Use of Acid Mine Drainage (AMD) Waste as a Soil Amendment

OSMRE Cooperative Agreement Number: S21AC10054

Draft Final Report

Principle Authors

Dr. Leslie Hopkinson., Principal Investigator

Dr. John D. Quaranta, P.E., Co-Principal Investigator

Jason Fillhart, Co-Principal Investigator

Graduate Students

Amanda Rodrigues Silva, MSCE

Grace Kerr, MSCE

Brady Watters, MSCE

Johah Tyson, MSCE

Luke Daugherty, MSCE

(April 2024)

Wadsworth Department of Civil and Environmental Engineering

Benjamin M. Statler College of Engineering and Mineral Resources

West Virginia University

P.O. Box 6103

Morgantown, WV 26506-6103

DISCLAIMER

ABSTRACT

Costs associated with sludge management and handling are high, often several times greater than the cost of chemical treatment. Alternative uses of this material may help offset these costs and improve efficiency of coal mining and reclamation activities. The overall goal of the research was to evaluate the use of acid mine drainage (AMD) sludge, a waste by-product, as a soil amendment to support vegetation establishment and persistence. To be successful, high moisture content sludge must be dewatered by non-mechanical means to aid with costs and transport. This goal was addressed by developing methods to enhance AMD geotube dewatering and evaluating the use of AMD as a soil amendment.

Geotextile fabrics are commonly used in the dewatering and filtration of high-water content geomaterials. Acid Mine Drainage sludge is a geomaterial and has increasing production volumes in West Virginia. Large sludge storage sites exist for dewatering and long-term disposal. Currently the AMD is treated then transferred by pumping the material into geobags for long-term disposal in tubular shape geotextile bags that dewater the sludge. The current design of the geobags limits the pathways for the water to filter out due to the quality of the material. This research investigated the geotextile fabrics currently used and explored options to insert internal lateral drains to shorten drainage paths and accelerate dewatering.

Coal-mining activities expose sulfide minerals in rocks that, when in contact with oxidizing conditions, produce sulfate-rich drainage known as AMD. AMD treatment typically involves chemical treatments to raise pH and precipitate solubilized metals. This process produces a sludge precipitate known as AMD sludge. The AMD sludge has been commonly disposed of in ponds or underground mine works, in active coal mine refuse areas, and in onsite burial. AMD sludge disposal present management and environmental concerns due to large requirement of area, sludge properties, and the continuous sludge production even after mining activities are ceased. This research evaluated the use of AMD sludge as a soil amendment by evaluating soil development at a reclaimed site, characterizing sludge, completing a small-scale growth study, and completing field tests.

GRAPHICS MATERIAL LIST

Table of Contents

List of Tables

Table of Figures

INTRODUCTION

Treatment of acid mine drainage often involves active treatment systems that use alkaline chemicals to raise the pH, neutralize acid, and precipitate metals (Skousen et al., 1998). The resulting hydroxide sludge (referred to as AMD sludge in this text) must be disposed of. The sludge is often disposed of in abandoned mines, refuse piles, or in ponds (Skousen et al., 2000). Sludge management is a continuing concern as the amount of AMD sludge continues to increase (Zinck, 2006).

Costs associated with sludge management and handling are high, often several times greater than the cost of chemical treatment (Skousen et al., 2000). For example, Lovett and Ziemkiewicz (1991) estimated that sludge handling costs were 6.75 times the yearly cost of the alkaline chemicals for a site in West Virginia. Alternative uses of this material, for example as soil amendment or part of a manufactured soil, may help offset these costs. AMD sludge has shown potential as a soil amendment (Alder and Sibrell, 2003), and use of this by-product as a soil amendment or part of a manufactured soil media will be further evaluated in the proposed work.

The overall goal of the work was to evaluate the use of AMD sludge, a waste by-product, as a soil amendment to support vegetation establishment and persistence. To be successful, high moisture content sludge must be dewatered by non-mechanical means to aid with costs and transport. Specific objectives included the following:

- Objective #1: Develop methods to enhance AMD geotube dewatering with internal lateral drains.
- Objective #2: Evaluate the use of AMD as soil amendment.

The ability to dewater AMD sludge (up to 2500 % moisture content) reduces the area needed for sludge disposal and simplifies methods for reuse (Zinck, 2006). Geotubes are often used to dewater sludge by non-mechanical means. In the first objective, methods for enhanced dewatering of geotubes bags were developed by evaluating the use of internal lateral drains and numerical modeling. A field test was completed through collaboration with the West Virginia Department of Environmental Protection (WVDEP) and an industry partner, Solmax® Geosynthetics.

One strategy for AMD sludge disposal is to allow it to dry and age on land, resulting in a soil-like material (Skousen et al., 2019). Therefore, there is potential for the use in a manufactured growth media. In the second objective, the use of sludge as a soil amendment or as part of a manufactured soil media was series of tests: soil development analysis, sludge characterization, small-scale growth study, and large-scale growth study.

EXECUTIVE SUMMARY

Costs associated with sludge management and handling are high, often several times greater than the cost of chemical treatment. Alternative uses of this material may help offset these costs and improve efficiency of coal mining and reclamation activities. The overall goal of this work was to evaluate the use acid mine drainage (AMD) sludge, a waste by-product, as a soil amendment to support vegetation establishment and persistence. To be successful, high moisture content sludge must be dewatered by non-mechanical means to aid with costs and transport. This goal was addressed by developing methods to enhance AMD geotube dewatering and evaluating the use of AMD as a soil amendment as detailed in the following paragraphs.

Develop methods to enhance AMD geotube dewatering

Geotextile fabrics are commonly used in the dewatering and filtration of high-water content geomaterials. AMD sludge is a geomaterial and has increasing production volumes in West Virginia. Large sludge storage sites exist for dewatering and long-term disposal. Currently AMD is treated and transferred by pumping the material into geobags for long-term disposal in tubular shape geotextile bags that dewater the sludge. The current design of the geobags limits the pathways for the water to filter out due to the quality of the material. This research investigated the geotextile fabrics currently used and explores options to insert internal lateral drains to shorten drainage paths and accelerate dewatering.

AMD sludge was collected from the field to determine the current geotextile filtration and dewatering efficiencies with and without polymer additives. Analysis of column filtration tests concluded that a nonwoven geotextile exhibited the highest filtration efficiency (>91%) and a relatively efficient drainage hydraulic conductivity (1.5×10^{-3} cm/s) for all permutations tested. The influence of polymer dosing on the AMD sludge indicated that for the no-polymer dose condition and a woven geotextile, the sludge hydraulic conductivity stabilized at 3×10^{-4} cm/s after approximately 50 hrs but had a filtration efficiency of 75% particle retention. In contrast, the 20 ppm cation polymer dosed sludge exhibited a hydraulic conductivity at 3×10^{-5} cm/s within 150 hrs and a filtration efficiency of 91%. The polymer dosed sludge is preferred for minimizing solids pass through for environmental permit compliance.

Techniques to accelerate filtration and dewatering of AMD precipitate using geobags augmented with capillary channel fibers and internal lateral drainage structures were evaluated. Laboratory and field research investigated increasing the total solids retention of AMD precipitate in geobag storage systems. Current geobag design and field application of treated AMD precipitate exhibit limited filtration and drainage efficiency due to the high moisture content (2,500%) polymer amended AMD flocculated solids.

Capillary channel fibers (CCFs) are geosynthetic yarns formed with microgrooves and set into bundled arrangements capable of wicking water, via capillary action, from fine grained soils. This research studied CCF augmented fabrics and prefabricated vertical drain (PVD) geocomposites positioned mid-depth in geobags filled with AMD precipitate to accelerate drainage via a shortened drainage path. A potential decrease in dewatering times using the combination of CCF geotextiles with internal lateral drainage was observed.

Laboratory and field scale tests included two predominant methods: the Hanging Bag (HB) and Geotube Dewatering (GDT) tests. The Hanging Bag test results indicated that introduction of CCF internal drainage media generally increases dewatering potential (3.84% increase in Total

Solids Content). Geotube dewatering tests revealed that the CCF internal drainage media of larger surface area increased dewatering potential (11.29% Total Solids Content) in contrast to the PVD lateral drainage layer (10.32% Total Solids Content).

Evaluate the use of AMD as a soil amendment

Coal-mining activities expose sulfide minerals in rocks that, when in contact with oxidizing conditions, produce sulfate-rich drainage known as acid mine drainage (AMD). AMD treatment typically involves chemical treatments to raise pH and precipitate solubilized metals. This process produces a sludge precipitate known as AMD sludge. The AMD sludge has been commonly disposed of in ponds or underground mine works, in active coal mine refuse areas, in geobags, and in onsite burial. AMD sludge disposal present management and environmental concerns due to large requirement of area, sludge properties, and the continuous sludge production even after mining activities are ceased. This research evaluated the use of AMD sludge as a soil amendment by evaluating soil development at a reclaimed site, characterizing sludge, completing a small-scale growth study, and completing field tests.

Soil development was observed at a previously treated reclaimed surface mine located in Upshur County, West Virginia, USA. The soil profile was analyzed through a qualitative soil pit analysis in accordance with USDA-NRCS sampling guidelines. Observations on the present soil conditions within the site showed no evidence of AMD within the soil profile. A thin topsoil horizon consisting of 2 inches (5cm) of depth overtop a compacted overburden fill was observed.

The small-scale, growth study evaluated the use of AMD sludge as a soil amendment as an alternative means of reuse for this material. Six different mixtures containing sludge and topsoil with amounts of sludge of 0%, 10%, 20%, 30%, 40%, and 50% in volume, were analyzed for ground cover, biomass, and stem height during nine weeks of study. The sludge sample used in the study met Resource Conservation and Recovery Act (RCRA) toxicity requirements. Results showed that the addition of AMD sludge up to 50% in volume to topsoil did not reduce ground cover significantly when compared to the only topsoil baseline, suggesting that the sludge may be considered for land application with additional testing at field scale needed.

A plot study was completed with fall planting in September 2022. The study consisted of five mixtures of AMD sludge to topsoil at 0%, 25%, 50%, 75%, and 100% AMD by volume, each replicated three times, creating a total study of fifteen 3.28 ft by 3.28 ft (1 m by 1 m) growth plots. Plots were seeded with a grass mixture recommended and used by the West Virginia Department of Environmental Protection. Plots were monitored for ground cover, moisture content, conductivity, and temperature. Spring planting results showed that AMD mixed soils had from 5% to 30% more moisture within the matrix versus just topsoil. Soil conductivity, an indicator of available nutrients and salinity, showed values ranging from 0.05 to 0.35 mS/cm over topsoil values. A mixture of 25%AMD performed from 1% to 5% more in grass coverage when compared to topsoil values. Temperature had no substantial difference by soil mixture.

The field plots were improved and replanted in May 2023. Fifteen study plots (three repetitions of five treatments) were created in Monongalia County, West Virginia. The treatments included topsoil mixed with AMD sludge in volumetric ratios: 1) 25% AMD sludge/75% topsoil (25AMD), 2) 50% AMD sludge/50% topsoil (50AMD), 3) 75% AMD sludge/25% topsoil (75AMD), 4) 100% AMD sludge (100AMD), and 5) 100% topsoil (Topsoil, control). Ground cover, soil moisture, soil electrical conductivity, and soil temperature were monitored for each plot from May 25, 2023, to October 23, 2023. At the end of the data collection phase, soil and above-ground biomass samples were collected from each plot. Statistical analysis for all measurements, and final measurements were conducted using R-Studio and compared. Major results suggest that mean ground cover for the AMD treatment was significantly less than all other treatments when considering only final ground cover and was significantly less than all other treatments when considering the full study duration; mean soil moisture for the AMD treatment was significantly greater than all other treatments when considering the full duration of the study.

EXPERIMENTAL

Experimental methods are reported for Objective #1 followed by Objective #2 in the following sections.

Objective #1 Develop methods to enhance AMD geotube dewatering with internal lateral drains.

Characterize geotechnical properties: Column filtration testing

Material Testing

A selection of geotextile fabrics was tested with a variation of AMD slurry treatment conditions. The treatment conditions included the preferred condition and the undesirable conditions to account for potential field conditions. The filtration and dewatering conditions evaluated include:

1. No Polymer Sludge from Omega Clarifier
2. 20 ppm Polymer T&T Sludge going to Geotextile Bags (20 ppm)

Five different geotextile fabrics were evaluated for the study. These fabrics that were tested had different uses in their field applications. The selection of the fabrics was based on fabric applications, AOS, and filtration efficiency. The geotextile specimens consisted of two typar fabrics used with the PVDs, one woven, and two nonwoven fabrics as present in Table 1.

Table 1. Geotextile fabric properties.

Fabric Type		GT500 Woven	1100N Nonwoven	140NC Nonwoven	MD88 Nonwoven Typar	MD7407 Nonwoven Typar
Apparent Opening Size (mm)	ASTM D4751	0.425	0.15	0.212	0.09	0.23
Permittivity (sec^{-1})	ASTM D4491	N/A	0.8	2	0.3	0.4
Flow Rate ($L/min/m^2$)	ASTM D4491	815	3056	5704	N/A	N/A

Testing Procedure

The testing method used followed Weggel and Dortch (2012), who used column filtration test specimens consisting of a 5 cm clear PVC pipe mounted vertically to a wooden structure on a table. The PVC pipe has a ruler on the outside surface for measurements. The framing system secures the vertical tube to the table using a C-clamp. The selected geotextile is wrapped and tightened to the bottom of the pipe using a hose clamp. The fabric is mounted flush and covers the entire drainage surface area of the bottom of the pipe with no loose areas that could develop leakage. A graduated cylinder sits underneath the pipe to collect and measure the outflow. The outflow liquid is measured between time intervals to calculate the discharge flowrate.

Detailed test instructions are available in the Appendix.

Characterize geotechnical properties: Moisture distribution tests

The purpose of the total solids distribution testing will be accomplished by collecting samples from the side of the geotextile tubes at different depths and across different distances at one cross section. The testing will be done following ASTM D2216 which is the Standard Test Methods for Laboratory Determination of Water (Moisture) Content of Soil and Rock by Mass. Following this ASTM will produce the moisture content for each sample that was collected and by using the total solids percentage from the sample a current model will be created that presents the current distribution of moisture based on the different cross sections that were selected.

To accomplish the purpose the following objectives will be performed:

1. Build a Sampler
2. Obtain Samples
3. ASTM Tests
4. Reduce Data
5. Build Figures

Testing Procedure

In situ sludge samples were collected from different depths within the geotextile bag by using a 2 in pvc pipe that had 9-10 cm holes set at 10 cm increments. Five to six different samples for each hole dug in the geotextile tube were taken. The PVC pipe was constructed by cutting a semicircle hole in the pvc pipe on one side and having a thin slit cut parallel to the flat edge of the semicircle. A piece of aluminum was used to scoop the sludge into the opening in the pvc pipe. Figure 1 is the second sampler that was constructed with a longer pipe section to allow for more scoops/holes.

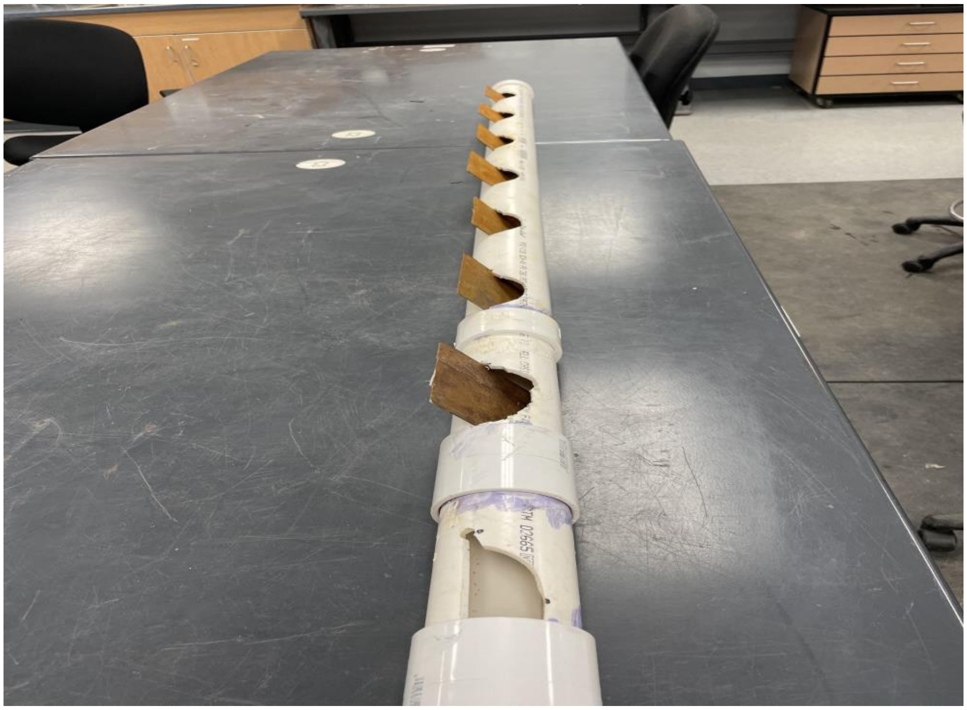

Figure 1. Version 2 6ft Sampler with 7 holes.

The testing method to determine the moisture contents was done following the ASTM D2216-19: Standard Test Methods for Laboratory Determination of Water (Moisture) Content of Soil and Rock by Mass. Each test was run using triplicate testing and then determining the average value of the 3 for the reported value. The specific gravity was also determined for each of the cross sections that were being tested. This test was done by following the ASTM D854-14: Standard Test Methods for Specific Gravity of Soil Solids by Water Pycnometer.

Design prototype dewatering system

AMD sludge management and handling costs remain high after geobag implementation. Further dewatering of AMD sludge via nonmechanical means would aid with the high handling and transport costs. Introducing internal lateral drainage in current field scale geobags has the potential to enhance geobag dewatering. Solmax manufactured bench scale hanging bags and geobags outfitted with various internal drainage configurations to investigate field scale internal lateral drainage feasibility.

<u>Lateral Drainage Approach Concept</u>

When an AMD sludge filter cake develops and increases in thickness on the inside surface of geobags, the result is a reduction in dewatering as the sludge material drains. The result of this is internal zones of low Total Solids Content and high Gravimetric Moisture Content remaining saturated with low permeability inside the geobags.

The *in situ* lateral drainage approach proposed herein is an innovative technique in that it provides the opportunity to dewater the centrally located, saturated, low permeability zones within geobags through passive gravity driven *in situ* drainage. In order to accomplish this, wick or band drain material was used. Specifically, Prefabricated Vertical Drains and Capillary Channel Fibers were proposed for implementation as lateral drainage mechanisms within geobags. Band drains are conventionally installed in a vertical orientation to remove pore water from low permeability soil, which induces and accelerates saturated ground settlement. This research proposed to install band drains horizontally within AMD sludge filled geobags to increase drainage effectiveness, with installation design executed using established radial consolidation theory (Richart, 1957).

Band drain orientation was proposed as parallel to the length of the geobags. Band drain positioning was proposed at mid-depth within the geobags to intersect the identified internal low permeability saturated AMD sludge zone. Figure 2 below illustrates this concept, with a circumferential filter cake zone at the geobag surface and 4 rows and 8 columns of band drains intersecting the internal AMD sludge low permeability zone and running parallel to the geobag length extending into the page.

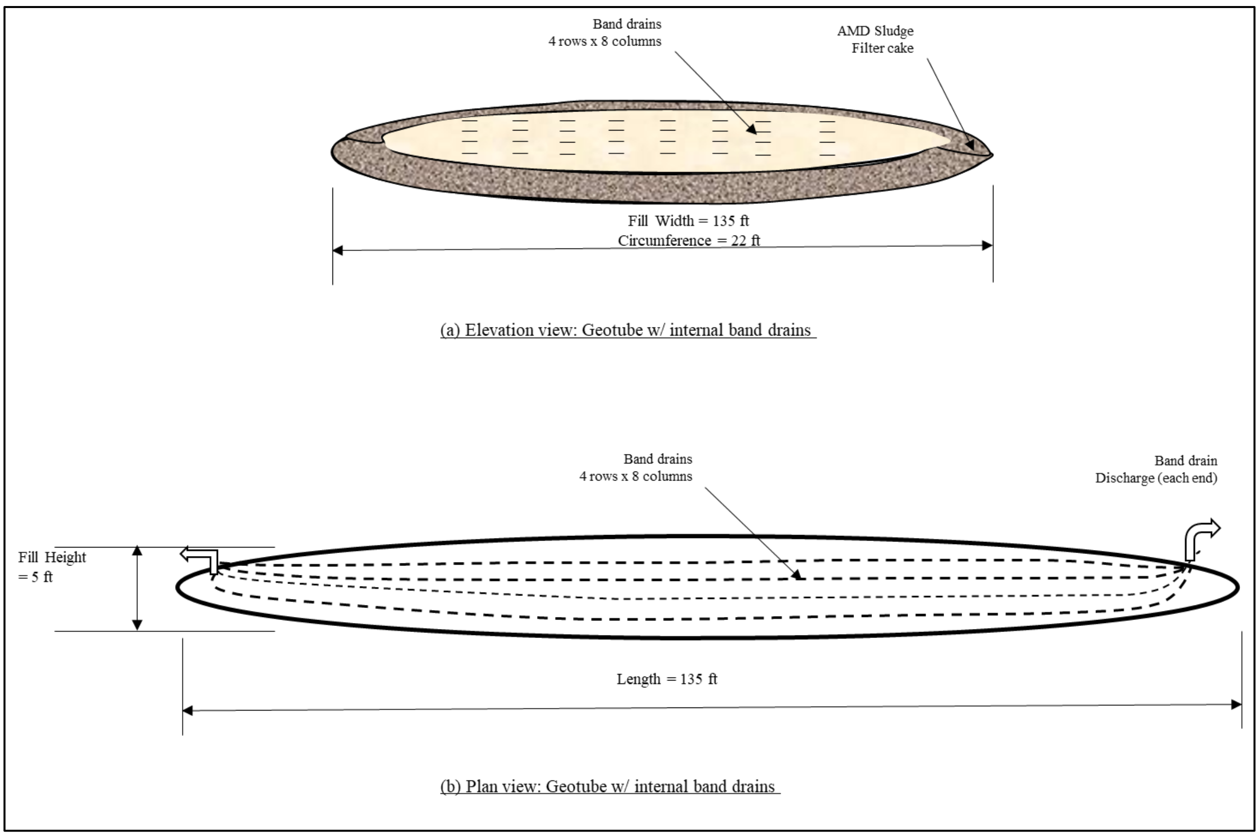

Figure 2. Lateral drainage approach concept (Source: Quaranta, personal communication).

Prefabricated Vertical Drain (PVD) overview

Prefabricated Vertical Drains (PVDs) are defined as a category of geocomposite, or combined woven and non-woven geotextile.

PVDs are known to decrease a drainage path for the purpose of consolidation acceleration. PVD components consist of an outer layer filter with an inner drainage core as illustrated in Figure 3 and Figure 4 (Fannin, 2007).

Figure 3. Plan view of PVD (Source: Author).

Figure 4. Cross-section view of PVD (Source: Author).

The inner drainage core is corrugated polypropylene with flow channels present on either side. The outer layer filter is a non-woven geotextile. PVDs are implemented with the intent to create a hydraulic gradient, which allows for removal of water from soil voids. PVDs function as intended when there is a surface surcharge present developing pore pressure and hydraulic gradient (Gabr et al., 1997). While PVDs are commonly installed in a vertical orientation, alternate orientation installations have also been implemented (Warren et al., 2006).

Capillary Channel Fiber (CCF) overview

Capillary Channel Fibers (CCF) are defined as fabrics that possess microgrooves capable of wicking water, via capillary action, out from a porous media. This wicking action causes water to be pulled from the wet towards the dry side of the CCF because of surface tension, or negative drainage (Santos, 2022). CCFs are implemented with the intent to minimize adverse dewatering conditions brought about by the presence of a capillary barrier in unsaturated conditions (Azevedo and Zornberg, 2013; Tyson, 2023). CCFs have previously been identified as having dewatering potential in industries pertaining to flocculated materials, including wastewater treatment, mine tailings, and dredging (Santos, 2022). In unsaturated soil conditions, the wicking fabric is heavily dependent on the suction gradient from evaporation to promote water drainage (Zhang et al., 2014). A CCF fabric is illustrated in Figure 5.

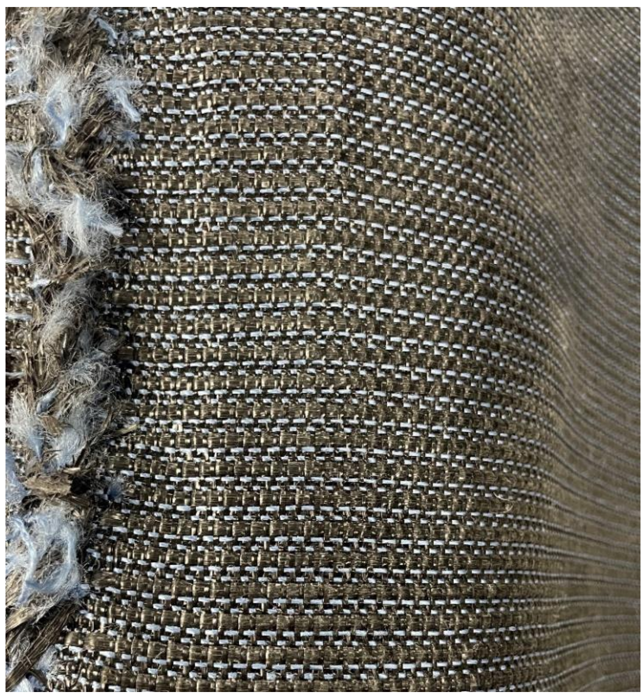

Figure 5. CCF fiber (Source: Tyson, 2023).

Approach

The test approach was to perform HBTs and GDTs using AMD HDS. This consisted of developing tests that evaluated HDS filtration and dewatering using geosynthetics. The approach was to use the HBTs and GDTs on geosynthetic specimens using HDS permeants. Three test sets (2 HBTs and 1 GDT) were followed and discussed as follows:

1. Hanging Bag Test (HBT)
    1.1. Test Set 1 = radial drainage in 3 configurations, 3 hanging bags in total
    1.2. Test Set 2 = radial drainage in 5 duplicate configurations, 10 hanging bags in total
2. Geotube Dewatering Test (GDT)
    2.1. Test Set 3 = lateral drainage in 5 duplicate configurations, 10 GDT bags in total
    2.2. Handheld Temperature Gauge Testing = temporal temperature monitoring of 10 GDT bags

Numerical modeling

A steady-state 2-dimensional model was created using Plaxis 2D Groundwater, which is a finite-element software for 2D analysis of deformation and stability in geotechnical and rock mechanics. The groundwater software module was used for the analysis for a flow of water in saturated and unsaturated soils. Groundwater allows for modeling dewatering in either a steady-state model or a time-dependent (transient) model. Using Plaxis to model flow in saturated soil follows Darcy's Law in which the rate of water flow through a soil mass is proportional to the hydraulic gradient. The flow for soil in an unsaturated state applies a mathematical function relating hydraulic conductivity to the soil saturation.

<u>Materials Properties</u>

The model is comprised of the input slurry material which was collected from a WVDEP site that was treating AMD. When running through oven-dried material through the ASTM D6913 (Standard Test Methods for Particle-Size Distribution (Gradation) of Soils Using Sieve Analysis) for grain size classification, the material was found to be a silt. A woven geotextile called GT500 was used and has the properties listed in Table 2. The properties that are present are the apparent opening size and the flow rate for the geotextile as well as the ASTM that are used in order to determine those values.

Table 2. Finite Element Modeling Woven Geotextile Properties.

Mechanical Property	ASTM Test Method	GT500
Fabric type		Woven
Apparent Opening Size (AOS) (mm)	ASTM D4751	0.425
Flow Rate (L/min/m^2)	ASTM D4491	815

The next set of data is the hydraulic conductivity used to create the unsaturated functions. The data for this was collected from Section 3 Column Filtration Testing. Where the average hydraulic conductivity from the first stages of filtration were used for the AMD Slurry and the steps to calculate the hydraulic conductivity for the GT500 fabric was done by taking the Flow Rate from Table 2 and putting it into the Darcy's Law equation. In this equation the Flow Rate equates for $\frac{Q}{A}$, so the only value that was needed is the hydraulic gradient (i).

$$k = \frac{Q}{iA} \tag{1}$$

$$i = \frac{\Delta h}{L} \tag{2}$$

Since the values for the slurry were calculated from the Column Filtration Testing, the value for L was taken to be 1 cm and the value for the change in head was taken from the average change in head from the start of the first stage of filtration to the end of that stage when there was no change. The value used to calculate for the change in head in this equation was 20 cm. The hydraulic gradient the value used in the Darcy's Law equation was 20. The hydraulic conductivity for the filter cake for each model decreases as time passes because the filter cake thickens and the pore spaces between material decreases. The equations that was used to solve for the hydraulic conductivity for the AMD Slurry is taken from the Falling Head:

$$k = \frac{aL}{A\Delta t} \ln \left(\frac{h1}{h2}\right). \qquad (3)$$

The values taken from the Column Filtration Testing have the dimensions for hydraulic conductivity (cm/s) which have to be converted to m/hr for the Plaxis models. The hydraulic conductivity values that are used for the model are listed in Table 3.

Table 3. Finite Element Modeling Material Hydraulic Conductivity Values.

Material	Hydraulic Conductivity (m/hr)
AMD Slurry	1.05×10^{-1}
Filter Cake Stage 1	5.27×10^{-2}
Filter Cake Stage 2	2.64×10^{-2}
Filter Cake Stage 3	1.32×10^{-2}
GT500 Fabric	2.44

Methodology

The model is just the slurry or sludge inside as the center core and the GT500 fabric outlines it where it acts as the filter for water flowing out of the system. The model is created on a four-stage system where the value that changes is the hydraulic conductivity of the slurry that is the proximity of the GT500 fabric. Based on the filter testing, the fabric develops a filter cake build-up over time due to the particle solids clogging the fabric. The increased density of the filter cake decreases hydraulic conductivity. The area of the filter cake is constant with the hydraulic conductivity changing between the 2^{nd}, 3^{rd}, and 4^{th} stage injections. The model's stages were simulated to be 7 days for the first stage and 21 days for the next three stages. A data point is collected and shown for every 24 hours, to show the model changing over time. The overall duration of the model is 1,680 hours (70 days).

Figure 6 is the design for the base model in Plaxis. The size of the model was created in a range to simulate the cross section of a geotextile tube that is currently in the field. The dimensions of the model have a length of 2 meters and a heigh of 0.5 meters. The area for the GT500 fabric in the model is not consistent with the thickness that is typically found out in the field. The thickness for the filter cake in the 2^{nd}, 3^{rd}, and 4^{th} stages is the same as the GT500 in the model. In the filter test the thickness decreases over time but maintained a constant area to eliminate another variable to be calculated for.

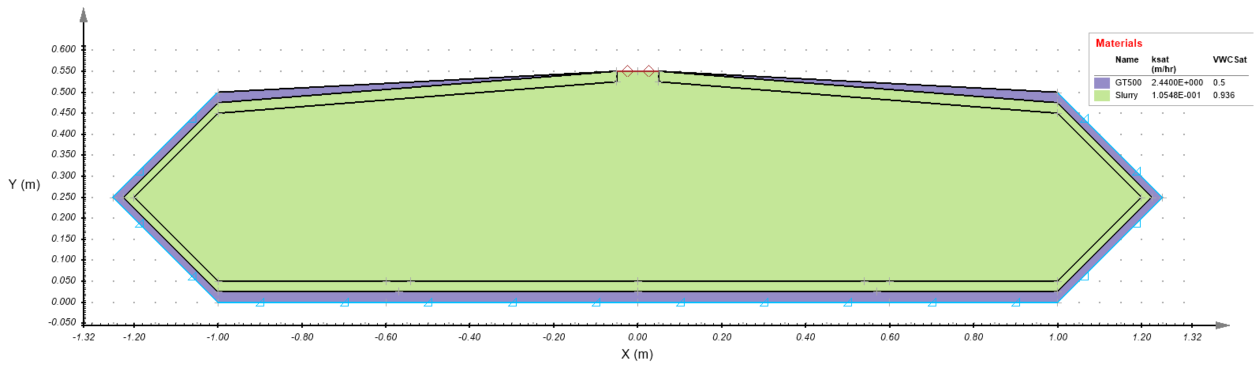

Figure 6. Plaxis Model Design.

The AMD slurry injection is at the top center of the model so that the inflow of material is within the geobag volume to simulate the geotextile fabric to only act as radial drainage. Where the darker shaded region is the geotextile, and the lighter shaded region is the AMD slurry. The filter cake region is filled in with the AMD slurry material in the first stage and then changed to the filter cake for the other stages.

Both the GT500 fabric and the AMD Slurry was modeled as unsaturated material and required a function that relates hydraulic conductivity to the slurry saturation. The Van Genuchten and Mualem Estimation function was used as listed below.

$$\theta_w = \theta_r + \frac{\theta_s - \theta_r}{(1+(a\varphi)^n)^m} \quad (4)$$

$$k_w = k_s \frac{(1-(a\varphi)^{(n-1)}\{1+(a\varphi)^n\}^{-m})^2}{(1+(a\varphi)^{n^{m/2}}} \quad (5)$$

$$n = \frac{1}{1-m} \quad (6)$$

Where:

k_s is the Saturated Hydraulic Conductivity

k_w is the Hydraulic Conductivity at a particular suction value

θ_w is the Volumetric Water Content

θ_s is the Saturated Water Content

θ_r is the Residual Water Content

φ is the Negative Pore Water Pressure

α, n, and m are the Model Fitting Parameters

The k_s values are taken from Table 3. The values for the AMD slurry saturated water content is calculated using the average water content within a geotextile tube. These values are taken from

Section 4 data points. The residual water content in the Van Genuchten function is defined as the water content at a soil suction value of 1500 kPa where this value for soil suction is defined as the wilting point (Vanapali et al., 1998). According to Luckner et al. (1989), the residual water content is specified by the maximum amount of water in a soil that will not contribute to the liquid flow because there is a blockage in the flow paths. The value for the AMD slurry's residual water content is related to the values for a Silt Loam which are taken from the Soil Water Storage Properties from the Minnesota Stormwater Manual which shows the wilting point, residual water content, for different soils. The wilting point value for a loam soil are between 10 to 15% (Northeast Region Certified Crop Advisor, 2010). Based on the research by Bouazza et al. (2006) the saturated water content is typically a large value for non-woven geotextiles with large porosities and the residual water content is small when the suction is high. The value for the GT500 fabric's residual water content are similar to the values from this article while the water content is estimated to be 0.5 to simulate that the bag is the driest at the outside edge.

The model fitting parameters (a, n, and m) for the AMD slurry are also based on values for a Silt Loam (Rawls et al., 1982). In order to calculate the model parameters for the geotextile fabric a computer program called Retention Curve (RETC) (van Genuchten et al., 1991). Bouazza et al. (2006), Stormont & Morris (2000), and Vanapalli et al. (1998) developed values from the RETC program for the geotextile fabrics. The steps that were taken when running the RETC program were to estimate the parameters. The predications are similar to the values for sand since nonwoven geotextiles have similar characteristics to coarse material. The initial estimated values used are shown in Figure 7. RETC uses the sum of squares (SSQ) in order to estimate the values. The SSQ for the estimation of the n parameter is shown in Figure 8.

```
INITial values of the coefficients
==================================
No      Name          INITial value
 1      ThetaR            .0000
 2      ThetaS            .9900
 3      Alpha            5.0000
 4      n                1.0500
 5      m                 .0476
 6      l                 .5000
 7      Ks               2.4400
```

Figure 7. Initially Predicted Parameters from RETC Program (Source: RETC).

```
NIT     SSQ       n
 0   14.43292    1.0500
 1   14.43275    1.2154
 2   14.43235    1.1867
 3   14.43233    1.1790
 4   14.43233    1.1775
 5   14.43233    1.1772
 6   14.43233    1.1772


RSquated for regression of observed vs fitted values =-1.47415934
=================================================================



Nonlinear least-squares analysis: final results
===============================================
                                                95% Confidence limits
Variable      Value      S.E.Coeff.    T-Value     Lower        Upper
n            1.17715     2.45320         --       -4.2889      6.6432
```

Figure 8. Sum of Squares from RETC Program (Source: RETC).

The values that were used to create the models based on the Van Genuchten and Mualem Estimation function are listed below in Table 4. With an example of the Plaxis 2D window for inputting the parameters is shown in Figure 9.

Table 4. Van Genucthen and Mualem Estimation Parameters.

Material	**a (1/kPa)**	**n**	**Saturated Water Content (θ_s)**	**Residual Water Content (θ_r)**
AMD Slurry	0.048	1.211	0.9361	0.75
GT500	5	1.17715	0.5	0

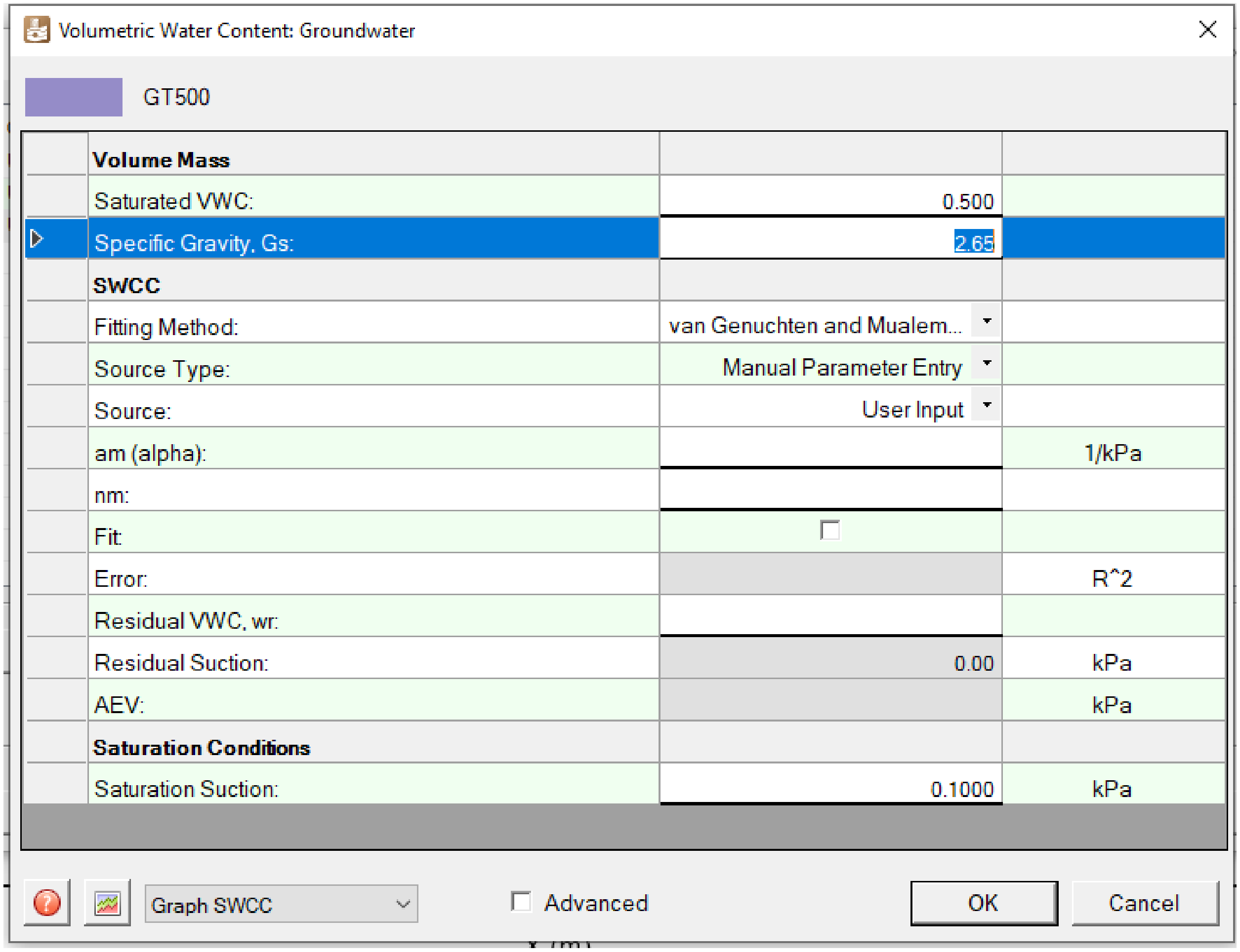

Figure 9. Plaxis 2D Van Genuchten Parameter Input Window (Source: Plaxis 2D).

The models that were developed in Plaxis 2D are listed in Table 5, with a brief description of what each model is showing. In total there are 9 output models and 1 input model.

Table 5. Plaxis Output Models.

Model #	Description
1	Hydraulic Conductivity Under Flow
2	Hydraulic Conductivity with Filter Cake Build Up
3	Initial Water Content
4	Water Content on Final Day of Stage 1
5	Water Content with Addition of Filter Cake
6	Final Water Content
7	Solids Content Distribution
8	Expected Moisture Flow
9	Unexpected Moisture Flow

Boundary Conditions

Boundary conditions (BC) are displacements assigned to the edges of the regions of the Plaxis model. The Plaxis model has boundary conditions that are placed on the lines the connect the regions and along the edge of the geotextile region. The boundary conditions that are: 1) the infiltration or inflow of water, which are weather conditions; 2) zero flux, meaning no flow through the zone; and 3) a unit gradient, which generates the flux outward of the model to be equal to the hydraulic conductivity. The value for the inflow is $850 m^3/hr/m^2$ is allowed to flow into the model for the first 12 hours of each week (or every 7 days) then continue for the next 156 hours as the water dewaters out of the model. The inflow is only allowed to enter the center port, shown in Figure 10, which shows an inflow of water and how many times water is input into the model's system. Where the AMD slurry injection flow rate is in cubic meters per hour. The zero-flux boundaries are along the top of the model, so the inflow is only allowed to flow through the injection port and not through the geotextile that immediately borders the injection port. The unit gradient boundary conditions are placed to surround the geotextile region, this is so that the injected flow of the material through the slurry region goes into the geotextile based on its hydraulic conductivity and then the material flows through the geotextile and out of the model based on the hydraulic conductivity of the geotextile fabric.

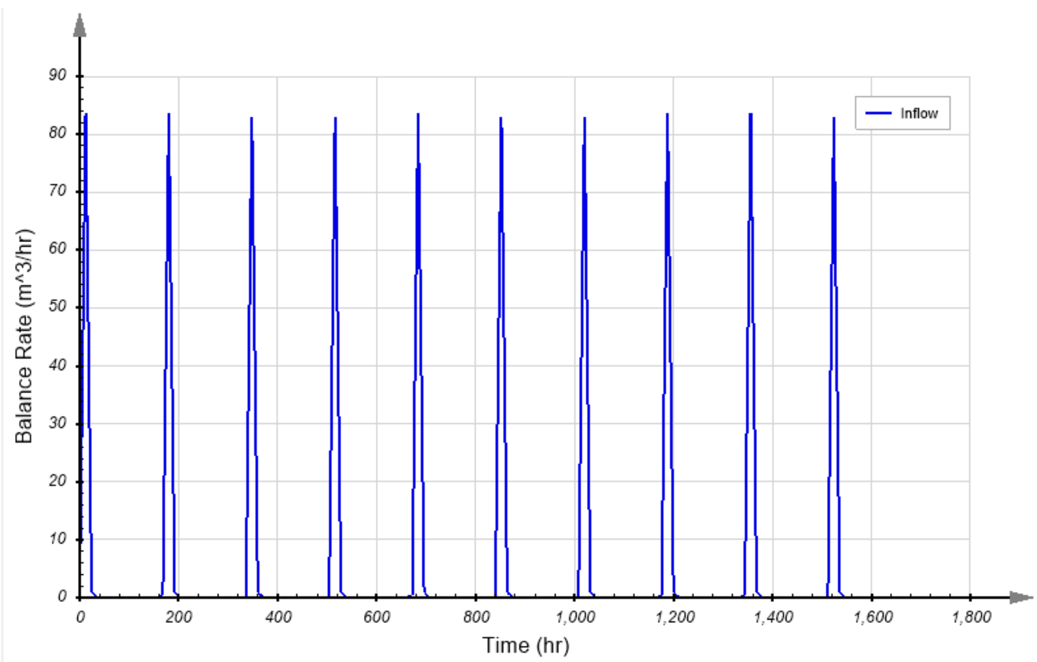

Figure 10. Plaxis Models Inflow Graph (During Injection).

Field-scale testing: Hanging Bag Tests (Test Set 1)

Test Set 1 consisted of hanging bags with prototype amended fibers in 2 configurations and a standard of comparison for a total of 3 tests. Each hanging bag consisted of dimensions of 35.5 cm in height and 30.5 cm in diameter. The individual tests were assigned a nomenclature of HB-

A, HB-B, and HB-C. HB-A was the standard of comparison and consisted of a woven shell lacking a central ribbon of prototype fiber. HB-B consisted of a woven shell with a vertically oriented central ribbon of prototype fiber. HB-C consisted of a woven shell with prototype fiber interwoven.

This information is concisely presented in Table 6. The nomenclature HB refers to Hanging Bags.

Table 6. Test Set 1 materials approach.

Sample Name	Description	
HB-A	Geotextile Shell Type = Woven AOS = 0.425 mm Wide Width Tensile Strength (Machine Direction) = 96.3 kN/m Water Flow Rate = 815 L/min/m^2	
HB-B	Geotextile Shell Type = Woven AOS = 0.425 mm Wide Width Tensile Strength (Machine Direction) = 96.3 kN/m Water Flow Rate = 815 L/min/m^2 Capillary Channel Fiber (internal drainage) Type = Bundled Prototype Drain Width = 111.1 mm Drain Length (per fiber) = 56.5 cm Quantity = 2	
HB-C	Geotextile Shell Type = Bundled Prototype	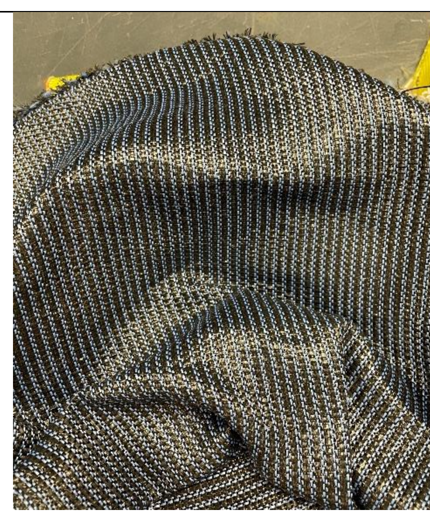

Field Operation

The Test Set 1 hanging bags and frame were transported to the T&T facility on July 14th, 2022. Upon reaching the site, the frame was assembled, and the bags were mounted to the frame. The wooden frame dimensions were 95 cm in height, a cross member 192 cm in length, 13.5 cm in depth and 2.5 cm in width with two supports of 20 cm width and 2.5 cm depth as illustrated in Figure 11.

Figure 11. Test Set 1 at the T&T site (Source: Author).

Frame dimensions were decided on based on ease of access to the hanging bags, hanging bag clearance with the ground and other hanging bags, and load bearing capacity. The initial filling of all 3 hanging bags took place at 10:20 AM and can be observed in Figure 12.

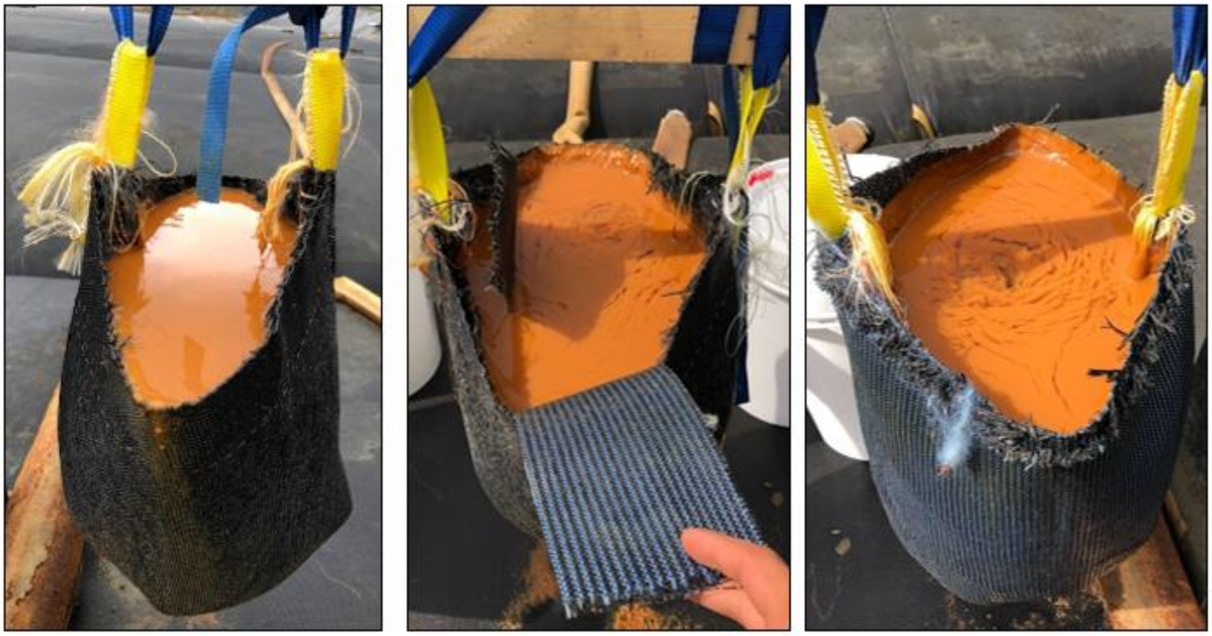

Figure 12. HB-A (standard-blank, left), HB-B ("V" orientation, middle) (Source: Author), HB-C (bundled prototype, right) (Source: Author).

The bags remained in the field for a total of 7 days and were filled 19 times. The initial time for the data collection plots was decided on as the end of the final bag filling in the field at 10:57 AM on July 21st, 2022, after which the test set was returned to the West Virginia University Evansdale Campus in the condition observed in Figure 13.

Figure 13. From left to right: HB-A, HB-B, HB-C (Source: Author).

Laboratory Monitoring

After the field specimens were retrieved from the field they were monitored in the laboratory. Once the bags were returned to the lab, re-mounting on the frame as specified by Koerner and Koerner (2006) was performed. The temporal air temperature of room B20, Engineering Sciences Building was recorded from July through September 2022. As can be observed in Figure 14, the air temperature remained relatively constant at approximately 22°C throughout the entirety of the experiment.

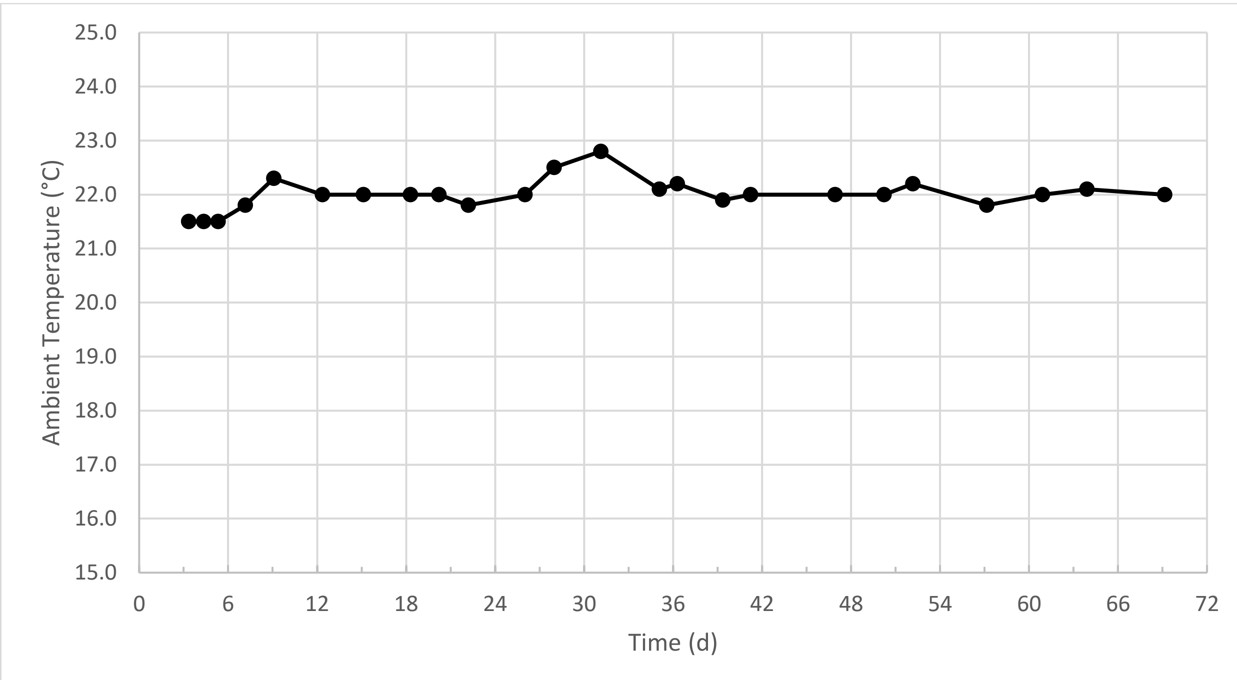

Figure 14. Ambient Room Temperature (°C) vs Time (d).

Test Set 1: Performance Testing Procedure (HBTs)

The following describes the performance testing procedure used for the Test Set 1 HBTs, adapted from Koerner and Koerner (2006):

1. The geotextile bags were attached to the frame by way of threading the loops of the bag onto screws. The screws were spaced at the diameter of the bag.
2. The geotextile bags were pumped to capacity with AMD sludge. Pumping was performed by notifying the on-duty WVDEP employee to turn on the pump, removing a hose from the quick connect to the field scale geobag, turning the valve to the ON position at the manifold, then orienting the hose to fill each individual bag to capacity with an effort to minimize AMD sludge spillover.
3. After each bag drained itself of free water, the geotextile bags were again pumped to capacity with AMD sludge.
4. Steps 2 and 3 were repeated until geotextile bag pumping resulted in minimal filter cake accumulation with additional pumping after which the valve was turned back to the OFF position and employee notified to turn off the pump.

5. Once the final pumping concluded, the timer was started and the number of times each bag was filled was recorded. This was time zero.
6. The bags were once again allowed to drain themselves of free water, then transported from the WVDEP treatment site to the geotechnical laboratory.
7. The bags were re-mounted on the frame and continued to let hang.
8. Each bag was monitored. This consisted of the following:
   8.1. Each bag was weighed weekly on a scale as in Figure 15 by freeing the bag from the hanger. The masses were recorded. The dry mass of each bag was obtained prior to initial AMD sludge pumping.

Figure 15. Test Set 1 Weighing Procedure (Source: Author).

   8.2. Representative samples were extracted from each bag on a bi-weekly schedule. ASTM Designation D2216-19 procedure was followed in order to determine the percent Total Solids Content and Gravimetric Moisture Content. Representative sample extractions were performed as follows:
      8.2.1. A sample of roughly 30 g material was extracted from the center position of the bag at a depth of roughly 2.5 cm (1 in) below the exposed filter cake layer.
      8.2.2. The sample was placed in the moisture content tin using a spatula, taking care to avoid smearing sample on the external surface of the tin as in Figure 16.

Figure 16. Test Set 1 sampling procedure (Source: Author).

8.2.3. The exposed filter cake layer was restored to approximate its pre-disturbed condition using the spatula.

8.3. Filter cake was monitored and characterized. This included filter cake formation, appearance, and intimate contact loss.

9. Once preliminary loss of intimate contact of AMD sludge with the drainage media was observed, a compression technique was employed weekly in an attempt to restore intimate contact. This technique involved folding over the top of the bag and “bear-hugging” the bag from different angles. Preliminary loss of intimate contact is defined as the initial visual observation of filter cake fracturing.
10. The test was concluded, and the timer stopped once significant loss of intimate contact of AMD sludge with the drainage media and cohesion of sludge was observed. Significant loss of intimate contact is defined as the point at which coherency of charged sludge to itself causes noticeable separation between the AMD filter cake and the internal drainage media. This was determined through visual inspection.
11. The following were plotted for each test:

    11.1. Time (d) vs. Normalized Change in Bag Mass (%)

    11.2. Time (d) vs. Total Solids Content (%)

    11.3. Time (d) vs. Normalized Change in Gravimetric Moisture Content (%)

Data plot normalization refers to the subtraction of each time step Bag Mass or Gravimetric Moisture Content from the initial time step Bag Mass or Gravimetric Moisture Content. This was done to allow for easier comparison among and between bags, since all bags were of different initial time step Bag Masses and Gravimetric Moisture Contents. The term time step refers to the time at which data was simultaneously collected for Bag Mass or sampling. Refer to the Measurement Calculations section for the equations for Normalized Change in Bag Mass (%) and Normalized Change in Gravimetric Moisture Content (%).

Deviations from the testing procedure followed in Koerner and Koerner (2006) was documented below:

1. The geotextile containers (bags) were not pre-wetted in prefiltered AMD water.
2. AMD sludge was not premixed in a container prior to being pumped into each bag.
3. Collection pans were not implemented, as effluent collection was not performed for reasons delineated in the Recommendations for Future Research, Test Set 1 (HBTs) section.
   3.1. Total Solids Content measurement of effluent was not monitored.
   3.2. Discharge flow rate of effluent was not monitored.
      3.2.1. Liquid level drop times were not recorded.
4. Multiple bag fillings with AMD sludge were done, rather than a single bag filling.
   4.1. Stopwatch timer was started after the final bag filling, rather than after the first bag filling.

Measurement Calculations

Measurement calculations for Total Solids Content (%) and Gravimetric Moisture Content (%) for Test Sets 1, 2, and 3 were performed as follows.

According to Howard and Carruth (2014), geotechnical engineers reference dry solid: (can be > 100%)

$$w = \frac{W_w}{W_s}(100\%) \qquad (7)$$

Where:

w = moisture content (water to solids (sludge)) expressed as a percentage,

W_w = mass of water (g), and

W_s = mass of solids (sludge) (g).

According to Howard and Carruth (2014), Dredging & Water Resources use Gravimetric Total Solids Content ($TS_{\%}$) by mass and Gravimetric Water ($W_{w\%}$) by mass as the following equations:

$$TS_{\%} = \frac{W_s}{W_w+W_s}(100) = \frac{W_w/W_{w\%}}{W_w+W_s}(100^2) \qquad (8)$$

$$W_{w\%} = \frac{W_w}{W_w+W_s}(100) \qquad (9)$$

$$TS_{\%} + W_{w\%} = 100 \qquad (10)$$

Where:

$W_{w\%}$ = total water by mass expressed as a percentage,

$TS_{\%}$ = Total Solids Content by mass expressed as a percentage,

W_w = mass of water (g), and

W_s = mass of solids (sludge) (g).

Bag weighing measures the mass of AMD contained within the bag. This was obtained by weighing the sludge-filled bag on an Ohaus® Defender 5000 scale precise to the nearest whole number in grams, then subtracting the empty Bag Mass from this value. All masses were then converted from grams to kilograms. Equation 8 demonstrates how Normalized Change in Bag Mass (%) was calculated.

$$Change\ in\ BM_{\%} = \left| \left[\frac{Current\ BM - Initial\ BM}{Initial\ BM}\right] x\ 100\% \right| \qquad (11)$$

Where:

Change in BM$_{\%}$ = absolute value of measured Bag Mass minus initial Bag Mass expressed as a percentage,

Current BM = Bag Mass at current time of experiment (g), and

Initial BM = Bag Mass at initial time of experiment (g).

Equation 9 demonstrates how Normalized Change in Gravimetric Moisture Content (%) was calculated by taking the difference of the Current Time Step Gravimetric Moisture Content (%)

and the Initial Time Step Gravimetric Moisture Content (%) then absolute value of the difference. Normalized Change in Gravimetric Moisture Content (%) and Total Solids Content (%) were calculated using data from weighed samples on an Ohaus® Gold Series scale precise to the hundredths place in grams.

$$Change\ in\ W_{w\%} = |Current\ W_{W\%} - \ Initial\ W_{W\%}| \tag{12}$$

Where:

Change in $W_{W\%}$ = absolute value of change in Gravimetric Moisture Content expressed as a percentage,

Current $W_{W\%}$ = Gravimetric Moisture Content at current time of experiment expressed as a percentage, and

Initial $W_{W\%}$ = Gravimetric Moisture Content at initial time of experiment expressed as a percentage.

The fact that Normalized Change in Bag Mass and Normalized Change in Gravimetric Moisture Content were expressed as an absolute value resulted in increasing or positive trends over time appearing in all figures, while the measured Bag Mass and Gravimetric Moisture Content reported values that decreased over time. That is, if Normalized Change in Bag Mass and Normalized Change in Gravimetric Moisture Content had not been expressed as an absolute value, the result would have been figures reporting decreasing or negative trends over time. Normalized Change in Bag Mass and Normalized Change in Gravimetric Moisture Content were not calculated for the initial time step since this resulted in either an undefined or zero value. These comments on Normalized Change in Bag Mass and Normalized Change in Gravimetric Moisture Content apply throughout.

The change in the mass of each individual bag over the experiment primarily was from water loss. A trace amount of fines passed through the geotextile shell of each bag but measurement attempts of the passing fines produced negligible mass measurements when the hanging bags were in the laboratory and effluent collection in the field was not performed due to the reasons delineated in the Recommendations for Future Research section.

ASTM Designation D6026-21 procedure was followed in order to determine significant digits in the calculation of all measured data.

Field-scale testing: Hanging Bag Tests (Test Set 2)

<u>Materials</u>

Test Set 2 consisted of hanging bags in four configurations and a standard of comparison in duplicates with various internal modifications for a total of 10 tests. The dimensions of each bag were 25.4 cm in diameter and 66.0 cm in depth. Ten individual tests were performed in total, as each configuration and the standard were duplicated. Each hanging bag had a two-layer shell, with the outside layer consisting of woven and the inside layer consisting of non-woven. The four configurations were variations of a vertically oriented CCF fiber. The CCF fabrics were either 1 or 2 centrally oriented strips, with either 2.54 cm or 10.2 cm widths. The four CCF fabrics were secured in the intended vertical orientation with metal wire which passed through the both sides of the hanging bag composite shell and the CCF fabric.

This information is presented concisely in Table 7. The nomenclature HB refers to Hanging Bags, (#_) refers to primary bags, and (#_D) refers to duplicate bags. It should be noted that the composite shell description reported for sample names HB#1 and HB#1D is applicable to all 5 configurations, as all 10 tests consisted of, at minimum, a composite shell.

Table 7. Test Set 2 materials approach.

Sample Name	Description	
HB#1 and HB#1D	Composite Shell (typical all specimens) Type = Nonwoven (inner) AOS = 0.15 mm Tensile Strength = 1113 N Type = Woven (outer) AOS = 0.425 mm Wide Width Tensile Strength (Machine Direction) = 96.3 kN/m Water Flow Rate = 815 L/min/m^2	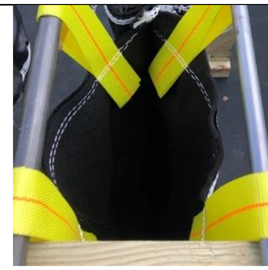
HB#2 and HB#2D	Capillary Channel Fiber (internal drainage) Type = Woven AOS = 0.425 mm Tensile Strength (Minimum Average Roll Value) = 77.0 kN/m Drain Width = 25.4 mm Drain Length (per fiber) = 66.0 cm Quantity = 1	
HB#3 and HB#3D	Capillary Channel Fiber (internal drainage) Type = Woven AOS = 0.425 mm Tensile Strength (Minimum Average Roll Value) = 77.0 kN/m Drain Width = 25.4 mm Drain Length (per fiber) = 66.0 cm Quantity = 2	
HB#4 and HB#4D	Capillary Channel Fiber (internal drainage) Type = Woven AOS = 0.425 mm Tensile Strength (Minimum Average Roll Value) = 77.0 kN/m Drain Width = 101.6 mm Drain Length (per fiber) = 66.0 cm Quantity = 1	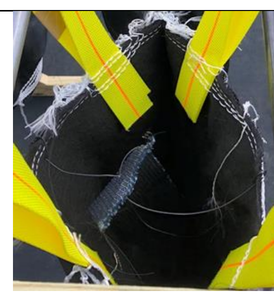
HB#5 and HB#5D	Capillary Channel Fiber (internal drainage) Type = Woven AOS = 0.425 mm Tensile Strength (Minimum Average Roll Value) = 77.0 kN/m Drain Width = 101.6 mm Drain Length (per fiber) = 66.0 cm Quantity = 2	

Field Operation

The Test Set 2 hanging bags and frame were transported to the T&T facility on August 31st, 2022 at 1:00 PM. Upon reaching the site, the frame was assembled, and the bags were mounted to the frame. The wooden frame dimensions were 138 cm in height, 2.44 m in length, and 1.22 m in width with four supports and two cross members of 8.9 cm width and depth. Frame dimensions were decided on based on identical criteria to that in Test Set 1. The initial filling of all 10 hanging bags took place at 1:50 PM. The bags remained in the field in the state illustrated in Figure 17 and Figure 18 for a total of 70 days and were filled 11 times. Plan views of all bag configurations in the field after a filling and dewatering cycle can be observed in Figure 19 and Figure 20.

Figure 17. Empty composite hangings bags and frame, T&T site (Source: Author).

Figure 18. Filled composite hangings bags and frame, T&T site (Source: Author).

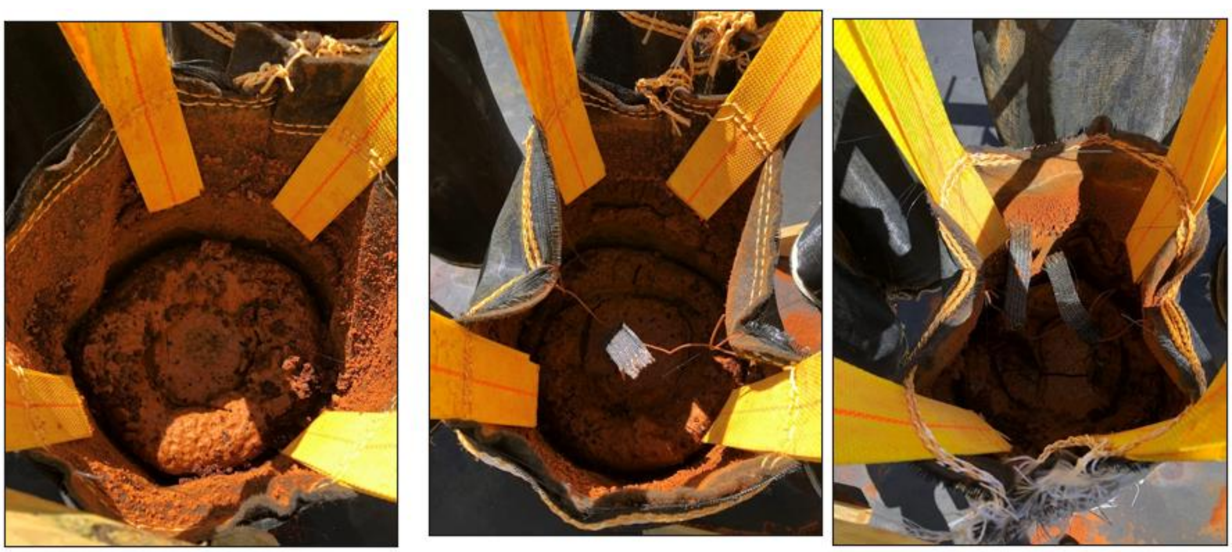

Figure 19. HB#1 (standard-blank, left), HB#2 (vertical orientation, middle), HB#3 ("V" orientation, right) (Source: Author).

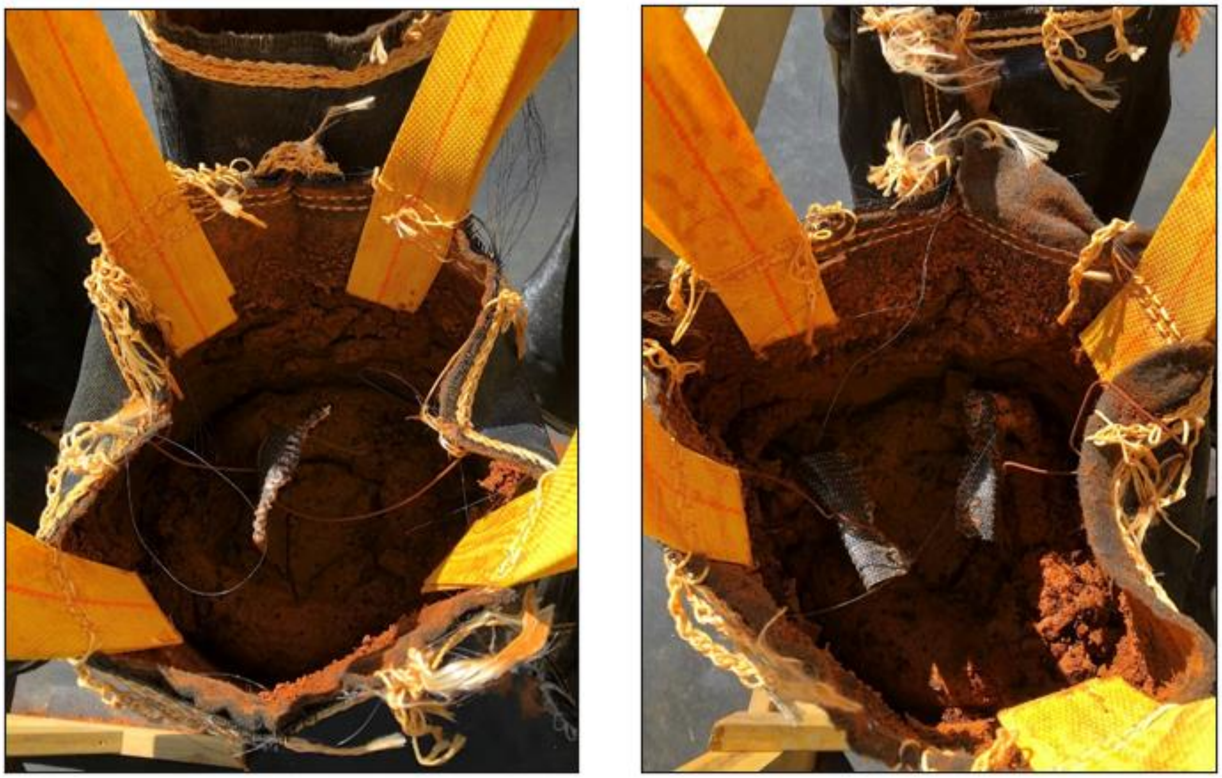

Figure 20. HB#4 (vertical orientation, left) and HB#5 (“V” orientation, right) (Source: Author).

Laboratory Monitoring

The initial time for the data collection plots was decided on as the return of Test Set 3 to the lab at 2:45 PM on November 9th, 2022. Once the bags were returned to the lab, re-mounting on the frame as specified by Koerner and Koerner (2006) was not performed due to limited storage space for the frame in the geotechnical laboratory and the significant difficulty presented by the task of mounting and dismounting bags from the secured rebar. Rather, the bags were placed in a stationary position on the laboratory floor as illustrated in Figure 21 and Figure 22. This exception was not made for Test Set 1. Allowing the bags to rest on the floor rather than remain suspended could have impacted dewatering on the bottom geotextile surface of the hanging bags and the extent to which this impacted the dewatering results is unknown.

Figure 21. HB#1(left), HB#2 (middle), HB#3 (right) (Source: Author).

Figure 22. HB#4 (left) and HB#5 (right) (Source: Author).

Test Set 2: Performance Testing Procedure (HBTs)

The following describes the performance testing procedure used for the Test Set 2 HBTs, adapted from Koerner and Koerner (2006):

1. The geotextile bags were attached to the frame by way of threading the loops of the bag onto secured rebar perpendicular to the length of the frame. The 2.5 cm diameter by 82 cm length rebar was spaced at the width of the hanging bag straps, which was 20 cm center-to-center spacing.
2. The geotextile bags were pumped to capacity with AMD sludge as detailed in the "Test Set 1: Performance Testing Procedure".
3. After each bag had drained itself of free water, the geotextile bags were again pumped to capacity with AMD sludge.
4. Steps 2 and 3 were repeated until geotextile bag pumping resulted in minimal filter cake accumulation with additional pumping.
5. The number of times each bag was filled was recorded.
6. The bags were once again allowed to drain themselves of free water, then transported from the WVDEP treatment site to the geotechnical laboratory.
7. Once the bags were returned to the geotechnical laboratory, the timer was started. This was time zero.
8. Each bag was monitored. This consisted of the following:
    a. Each bag was weighed weekly on a scale as in Figure 23. The masses were recorded. The dry mass of each bag was obtained prior to initial AMD sludge pumping.

Figure 23. Test Set 2 weighing procedure (Source: Author).

    b. Representative samples were extracted from each bag on a bi-weekly schedule. ASTM Designation D2216-19 procedure was followed in order to determine the percent Total Solids Content and Gravimetric Moisture Content. Representative sample extraction was performed as follows:

i. A sample of roughly 30 g material was extracted from the center position of the bag at a depth of roughly 2.5 cm (1 in) below the exposed filter cake layer.
ii. The sample was placed in the moisture content tin using a spatula, taking care to avoid smearing sample on the external surface of the tin as in Figure 24.

Figure 24. Test Set 2 sampling procedure (Source: Author).

iii. The exposed filter cake layer was restored to approximate its pre-disturbed condition using the spatula.

c. Filter cake was monitored and characterized. This included filter cake formation, appearance, and intimate contact loss.

9. Once preliminary loss of intimate contact of AMD sludge with the drainage media was observed, a compression technique was employed weekly in an attempt to restore intimate contact. This technique involved folding over the top of the bag and "bear-hugging" the bag from different angles.
10. The test was concluded, and the timer stopped once significant loss of intimate contact of AMD sludge with the drainage media and cohesion of sludge was observed.
11. The following was plotted for each test:
    a. Time (d) vs. Normalized Change in Bag Mass (%)
    b. Time (d) vs. Total Solids Content (%)
    c. Time (d) vs. Normalized Change in Gravimetric Moisture Content (%)

Deviations from the testing procedure in Koerner and Koerner (2006) that were different from those discussed in "Test Set 1: Performance Testing Procedure" are presented below:

1. Multiple bag fillings with AMD sludge were done, rather than a single bag filling.
    1.1. Stopwatch timer was started upon arrival of the bags back to the geotechnical lab, rather than after the first bag filling.

Field-scale testing: Geotube Dewatering Tests (Test Set 3)

Materials

Test Set 3 consisted of GDT bags with varying width laterally configured CCFs and PVDs and a standard of comparison in duplicates for a total of 10 tests. The GDTs incorporated PVD internal drainage systems for testing as GDT tests allowed for an AMD sludge surcharge load to be placed on top of the PVDs. In contrast, the vertical radial orientation of the HBTs did not allow for a surcharge load to be placed on PVDs for that test. This is the reason for absence of PVDs in the HBTs. The dimensions of each GDT bag are: 55.9 cm by 55.9 cm. Individual tests were assigned a nomenclature of Bag #1-5. Bag 1 was the standard of comparison and lacked internal drainage. Bags 2 and 3 consisted of the PVD internal drainage configurations of 25.4 mm and 101.6 mm width and 61.0 cm length. Bags 4 and 5 consisted of the CCF internal drainage configurations of 25.4 mm and 101.6 mm width and 61.0 cm length. Bags 2 through 5 were constructed with a total runout length of 50.8 mm, or 25.4 mm of runout length past each seam, where runout length is defined as the length of internal lateral drainage media that extends beyond the seam of the geobag. The internal drainage media were secured via stapling at the GDT bag seams. PVD internal lateral drainage media were manufactured in rolls of 101.6 mm width. This required the PVD internal lateral drainage media strips of 25.4 mm width to have the outer filter layer stapled together to restore filter-to-filter contact that was lost by trimming the PVD roll, as illustrated in Figure 25. PVD and CCF internal drainage media implemented in Bags 2 through 5 can be observed in Figure 26.

Figure 25. PVD Internal Drainage Component (Source: Author).

Figure 26. CCF and PVD Internal Drainage Components (Source: Author).

This information is presented concisely in Table 8. The nomenclature GD refers to Geotube Dewatering, (#_) refers to primary bags, and (#_D) refers to duplicate bags.

Table 8. Test Set 3 materials approach.

Sample Name	Description	
GD#1 and GD#1D	Geotextile Shell (typical all specimens) Type = Woven AOS = 0.425 mm Wide Width Tensile Strength (Machine Direction) = 96.3 kN/m Water Flow Rate = 815 L/min/m^2	
GD#2 and GD#2D	Prefabricated Vertical Drain (internal lateral drainage) Type = Composite AOS = 0.090 mm Grab Tensile Strength = 710 N Discharge Capacity @ 10 kPa = 1.45 x 10^{-4} m^3/s Lateral Drain Width = 25.4 mm Lateral Drain Length = 61.0 cm Lateral Drain Runout Length (per seam) = 25.4 mm	
GD#3 and GD#3D	Prefabricated Vertical Drain (internal lateral drainage) Type = Composite AOS = 0.090 mm Grab Tensile Strength = 710 N Discharge Capacity @ 10 kPa = 1.45 x 10^{-4} m^3/s Lateral Drain Width = 101.6 mm Lateral Drain Length = 61.0 cm Lateral Drain Runout Length (per seam) = 25.4 mm	
GD#4 and GD#4D	Capillary Channel Fiber (internal lateral drainage) Type = Woven AOS = 0.425 mm Tensile Strength (Minimum Average Roll Value) = 77.0 kN/m Flow Rate = 1,222 L/min/m^2 Lateral Drain Width = 25.4 mm Lateral Drain Length = 61.0 cm Lateral Drain Runout Length (per seam) = 25.4 mm	
GD#5 and GD#5D	Capillary Channel Fiber (internal lateral drainage) Type = Woven AOS = 0.425 mm Tensile Strength (Minimum Average Roll Value) = 77.0 kN/m Flow Rate = 1,222 L/min/m^2 Lateral Drain Width = 101.6 mm Lateral Drain Length = 61.0 cm Lateral Drain Runout Length (per seam) = 25.4 mm	

Configuration Approach

A method of comparison between GDT bags and field scale geobags was produced. The result of this were the spreadsheet matrices in Table 9 and Table 10 where geobag dimensions, GDT bag dimensions, internal lateral drainage media dimensions, and internal lateral drainage media spacing could be input to yield output parameters, area coverage ratio and drainage area (in^2). The purpose of this spreadsheet was to identify what field scale geobag equipped with internal lateral drainage media would be equivalent with respect to area coverage ratio or drainage area to a bench scale GDT bag equipped with internal lateral drainage media. The spreadsheet also allowed for identification of equivalent GDT bags of alternative internal lateral drainage media dimensions and spacing with respect to area coverage ratio and drainage area. The result of this spreadsheet was the selection of 25.4 mm and 101.6 mm internal lateral drainage media strip widths at an equal spacing between strips of 26.7 cm and 22.9 cm respectively for Test Set 3.

Table 9. GDT Internal Drainage Component Width Selection Matrix (Source: Quaranta, personal communication).

GDT							
	GDT		**Area Coverage Ratio**				
	usable width or length (inch)		**(Strip width * NumberStrips / GDT width) %**				**Determine this Parameter "Drainage Width Equivalent"**
Strip Width (inch)	22	Number of Strips	**22**		Equal Spacing between Strips (inches)	Ratio (Ds/Geotube Length)	**Drainage Area (in2)**
Sw					**Ds**		
1	22	1	**4.55**		10.50	0.48	**231.0**
1	22	2	**9.09**		6.67	0.30	**146.7**
1	22	3	**13.64**		4.75	0.22	**104.5**
1	22	4	**18.18**		3.60	0.16	**79.2**
1	22	5	**22.73**		2.83	0.13	**62.3**
2	20	1	**9.09**		10.00	0.50	**200.0**
2	20	2	**18.18**		6.00	0.30	**120.0**
2	20	3	**27.27**		4.00	0.20	**80.0**
2	20	4	**36.36**		2.80	0.14	**56.0**
2	20	5	**45.45**		2.00	0.10	**40.0**
3	20	1	**13.64**		9.50	0.48	**190.0**
3	20	2	**27.27**		5.33	0.27	**106.7**
3	20	3	**40.91**		3.25	0.16	**65.0**
3	20	4	**54.55**		2.00	0.10	**40.0**
3	20	5	**68.18**		1.17	0.06	**23.3**

Table 10. Geobag Internal Drainage Component Width Selection Matrix (Source: Quaranta, personal communication).

FULL SCALE								
		GEOTUBE		Area Coverage Ratio				
		15C Strip Length (Ft) is Geotube Width		(Strip width * NumberStrips / Geotube Length) %				Determine this Parameter "Drainage Width Equivalent"
Strip Width		19	Number of Strips w/Full Geotube Length	120		Equal Spacing between Strips (Ft)	Ratio (Ds/Geotube Length)	Drainage Area (Ft2)
Sw (inch)	Sw (Ft)					Ds		
4	0.33	19	10	2.75		10.61	0.56	201.6
4	0.33	19	12	3.30		8.93	0.47	169.6
4	0.33	19	14	3.85		7.69	0.40	146.1
4	0.33	19	16	4.40		6.75	0.36	128.2
4	0.33	19	18	4.95		6.00	0.32	114.1
8	0.66	19	10	5.50		10.31	0.54	195.9
8	0.66	19	12	6.60		8.62	0.45	163.8
8	0.66	19	14	7.70		7.38	0.39	140.3
8	0.66	19	16	8.80		6.44	0.34	122.3
8	0.66	19	17	9.35		6.04	0.32	114.8
12	1	19	10	8.33		10.00	0.53	190.0
12	1	19	12	10.00		8.31	0.44	157.8
12	1	19	14	11.67		7.07	0.37	134.3
12	1	19	17	14.17		5.72	0.30	108.7
12	1	19	18	15.00		5.37	0.28	102.0
16	1.33	19	10	11.08		9.70	0.51	184.3
16	1.33	19	12	13.30		8.00	0.42	152.1
16	1.33	19	14	15.52		6.76	0.36	128.4
16	1.33	19	16	17.73		5.81	0.31	110.3
16	1.33	19	18	19.95		5.06	0.27	96.1
24	2	19	10	16.67		9.09	0.48	172.7
24	2	19	12	20.00		7.38	0.39	140.3
24	2	19	14	23.33		6.13	0.32	116.5
24	2	19	16	26.67		5.18	0.27	98.4
24	2	19	18	30.00		4.42	0.23	84.0

Field Operation

The Test Set 3 pillows bags and PVC frame were transported to the T&T facility on October 5th, 2022 at 5:30 PM. Upon reaching the site, the PVC frame was mounted to the hose, and the bags were mounted to the PVC frame illustrated in Figure 27.

Figure 27. PVC frame (Source: Author).

The PVC pipe was of 57.2 mm outside diameter. Laterals of the PVC frame were spaced at 1.57 m measured outside-to-outside of each lateral and GDT bag geoport inserts were spaced at 78.5 cm center-to-center to accommodate GDT bag rotation when seating. The total length of each lateral was 3.05 m. The initial filling of all 10 GDT bags took place at 5:38 PM and is illustrated in Figure 28 and Figure 29.

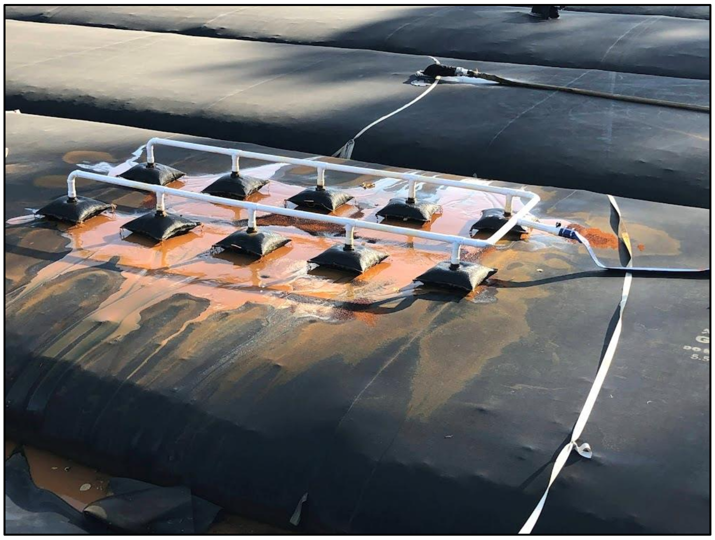

Figure 28. Feed stock inflow via PVC frame, T&T site (1/2) (Source: Author).

Figure 29: Feed stock inflow via PVC frame, T&T site (2/2) (Source: Author).

The discoloration of the permeant was a result of pressurized AMD sludge fine particles passing through the GDT bag geotextiles and was typical for all GDT bags at the T&T site. The PVDs drained properly up until the third field filling, by which time the PVDs clogged as shown in Figure 30 and Figure 31 . This further confirmed that the typar outer layer filter displayed faster clogging or particle blinding, lower hydraulic conductivity, and lower filtration efficiency than the GDT bag woven geotextile previously identified by Tyson (2023). The fast clogging of the outer filter layer of the PVDs could have impacted the development of a long-term stable filter cake formation in the PVD configured GDT bags. There did not appear to be any impact to

AMD sludge dewatering of the internal drainage configured GDT bags as a result of seam stapling, since no leaks at the seams were observed during any of the bag fillings. The GDT bags remained in the field for a total of 35 days and were filled 8 times.

Figure 30. PVD draining, typical all PVD configurations (Source: Author).

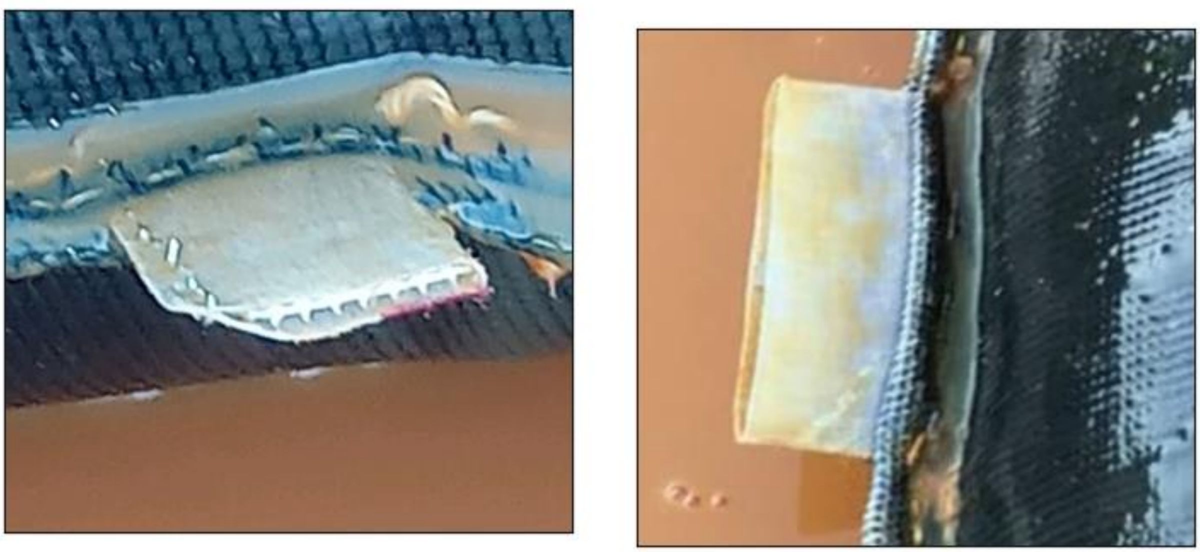

Figure 31. PVD clogging, typical all PVD configurations (Source: Author).

<u>Laboratory Monitoring</u>

The initial time for the data collection plots was decided on as the return of Test Set 3 to the lab at 2:45 PM on November 9th, 2022 in the condition illustrated in Figure 32.

Figure 32. GD#1 (left, top), GD#2 (left, bottom), GD#3 (middle, top), GD#4 (middle, bottom), and GD#5 (right) (Source: Author).

<u>Test Set 3: Performance Testing Procedure (GDTs)</u>

The following describes the performance testing procedure used for the Test Set 3 GDTs, adapted from Stephens (2007) and ASTM D7880/D7880M – 13:

1. The geotextile bags were threaded onto each of the ten outflow point source segments of the PVC frame via the 5.1 cm (inner diameter) geoport in the top of each GDT bag.
2. The inflow hose was threaded onto the inflow point source segment of the PVC frame and the valve on the PVC frame was turned to the ON position.
3. After notifying the on duty WVDEP employee to turn on the pump, the valve at the manifold was turned to the ON position and the geotextile bags were pumped to capacity with AMD sludge, after which the manifold and PVC frame valves were turned back to the OFF position and the employee notified to turn off the pump.
4. After each bag had drained itself of free water, the geotextile bags were again pumped to capacity with AMD sludge.
5. Steps 3 and 4 were repeated until geotextile bag pumping resulted in minimal noticeable change in bag volume with additional pumping.
6. The number of times each bag was filled was recorded.
7. The bags were once again allowed to drain themselves of free water, then unthreaded from the PVC framework, capped, and transported from the WVDEP treatment site to the geotechnical laboratory, making an effort to minimize physical disturbance of the bags.
8. Once the bags were returned to the geotechnical laboratory, the timer was started. This was time zero.
9. Each bag was monitored. This consisted of the following:

9.1. Each bag was weighed weekly on a scale as in Figure 33. The masses were recorded. The dry mass of each bag was obtained prior to initial AMD sludge pumping.

Figure 33. Test Set 3 weighing procedure (Source: Author).

9.2. Representative samples were extracted from each bag on a bi-weekly schedule. ASTM Designation D2216-19 procedure was followed in order to determine the percent Total Solids Content and Gravimetric Moisture Content. Representative sample extractions were performed as follows:

9.2.1. The cap that was previously threaded onto the center geoport was unscrewed and removed.

9.2.2. A sample of roughly 30 g material was extracted from the center geoport of the bag.

9.2.3. The sample was placed in the moisture content tin using a spatula, taking care to avoid smearing sample on the external surface of the tin as in Figure 34.

Figure 34. Test Set 3 sampling procedure (Source: Author).

9.2.4. The cap was rethreaded onto the central geoport.

9.3. Filter cake was monitored and characterized. This included filter cake formation, appearance, and intimate contact loss.

10. The test was concluded, and the timer stopped once significant loss of intimate contact of AMD sludge with the drainage media and cohesion of sludge was observed. Since bags were not cut open for dewatered sludge sampling as outlined in Stephens (2007), these properties were determined via visual examination through the central geoport hole and gentle shaking of each bag.
11. The following were plotted for each test:
    11.1. Time (d) vs. Normalized Change in Bag Mass (%)
    11.2. Time (d) vs. Total Solids Content (%)
    11.3. Time (d) vs. Normalized Change in Gravimetric Moisture Content (%)

Deviations from the testing procedure followed in Koerner and Koerner (2006) and ASTM D7880/D7880M – 13 was documented below:

1. The geotextile containers (bags) were not pre-wetted in prefiltered AMD water.
2. Collection pans were not implemented, as effluent collection was not performed.
    2.1. Total suspended solids of effluent were not monitored.
    2.2. Flow rate of effluent was not monitored.
3. AMD sludge was not uniformly mixed in a container prior to being pumped into each bag.
4. Pressure assessment was not performed.
    4.1. PVC frame was used in favor of a standpipe.
    4.2. Supply valve at the treatment facility did not include a pressure gauge.
5. Bags were not cut open to obtain sludge samples. Samples were extracted from the geoport hole sewn into the top side of each bag. This made sample extraction from the AMD filter cake within the bag from any location other than the open geoport hole difficult without considerable AMD filter cake disturbance or cutting open the GDT bag surface.

Objective #2: Evaluate the use of AMD as soil amendment

Evaluate soil development at a reclaimed site

Site location

The field site was located on a 160-ha reclaimed surface mine in Upshur County, West Virginia, USA (38°48'57.8"N, 80°11'44.5"W, Figure 35). The site operated from 1974 to 1984 (Kittanning coal with truck-shovel equipment) and had been reclaimed since 1985 (Faulkner et al., 2000; Scagline-Mellor et al. 2018). Reclamation included backfilling a mixed sandstone-siltstone overburden, topping with 15-cm of native forest topsoil (Gilpin silt loam), fertilizing and liming according to regulations, and seeding with a grass mixture (i.e., *Lolium arundinaceum* (Schreb.) S.J. Darbyshire, *Dactylis glomerata* L., *Lotus corniculatus* L., and *Trifolium* spp.) (Scagline-Mellor et al. 2018). There has been substantial ground cover since reclamation (Faulkner et al., 2000; Scagline-Mellor et al. 2018).

The field site is located within the Central Appalachians ecoregion (Woods et al. 1999), has an annual average precipitation of 47.6 in (120.9 cm), and has an annual average temperature of 53.4°F (11.9°C) (US Department of Commerce). The soil is classified by USDA-NRCS Web Soil Survey (WSS) as Bethesda loam (BsB) at 0%-8% slope and A-C horizonation. There are areas with sludge disposal and sustained vegetation growth (personal communication, P. Ziemkiewicz).

Geology in the region consists of Pennsylvanian resistant sandstones and conglomerates from the Pottsville Group, Mississippian sandstones from the Pocono Formation, and Mississippian sedimentary rocks from the Mauch Chunk formations. Most of the soils are frigid and mesic Ultisols and Inceptisols that are typically acidic, steep, stony, and low in nutrients (Woods et al. 1999).

Figure 35. Study location, located within Upshur County, WV. Photo from Google Earth.

<u>Field methods and analysis</u>

A pit was excavated by a Caterpillar 313F excavator on May 11, 2022. The study pit dimensions were approximately 5 ft (1.52 m) deep, 3 ft (0.91 m) wide, and with a sloping length of roughly 8 ft (2.43 m) (Figure 36). The soil was evaluated following methods by Schoeneberger et al. (2012). Soil color was documented using Globe (2005), and soil pH was measured using a LaMotte TesTabs Kit (no. 5912). Samples (approximately 3.8 L) of each horizon were collected and analyzed for moisture content (ASTM D2216) and grain size distribution (ASTM D6913). Location was documented using Garmin e-trex 20 GPS unit (WGS84) and slope was measured using a Suunto PM-5/360 Clinometer. Saturated hydraulic conductivity of the topsoil was quantified using a Turf-tech double ring infiltrometer (ASTM D3385). Four repetitions were completed, and individual tests ranged from approximately 1 hour to 1.5 hours.

Figure 36. Soil pit progression. a) Pit being dug by Caterpillar 313F Excavator. b) Dug soil pit with dimensions. c) Student observing soil pit. d) Soil pit with testing equipment.

Sludge characterization

Six AMD sludge samples were characterized by Pace Analytical laboratory by the following methods: EPA 6010D, EPA 7471B, SM 2540G-2015 (Table 11). A second sample of VMS was collected after the first resulted in high concentration of lead.

Table 11. Location of samples for sludge characterization.

Sample	Sample Type	Site Location	Site Coordinates
OMEGA-B	Geobag	Ringgold, WV	39°31'56.5"N 79°56'19.5"W
OMEGA-AR	Open Air Cell	Ringgold, WV	39°31'56.5"N 79°56'19.5"W
ED-E-CL	Open Air Cell	Cheat Lake, WV	39°42'04.8"N 79°51'47.5"W
ED-T-B	Geobag	Kingwood, WV	39°28'32.0"N 79°44'56.1"W
TNTB01	Geobag	Albright, WV	39°32'37.2"N 79°37'49.6"W
VMS B01	Geobag	Gladesville, WV	39°28'38.8"N 79°54'36.7"W

Complete a small-scale growth study

AMD source

The AMD sludge used for this study was sourced from the OMEGA impoundment (39º31’57.9” N, 79º56’21.0” W), a treatment station located south of Morgantown, West Virginia, operated by the Department of Environmental Protection (WVDEP). The raw AMD treated on this site is a product of multiple underground mines. The treatment consists of the use of calcium hydroxide (lime) to raise the pH from 3.2 to 6.7 (clarification) and precipitate solids. The supernatant is settled in a series of ponds and the clean water is discharge into the environment through a National Pollutant Discharge Elimination System (NPDES). The precipitated sludge underflow is treated with polymers to create flocks that are dewatered through geotubes (Dalen, 2021). The sludge used for this study was collected from an old sludge pond located on the site.

Test set-up

A small-scale growth analysis was completed to evaluate the establishment and cover capacity of different media composed by topsoil and AMD sludge.

The medias consisted of six volume-based mixtures of topsoil and sludge: (i) 100% topsoil, (ii) 10% sludge and 90% topsoil, (iii) 20% sludge and 80% topsoil, (iv) 30% sludge and 70% topsoil, (v) 40% sludge and 60% topsoil, and (vi) 50% sludge and 50% topsoil.

Four replicates of each mixture were made, resulting in twenty-four samples in total. The mixtures were put in pots of 20-cm diameter and 18-cm height. The pots were filled with the mixtures to the height of 15 cm. The bulk density of the medias ranged between 0.29 g/cm^3 (100% topsoil) and 0.50 g/cm^3 (50% topsoil and 50% sludge) (Table 12, Figure 37).

Table 12. Bulk densities of mixtures.

Treatment	ρ_b (g/cm$^{3)}$
100% topsoil (100T)	0.29
10% sludge and 90% topsoil (10S90T)	0.29
20% sludge and 80% topsoil (20S80T)	0.37
30% sludge and 70% topsoil (30S70T)	0.37
40% sludge and 60% topsoil (40S60T)	0.46
50% sludge and 50% topsoil (50S50T)	0.50

Figure 37. Soil-sludge mixing process.

The samples were seeded with 2 g of Kentucky 31 tall fescue grass seed (*Festuca arundinacea*) (Pennington seed inc., Greenfield, MO). Seeding methods followed four steps, as recommended by the manufacturer: (1) the top layer was loosed and smoothed, (2) the seeds were spread by hand, (3) the surface was slightly tapped to guarantee the seeds were in contact with the soil, and (4) the samples were watered with 250 ml of water each (Figure 38).

Figure 38. Progression of study preparation: (from left to right: topsoil and sludge mixing; seeding; watering; straw layer; final setup.

The pots were then randomly arranged in four plastic storage containers (96.5-cm deep, 56-cm wide, and 41-cm tall) - six pots in each container, one of each kind of media (Figure 3). The containers were labeled as “A”, “B”, “C”, and “D”, and the pots were labeled according to the media and the container where they were located (Figure 39).

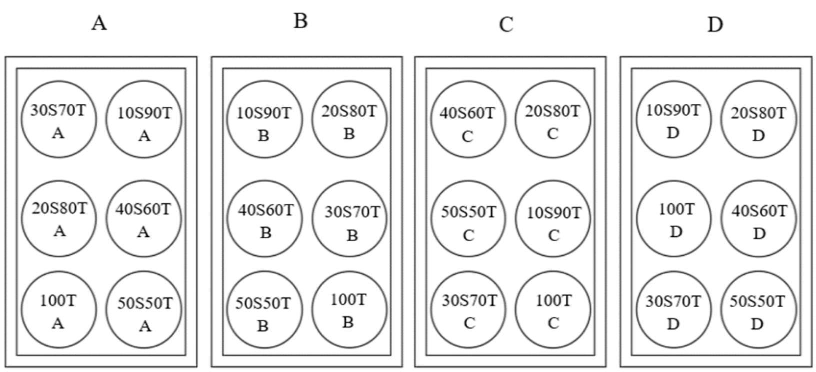

Figure 39. Organization of mixtures per container and container position in the research area. (S = sludge, T = topsoil).

Drainage holes were made on the bottom of the containers and the samples were placed over a 15 cm topsoil layer. A layer of seeding straw with tackifier (Pennington Seed, Madison, GA) was put on the top of the samples after seeding to protect the seeds. The straw layer was mostly removed after the seed germination to facilitate ground cover measurements. The containers were surrounded by a 1.20 m tall green garden fence (TENAX®) and covered with a piece of the same kind of fence by which it was surrounded (Figure 40). The watering schedule was initially determined as 250 ml each day during the first week of germination, and 2-3 times a week during the following weeks. Due to rain and night frostings, the watering schedule was modified as shown in Appendix B and Figure 41.

Figure 40. Final setup (Containers A, B, C, and D from left to right).

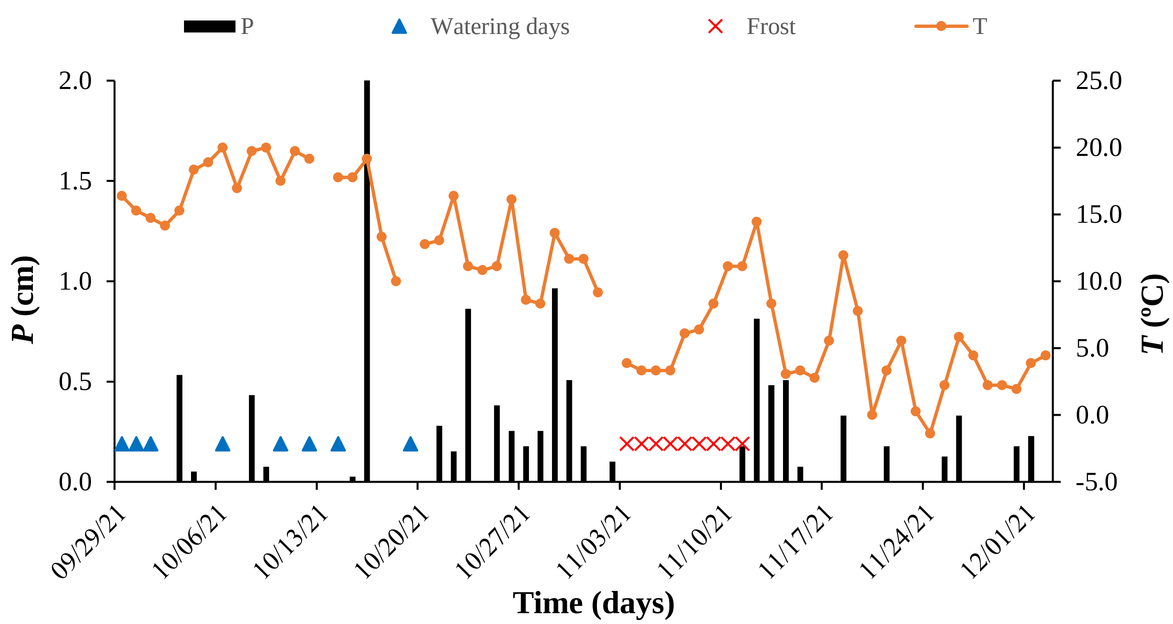

Figure 41. Watering schedule with mean daily temperature, T, and total daily precipitation, P, and days with frost observed.

<u>Data collection</u>

Samples of 500 g ± 50 g of each soil mixture were collected for analysis before (09/24/21) and after (12/09/21) growth season. The samples were sent to WVU Soil Test Laboratory (Morgantown, WV) and were analyzed for pH (1:1 – soil:water), P, K, Ca, Mg (extraction using Mehlich 3), Psat (Khiari, L. et al 2000), Organic Matter (OM) (Loss on ignition), and electric conductivity (EC).

Photographs were taken weekly to monitor the ground cover during the nine weeks of study (September 29, 2021 – December 2, 2021). The photographs were analyzed for ground cover by area using Adobe Photoshop 2022. Steam sizes were measured for at least 10 random live steams from each sample at week 5 (November 1). At the end of the study, total live above-ground biomass was collected and weighted following guidance by Franks and Goings (1997).

Statistical methods

Comparisons of ground cover, stem height, and biomass were made among treatments. The data were tested for normal distribution using the Shapiro-Wilk test and Anderson Darling tests. Both tests have the null hypothesis that the data is normally distributed. The validation of the null hypothesis means that a parametric analysis can be applied to the data.

After the distribution analysis, the data was submitted to an analysis of variance (one-way ANOVA) when normally distributed, or to a Wilcoxon/ Kruskal-Wallis non-parametric analysis, when not normally distributed (Ott and Longnecker, 2001). Statistical analysis was completed using the software JMP 16.

Complete a field study: Fall planting

Site description

The field site was located at an open-air AMD sludge cell, in Monongalia County, West Virginia (39°28'38.8"N, 79°54'36.7"W) (WGS84) (Figure 42). The site is located on a hill crest with a mean surface elevation recorded at 1,970 ft (600 m) (EGM96). The sludge cell is a storage location for AMD waste and is a large pit that was dug down into the hilltop to contain runoff (Figure 43). The AMD within the site is bagged from other treatment facilities and transported to the study site. The field site was chosen for the study because it is located on flat unused ground, runoff from the growth study would run into the sludge cell, and primarily because the AMD waste that was dumped onsite allows for easy collection and use for mixing testing.

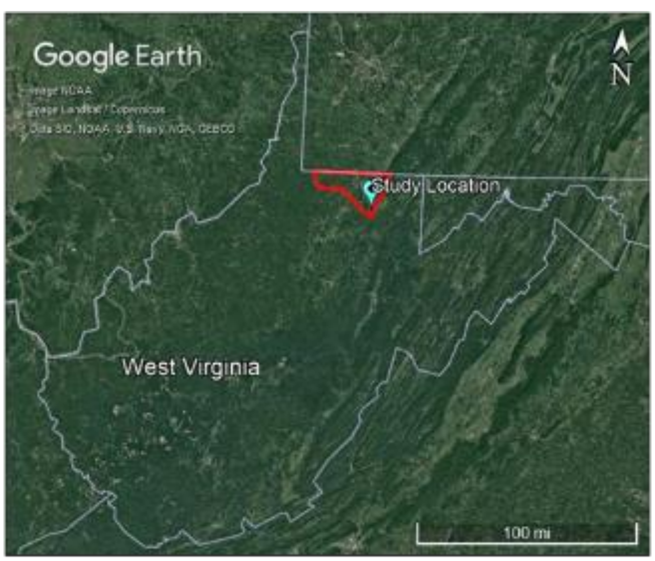

Figure 42. Field plot study location, Highlighted within Monongalia County, WV. Photo from Google Earth.

Figure 43. Aerial image of sludge cell. Photo from Google Earth.

The study site is located within the Central Appalachians EPA ecoregion (Woods et al. 1999) and has a mean annual precipitation of 43.1 in (109 cm). Temperatures range are 21°F to 43°F and 69°F to 83°F in the winter and summer, respectively. Over the duration of the growth study the average temperature ranges from an average high of 76°F to a low of 25°F and precipitation amounting to an average of 12.88 in (32.7 cm) (Table 13).

Table 13. Average high and low temperature and average precipitation data over study duration for the months of September through December 2022.

	Sept	Oct	Nov	Dec
Average High Temp. (ºF)	76	65	54	42
Average Low Temp. (ºF)	55	43	33	25
Average Precipitation (in)	3.16	2.82	3.57	3.33

The EPA Ecoregion is #69 Central Appalachians – 69a Forested Hills and Mountains. The region is described as occupying the highest and most rugged parts of Ecoregion 69. The region is filled with dissected hills, mountains, and ridges that are steep sided with narrow valleys.

Crestal elevations range from 1,800 to 2,600 ft (549 to 793 m) and have a maximum elevation of about 4,600 ft (1,402 m) within West Virginia. Generally, the higher elevations get more precipitation and have a shorter growing season than lower elevations (Woods et al. 1999).

Geology in the region consists of Pennsylvanian resistant sandstones and conglomerates from the Pottsville Group, Mississippian sandstones from the Pocono Formation, and Mississippian sedimentary rocks from the Mauch Chunk formations. Most of the soils are frigid and mesic Ultisols and Inceptisols that are typically acidic, steep, stony, and low in nutrients. The relatively infertile soils, cool climate, short growing season, and ruggedness within the ecoregion make the area particularly unsuited to agriculture (Woods et al. 1999).

AMD sludge source

The AMD sludge used in this research was produced from a treatment site located in Preston County, WV (39°29'39.3" N, 79°46'06.0" W) (WGS84) (Figure 44**).**

Figure 44. Location of AMD treatment facility within Preston County, WV. Photo from Google Earth.

The treatment plant collects AMD seepage using seep collectors that route the drainage into two aeration beds. Then the AMD is dosed with activated lime and gravity fed into a settling pond. Where it is then pumped into Solmax® Geotube Geobags from a sump at the bottom of the settling pond (Figure 45, Figure 46). After pumping, the Geobags fill with sludge and are transported to the study site for final disposal.

Figure 45. Aerial photo of the treatment facility. Photo from Google Earth.

Figure 46. Photo showing the Geotube (Left) During filling at the treatment facility within its transportation container. (Right) At the field site on the edge of the sludge cell, cut open for AMD extraction.

<u>Experimental design</u>

Soil plots consisted of three repetitions of five treatments, resulting in 15 plots total. The treatment mixtures were as follows: 100% Soil 0% AMD (TS – Total Soil), 75% Soil 25%AMD (25AMD), 50% Soil 50% AMD (50AMD), 25% Soil 75% AMD (75AMD), & 0% Soil 100% AMD (AMD). The location of each plot among the 3 plot by 5 plot grid was randomly determined (Figure 47). The plots were designed to be 5 ft by 5 ft (1.5 m by 1.5 m) with space in-between to allow for movement between plots. Total dimensions of the study area were 15 ft (4.5 m) in width by 25 feet (7.6 m) in length.

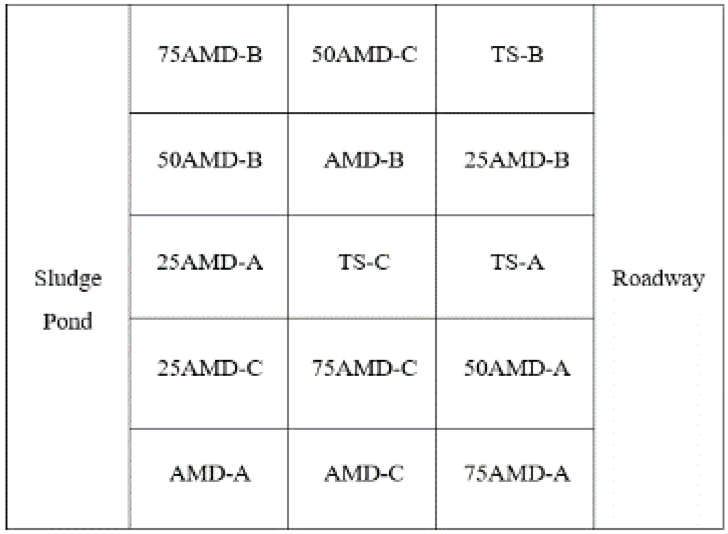

Figure 47. Growth study plot layout.

The seed mix chosen for the plot was in accordance with WVDEP current practices. The seed choice and ratios for the chosen mixture are in the table below.

Table 14. Seed mixture by percentage.

Scientific Name	Seed Type	Quantity (%)
Dactylis glomerata	Orchard Grass	48
Trifolium pratense	Medium Red Clover	20
Phleum pratense	Climax Timothy	12
Lolium perenne	Perennial Ryegrass	8
Poa pratensis	Kentucky Bluegrass 85/80	8
Trifolium repens	Ladino Clover	4

Construction of the plots was completed on September 26th, 2022. The topsoil was bought and transported out to the site, Scotts all-purpose lawn and garden topsoil. The plots were marked out with level lines and spray-paint to meet design dimensions of 5 feet by 5 feet (1.5 m by 1.5 m) for each plot, resulting in a total layout of 25 feet by 50 feet (7.6 m by 15.2 m). Then using precalculated mixtures by the number of 5-gallon buckets for AMD sludge and number of 0.75 cubic foot (0.02 cubic meter) bags, the plots were constructed. The AMD sludge was removed from a previously deposited Geotube from the nearby treatment facility. Once the soil mixtures were in their respective plots, 0.575 lbs (260 g) of 10/10/10 N, P, K fertilizer and 0.034 lbs (15.4 g) of the seed mix were applied by weight to each plot. The rates were scaled to the designed plot size based on seeding rates of 60 lbs (27.2 kg) per acre and fertilizer rates at 1000 lbs (453.5 kg) per acre. The seeding and fertilizer rates were in accordance with current WVDEP procedure.

Pennington Seeding Straw was spread to cover and protect the seeds during the early stages of seed growth. The progression of the plots being constructed can be seen in the figures below.

Figure 48. Construction progression of the growth study plots: a) after initial vegetation removal, b) marking plot locations, c) mixing media treatments, and d) final seeded plots with straw cover.

<u>Data collection</u>

Monitoring and data collection began on October 20th and ended on the 14th of December. Site visits were conducted every week until the first frost marking the end of the growing season.

The soil coverage net is a PVC pipe constructed net that results in a 10 by 10 grid of points that allow for reading of what is beneath the point to construct a matrix of growth within each plot. It is 3 ft by 3 ft (1 m by 1 m) and stands 6 in (15 cm) in height from the ground for all readings (Figure 49).

The constructed grid points act as a crosshair for readings. Readings would consist of standing as perpendicular to the apparatus as possible and logging whether the point on the plot had straw, bare ground, or grass beneath it. This is referenced as the point intercept ground coverage method (Elzinga et al. 1999).

The AMD sludge used for the study was sent to Pace Analytical for total waste analysis. Their test methods for contents of As, Ba, Ca, Cr, Pb, Se, and Ag follows analytical method EPA 6010D and preparation method EPA 3050B. A separate test for Hg used analytical and preparatory method EPA 7471B. Percent moisture was recorded using analytical method SM 2540G-2015. The AMD sludge from the study was then compared with previous sludge studies to compare heavy metal contents across AMD treatment locations.

Figure 49. Measuring ground cover.

Soil moisture, electrical conductivity, and soil temperature were measured with a Field Scout TDR 150 equipped with the 2-in (5 cm) soil probe option. The 2-in probe was used so that the probes would be fully within the treatment mixture. The probe was placed once randomly in each plot to take a reading then moved to the next plot (Figure 50).

Figure 50. Field Scout TDR 150 temperature, conductivity, and moisture reading.

Complete a field study: Spring planting

This section includes determining the site location, the construction of the site, how the data was monitored and how the data was analyzed.

Description of field site

The site is located in Monongalia County, West Virginia (39°28'38.8"N, 79°54'36.7"W) at an elevation of 1,970 ft (600m) (Figure 51). The soil composition consists of large rocks, and sandy soil. The site is within the #70 Western Allegheny Plateau ecoregion (U.S. EPA, 2016). Temperature (˚F) and precipitation (inches) were obtained from the U.S. Climate Data for the period of the data collection (Figure 52). This region's climate is characterized by an average temperature of 52 ˚F and the average precipitation ranges from 35-45 inches per year, which mostly is experienced in the spring, summer, and winter (*Western Allegheny Plateau Ecoregion*).

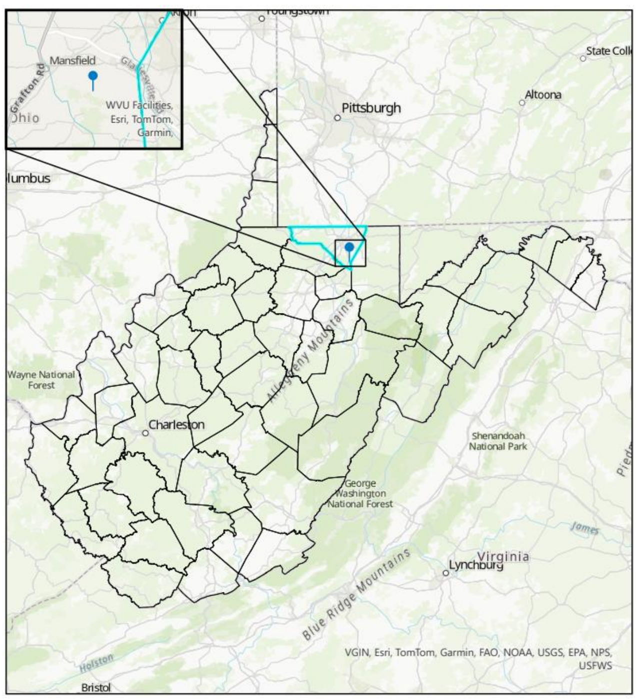

Figure 51. Map of site location.

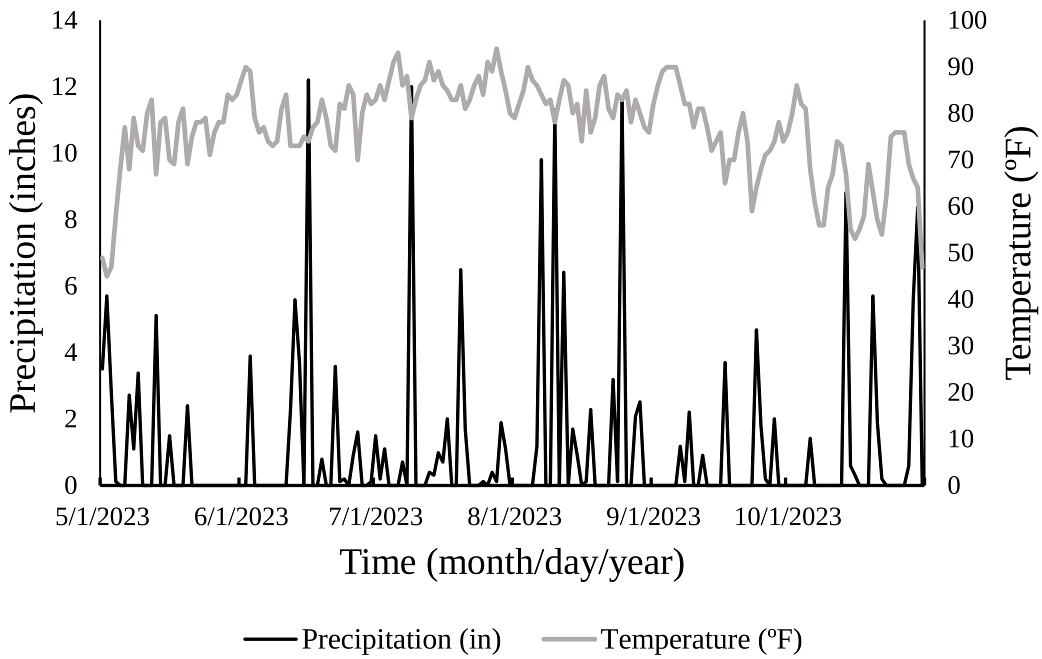

Figure 52. Average temperature and precipitation from U.S. Climate Data (NCEI).

Treatments and site development

The sludge used in this study was from a treatment plant in Preston County, West Virginia (same as previous section). The site consists of fifteen study plots (three repetitions of five treatments) were created. The treatments included topsoil mixed with AMD sludge in volumetric ratios: 1) 25% AMD sludge/75% topsoil (25AMD), 2) 50% AMD sludge/50% topsoil (50AMD), 3) 75% AMD sludge/25% topsoil (75AMD), 4) 100% AMD sludge (100AMD), and 5) 100% topsoil (Topsoil, control) (Figure 53). Each plot was formed by volume of AMD sludge and topsoil, that alternated AMD/soil, and was hand mixed. After the plots were mixed, 0.575 lbs (260 g) of 10/10/10 N, P, K fertilizer and 0.034 lbs (15.4 g) of the seed mix were applied by weight to each plot with a mixture that was developed based off WVDEP current practices. Table 15 represents the seed mixture by percentage that was scattered on each plot. After the seed mixture was scattered over each plot, Pennington Seeding Straw was placed on top of the plots. Constructing the plots consisted of following the WVDEP permanent seeding guidelines (WVDEP, 2012). Site development was completed on September 26, 2022 (Figure 54).

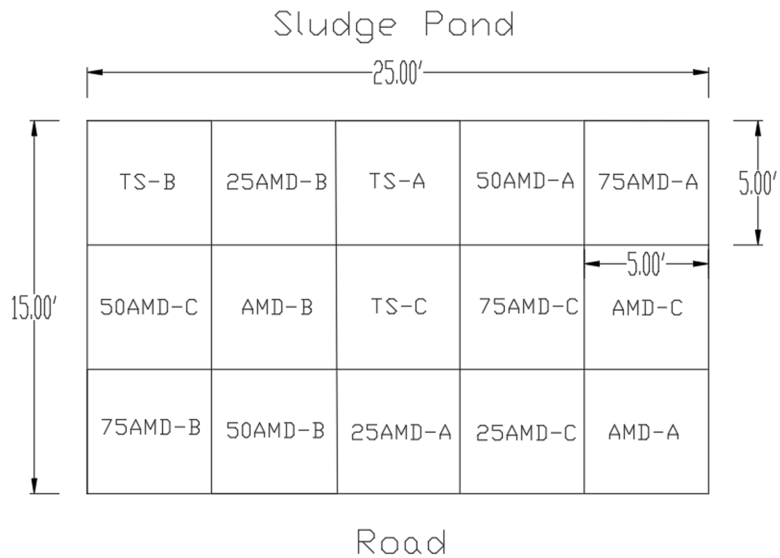

Figure 53: Site layout representing the mixture by subplots.

Table 15. Seed mixture.

Scientific Name	Seed Type	Quantity (%)
Dactylis glomerata	Orchard grass	48
Trifolium pratense	Medium red clover	20
Phleum pratense	Climax timothy	12
Lolium perenne	Perennial ryegrass	8
Poa pratensis	Kentucky bluegrass 85/80	8
Trifolium repens	Ladino clover	4

Figure 54. Site development.

Data collection

Ground cover, soil moisture, soil electrical conductivity, and soil temperature were monitored for each plot from May 25, 2023, to October 23, 2023. Ground cover was measured for each plot by an instrument that was made of PVC pipe and string (Figure 55). The instrument is 3 ft^2 in area that stands 6 inches off the ground. The instrument was placed on top of each plot and was read at each intersection that the string formed to see if the plot was covered in grass, straw, or was bare.

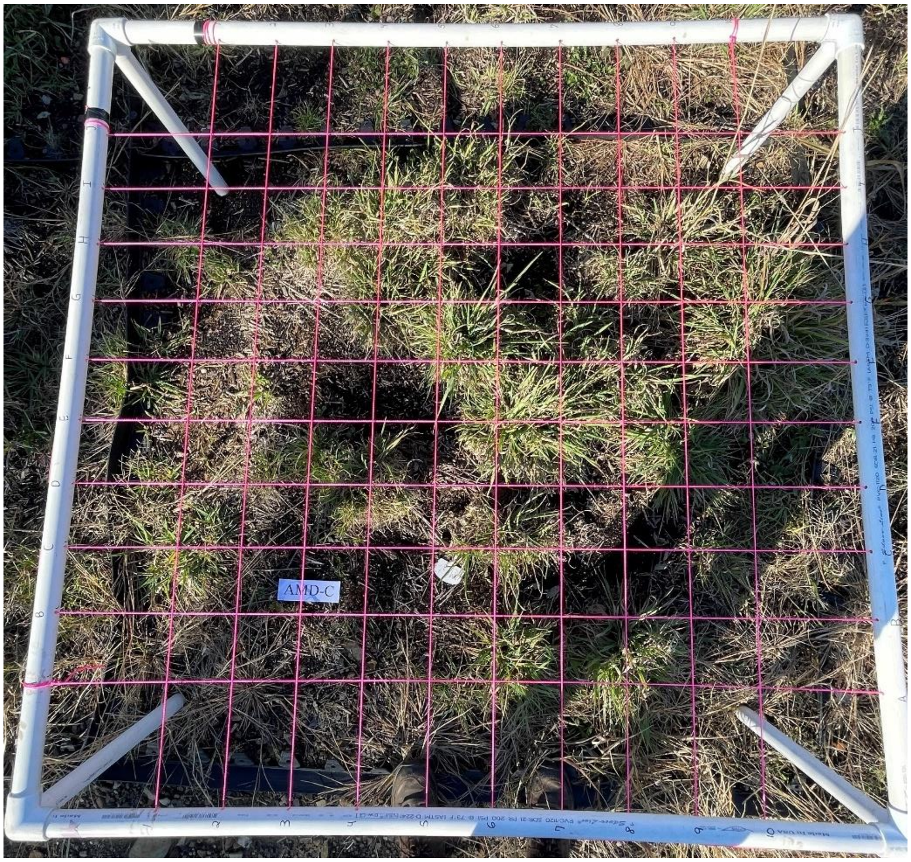

Figure 55. Instrument used to measure ground cover.

Soil moisture, electrical conductivity and temperature were all collected with the instrument Field Scout TDR 150 Soil Moisture Meter (Aurora, IL, USA), using the 2 in probe attachment. At each plot the Field Scout 150 was used to collect measurements in five randomly selected locations. At the end of the data collection phase, soil and above-ground biomass samples were collected from each plot. The biomass samples were collected by taking a 1 ft^2 square area, constructed out of PVC pipe, and randomly placing it on top of each of the plots (Figure 56). From there, the area that was enclosed by the PVC square was trimmed and placed into bags.

Figure 56. Instrument to collect biomass samples from each plot.

The biomass samples were weighed and recorded. The soil samples consisted of removing the roots and biomass to collect approximately 2 cups of soil. The soil samples were then sent to A & L Great Lakes Laboratories to have a saturated media extract report done, using NCR-13 No. 221, 1998 method, for each plot, excluding the 100% AMD treatments.

Analysis

Statistical analysis was completed for ground cover, electrical conductivity, temperature, biomass samples, and results from saturated media extract report. The analysis was completed in R Studio, a statistical software system. The tests that were performed included the last measurements of each plot, and all measurements for ground cover, electrical conductivity, and temperature, along with the biomass samples. The One-way Kruskal Wallis test was completed, with $\alpha = 0.05$. From there, if the p-value was less than 0.05, then the analysis was continued with the Dunns test for pairwise comparisons. Each measurement category was then plotted with a box and whiskers plot with statistically significant letters, if applicable. Results for the saturated media extract report that contained less than detected values, used half of the detected value to run the statistical analysis.

RESULTS AND DISCUSSION

Results are reported for Objective #1 followed by Objective #2 in the following sections.

Objective #1 Develop methods to enhance AMD geotube dewatering with internal lateral drains.

Characterize geotechnical properties: Column filtration testing

Results

The major results that are reported from the filter tests are the filtration efficiency, the total solid percentage of the slurry (inflow), the total solid percentage of the filter cake (output), and the hydraulic conductivity. The filtration efficiency is based on the weight of solids that do not pass through the filter compared to the weight solids that pass through the filter. The total solid from the output is the average between the top and the bottom after filtration is complete. The hydraulic conductivity is the average between each phase of the filtration test, where each test had 2 or 3 exposures. Where the first exposure was straight slurry and the second and third exposure being the addition of deionized water.

The first set of filter tests were run by using the No Polymer Sludge that was taken from the bottom of the clarifier at the Omega Site. This slurry was not dosed with polymer and only was treated with lime slurry. The fabrics tested in this set were the GT500, MD88 Typar, and MD7407 Typar. The GT500 fabric is the most common woven geotextile dewatering fabric, while the MD88 and MD7407 are both wicking drain Typar fabrics. The results for these tests are shown in Table 16 through Table 18.

Table 16. Initial No Polymer Omega GT500 Filtration Results.

		Filtration	Slurry	Filter Cake	Hydraulic Conductivity		
Test #	Volume of DI Water Added (mL)	Filtration Eff.	Inflow TS	Output TS	k (cm/sec) initial	k (cm/sec) DI	k (cm/sec) DI (2nd)
1	500	91.61%	1.01 %	2.40%	2.44×10^{-3}	1.71×10^{-4}	-
4	1,000	93.80%	1.05 %	2.43%	2.36×10^{-3}	1.46×10^{-3}	4.48×10^{-4}
6	1,000	95.87%	1.40 %	2.28%	1.25×10^{-3}	2.03×10^{-3}	1.22×10^{-3}

Table 17. Initial No Polymer Omega MD88 Filtration Results.

MD88 Data		Filtration	Slurry	Filter Cake	Hydraulic Conductivity		
Test #	Volume of DI Water Added (mL)	Filtration Eff.	Inflow TS	Output TS	k (cm/sec) initial	k (cm/sec) DI	k (cm/sec) DI (2nd)
3	1,000	94.83%	1.06%	2.07%	$2.09x10^{-3}$	$1.26x10^{-3}$	$6.43x10^{-4}$
5	1,000	96.21%	1.26%	2.40%	$3.46x10^{-3}$	$1.55x10^{-3}$	$5.06x10^{-4}$
8	1,000	95.79%	1.39%	2.69%	$1.59x10^{-3}$	$4.34x10^{-3}$	$2.88x10^{-3}$

Table 18. Initial No Polymer Omega MD7407 Filtration Results

MD7407 Data		Filtration	Slurry	Filter Cake	Hydraulic Conductivity		
Test #	Volume of DI Water Added (mL)	Filtration Eff.	Inflow TS	Output TS	k (cm/sec) initial	k (cm/sec) DI	k (cm/sec) DI (2nd)
2	500	92.72%	1.01%	2.31%	$1.97x10^{-3}$	$1.77x10^{-4}$	-
7	1,000	97.11%	1.40%	2.64%	$1.55x10^{-3}$	$3.45x10^{-3}$	$1.25x10^{-3}$
9	1,000	94.26%	1.41%	2.62%	$1.47x10^{-3}$	$2.46x10^{-3}$	$1.39x10^{-3}$

The second set of filter tests were also run using the No Polymer Sludge from the Omega Clarifier. The filters that were selected to be testing for this set were based on the filtration results from the first set. The fabrics that were tested in this set were the GT500, MD88, 140NC, and 1100N. Both the 140NC and 1100N are common woven fabrics which were selected to compare their relative efficiency. The results for the second set of tests are shown the following tables.

Table 19. Final No Polymer Omega GT500 Filtration Results.

GT500 Data		Filtration	Slurry	Filter Cake	Hydraulic Conductivity		
Test #	Volume of DI Water Added (mL)	Filtration Eff.	Inflow TS	Output TS	k (cm/sec) initial	k (cm/sec) DI	k (cm/sec) DI (2nd)
10	1,000	63.03%	0.35%	1.66%	$1.47x10^{-3}$	$8.45x10^{-4}$	$9.74\ x10^{-4}$
13	1,000	48.79%	0.34%	2.09%	$4.20x10^{-3}$	$3.36x10^{-3}$	$2.50\ x10^{-3}$
15	1,000	77.80%	0.54%	1.54%	$3.14x10^{-3}$	$8.15x10^{-3}$	$5.46x10^{-3}$

Table 20. Final No Polymer Omega MD88 Filtration Results.

MD88 Data		Filtration	Slurry	Filter Cake	Hydraulic Conductivity		
Test #	Volume of DI Water Added (mL)	Filtration Eff.	Inflow TS	Output TS	k (cm/sec) initial	k (cm/sec) DI	k (cm/sec) DI (2nd)
11	1,000	88.56%	0.70%	1.73%	1.81×10^{-3}	2.38×10^{-3}	1.34×10^{-3}
21	1,000	78.77%	0.46%	1.64%	8.55×10^{-3}	1.43×10^{-3}	6.23×10^{-3}
22	1,000	92.29%	0.49%	1.36%	4.43×10^{-3}	4.80×10^{-3}	1.31×10^{-2}

Table 21. Final No Polymer Omega 140NC Filtration Results.

140NC Data		Filtration	Slurry	Filter Cake	Hydraulic Conductivity		
Test #	Volume of DI Water Added (mL)	Filtration Eff.	Inflow TS	Output TS	k (cm/sec) initial	k (cm/sec) DI	k (cm/sec) DI (2nd)
17	1,000	92.44%	0.48%	1.76%	3.90×10^{-3}	2.35×10^{-3}	3.51×10^{-4}
19	1,000	91.24%	0.46%	1.78%	4.51×10^{-3}	2.12×10^{-3}	5.63×10^{-3}
20	1,000	91.27%	0.46%	1.66%	4.39×10^{-3}	9.50×10^{-4}	1.78×10^{-3}

Table 22. Final No Polymer Omega 1100N Filtration Results.

1100N Data		Filtration	Slurry	Filter Cake	Hydraulic Conductivity		
Test #	Volume of DI Water Added (mL)	Filtration Eff.	Inflow TS	Output TS	k (cm/sec) initial	k (cm/sec) DI	k (cm/sec) DI (2nd)
12	1,000	82.41%	0.14%	1.54%	1.12×10^{-3}	1.13×10^{-3}	9.76×10^{-4}
14	500	90.92%	0.37%	1.77%	1.55×10^{-3}	4.21×10^{-4}	
16	1,000	92.79%	0.48%	1.65%	3.76×10^{-3}	1.93×10^{-3}	3.74×10^{-3}
18	1,000	92.36%	0.46%	1.77%	3.43×10^{-3}	4.80×10^{-3}	3.15×10^{-3}

The third set of filter tests were run by using slurry collected from the T&T Site. This slurry was collected from the material headed for the geotextile tubes that were on site. This slurry had been treated with 20 ppm of polymer as well as the lime slurry. This set of tests used the same fabrics that the second set conducted with. The results for the third set of tests are shown in Table 23 through Table 26.

Table 23. 20 ppm Polymer T&T GT500 Filtration Results.

GT500 Data		Filtration	Slurry	Filter Cake	Hydraulic Conductivity		
Test #	Volume of DI Water Added (mL)	Filtration Eff.	Inflow TS	Output TS	k (cm/sec) initial	k (cm/sec) DI	k (cm/sec) DI (2nd)
23	1,000	91.05%	0.74%	2.89%	$6.98x10^{-4}$	$7.74x10^{-5}$	$4.84x10^{-5}$
24	1,000	92.08%	0.72%	1.95%	$6.19x10^{-4}$	$1.63x10^{-4}$	$6.06x10^{-5}$

Table 24. 20 ppm Polymer T&T MD88 Filtration Results.

MD88 Data		Filtration	Slurry	Filter Cake	Hydraulic Conductivity		
Test #	Volume of DI Water Added (mL)	Filtration Eff.	Inflow TS	Output TS	k (cm/sec) initial	k (cm/sec) DI	k (cm/sec) DI (2nd)
29	1,000	94.16%	1.15%	2.76%	$7.08x10^{-4}$	$5.78x10^{-5}$	$1.06x10^{-4}$
30	1,000	94.39%	0.89%	2.83%	$8.76x10^{-4}$	$7.61x10^{-5}$	$2.16x10^{-5}$

Table 25. 20 ppm Polymer T&T 140NC Filtration Results.

140NC Data		Filtration	Slurry	Filter Cake	Hydraulic Conductivity		
Test #	Volume of DI Water Added (mL)	Filtration Eff.	Inflow TS	Output TS	k (cm/sec) initial	k (cm/sec) DI	k (cm/sec) DI (2nd)
25	1,000	92.51%	0.75%	2.83%	$6.37x10^{-4}$	$8.13x10^{-5}$	$5.30x10^{-5}$
26	1,000	91.41%	0.74%	2.19%	$4.98x10^{-4}$	$5.73x10^{-5}$	$7.61x10^{-5}$

Table 26. 20 ppm Polymer T&T 1100N Filtration Results.

1100N Data		Filtration	Slurry	Filter Cake	Hydraulic Conductivity		
Test #	Volume of DI Water Added (mL)	Filtration Eff.	Inflow TS	Output TS	k (cm/sec) initial	k (cm/sec) DI	k (cm/sec) DI (2nd)
27	1,000	93.46%	0.75%	2.59%	$6.03x10^{-4}$	$5.89x10^{-5}$	$6.41x10^{-5}$
28	1,000	88.63%	0.75%	2.29%	$6.41x10^{-4}$	$1.08x10^{-4}$	$6.32x10^{-5}$

Discussion

Evaluation is based on their filtration efficiency, hydraulic conductivity, and the change in total solids between the slurry and the filter cake. Each fabric will also be compared between each of the polymer amounts to assess how a polymer addition effects.

Table 27 shows the average initial hydraulic conductivity, filtration efficiency, incoming total solids, and the filter cake total solids for each of the fabrics between the 2 polymer doses. In this table the values can be easily compared between the different polymer doses that were used. Where the addition of polymer is expected to decrease the hydraulic conductivity increase the filtration efficiency in the GT500 fabric and increase the total solid content in the filter cake after filtration is complete.

Table 27. Average Values from Column Filter Test Results.

Material	Fabric	Hydraulic Conductivity (cm/s)	Filtration Efficiency	Incoming Total Solid	Filter Cake Total Solid
Omega No Polymer	GT500	2.48×10^{-3}	78.50%	0.78%	2.07%
	MD7407	1.66×10^{-3}	94.70%	1.27%	2.52%
	MD88	3.66×10^{-3}	91.10%	0.89%	1.98%
	1100N	2.47×10^{-3}	89.60%	0.36%	1.68%
	140NC	4.26×10^{-3}	91.70%	0.47%	1.73%
T&T 20 ppm Polymer	GT500	6.59×10^{-4}	91.60%	0.73%	2.42%
	MD88	7.92×10^{-4}	94.30%	1.02%	2.79%
	1100N	6.22×10^{-4}	91.05%	0.75%	2.44%
	140NC	5.68×10^{-4}	91.96%	0.75%	2.51%

Filtration. The filtration results show that the MD88 fabric is more consistent and has a better average filtration efficiency between all three tests. In the following table, the filtration data that was collected after the tests that compare the results for the MD88 and MD7407 typar fabrics. Based off these results a decision to choose the MD88 wick drain in all future experiments and designs was made because of the higher filtration efficiency and higher solids retention trapped in the filter itself (this is found based on the grams lost per unit area).

Table 28. Initial No Polymer Omega MD88 Typar vs MD7407 Typar Filtration Data.

Test #	Fabric	AOS (mm)	% Retained	% Passing	Filtration Eff.	% Lost	grams lost per unit area (cm^2)
2	MD7407	0.23	92.41%	7.28%	92.72%	0.31%	0.1076
7	MD7407	0.23	97.00%	2.89%	97.11%	0.11%	0.0523
9	MD7407	0.23	94.17%	5.74%	94.26%	0.09%	0.0982
3	MD88	0.09	94.73%	5.17%	94.83%	0.10%	0.0804
5	MD88	0.09	95.84%	3.79%	96.21%	0.37%	0.0607
8	MD88	0.09	95.77%	4.21%	95.79%	0.03%	0.0750

The filtration efficiency results are consolidated in a box and whisker plot. For each of the fabric tested are shown in Figure 57. Filtration efficiency. Important metrics show the inconsistent filtration efficiency range of the GT500 fabric w from 50-96%. The MD88 fabric is by far the most efficient with having majority of the tests being above 94% with one outlier point. The comparison of the two woven fabrics, 140NC and 1100N, shows that the 140NC is more accurate between all the tests taken with all the values being above 91%, and the 1100N had one test that was far below the average of 90%.

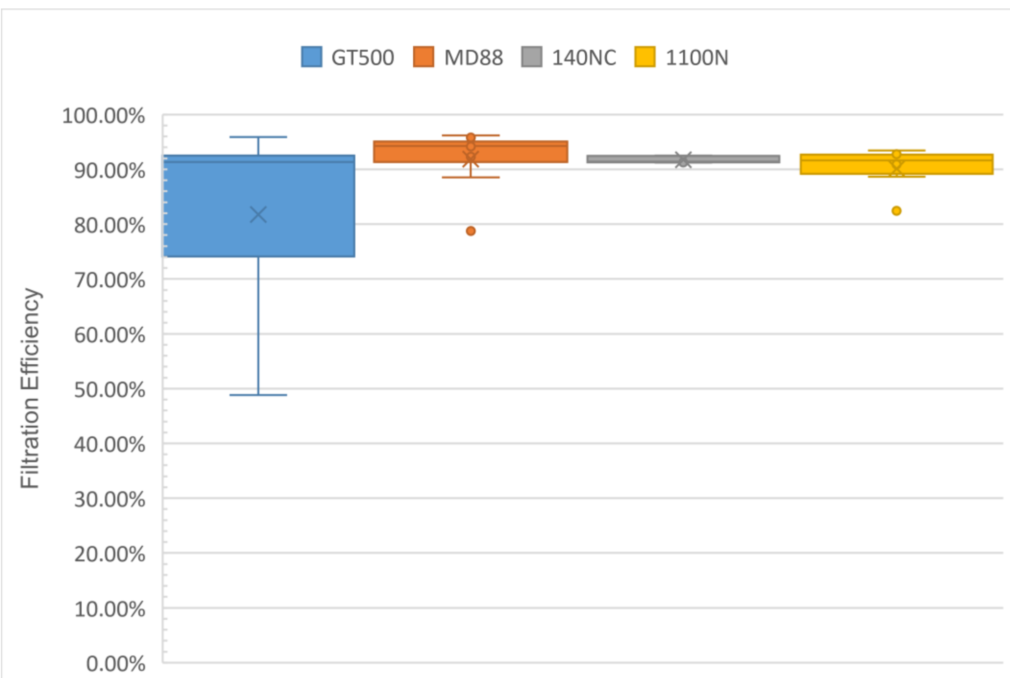

Figure 57. Filtration efficiency.

Hydraulic Conductivity. From the testing it was shown that the hydraulic conductivity decreased with time for each fabric. The significant difference was noticed when comparing either the total solids of the material that was being tested and if the slurry was using polymer or not. The decrease in hydraulic conductivity with time is more noticeable when comparing the different polymer dosages tested. Figure 58 shows the hydraulic conductivity (log scale) vs time for tests 10, 13, and 15 which were from the No Polymer Omega Slurry using the GT500 fabric. This figure combines all the data from each of the tests in order to create a line of best fit Based on the figure it shows that the hydraulic conductivity is expected to decrease with time. The following figures were created using JMP Statistical Software© in order to create the line of best fits with the confidence interval.

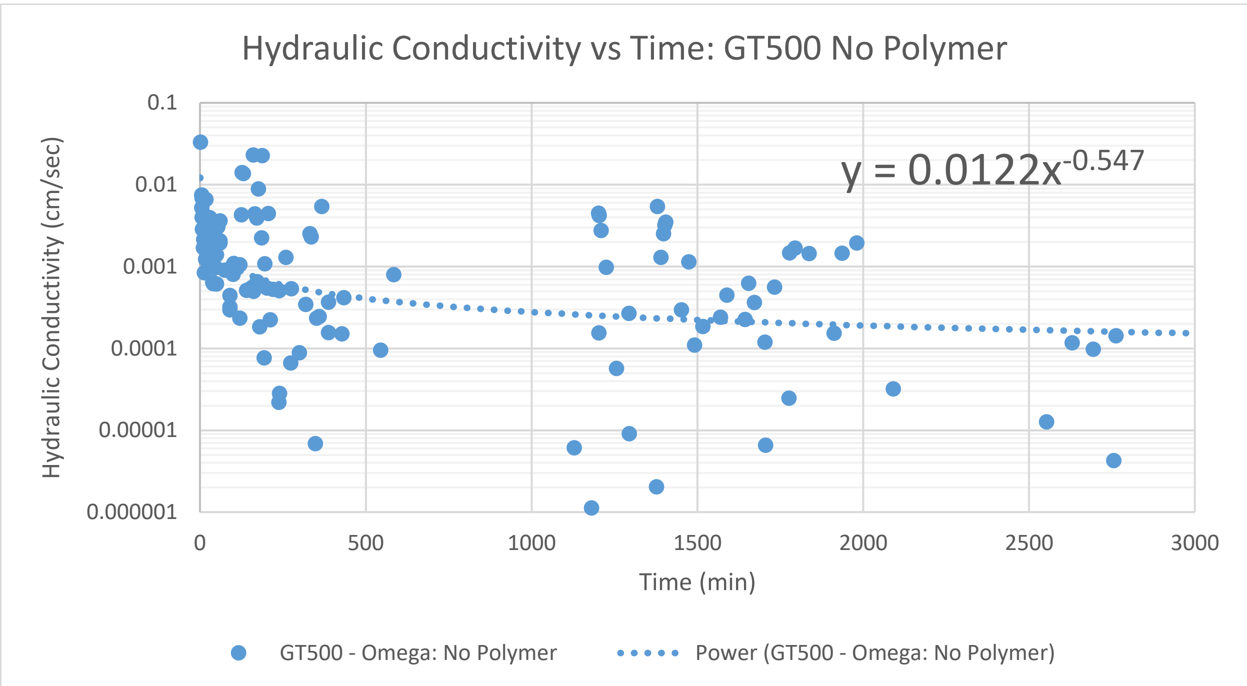

Figure 58. Hydraulic Conductivity GT500 with No Polymer Omega Sludge.

Figure 59 shows the hydraulic conductivity (log scale) vs time for tests 23 and 24 which were from the 20 ppm polymer dosed T&T Slurry using the GT500 fabric. This figure has both tests data combined in order to create a logarithmic line of best fit. This figure also shows that the hydraulic conductivity is expected to decrease with time. In comparison between Figure 58 and Figure 59, the hydraulic conductivity decreases at a faster rate when polymer is used in the slurry. Where Figure 6 decreases from 1×10^{-2} cm/s to 1×10^{-3} cm/s and Figure 7 decreases from 1×10^{-3} cm/s to 5×10^{-4} cm/s. The test duration for the polymer dosed tests was significantly longer than the raw slurry where Figure 58 ran for almost 3,000 minutes and Figure 59 ran for almost 15,000 minutes with is five times as long.

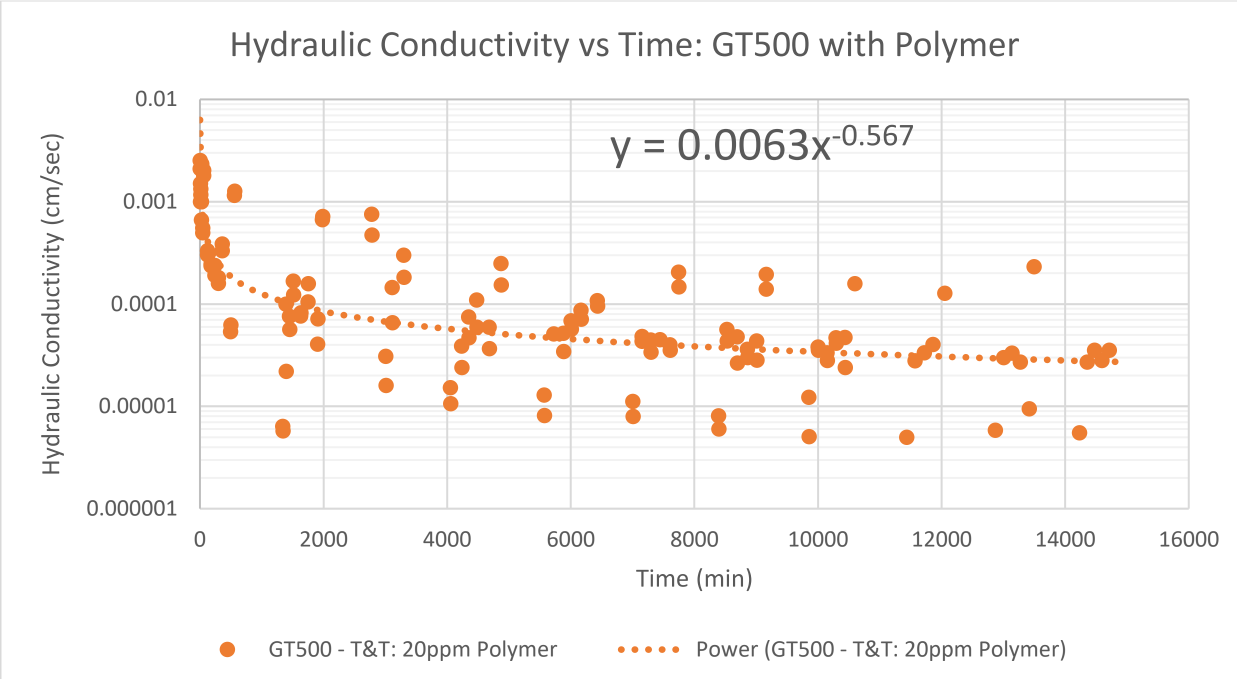

Figure 59. Hydraulic Conductivity GT500 with 20 ppm Polymer T&T Sludge.

Figure 60 shows the hydraulic conductivity (log scale) vs time for test 27 which was done using the 1100N nonwoven fabric using the 20 ppm polymer T&T slurry. This test follows the same trend from Figure 7 where the decrease in hydraulic conductivity with time is the same and then the duration of the test is also similar. Based on the comparison of the Figure 59 and Figure 60 it seems that the fabric used does not play a factor into the change in hydraulic conductivity. The fabrics are dependent on the filtration efficiency and solids retained based on the AOS of the fabric.

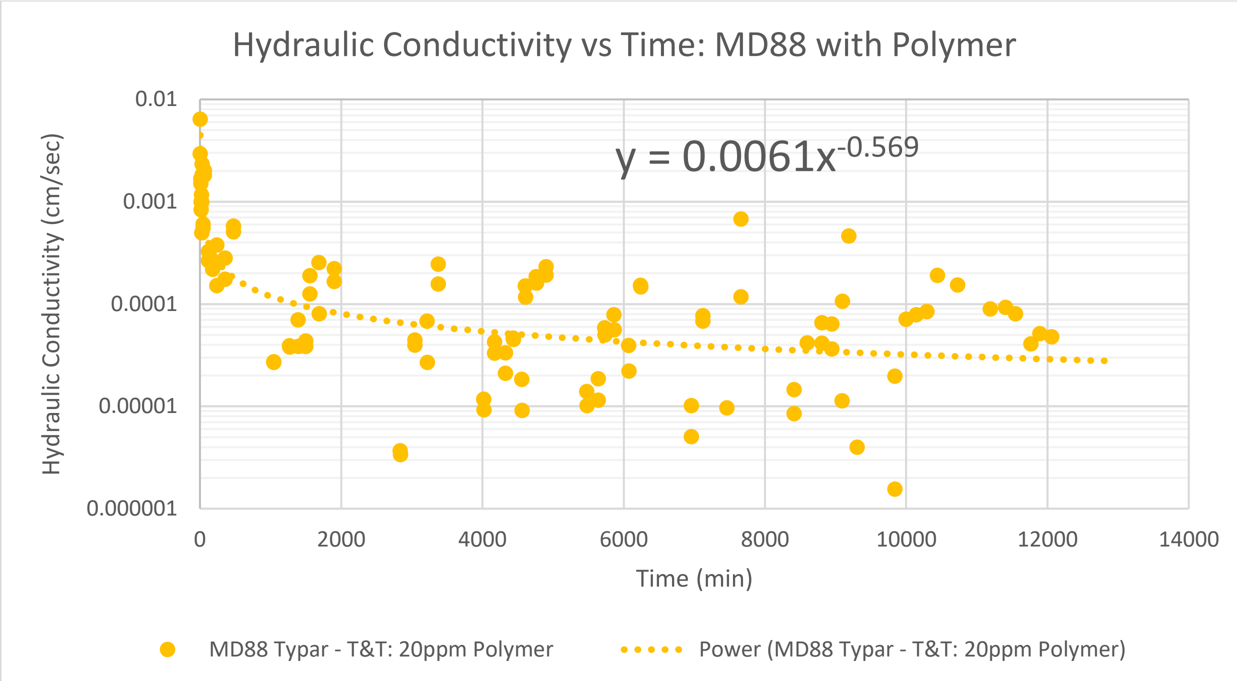

Figure 60. Hydraulic Conductivity 1100N with 20 ppm Polymer T&T Sludge.

More plots for hydraulic conductivity vs time are listed in the Appendix where the lines are separated between the different filling cycles. In these plots all the different test's lines are independent.

Total Solids. The total solids in the material were measured for each test at two separate times. The first time was to determine the total solids of the incoming slurry, this was done by averaging three samples taken from a bucket filled with AMD slurry. The second time it was collected was from the filter cake once the filtration tests was complete, this was done by taking the average TS% from the top and the bottom of the filter cake. Figure 61 and Figure 62 are two box and whisker plots which show the difference in total solids between the incoming slurry and the filter cake. Figure 61 shows the change when using the No Polymer Omega AMD Slurry and Figure 62 shows the change when using the 20 ppm polymer T&T AMD Slurry.

For Figure 61 the average total solids for the slurry is 0.76% which than increases to an average of 1.99% for the filter cake. In Figure 62 the average total solids for the slurry is 0.81% and the average for the filter cake is 2.54%. This means that the incoming total solids is very similar between the 2 samples of AMD Slurry but with the introduction of polymer the filter cake is expected to increase in the total solids percentage. The no polymer Omega slurry has an increase in total solids by 162% and the 20 ppm polymer T&T slurry increases by 214%

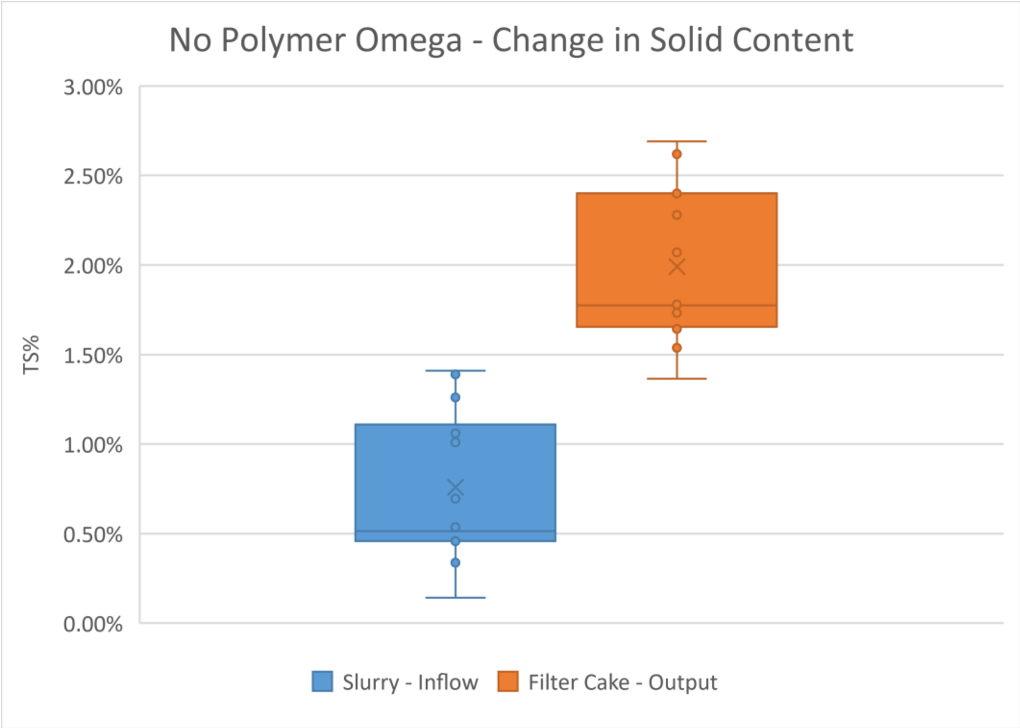

Figure 61. Raw (no polymer) Omega Change in Solid Content from Slurry to Filter Cake.

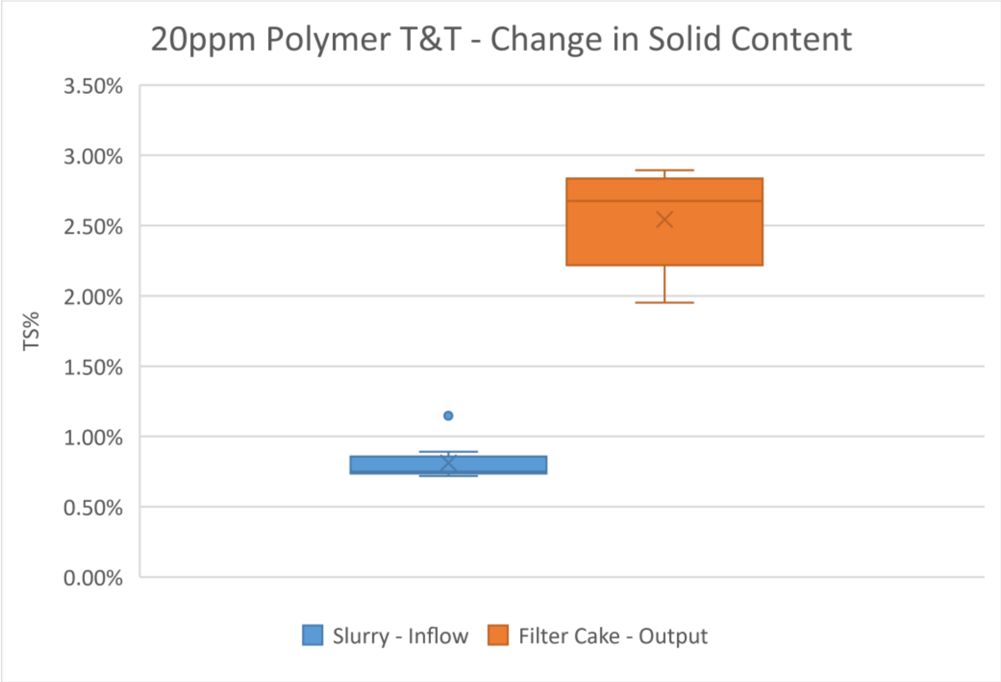

Figure 62. 20 ppm polymer dose T&T Change in Solid Content from Slurry to Filter Cake.

Characterize geotechnical properties: Moisture distribution tests

Results

The moisture content and total solids percentage results for the sampler tubes tested are listed in the Appendix with Table 29 shown as a reference indicating how the data is further reported. For the bags with full cross sections tested the specific gravity results are shown in Table 30. Out of the bags sampled there were 2 samples taken from a center port only (Bag 5 and 11), 3 bags with 1 cross section sampled (Bag 6, 7, and 9), and 1 bag with 2 cross sections sampled (Bag 11).

Table 29. Omega Geobag 11 Center Port.

Distance from Surface (cm)	Moisture Content	Total Solids
0	97.51%	2.49%
9		
20	96.01%	3.99%
29		
40	96.33%	3.67%
49		
60	95.39%	4.61%
69		
80	95.20%	4.80%
89		

Table 30. Omega Geobags Specific Gravity.

Specific Gravity	Bag 6	Bag 7	Bag 9	Bag 11
Mass Pyc. (g)	160.3	168.3	159.5	160.6
Mass Pyc + Water (g)	657.7	666.3	660.0	658.0
Calibration Temp (Degrees C)	21.0	20.2	24.0	19.8
Density @ Cal. Temp (g/mL)	0.997	0.998	0.997	0.998
Calibrated Vol (mL)	498.40	498.92	501.84	498.27
Mass Pyc. + Water @ Test Temp (g)	657.7	666.3	660.0	658.0
Mass Pyc + Water + Soil (g)	690.01	697.68	691.00	690.10
Mass Soil (g)	49.43	48.87	48.90	49.50
Volume Pyc (mL)	498.40	498.92	501.84	498.27
Test Temp (Degrees C)	21.0	20.2	24.0	19.8
Density Water @ Test Temp (g/mL)	0.997	0.998	0.997	0.998
Specific Gravity	2.89	2.79	2.73	2.84
Temp. Coeff (K)	0.998	0.998	0.998	0.998
Specific Gravity @ 20°C	2.88	2.79	2.73	2.84

Discussion

Moisture Distribution. The moisture distribution throughout each of geobags the points were transposed into AutoCAD. For synthesis, the first two tests that were conducted only 1 dig sample was done. These tests were done on a dry bag (Bag 5) and in a new bag that was still being pumped into (Bag 11). The cross-sectional distribution models are shown in Figure 63 and Figure 64. When looking at each of the cross sections the black rectangles indicate the sampler hole spacing and where the sludge was collected.

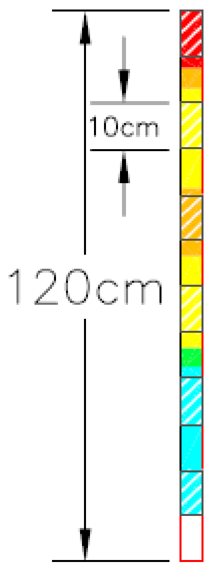

Percent Total Solid Ranges			
Range #	Minimum TS	Maximum TS	Color
1	5.00	5.25	
2	5.25	5.50	
3	5.50	5.75	
4	5.75	6.00	
5	6.00	6.25	
6	6.25	6.50	
7	6.50	6.75	

Figure 63. Omega Geotextile Bag #5 – Sampled 5/23/22.

The spacing in the 5th geotextile bag is in 10 cm increments with the data being collected using one of the early iterations of the sampler design. The model shows that the bag has a higher TS% closer to the top of the bag. With this being an older bag, it has had more time than other bags to be able to dewater and have the sun evaporate any moisture near the top of the bag. It can be inferred since this was a relatively old bag that there was limited moisture movement out of the bag but it all pools near the bottom along the formed filter cake.

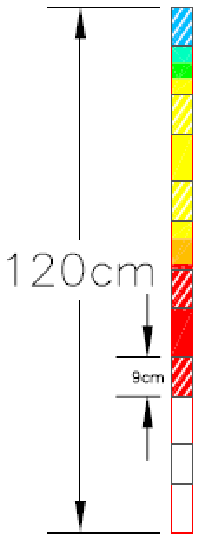

Percent Total Solid Ranges			
Range #	Minimum TS	Maximum TS	Color
1	1.00	1.50	
2	1.50	2.00	
3	2.00	2.50	
4	2.50	3.00	
5	3.00	3.50	
6	3.50	4.00	
7	4.00	4.50	
8	4.50	5.00	

Figure 64. Omega Geotextile Bag #11 – Sampled 6/03/22.

The data for the 11th geotextile bag has 9 cm holes because it was using the 2nd iteration of the sampler design. The data show that the geotextile bag is wetter at the top than at the bottom of the bag. The difference between bag 11 and bag 5 is that bag 11 was still being pumped into so the viscosity of the sludge allowed for the solids to flow to the bottom of the bag easier. This is because the bags were still being pumped into so all the fresh sludge was at the top of the bag and the older sludge was at the bottom which had a longer time to dewater. When collecting the material from this bag it was the 2nd newest bag and had been pumped into since the first of March 2022, and the material was collected the third of June 2022.

The data collected from the 6th, 7th, and the 9th Geotextile bags at the Omega site had enough information to create a plot of the moisture distribution throughout a cross sectional area. The plot for the moisture distribution is shown in Figure 65 and Figure 66 for bag 7 and 9, respectively. Figure 67 is the legend used for both models. Figure 68 shows the moisture distribution model for bag 6 with Figure 69 showing the corresponding legend similar to the other two plots the black rectangles indicate where each of the holes in the sampler were and then the red rectangles indicate where the sampler was inserted for each dig.

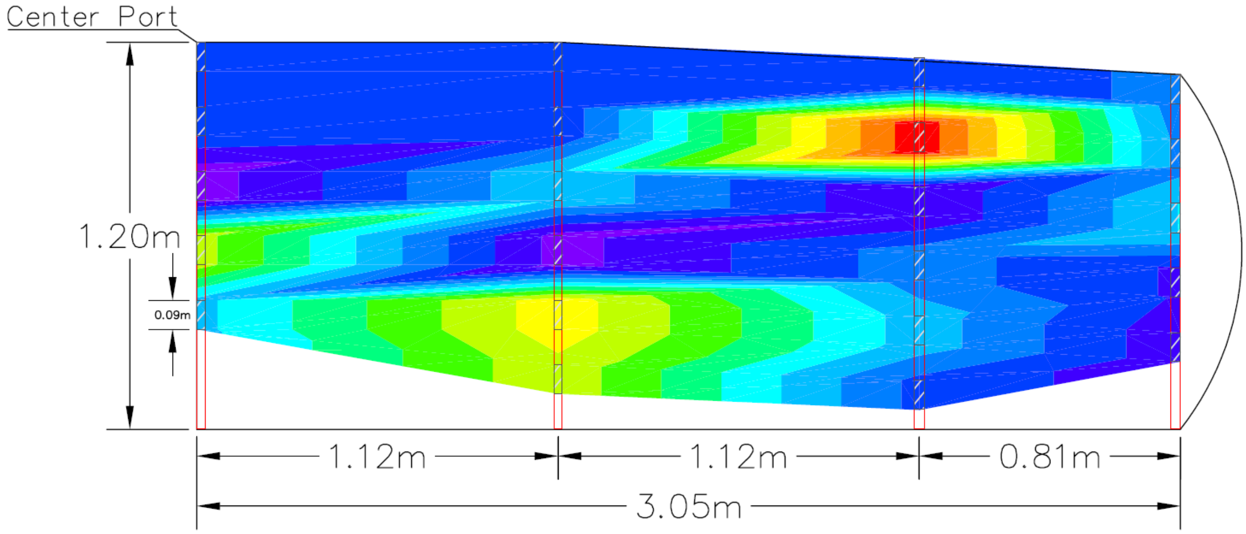

Figure 65. Total Solids Distribution Omega Geotextile Bag #7 – Sampled 6/08/22.

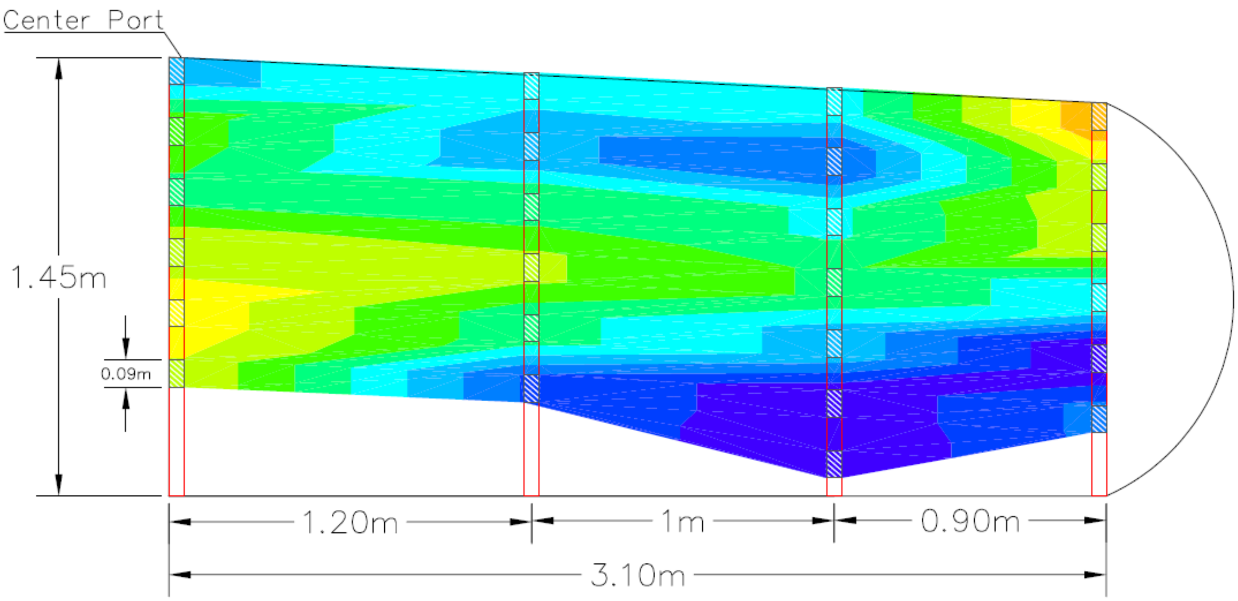

Figure 66. Total Solids Distribution Omega Geotextile Bag #9 – Sampled 9/09/22.

Percent Total Solid Range			
Range #	Minimum TS	Maximum TS	Color
1	5.00	5.50	
2	5.50	6.00	
3	6.00	6.50	
4	6.50	7.00	
5	7.00	7.50	
6	7.50	8.00	
7	8.00	8.50	
8	8.50	9.00	
9	9.00	9.50	
10	9.50	10.00	
11	10.00	10.50	
12	10.50	11.00	
13	11.00	11.50	

Figure 67. Omega Geotextile Bag #7 and #9 TS Legend.

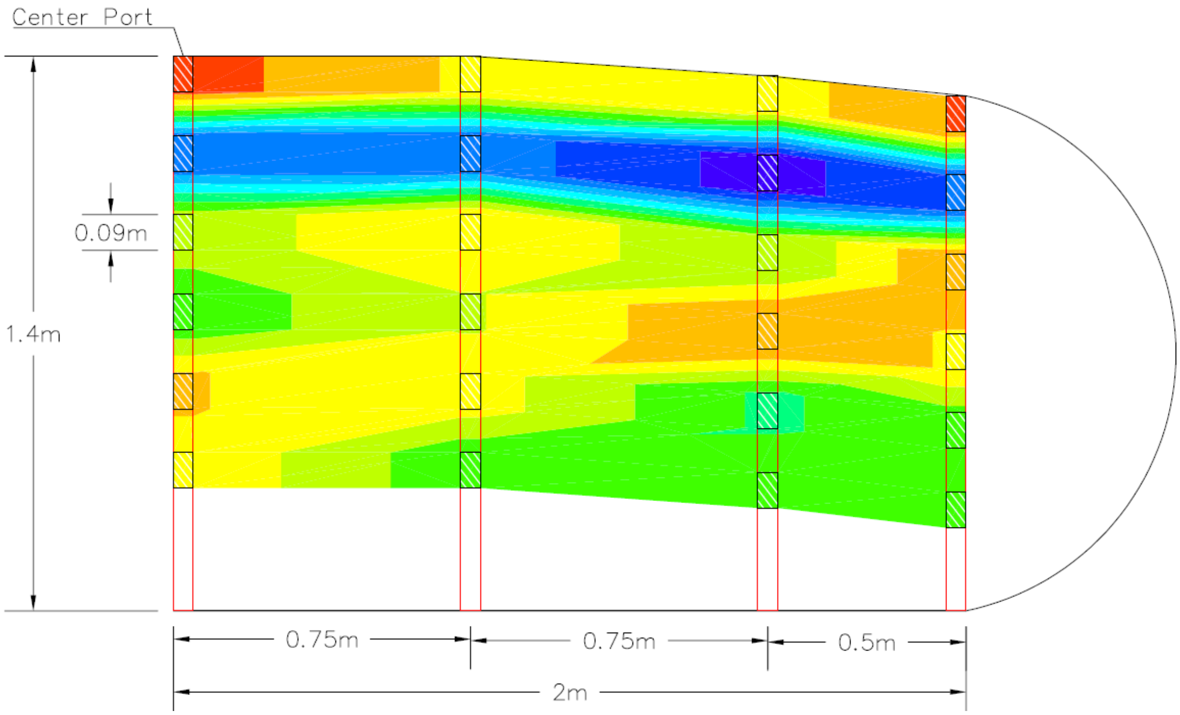

Figure 68. Total Solids Distribution Omega Geotextile Bag #6 – Sampled 1/17/23.

Percent Total Solid Range			
Range #	Minimum TS	Maximum TS	Color
1	4.50	4.75	
2	4.75	5.00	
3	5.00	5.25	
4	5.25	5.50	
5	5.50	5.75	
6	5.75	6.00	
7	6.00	6.25	
8	6.25	6.50	
9	6.50	6.75	
10	6.75	7.00	
11	7.00	7.25	
12	7.25	7.50	

Figure 69. Omega Geotextile Bag #6 TS Legend.

With the 6th, 7th, and 9th bag all getting 4 digs across half the length of the bag a plot was created to show how the moisture distributes throughout the axisymmetric cross section. There are layers developed by the different filling cycles. The shape of these layers are in a similar shape as a parabola, where the bottom of the parabola is in the center and then arcs up towards the top edges. The moisture profile is not uniform this may be a result of high variability of the polymer dosage that is used and the different AMD treatment flow rates. When comparing the 7th bag and the 9th bag, there are zones that have an elevated zone when looking at the total solids. When comparing the 7th and 9th bags, they are not uniform where the top of the 9th bag has more solids than the 7th bag. This may be due to inconsistencies in polymer addition, filling cycles, and the material coming to the site. When comparing the 6th bag to the 7th and 9th bags, the 6th bag has different layers and average total solids than the other 2. This bag is wetter than the other 2, which could be different variables involved. These variables could be different weather and different time of year, where the 7th and 9th bag were collected in the summer and the 6th bag was collected in the winter.

After comparing how the moisture and TS% distribute between three different bags, the test objective advanced to assess the moisture profile within a single bag. To answer this question samples were collected from one of the geotextile bags at two different points along the length of the bag. Similar to the other cross sections each had 4 digs across half of the bag to create the model. The cross sections were taken from Omega Geotextile bag 11, which is also a bag that had been tested back in June 2022 but only material was taken from the center port. This geotextile bag was placed in March of 2022 with this sampling occurring on 2 November 2022. This bag was last filled in October of 2022prior to the sampling as well as that all pumping into the bag did not take place from either port that sample was taken from (all pumping took place from Cross Section C, see Figure 25 below). Figure 70 shows the moisture distribution for Cross Section A and Figure 71 shows the moisture distribution for Cross Section B with Figure 72 providing the legend for both cross sections.

One thing to compare from the Cross Section B from Bag 11 is to the singular dig above. The sampling from the center port is the same region just 3 months apart. It shows that there is a significant change in the solids content in this region over time going from a range of 3-5% to a range of 4-6%.

The coring layout is illustrated in Figure 73 on a planar view of the 11th Geotextile bag, which was created to show where each of the ports are situated and the distance from the edge the samples were cored.

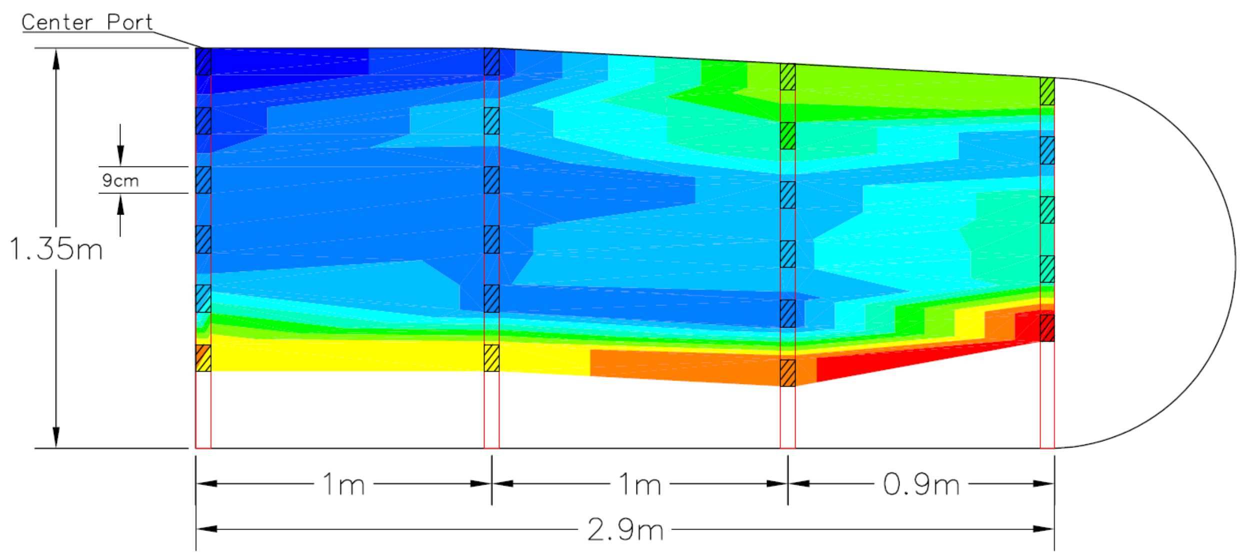

Figure 70. Total Solids Distribution Omega Geotextile Bag #11 Cross Section A – Sampled 11/02/22.

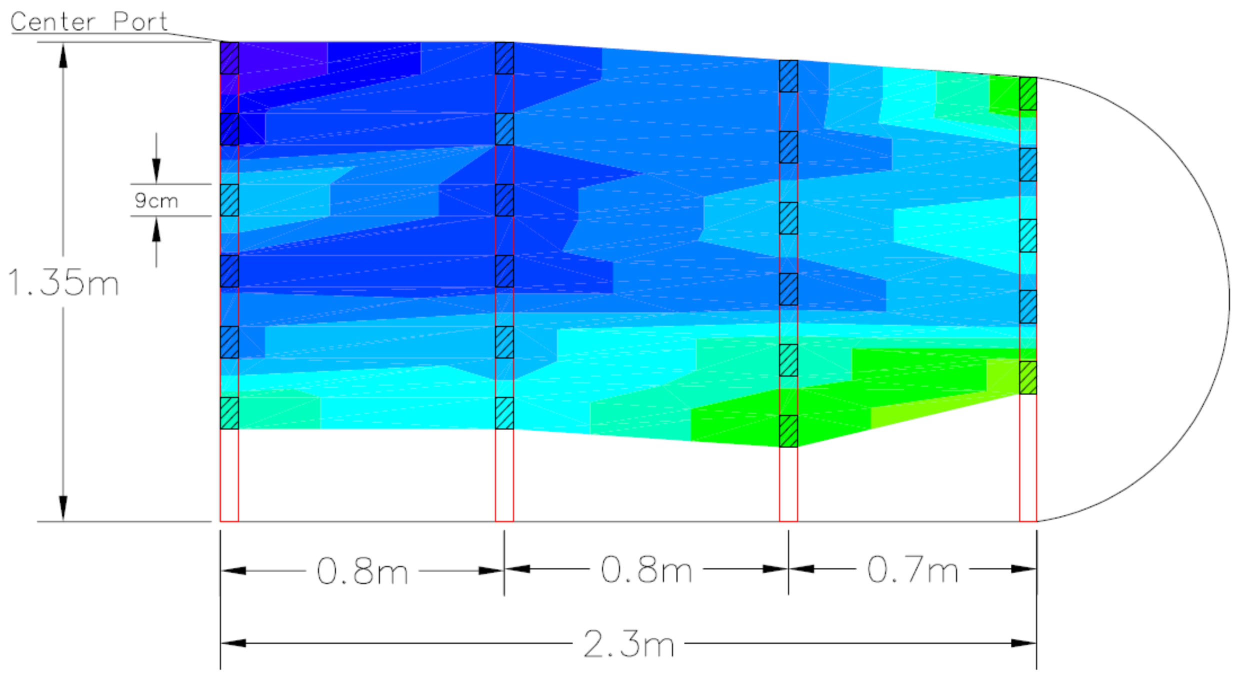

Figure 71. Total Solids Distribution Omega Geotextile Bag #11 Cross Section B – Sampled 11/02/22.

Percent Total Solid Range			
Range #	Minimum TS	Maximum TS	Color
1	4.00	4.25	
2	4.25	4.50	
3	4.50	4.75	
4	4.75	5.00	
5	5.00	5.25	
6	5.25	5.50	
7	5.50	5.75	
8	5.75	6.00	
9	6.00	6.25	
10	6.25	6.50	
11	6.50	6.75	
12	6.75	7.00	
13	7.00	7.25	

Figure 72. Omega Geotextile Bag #11 TS Legend.

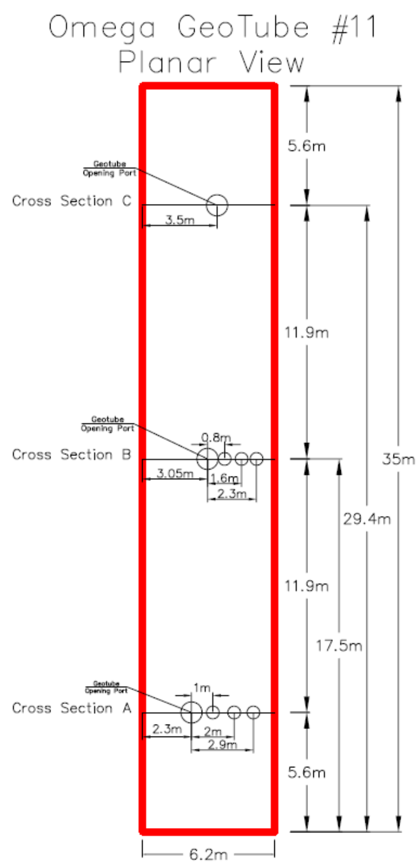

Figure 73. Planar View of Omega Geotextile Bag #11.

Specific Gravity. Besides the moisture content that was collected the specific gravity was also collected by getting a large sample of sludge from each bag. This was because of the low solids content of the material and the necessity of about 50grams of solids to run Specific Gravity Tests following the ASTM D854. A condensed table showing the bags number, date the sample was collected, and the bags specific gravity are shown below in Table 31. The significance of the specific gravity is in correlation with how most soils fall between the range of 2.65 and 2.8 with the large the specific gravity the finer the soil. With the average between the four bags being 2.81. In this case bag 6 has the finest soil particles and bag 9 has the coarsest soil particles.

Table 31. Specific Gravity.

Bag #	Date Sample Collected	Specific Gravity
6	1/17/23	2.88
7	6/8/22	2.79
9	9/9/22	2.73
11	11/2/22	2.84
Average		2.81
Standard Deviation		0.056

Design prototype dewatering system

Modified geotextile bags were evaluated to enhance dewatering efficiency for AMD sludge dewatering and long-term stability. HBTs (Method 1) and GDTs (Method 2) were performed with different shell fibers and internal lateral drains.

HBT Test Set 1 shell fibers consisted of woven fabric type. HBT Test Set 2 shell fibers consisted of geocomposite fabric type. GDT Test Set 3 GDT bag fibers consisted of woven fabric. HBT Test Set 1 internal drainage components consisted of a vertically oriented prototype fabric to provide radial drainage. The prototype internal drainage component was sewn into the base of the bag at the manufacturing facility. HBT Test Set 2 internal drainage components consisted of vertically oriented CCF fabrics to provide radial drainage. The CCF fabrics were cut to a specific width using scissors then secured to the base of the respective bags at the West Virginia University campus by threading a screw through the base of the bag, a piece of wood, and the CCF fabric. GDT Test Set 3 internal drainage components consisted of horizontally oriented CCF fabrics and PVD geocomposites to provide lateral drainage. The CCFs and PVDs were installed at the West Virginia University campus by removing the stitching at opposite, central location of the GDT bag. The CCFs and PVDs were then cut to a specific width using scissors, threaded through the opening, then stapled in place. Method 1 and 2 modified geotextile bags were configured as illustrated in Figure 74 and Figure 75.

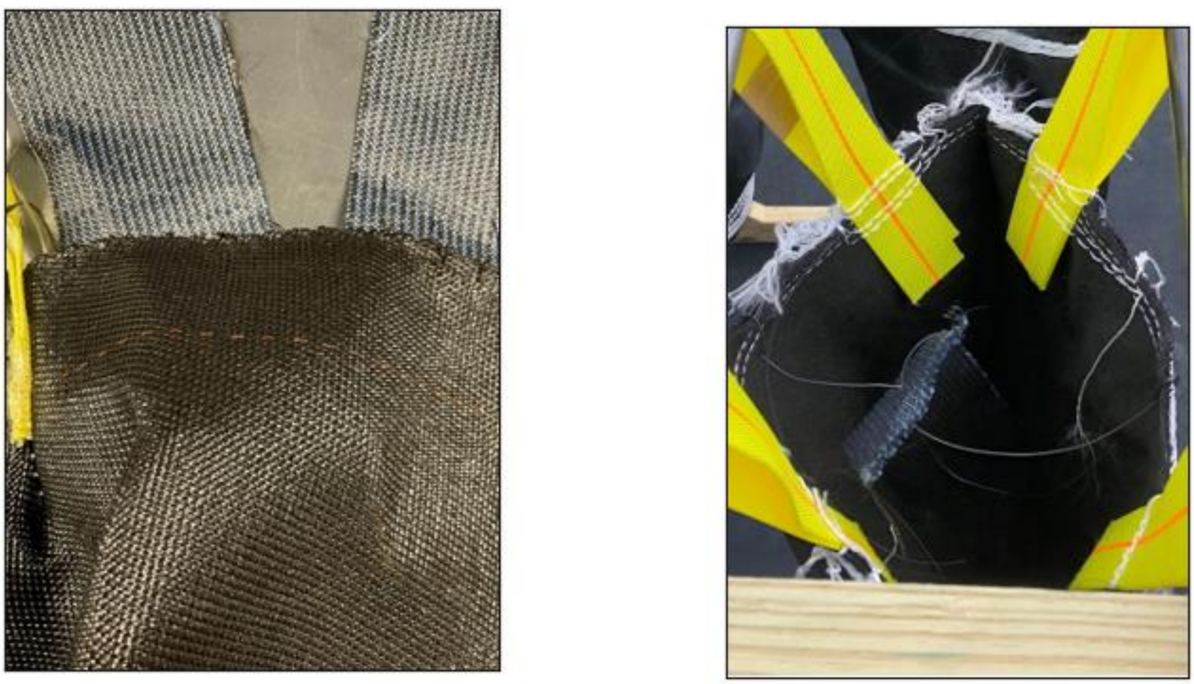

Figure 74. HBT Test Set 1 (left) and HBT Test Set 2 (right) (Source: Author).

 

Figure 75. GDT Test Set 3 bag with PVD (left) and CCF (right) (Source: Author).

HBT internal drainage components were oriented vertically due to the HBT bags lacking seams in the lateral direction, through which internal drainage components were oriented in the GDT bags, and the HBT bags possessing an opening in the vertical direction. This difference in orientation of internal drainage components made the GDTs more representative of a lateral drainage application than the HBTs. However, both internal drainage component orientations served the purpose of removing excess water from the center of the respective bags.

Numerical modeling

<u>Hydraulic Conductivity</u>

The first discussion of results will be based on the hydraulic conductivity changes due to the variation in the density of the filter cake. The Plaxis model resulted in 2 significant output models that show how the hydraulic conductivity changed during the models duration. Model #1 in Figure 76 show as water flows throughout region and has a relatively large contour range due to the low hydraulic conductivity ($2.93x10^{-3}$ cm/s or $1.05x10^{-1}$E m/hr) used for the slurry and the relatively large value for the GT500's permittivity. Model #2 in Figure 77 shows there is limited flow out (dewater) of the system, and the buildup of the filter cake. The built-up filter cake is evident of the steep increase in hydraulic conductivity in the proximity of the geotextile fabric. This region has a consistent hydraulic conductivity throughout the system in the AMD slurry region, and the hydraulic conductivity for the filter cake changes between stages of the model, meaning as the stages progress the flow through that zone decreases.

The color scheme for these models has the blue regions being the larger hydraulic conductivity and the red region being the smallest hydraulic conductivity. So, for Figure 76 the outer zone, where the GT500 fabric is, has permittivity. In Figure 77 the AMD slurry's region has a larger hydraulic conductivity than the material that is in the vicinity of the filter cake and the inner edge of the GT500 fabric.

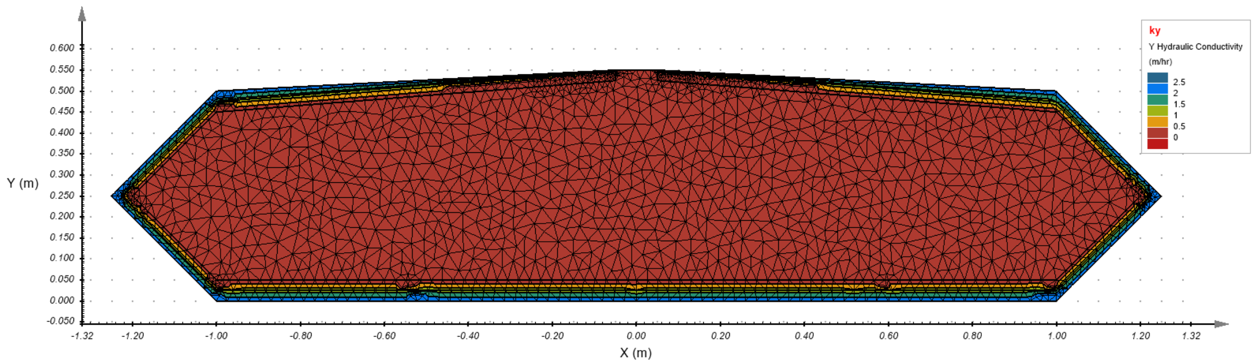

Figure 76. Plaxis Model #1 - Hydraulic Conductivity under Flow.

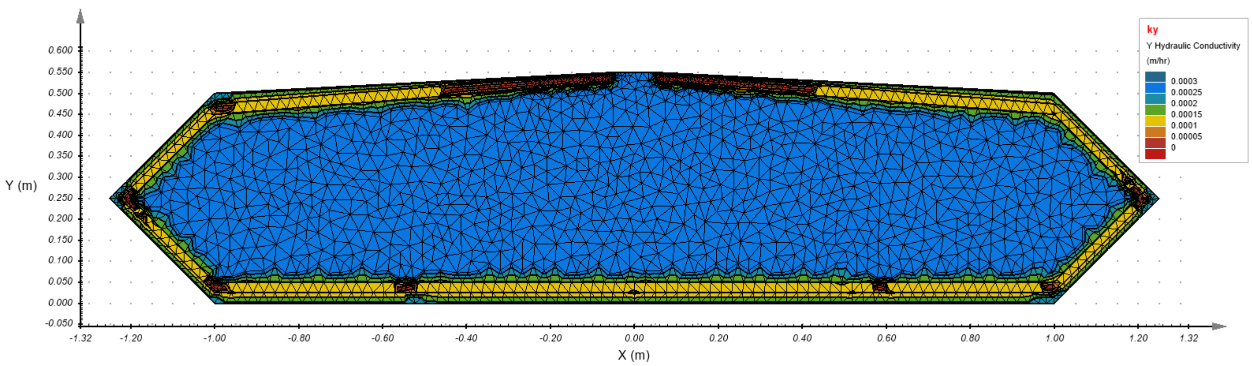

Figure 77. Plaxis Model #2 - Hydraulic Conductivity Filter Cake Build Up.

Water Content

The next discussion of model analysis outputs addresses the changes in water content over time throughout the system. The models that were collected from the water content can be compared with the field sampling in Section 4. These models are to predict water content percent when AMD sludge is pumped into a bag that already has a slurry sludge mixture inside. The models which have the largest relevance when looking at the water content occur from the first stage and the final day of the first stage, then when AMD sludge is pumped into the system and then the final model from the fourth stage. Each model has the same scale for comparison. Model #3 in Figure 78 has only the GT500 fabric and the AMD slurry. In this model the fabric is defined as a clogged zone with a moisture content of 50% and the AMD slurry has its water content set at 93%. Model #4 in Figure 79 is the final day of stage 1 where the internal area's water content is expected to decrease, and the water content decreases as the material gets closer to the GT500 fabric shown by the increase in contour lines.

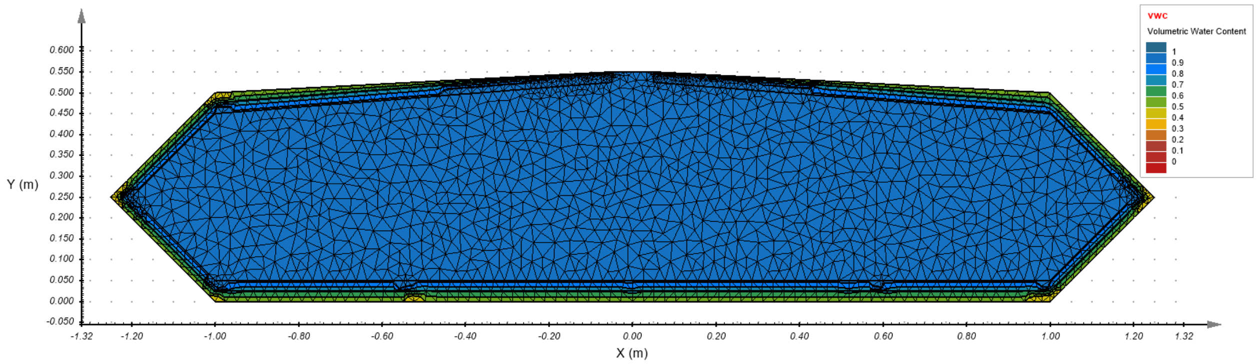

Figure 78. Plaxis Model #3 - Water Content Initial Model Results.

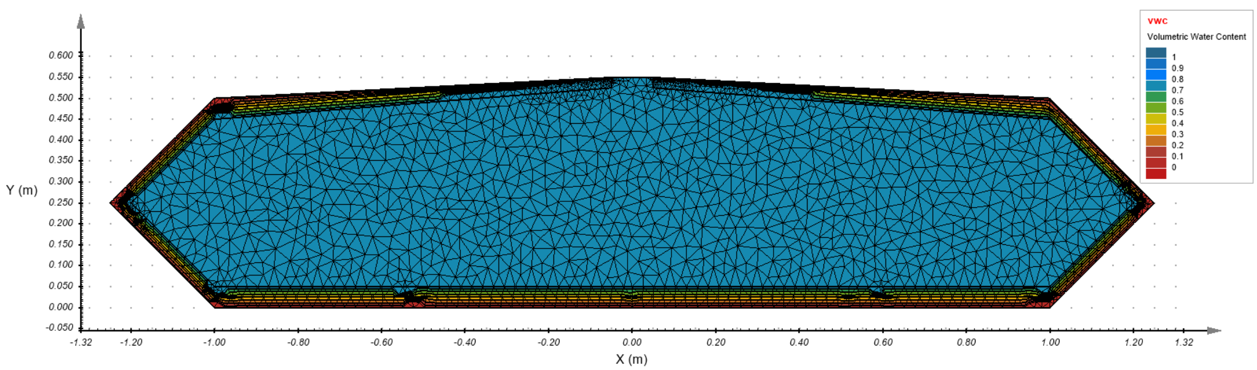

Figure 79. Plaxis Model #4 - Water Content First Stage Final Day Results.

The next two output models include the filter cake. Where Model #5 in Figure 80 is showing the output from the first day of stage 2. Model #6 in Figure 81 shows that the center regions water content increases back to the initial water content because of the inflow of more AMD slurry. Comparing this figure to the initial results in Figure 78 the main difference is that the filter cakes region has a lower water content, because of the density of the filter cake. Figure 81 from the final output is similar to the final day from the initial stage with the main difference being the region near the top center because of the introduction of the filter cake that there is a change in water content in that region that was originally just AMD slurry in Figure 79.

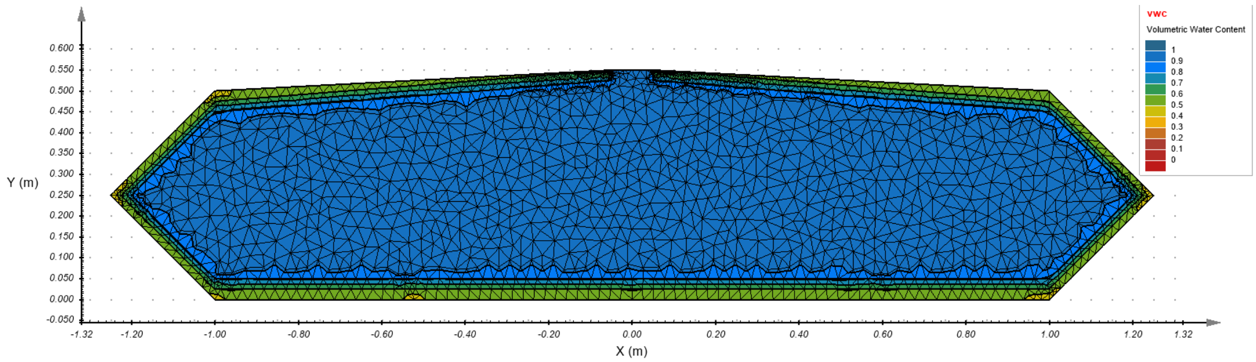

Figure 80. Plaxis Model #5 - Water Content Addition of Filter Cake Results.

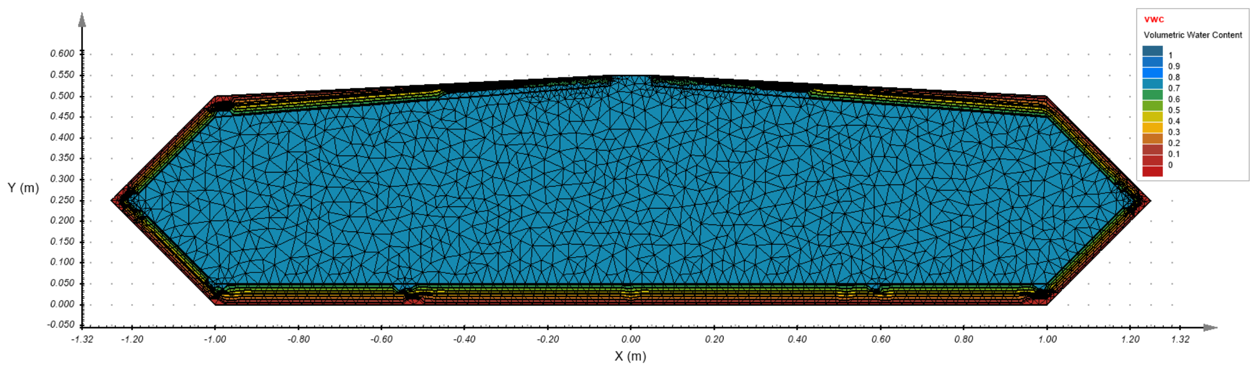

Figure 81. Plaxis Model #6 - Water Content Final Model Results.

<u>Total Solids Content</u>

The distribution of total solids content in the AMD Sludge is discussed in this analysis shows the largest solids content region and to maximize for higher solids percentage throughout the geotextile tube cross section. An important finding is that the change in solids content over time and with the addition of AMD slurry is that there was no change. This means there is a difference between the metrics used to calculate the solids content and the water content. This is due to the water content calculation is based on volumetric water content. Model #7 in Figure 82 is the model showing the distribution of the solids content within the system. Where the model shows that the solids content within the AMD slurry is about 15% and majority of the solids is within the region for the GT500 fabric, and some contour lines are shown to be within the filter cakes region.

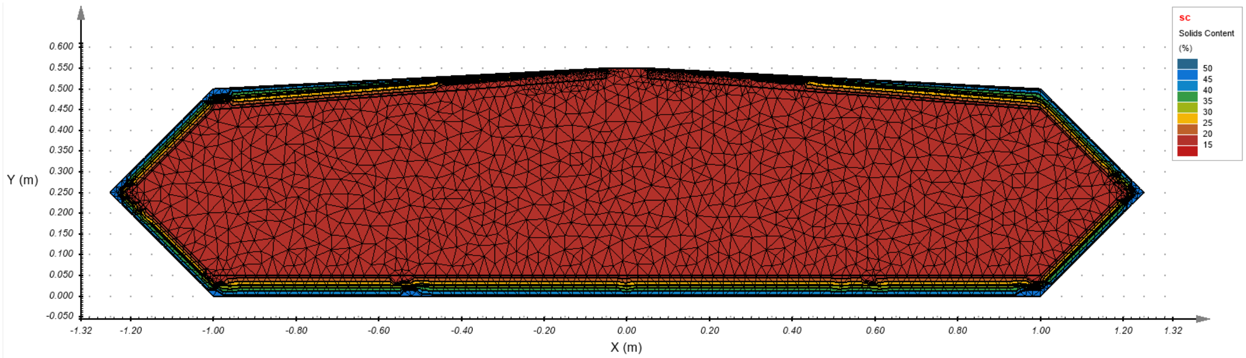

Figure 82. Plaxis Model #7 - Total Solids Content Distribution.

<u>Moisture Flow</u>

This analysis addresses how the moisture is expected to dewater within the geotextile tubes. The direction to show this result was by creating stream tracers within the system at different time steps for the model. This illustrates that the flow of moisture is inconsistent between the stages of the model and where the water is expected to dewater. Model #8 in Figure 83 shows the flow of material during the first stage, but it is also the predicted flow throughout most of the models duration. The figure shows that the flow in the system is symmetrical, and all saturated flow lines are originating from the midpoint of the inflow port.

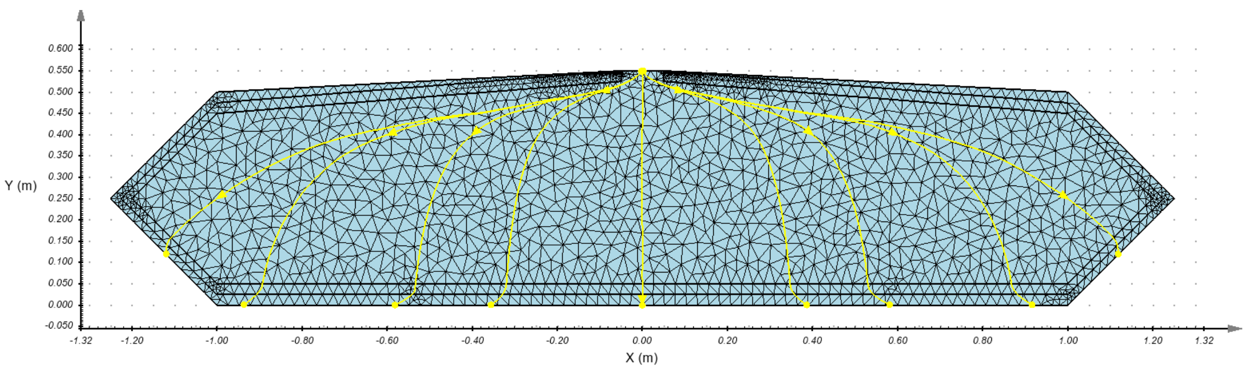

Figure 83. Plaxis Model #8 - Expected Moisture Flow.

Model #9 in Figure 84 shows a second model displayed for moisture flow at the end of each week prior to a second pumping into the system. The results illustrate the AMD slurry flows from the filter cake region up to the input port and flows through GT500 region before flowing out of the system at the bottom. This output creates a problem in the Plaxis model because it simulates that the moisture will flow inwards and around the GT500 fabrics outline. The goal of the model is to only allow moisture to flow out of the system once it flows through the GT500 fabric.

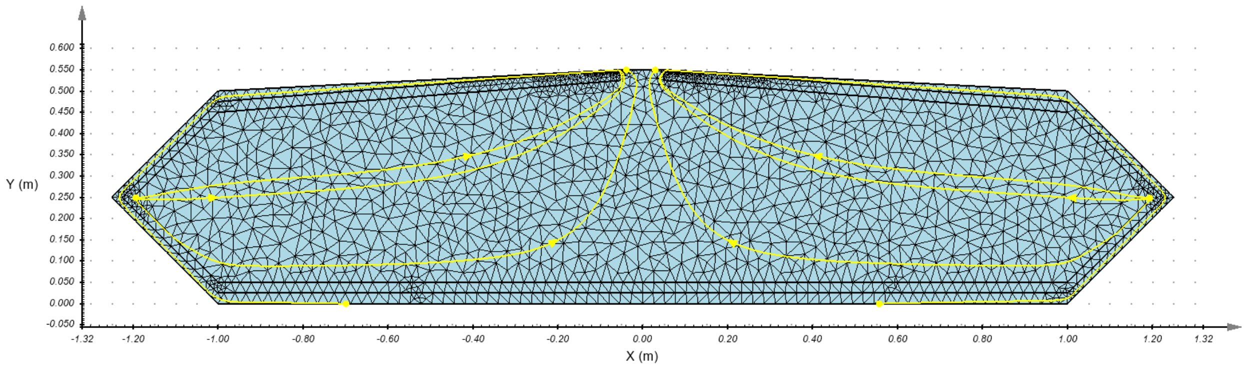

Figure 84. Plaxis Model #8 - Unusal Moisture Flow.

Field-scale testing: Hanging Bag Tests (Test Set 1)

The major results that were reported for Test Set 1 were the Time (d), Bag Mass (kg), Normalized Change in Bag Mass (%), Total Solids Content (%), and Normalized Change in Gravimetric Moisture Content (%). Typical sample data reduction is presented in Table 32 and Table 33.

Table 32. Test Set 1 Data Collection for HB-A, Bag Mass.

Last Filling End	7/21/2022 10:57:15			
Time	**Time (hr)**	**Time (d)**	**BM (kg)**	**Change in BM%**
7/22/2022 18:58	32	1	15.900	0.00%
7/23/2022 18:00	55	2	14.650	7.86%
7/24/2022 19:07	80	3	13.952	12.25%
7/30/2022 12:48	217	9	12.120	23.77%
8/10/2022 16:14	485	20	9.638	39.38%
8/21/2022 14:14	747	31	7.468	53.03%
8/31/2022 16:21	989	41	6.030	62.08%
9/16/2022 14:46	1371	57	4.012	74.77%
9/28/2022 14:38	1659	69	2.944	81.48%

Table 33. Test Set 1 Data Collection for HB-A, Total Solids Content and Gravimetric Moisture Content.

Last Filling End	7/21/2022 10:57:15								
Sample #	**1**	**2**	**3**	**4**	**5**	**6**	**7**	**8**	**9**
Day	7/22	7/23	7/23	7/24	8/3	8/21	8/26	9/16	9/28
Time	19:08	8:47	18:04	9:24	16:51	16:26	18:02	15:01	15:01
Time (hr)	32	45	55	70	317	749	871	1372	1660
Time (d)	1	1	2	2	13	31	36	57	69
Tin (g)	14.04	13.88	13.82	13.76	13.83	13.83	13.84	13.82	13.82
Tin + Sludge (g)	29.55	23.23	19.96	19.71	20.72	16.89	17.12	20.99	17.54
Dry Tin + Sludge (g)	14.67	14.29	14.12	14.05	14.32	14.13	14.20	14.95	15.14
W_w	14.88	8.94	5.84	5.66	6.40	2.76	2.92	6.04	2.40
W_s	0.63	0.41	0.30	0.29	0.49	0.30	0.36	1.13	1.32
$TS_{\%}$	4.06	4.39	4.89	4.87	7.11	9.80	10.98	15.76	35.48
$W_{w\%}$	95.94	95.61	95.11	95.13	92.89	90.20	89.02	84.24	64.52
Change in $W_{w\%}$	-	0.32	0.82	0.81	3.05	5.74	6.91	11.70	31.42

Experimentation Results

For Test Set 1 the results are illustrated in Table 34 through Table 38 and Figure 85. Notable numbered observations were made for the table or figure of interest, followed by the table or figure of interest or a direction to the table or figure of interest. Bag HB-C generally outperformed HB-A in dewaterability measures but not to the extent that HB-A did. Therefore, dewatering comparisons are primarily made between HB-A and HB-C. Only the Total Solids Content (%) vs Time (d) plot for HB-A, HB-B, and HB-C is discussed here. The Normalized Change in Gravimetric Moisture Content (%) and Normalized Change in Bag Mass (%) vs Time (d) plots for HB-A, HB-B, and HB-C can be found in section Test Set 1 (HBTs) of the Appendices.

The maximum difference in Percent Change in Bag Mass between HB-B and HB-A was 0.56%. This occurred at 20 days after the timer was started.

The difference in Percent Change in Bag Mass between HB-C and HB-A at 20 days after the timer was started was 2.35% (see Table 34).

Table 34. Test Set 1 Results at Maximum Difference in Air Dried Bag Mass between HB-B and HB-A.

Bag ID	**Time**	**Time (hr)**	**Time (d)**	**BM (kg)**	**Change in $BM_{\%}$**
HB-A	8/10/2022 16:14	485	20	9.638	39.38%
HB-B	8/10/2022 16:15	485	20	9.244	39.94%
HB-C	8/10/2022 16:15	485	20	10.736	41.73%

A difference in 0.22% Change in Bag Mass between HB-B and HB-A occurred 36 days after timer start. The gap in the difference in Percent Change in Bag Mass between HB-B and HB-A had narrowed by this point, indicating that initial intimate contact loss could have occurred sometime between 20 and 36 days after the timer was started, even though it was officially confirmed by 40 days after the timer was started (see Table 35).

HB-C had regressed by this point to have a lower Percent Change in Bag Mass than HB-A of 0.39% (see Table 35) and performance of this nature remained similar for the rest of the experiment.

Table 35. Test Set 1 Results at Final Reading Before Observed Intimate Contact Loss, Bag Mass.

Bag ID	Time	Time (hr)	Time (d)	BM (kg)	Change in $BM_{\%}$
HB-A	8/26/2022 17:56	870	36	6.696	57.89%
HB-B	8/26/2022 17:57	870	36	6.448	58.11%
HB-C	8/26/2022 17:58	870	36	7.830	57.50%

A difference in 0.15% Change in Bag Mass between HB-B and HB-A occurred 69 days after the timer start and the gap in Percent Change in Bag Mass between HB-B and HB-A had narrowed further by this point (see Table 36).

Table 36. Test Set 1 Results at Final Reading, Bag Mass.

Bag ID	Time	Time (hr)	Time (d)	BM (kg)	Change in $BM_{\%}$
HB-A	9/28/2022 14:38	1659	69	2.944	81.48%
HB-B	9/28/2022 14:38	1659	69	2.828	81.63%
HB-C	9/28/2022 14:38	1659	69	3.516	80.92%

The maximum difference of 2.92% Total Solids Content and 2.69% Change in Gravimetric Moisture Content between HB-B and HB-A over the duration of the test occurred 36 days after the timer was started (see Table 37).

A difference of 0.65% Total Solids Content and 1.25% Change in Gravimetric Moisture Content between HB-C and HB-A occurred 36 days after the timer was started. This was roughly 4 days prior to initial intimate contact loss being observed (see Table 37).

Table 37. Test Set 1 Results at Final Reading Before Observed Intimate Contact Loss, Total Solids Content and Gravimetric Moisture Content.

Bag ID	HB-A	HB-B	HB-C
Time	8/26/2022 18:02	8/26/2022 18:02	8/26/2022 18:02
Time (hr)	871	871	871
Time (d)	36	36	36
$TS_{\%}$	10.98%	13.90%	11.63%
Change in $W_{w\%}$	6.91%	9.60%	8.16%

By 69 days after the timer was started, HB-A had overtaken HB-B after initial intimate contact loss, with the difference being 10.72% Change in Gravimetric Moisture Content. However, the results relevant to the findings of this study were confined to dewatering behavior of AMD sludge that maintained intimate contact with internal drainage media, as AMD sludge dewatering behavior beyond the point of intimate contact loss of AMD sludge to internal drainage media did not allow for comparison to a standard. Therefore, findings and results beyond this point in the document focused more on AMD sludge dewatering behavior at or before observed intimate contact loss (see Table 38).

Table 38. Test Set 1 Results at Final Reading, Total Solids Content and Gravimetric Moisture Content.

Bag ID	HB-A	HB-B	HB-C
Time	9/28/2022 15:01	9/28/2022 15:01	9/28/2022 15:01
Time (hr)	1660	1660	1660
Time (d)	69	69	69
$TS_{\%}$	35.48%	25.00%	24.84%
Change in $W_{w\%}$	31.42%	20.70%	21.37%

It was observed that there was preliminary intimate contact loss between Day 36 and Day 57 of the test in all three bags (see Figure 85). Immediately following the observation of intimate contact loss, the compression technique was applied identically to each bag to restore intimate contact, with no observed impact on restoring intimate contact.

By Day 69, significant loss of intimate contact of AMD sludge with the drainage media and cohesion of sludge was observed in all three bags and the test concluded (see Figure 85).

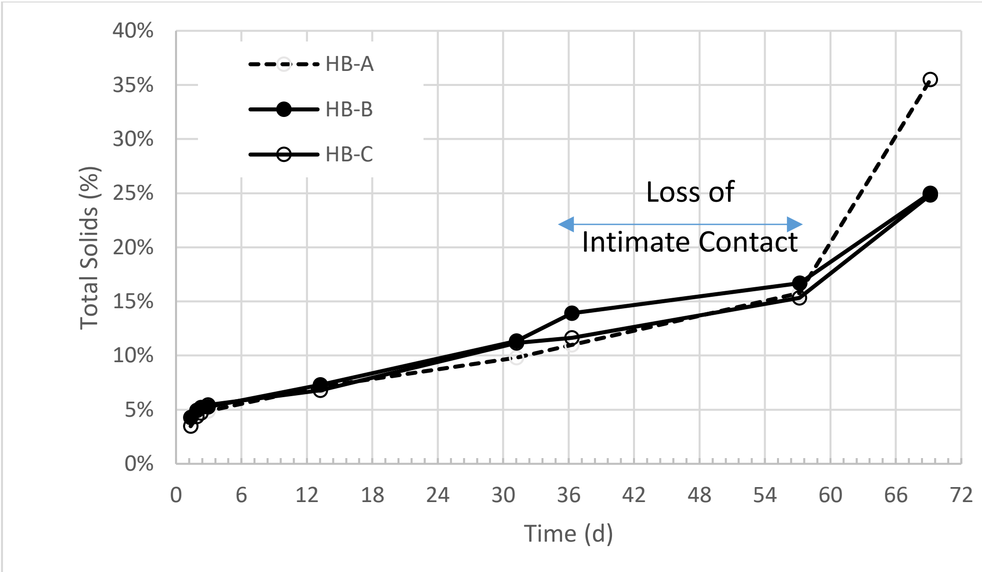

Figure 85. Total Solids Content (%) vs Time (d) for HB-A, HB-B, and HB-C.

Field-scale testing: Hanging Bag Tests (Test Set 2)

<u>Sample Data</u>

The major results that were reported for Test Set 2 were the Time (d), Bag Mass (kg), Normalized Change in Bag Mass (%), Total Solids Content (%), and Normalized Change in Gravimetric Moisture Content (%). Typical sample data reduction is presented in Table 39 and Table 40.

Table 39. Test Set 2 Data Collection for HB#1, Bag Mass.

Return to Campus	11/9/2022 14:45			
Time	**Time (hr)**	**Time (d)**	**BM (kg)**	**Change in $BM_{\%}$**
11/9/2022 15:16	0	0	39.508	0.00%
11/16/2022 19:36	172	7	34.946	11.55%
11/23/2022 14:27	335	13	31.236	20.94%
11/30/2022 12:04	501	20	28.496	27.87%
12/9/2022 16:45	722	30	25.170	36.29%
12/21/2022 9:18	1002	41	21.006	46.83%
1/5/2022 11:32	1364	56	16.958	57.08%
1/11/2022 16:45	1513	63	15.268	61.35%

Table 40. Test Set 2 Data Collection for HB#1, Total Solids Content and Gravimetric Moisture Content.

Return to Campus	11/9/2022 14:45:00				
Sample #	1	2	3	4	5
Day	11/11	11/23	12/15	1/6	2/3
Time	11:57	17:12	16:45	9:15	9:00
Time (hr)	45	338	866	1386	2058
Time (d)	1	14	36	57	85
Empty Tin (g)	13.99	13.99	13.99	13.99	14.00
Tin + Sludge (g)	18.20	17.25	18.12	18.96	27.48
Dry Tin + Sludge (g)	14.34	14.37	14.55	14.80	16.38
W_w	3.86	2.88	3.57	4.16	11.10
W_s	0.35	0.38	0.56	0.81	2.38
$TS_{\%}$	8.31	11.66	13.56	16.30	17.66
$W_{w\%}$	91.69	88.34	86.44	83.70	82.34
Change in $W_{w\%}$	-	3.34	5.25	7.98	9.34

Experimentation Results

For Test Set 2 the results are illustrated in Tables 12 through 16 and Figure 86 through Figure 88. Notable numbered observations were made for the table or figure of interest, followed by the table or figure of interest or a direction to the table or figure of interest. Results reported in this section for the primary bags were also applicable to the duplicate bags (see Test Set 2 (HBTs) in the Appendices). Results for the 25.4 mm radial internal drainage configuration bags (HB#2, 2D, 3, and 3D) were omitted from discussion in this section. The smaller width CCF configurations generally produced data inconclusive of indicating increased dewatering performance with respect to the standard hanging bags due to negligible intimate contact (see Test Set 2 (HBTs) in the Appendices). This observation followed the laboratory testing results discussed previously in Section 5.1.3 Laboratory Monitoring; herein which concluded that sample size and aspect ratios of surface area and AMD sludge mass tends to drive the noticeable changes in dewatering.

A difference in 2.42% Change in Bag Mass between HB#4 and HB#1 was observed 20 days after the timer start (see Table 41). Difference in 1.76% Change in Bag Mass between HB#4 and HB#5 was observed 20 days after the timer start (see Table 41). Both HB#4 and HB#5 outperformed HB#1 with respect to Percent Change in Bag Mass at this time step (see Table 41).

Table 41. Test Set 2 Results at Final Reading Before Observed Intimate Contact Loss, Air Dried Bag Mass (Primary Bags).

Bag ID	Time	Time (hr)	Time (d)	BM (kg)	Change in $BM_{\%}$
HB#1	11/30/2022 12:04	501	20	28.496	27.87%
HB#4	11/30/2022 12:09	501	20	23.212	30.29%
HB#5	11/30/2022 12:10	501	20	26.870	28.53%

The maximum difference in Change in Bag Mass between HB#4 and HB#1 occurred at 41 days after the timer start and was 3.03% (see Table 42). A difference in 1.52% Change in Bag Mass between HB#4 and HB#5 was observed 41 days after timer start (see Table 42). Both HB#4 and HB#5 outperformed HB#1 with respect to Percent Change in Bag Mass at this time step (see Table 42).

Table 42. Test Set 2 Results at Maximum Difference in Air Dried Bag Mass between HB#4 and HB#1 (Primary Bags).

Bag ID	Time	Time (hr)	Time (d)	BM (kg)	Change in $BM_{\%}$
HB#1	12/21/2022 9:18	1002	41	21.006	46.83%
HB#4	12/21/2022 9:21	1002	41	16.698	49.86%
HB#5	12/21/2022 9:22	1002	41	19.42	48.34%

A difference in 2.19% Change in Bag Mass between HB#4 and HB#1 occurred at 63 days after timer start. A difference in 1.45% Change in Bag Mass between HB#4 and HB#5 63 days after timer start. Both HB#4 and HB#5 still outperformed HB#1 with respect to Percent Change in Bag Mass at this time step, but the gap between HB#5 and HB#1 and HB#4 and HB#1 narrowed in later time steps, possibly because of intimate contact loss (see Table 43).

Table 43. Test Set 2 Results at Final Reading, Air Dried Bag Mass (Primary Bags).

Bag ID	Time	Time (hr)	Time (d)	BM (kg)	Change in $BM_{\%}$
HB#1	1/11/2022 16:45	1513	63	15.268	61.35%
HB#4	1/11/2022 16:45	1513	63	12.14	63.54%
HB#5	1/11/2022 16:45	1513	63	13.994	62.78%

A difference in 3.84% Total Solids Content between HB#4 and HB#1 and 2.10% Change in Gravimetric Moisture Content between HB#4 and HB#1 occurred at 36 days after the timer was started. A difference in 3.56% Total Solids Content between HB#5 and HB#1 and 1.28% Change in Gravimetric Moisture Content between HB#5 and HB#1 occurred 36 days after the timer was started. Both HB#4 and HB#5 outperformed HB#1 with respect to Total Solids Content and Change in Gravimetric Moisture Content at this time step, which was closest to observed intimate contact loss (see Table 44).

Table 44. Test Set 2 Results at Final Reading Before Observed Intimate Contact Loss, Total Solids Content and Gravimetric Moisture Content (Primary Bags).

Bag ID	HB#1	HB#4	HB#5
Time	12/15/2022 16:45	12/15/2022 17:15	12/15/2022 17:25
Time (hr)	866	866	866
Time (d)	36	36	36
$TS_{\%}$	13.56%	17.40%	16.12%
Change in $W_{w\%}$	5.25%	7.35%	6.53%

A difference in 2.40% Total Solids Content and 0.86% Change in Gravimetric Moisture Content between CCF (10 cm, x1) and Standard occurred 36 days after the timer was started. This was the maximum difference observed in both Total Solids Content and Change in Gravimetric Moisture Content between CCF (10 cm, x1) and Standard at the time step closest to observed intimate contact loss (see Table 45).

A difference in 1.05% Total Solids Content and 0.29% Change in Gravimetric Moisture Content between CCF (10 cm, x2) and Standard occurred 36 days after the timer was started. This was the maximum difference observed in both Total Solids Content and Change in Gravimetric Moisture Content between CCF (10 cm, x2) and Standard at the time step closest to observed intimate contact loss (see Table 45).

Table 45. Test Set 2 Results at Estimated Final Reading Before Intimate Contact Loss, Total Solids Content and Change in Gravimetric Moisture Content (Average of Configuration Type).

Configuration ID	Standard	CCF (10 cm, x1)	CCF (10 cm, x2)
Time	12/15/2022 16:45	12/15/2022 17:15	12/15/2022 17:25
Time (hr)	866	866	866
Time (d)	36	36	36
$TS_{\%}$	13.51%	15.91%	14.56%
Change in $W_{w\%}$	4.88%	5.74%	5.17%

The plot was normalized to percent change. An observed trend was that the 10 cm CCF configuration of vertical orientation and the 10 cm CCF configuration of "V" orientation slightly outperformed the standard (see Figure 86).

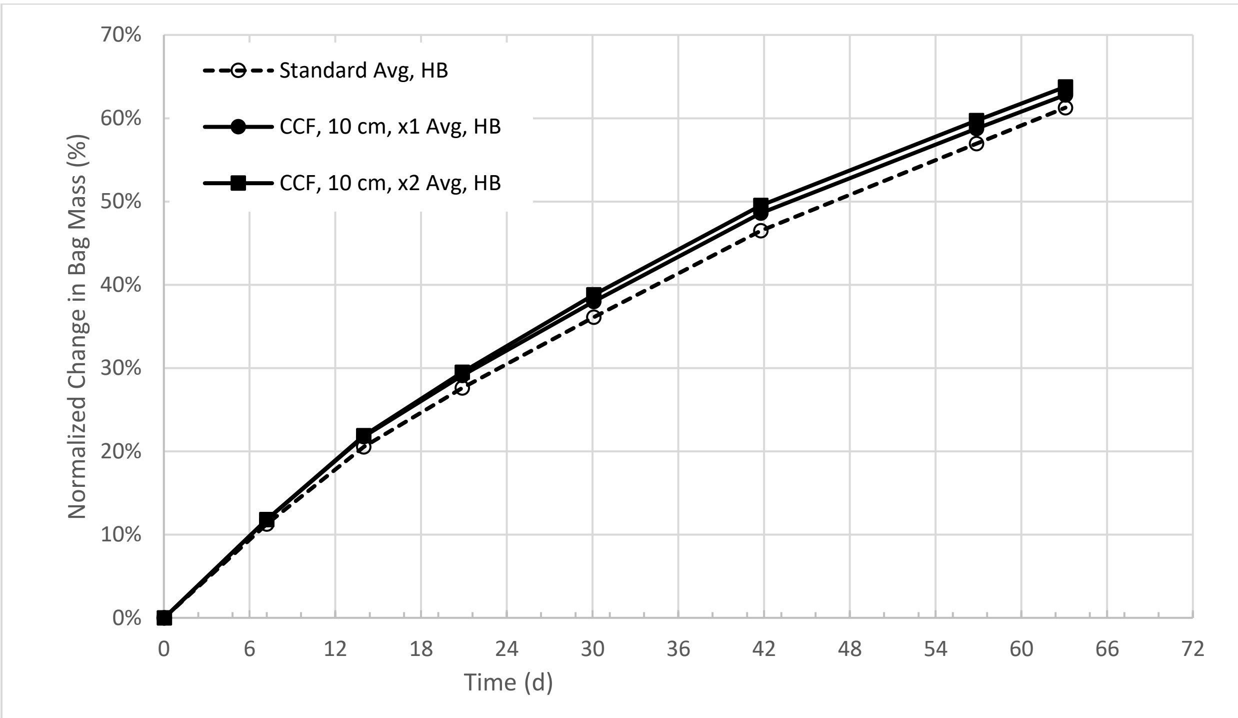

Figure 86. Normalized Change in Bag Mass (%) vs Time (d) for Standard, [CCF, 10 cm, x1], and [CCF, 10 cm, x2] Configuration Average.

The plot was normalized to percent change. An observed trend was that the CCF outperformed the standard at later time steps. The final data point collected at 85 days between the identical 10 cm CCF configurations exhibited a large difference in the normalized change in Gravimetric Moisture Content data (8.21%) compared to earlier time steps of the experiment. This erratic dewatering behavior is attributed to a result of the filter cake having broken up into multiple contracted separate clods of material at this time and only one representative sample being taking from each bag (see Figure 87). This behavior was typical across all configuration type duplicates and variation between duplicates was observed with greater frequency as the experiment progressed.

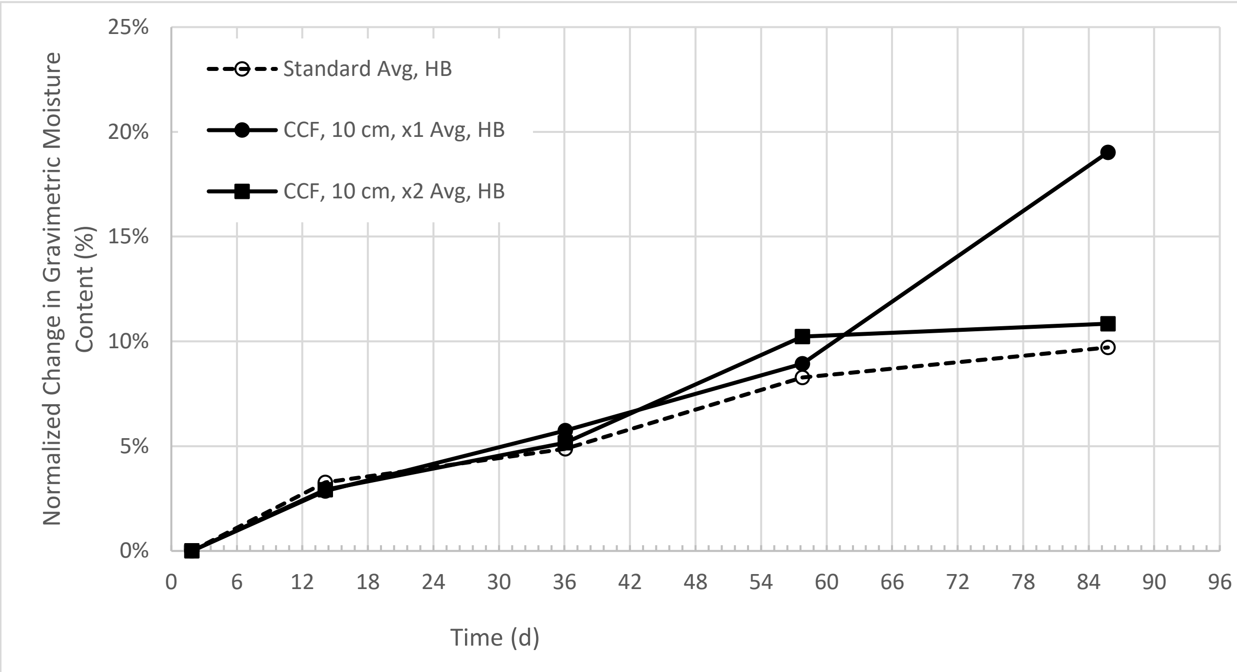

Figure 87. Normalized Change in Gravimetric Moisture Content (%) vs Time (d) for Standard, [CCF, 10 cm, x1], and [CCF, 10 cm, x2] Configuration Average.

An observed trend was that the CCF outperformed the standard at every time step. The final data point for CCF (10 cm, x1) displayed uncharacteristic dewatering behavior compared to earlier time steps (see Figure 88).

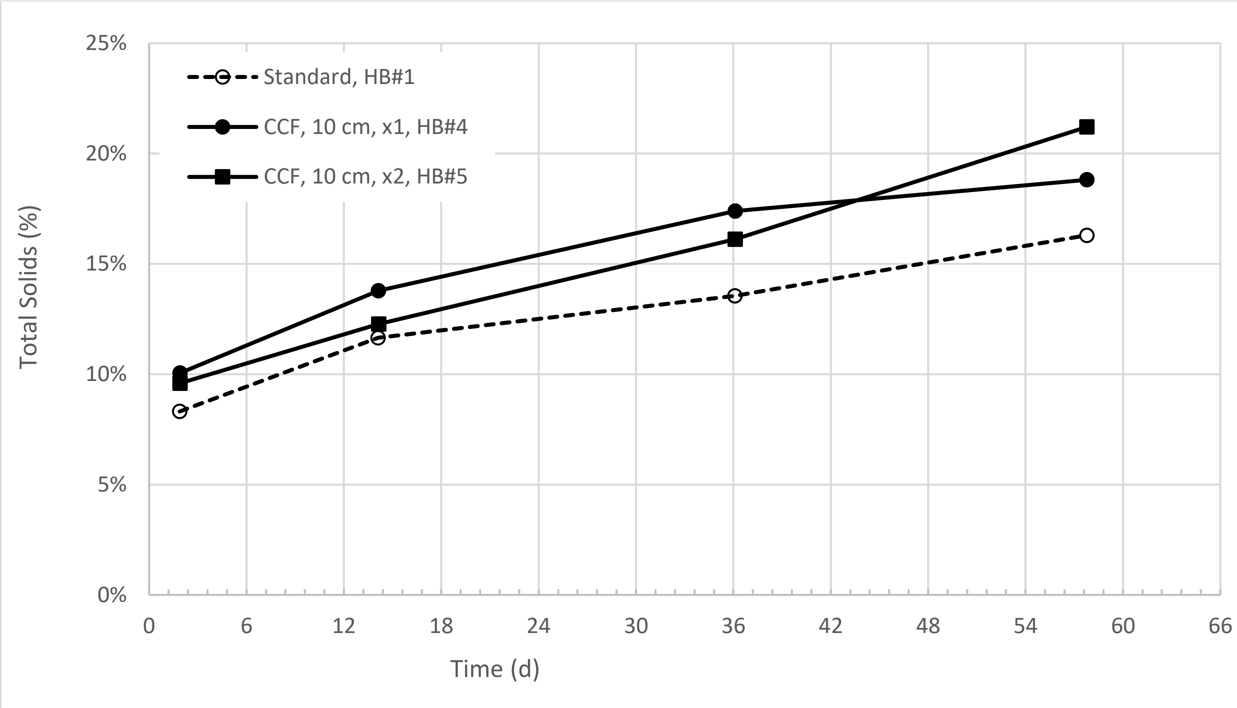

Figure 88. Total Solids Content (%) vs Time (d) for HB#1, HB#4, and HB#5.

Field-scale testing: Geotube Dewatering Tests (Test Set 3)

<u>Sample Data</u>

The major results that were reported for the GDTs were the Time (d), Bag Mass (kg), Normalized Change in Bag Mass (%), Total Solids Content (%), and Normalized Change in Gravimetric Moisture Content (%). Typical sample data reduction is presented in Table 46 and Table 47.

Table 46. Test Set 3 Data Collection for GD#1, Bag Mass.

Return to Campus	11/9/2022 14:45			
Time	**Time (hr)**	**Time (d)**	**BM (kg)**	**Change in $BM_{\%}$**
11/9/2022 20:35	5	0	18.726	0.00%
11/16/2022 19:45	173	7	16.264	13.15%
11/23/2022 15:52	337	14	13.384	28.53%
12/3/2022 19:20	580	24	10.954	41.50%
12/9/2022 16:56	722	30	9.732	48.03%
12/21/2022 11:28	1004	41	7.204	61.53%
1/5/2022 11:32	1364	56	4.642	75.21%
1/11/2022 5:10	1502	62	3.702	80.23%

Table 47. Test Set 3 Data Collection for GD#1, Total Solids Content and Gravimetric Moisture Content.

Return to Campus	11/9/2022 14:45:00			
Sample	1	2	3	4
Day	11/11	11/23	12/9	1/6
Time	15:51	16:48	18:00	10:05
Time (hr)	49	338	723	1387
Time (d)	2	14	30	57
Tin (g)	14.00	14.00	14.00	14.00
Tin + Sludge (g)	28.78	19.38	21.58	26.49
Dry Tin + Sludge (g)	14.95	14.50	14.88	15.81
W_w	13.83	4.88	6.70	10.68
W_s	0.95	0.50	0.88	1.81
$TS_{\%}$	6.43	9.29	11.61	14.49
$W_{w\%}$	93.57	90.71	88.39	85.51
Change in $W_{w\%}$	-	2.87	5.18	8.06

Experimentation Results

For Test Set 3: GDTs the results are illustrated in Table 48 through Table 50 and Figure 89 through Figure 92. Observations from the tables and figures are laid out below. Notable numbered observations were made for the table or figure of interest, followed by the table or figure of interest or a direction to the table or figure of interest. Results reported in this section for the duplicate bags are also applicable to the primary bags (see Test Set 3 (GDTs) in the Appendices). Results for the 25.4 mm radial internal drainage configuration bags (GD#2, 2D, 4, and 4D) were omitted were omitted from discussion in this section. The smaller width PVD and CCF configurations generally produced data inconclusive of indicating increased dewatering performance with respect to the standard hanging bags as due to negligible intimate contact (see Test Set 3 (GDTs) in the Appendices).

A maximum difference prior to observed intimate contact loss of 6.59% Change in Bag Mass between GD#5D and GD#3D occurred 30 days after timer start.The relationship between GD#5D and GD#1D was of similar performance, with a marginal difference of 0.86% Change in Bag Mass between occurring 30 days after timer start. This was the last data point when observed intimate contact loss was identified via the method outlined in the Test Set 3: Performance Testing Procedure (see Table 48).

Table 48: Test Set 3 Results at Estimated Final Reading Before Intimate Contact Loss, Air Dried Bag Mass (Duplicate Bags).

Bag ID	Time	Time (hr)	Time (d)	BM (kg)	Change in $BM_{\%}$
GD#1D	12/9/2022 16:58	722	30	10.146	49.87%
GD#3D	12/9/2022 16:59	722	30	11.792	42.42%
GD#5D	12/9/2022 17:00	722	30	10.392	49.01%

A difference in 0.97% Total Solids Content and 0.67% Change in Gravimetric Moisture Content between GD#5D and GD#3D occurred 30 days after the timer was started. This was the maximum difference in both Total Solids Content and Gravimetric Moisture Content between GD#5D and GD#3D when observed intimate contact loss occurred (see Table 49).

A difference of 0.32% Total Solids Content between GD#5D and GD#1D and 0.48% Change in Gravimetric Moisture Content between GD#1D and GD#5D occurred 30 days after timer start (see Table 49).

Table 49: Test Set 3 Results at Estimated Final Reading Before Intimate Contact Loss, Total Solids Content and Gravimetric Moisture Content (Duplicate Bags).

Bag ID	GD#1D	GD#3D	GD#5D
Time	12/9/2022 18:00	12/9/2022 18:10	12/9/2022 18:20
Time (hr)	723	723	723
Time (d)	30	30	30
$TS_{\%}$	10.97%	10.32%	11.29%
Change in $W_{w\%}$	4.71%	3.56%	4.23%

A difference in 0.56% Total Solids Content and 0.46% Change in Gravimetric Moisture Content between CCF (10 cm) and PVD (10 cm) occurred 30 days after the timer was started. A difference of 0.24% Total Solids Content between Standard and CCF (10 cm) occurred 30 days after timer start. These Total Solids Content and Gravimetric Moisture Content samples were obtained when intimate contact loss was observed (see Table 50).

Table 50: Test Set 3 Results at Estimated Final Reading Before Intimate Contact Loss, Total Solids Content and Gravimetric Moisture Content (Average of Configuration Type).

Configuration ID	Standard	PVD (10 cm)	CCF (10 cm)
Time	12/9/2022 18:00	12/9/2022 18:10	12/9/2022 18:20
Time (hr)	723	723	723
Time (d)	30	30	30
$TS_{\%}$	11.29%	10.49%	11.05%
Change in $W_{w\%}$	4.95%	3.89%	4.35%

The plot was normalized to percent change. The CCF maximum width configuration and standard outperformed the PVD maximum width configuration (see Figure 89).

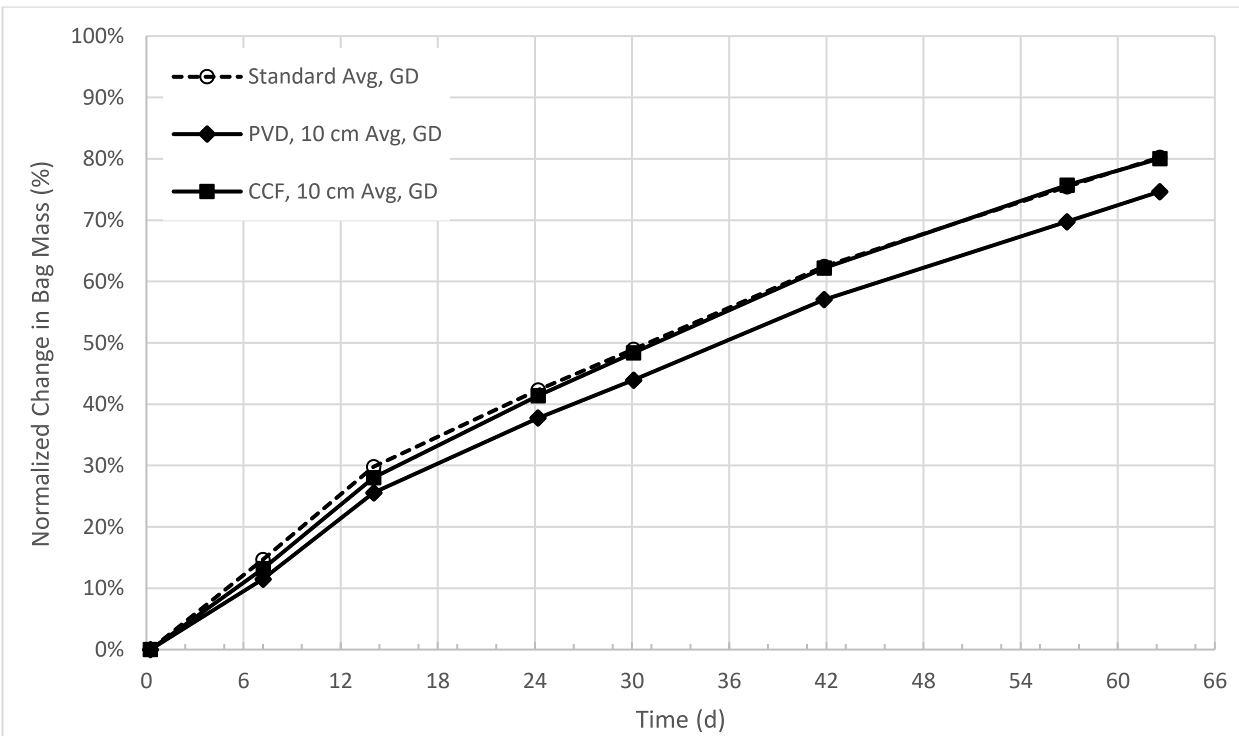

Figure 89: Normalized Change in Bag Mass (%) vs Time (d) for Standard, [PVD, 10 cm], and [CCF, 10 cm] Configuration Average.

The CCF maximum width configuration and standard outperformed the PVD maximum width configuration at later time steps (see Figure 90).

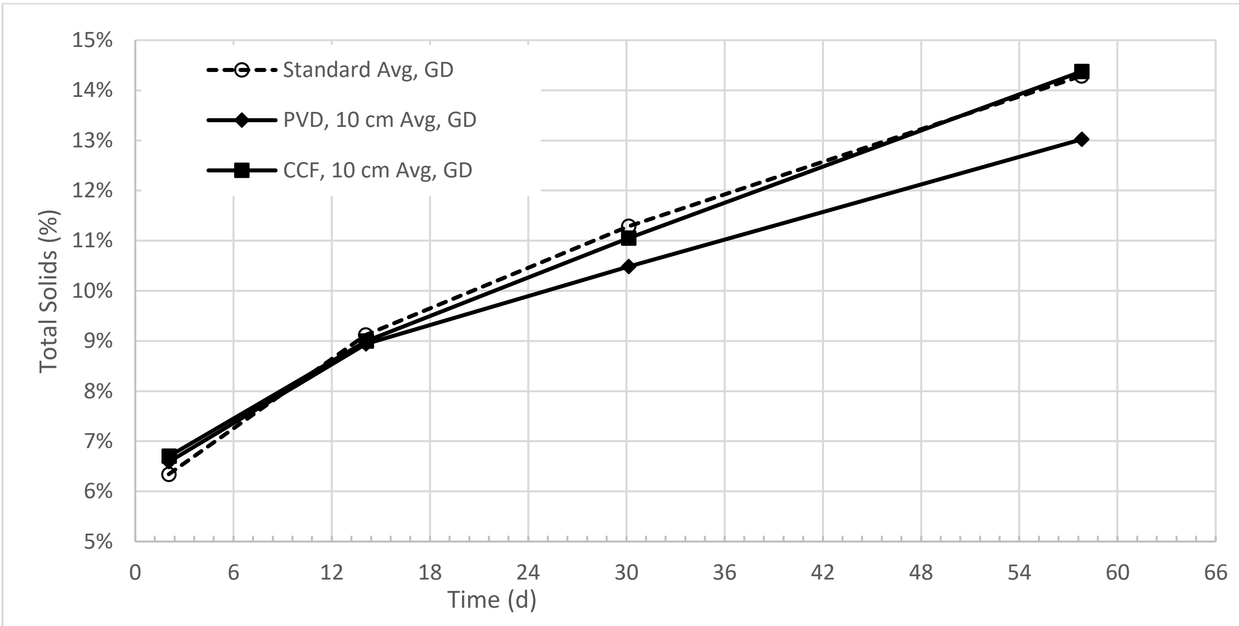

Figure 90: Total Solids Content (%) vs Time (d) for Standard, [PVD, 10 cm], and [CCF, 10 cm] Configuration Average.

The CCF maximum width configuration outperformed standard. The standard outperformed the PVD maximum width configuration (see Figure 91).

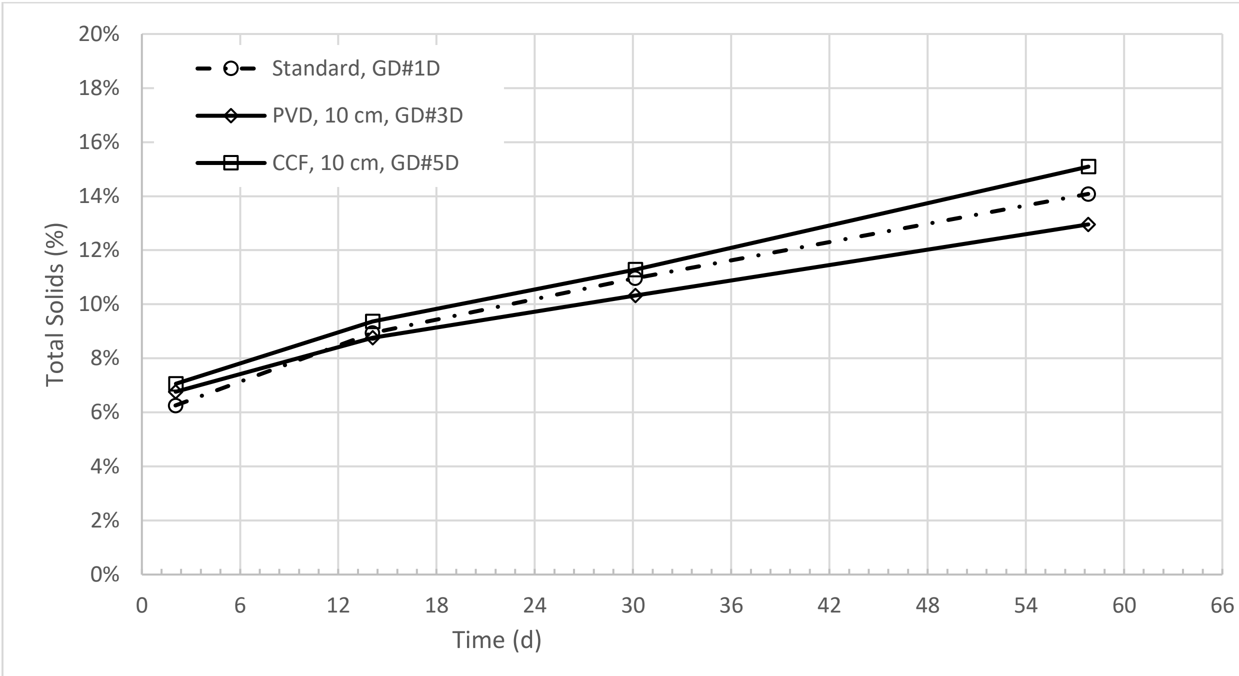

Figure 91: Total Solids Content (%) vs Time (d) for GD#1D, GD#3D, and GD#5D.

The plot was normalized to percent change. CCF and standard performed similarly. Both the CCF maximum width configuration and standard outperformed the PVD maximum width configuration (see Figure 92).

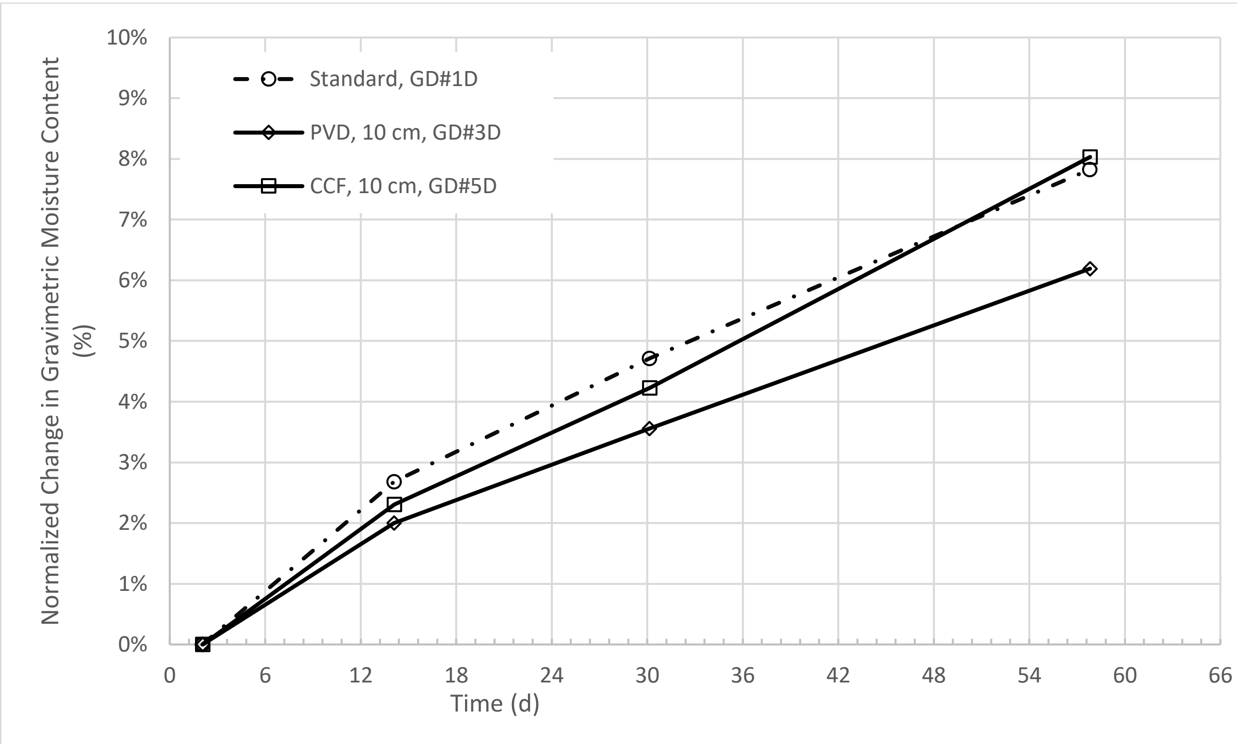

Figure 92: Normalized Change in Gravimetric Moisture Content (%) vs Time (d) for GD#1D, GD#3D, and GD#5D.

Objective #2: Evaluate the use of AMD as soil amendment

Evaluate soil development at a reclaimed site

Field results

Observed weather for the day, May 11th, 2022, felt like a hot sunny day, temperatures ranging from 72 to 80°F with a bluebird sky. The location of the study pit was recorded at 38°48’57.8” N, 80°11’44.5” W using a WGS84 datum. The aspect was measured as 221° and the slope grade was measured at 3%.

Considering the localized topographic features, the pit is located on a hill slope in a slight open depression, within the Appalachian Highlands Province. No flooding, ponding, or standing water on the surface was noted. The land is best described as pasture or grassland area with no vegetation larger than grass within the reclaimed area. The location of the soil pit was close to previous switchgrass study where grasses were still standing and growing.

A large quantity of varying sizes of sandstone rocks, ranging from gravels to cobbles, were observed throughout the entire profile. Four notable horizons were observed: A, B, C, Cg at depths of 0-2”, 2-12”, 12-24”, 24”+ respectively (0-5 cm, 5-30 cm, 30-60 cm, 60+ cm) (Figure 93, Table 51).

Table 51. Profile description.

Horizon	Depth, cm	Description
A	0-5	Very dark brown (7.5YR 2.5/2), clay loam, fine angular blocky structure, many fine roots, 60% subangular rock fragments (bolder to cobbles), neutral (pH 7)
B	5-30.5	Weak red (2.5YR 4/2), sandy loam, medium angular blocky soil structure, few roots, 60% subangular rock fragments (bolder to cobbles), moderately acid (pH 6)
C	30.5-61	Weak red (2.5YR 4/2), sandy loam, coarse angular blocky soil structure, few roots, 60% subangular rock fragments (bolder to cobbles), moderately acid (pH 6)
Cg	61+	Yellowish brown (10YR 5/8), sandy loam, coarse angular blocky soil structure, few roots, 60% subangular rock fragments (bolder to cobbles), moderately acid (pH 6), redoximorphic features and mottling visible N5 (5GY 5/1), major increase in soil saturation

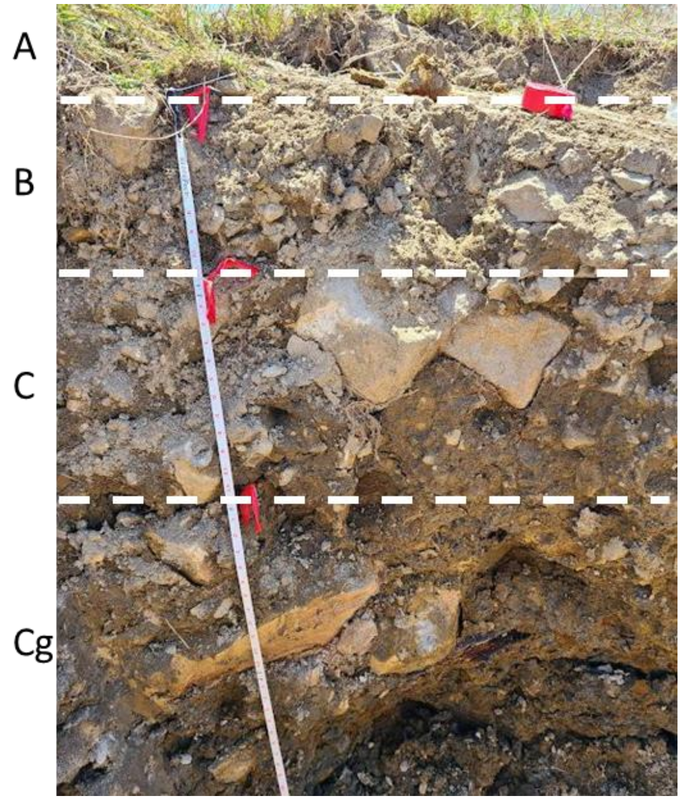

Figure 93. Observed soil horizons.

Hydraulic conductivity testing resulted in a range of values from 3.5 x 10^{-4} to 3.9 x 10^{-4} in/hr (9 x 10^{-4} to 1 x 10^{-3} cm/hr) (Table 52). All recorded values fell below the saturated hydraulic conductivity (K_{SAT}) classification of Very Low (Schoeneberger et al. 2012).

Table 52. Hydraulic Conductivity from Infiltrometer Tests.

Test Number	Hydraulic Conductivity (K_{SAT}) [cm/hr]
1	9.63 x 10^{-4}
2	2.76 x 10^{-3}
3	4.62 x 10^{-4}
4	1.85 x 10^{-3}

The median particle size for topsoil was 0.035 in (0.9 mm), A horizon was 0.098 in (2.5 mm), B horizon was 0.12 in (3 mm), and C horizon was 0.20 in (5 mm). The smallest recorded particle size 0.003 in (0.075 mm) marks the separation between fine and coarse grains and no soil sample was comprised of more than 7% fines. These results show that sampled soils are in a dual class well graded sand range.

Sludge characterization

Sludge was characterized for six locations (Table 53). Parameter concentrations were consistently less than the detection limit. A second VMS sample was collected and analyzed after the high concentration of lead was determined; however the second sample indicated that lead concentrations did not meet the detection limit. This result highlights the variability of sludge from a single geobag. When considering the values at half the detection limit, the regulatory limit of selenium was exceeded for the open air cell at OMEGA. All other values were within the limit, but further testing should be considered. Further discussion is in following sections.

Table 53. AMD sludge characterization results; bolded values are measured concentrations and all other values are reported as half of the detection limit.

Parameters	OMEGA-B	OMEGA -AR	ED-E-CL	ED-T-B	TNTB01	VMS	VMS-B
Arsenic (mg/kg)	4.15	16.85	4.90	3.40	4.1	10.55	4.55
Barium (mg/kg)	4.30	**462**	5.05	3.55	4.25	10.95	4.7
Calcium (mg/kg)	**16800**	**179000**	**67000**	**20700**	**16800**	**9690**	**6520**
Chromium (mg/kg)	4.40	17.80	5.15	3.60	4.35	11.15	4.8
Lead (mg/kg)	3.65	14.75	4.30	3.00	3.6	**1310**	4
Selenium (mg/kg)	7.95	32.30	9.35	6.55	7.9	20.3	8.7
Silver (mg/kg)	3.20	12.95	3.75	2.60	3.15	8.15	3.5
Mercury (mg/kg)	0.07	0.29	0.08	0.06	0.07	0.18	0.15
Moisture (%)	**93.3**	**98.4**	**94.2**	**91.9**	**93.3**	**94.8**	**93.7**

Complete a small-scale growth study

Groundcover

The treatments presented groundcover results varying from 14.6% (50S50T D) to 70.1% (50S50T A). The samples composed of 100% topsoil (100T) presented the best weekly average ground cover results during the study. There was one exception during week 2 when the treatment 30S70T had the highest ground cover on average (= 29.46%) (Figure 94).

Differences were observed in one of the 50% sludge samples (50S50T D) since week one, potentially due to errors in the mixing process. This mixture presented a constant-saturated condition with low permeability throughout the study. It was observed that the water would remain pooled after watering for more time than the other samples. This constantly-submerged sample had a ground cover value 78% less than the other 50% sludge samples, on average, by the end of the study.

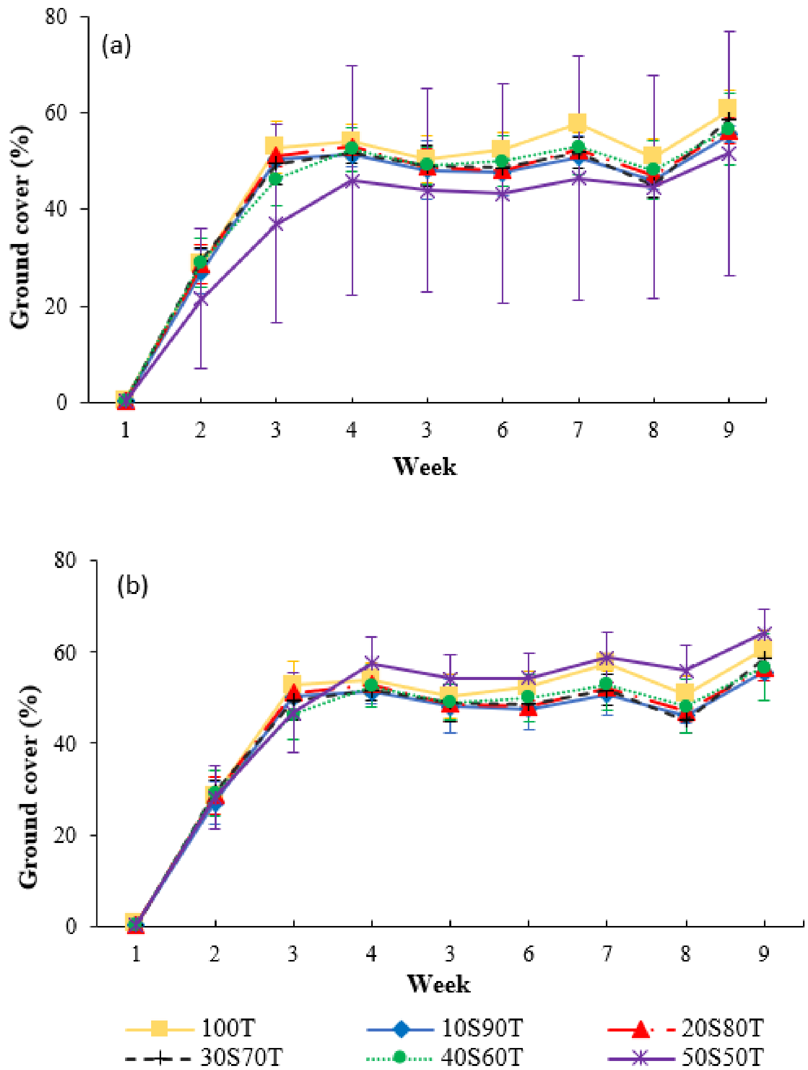

Figure 94. Mean ground cover: (a) all samples, (b) outlier 50S50T D sample removed; error bars denote standard deviation.

As can be observed in Figure 94a, this outlier lowered the mean ground cover of the 50S50T mixtures, resulting in the lowest mean ground cover during the study. However, if the sample 50S50T D was removed, the mixtures with 50% sludge would show the greatest mean ground cover analysis, exceeding all mixtures for weeks 4 to 9 (Figure 94b).

The ground cover data for week 9 presented a normal distribution when the results for treatment 50S50T D were excluded. On Figure 95, the letters *a* and *b* above plot connect the similar treatments: matching letters indicate that the treatments showed to be statistically the same. When the outlier was removed, the 50% sludge treatment was significantly greater than some of the other treatments with sludge (showing differences from 10S90T, 20S80T, and 40S60T), all treatments containing sludge were determined statistically the same as the topsoil control (100T) (Figure 95).

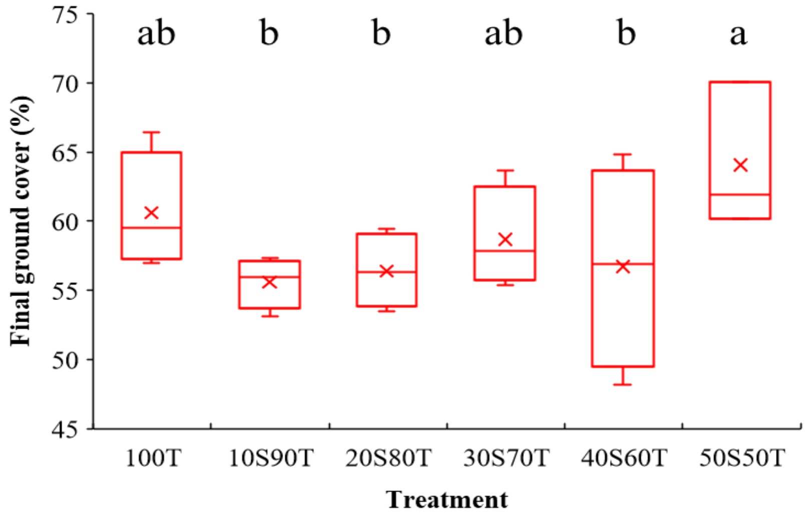

Figure 95. Comparison of final ground cover by treatment (n = 23). Summary values for the tenth percentile, first quartile, median, third quartile, and ninetieth percentile. Treatments not connected by the same letters are significantly different; outlier removed from statistical analysis shown.

<u>Biomass</u>

The total biomass ranged from 1.41 g (50S50T D) to 6.22 g (50S50T C). The 100% treatment (100T) presented total biomass ranging from 4.86 g to 5.62 g. The media with 50% sludge (50S50T) presented the two largest biomasses among all mixtures: 6.22 g (50S50T C) and 6.12 g (50S50T A) (Figure 96).

As previously discussed, 50S50T D had the lowest live biomass (1.41 g) due to excessive water content. The biomass data presented a normal distribution when the 50S50T D mixture was removed. The results of the analysis of variance are presented in Figure 97, where letters a, b, and c above plots connect the statistically proved similar treatments. All treatments with up to 30% sludge had biomass values significantly less than the control (100% topsoil). The 50% sludge treatment had biomass significantly greater than the 100% topsoil treatment.

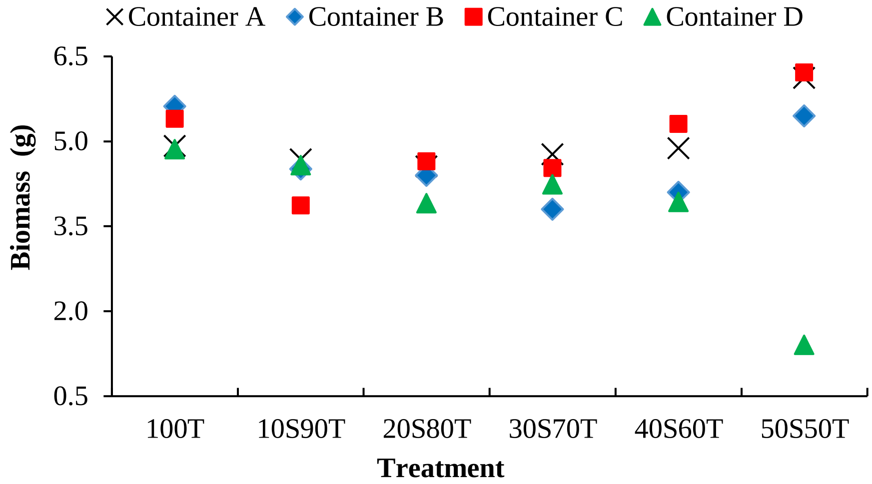

Figure 96. Biomass per treatment per container.

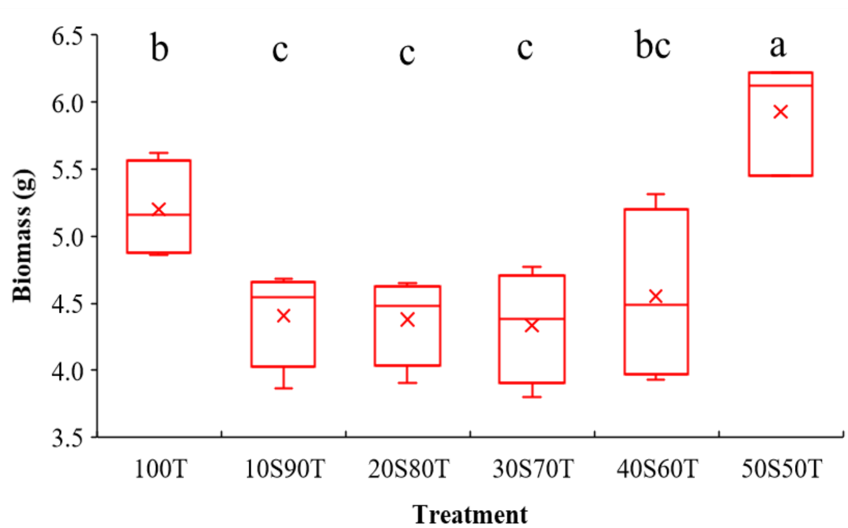

Figure 97. Comparison of biomass by treatment (n = 23). Summary values for the tenth percentile, first quartile, median, third quartile, and ninetieth percentile. Treatments not connected by the same letters are significantly different; outlier removed from statistical analysis show.

Stem height

Stem heights were measured at week 5 for at least 10 stems for each treatment. Generally, the average stem height did not vary substantially among medias (Figure 98). Sample 50S50T A presented the highest average stem height (5.3 cm), and sample 10S90T B presented the lowest average stem height (3.5 cm).

The stem height data set did not present a normal distribution ($p < 0.05$), so a non-parametric analysis (Wilcoxon / Kruskal-Wallis) was used for statistical analysis. As shown by the matching letters a and b in Figure 99, all treatments were found statistically the same as the baseline. However, differences were determined among treatments 10S90T and 30S70T and 50S50T.

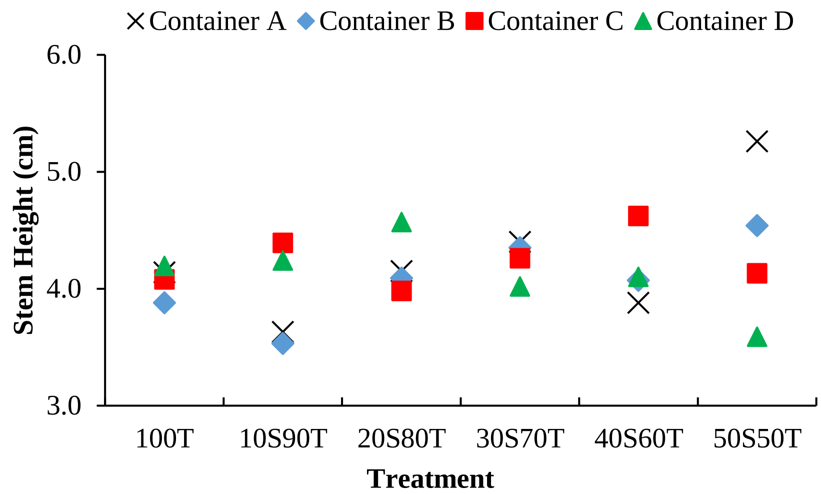

Figure 98. Mean stem height.

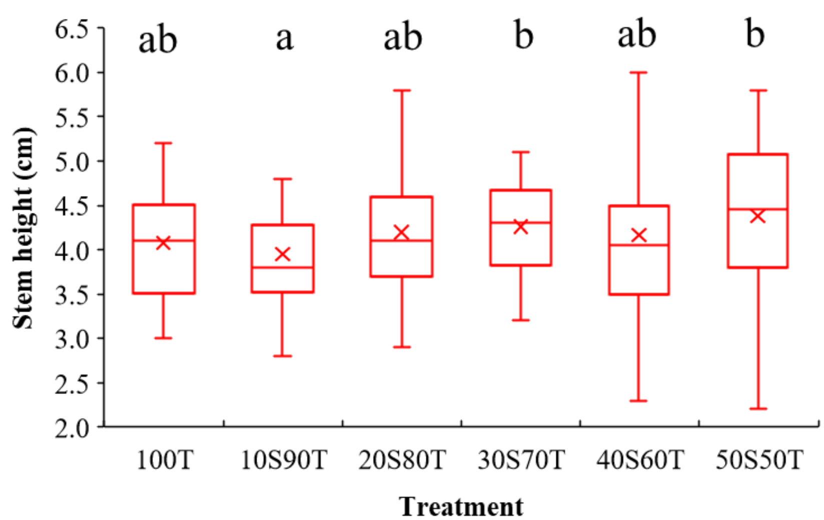

Figure 99. Comparison of stem height by treatment (n = 240). Summary values for the tenth percentile, first quartile, median, third quartile, and ninetieth percentile. Treatments not connected by the same letters are significantly different; outlier removed from statistical analysis shown.

<u>Soil analysis</u>

The results for the soil analysis are presented in Table 54. The treatments presented pH ranging from 6.7 to 7.3 for the duration of the study; the highest pH (7.3) was recorded in the 50% sludge treatment. OM was greater than 38% due to use of commercially available topsoil. EC ranged from 1.1 to 1.3 dS/m at the beginning of study and 0.3 to 0.9 dS/m at end of study. In general, at the end of the study treatments with 40% and 50% sludge presented larger differences from the control than treatments with less sludge.

Table 54. Soil analysis results per treatment before and after growth season. Letters under values denote statistical significance.

Date	Treatment	pH	OM (%)	EC (dS/m)	P (ppm)	K (ppm)	Ca (ppm)	Mg (ppm)
24 September 2021	100T	6.7	42.6	1.1	61.0	540.0	2690.0	490.0
	10S90T	6.8	42.7	1.2	30.0	570.0	3160.0	530.0
	20S80T	7.0	40.3	1.2	5.3	540.0	3680.0	600.0
	30S70T	6.9	41.4	1.3	5.5	560.0	3680.0	580.0
	40S60T	7.0	39.7	1.3	5.7	330.0	3650.0	570.0
	50S50T	7.3	38.0	1.3	0.8	350.0	3120.0	570.0
10 December 2021	100T	6.95 ± 0.18 ab	41.24±1.38 a	0.275 ± 0.04 a	51.5 ± 4.39 a	365 ± 16.58 a	3745 ± 318.79 a	560 ± 47.44 a
	10S90T	7.15 ± 0.11 ab	39.1 ± 1.02 ab	0.3 ± 0 a	23.5 ± 3.20 b	357.5 ± 24.87 a	4210 ± 294.79 ac	647.5 ± 46.03 ab
	20S80T	7.18 ± 0.08 ab	38.98 ± 0.78 ab	0.38 ± 0.04 ac	11.33 ± 2.48 c	352.5 ± 33.45 a	4330 ± 139.10 ac	657.5 ± 29.47 ab
	30S70T	7.08 ± 0.08 ab	39.33 ± 0.65 ab	0.43 ± 0.04 c	10.18 ± 4.46 c	432.50 ± 19.20 b	5112.50 ± 395.81 b	730.0 ± 14.14 bc
	40S60T	7.05 ± 0.09 a	37.675 ± 0.86 b	0.7 ± 0.07 b	5.12 5± 0.36 d	435 ± 16.58 b	4642.5 ± 265.46 bc	685.0 ± 26.93 b
	50S50T	7.25 ± 0.05 b	35.20 ± 1.52 b	0.93 ± 0.18 b	2.83 ± 0.16 e	382.50 ± 25.86 a	5285.00 ± 353.94 b	822.50 ± 57.61 c

Discussion

While AMD sludge is produced in high amounts during the AMD chemical treatment (Wei et al, 2008), the safe handling and disposal is a costly environmental concern. Before this, finding a sustainable application for this material represents a benefit not only by reducing environmental impacts or costs, but by transforming a waste into a valuable material. Besides adsorptive pollution control, microbially facilitated ferric reduction, and catalytic degradation of wastes, AMD land application is another alternative way of disposal that has been studied for this material (Anwar, 2021).

For land application, the AMD sludge must be demonstrated to be non-hazardous as defined by the Resource Conservation and Recovery Act (RCRA) Subtitle C. Intending to identify wastes likely to leach toxic compounds into underground water, EPA developed lab procedures known as Toxicity Characteristic Leaching Procedure (TCLP). Under this procedure, a leachate is created using the considered material and it must comply with specific regulatory levels for 40 different toxic chemicals to be considered safe (EPA, 2015). As TCLP can be expensive, a solid waste can be analyzed by the Rule of 20, where, instead of creating the leachate, the total concentration levels of toxic compounds are defined. The results of the total concentration are divided by 20 to determine the Maximum Theoretical Leachate Concentration (MTLC). If the MTLC is less than the regulatory levels, the sample cannot exhibit the toxicity characteristic. Otherwise, the TCLP should be run (Minnesota PCA, 2011).

All metal concentrations were below the minimum detection limits except for barium (4.62 ppm) and are reported as half of the detection limit (Table 55). Considering the Rule of 20, arsenic, barium, chromium, lad, mercury, and silver meet basic requirements for land application. Selenium concentrations need to be further evaluated; however, concentrations for the sampled sludge were below detection limits. Cadmium was not tested in this study and needs to be considered in the future. It should be noted that AMD sludge characteristics vary by source and the sludge should be tested prior to land application.

Zink (2006) suggested that sludges with low metal concentrations and excess alkalinity may be used to increase soil pH. Presence of acidic soils is a common concern of disturbed sites, but soil pH was not a concern in this small study because commercially available soil was used the substrate combined with the sludge; however, soil pH increased from 6.7 to 7.3 with the addition of 50% sludge (Table 54), providing support that AMD sludge can impact pH.

Table 55. Metal concentration of sludge with regulatory limits.

Metal	Regulatory limit (ppm)	Sludge (ppm)
Arsenic	5.0	*16.85*
Barium	100	4.62
Chromium	5.0	*17.8*
Lead	5.0	*14.75*
Mercury	0.2	*0.29*
Selenium	1.0	*32.30*
Silver	5.0	*12.95*

Note: Italicized values reported as half of the minimum detection limit

This study did not include fertilizer or lime that will likely be considered in field applications. With addition of AMD, levels of P decreased below optimum levels (<15) (AgSource 2022), suggesting that soil test with fertilizer requirements will be important for the implementation of AMD in land application.

General water-pollution-control permits for the National Pollutant Discharge Elimination System (NPDES) require 70% ground cover (USEPA 2007). This metric was reached for only one sample in this small-scale study.

Complete a field study: Fall planting

<u>Field measurements</u>

Grass coverage for the focus of the growth study ranged from 3% to 20%. Average increase in coverage from week to week was calculated at 6%. After the first frost (November 17th), all mixtures except total soil saw a reduction in grass coverage. The 25% AMD mixture was the best performing over the course of the study ending at 30% coverage. Total soil had a grass coverage of 28% (Figure 100).

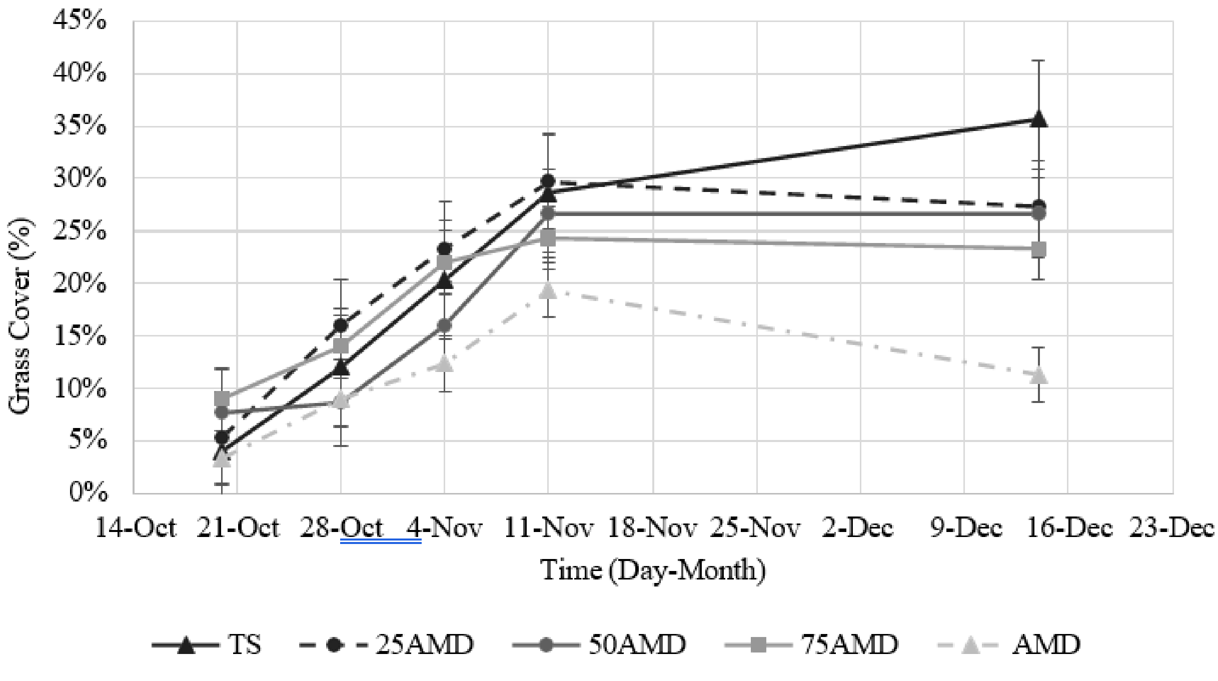

Figure 100. Mean ground cover by treatment.

Ground temperature fluctuations were in direct correlation with air temperature. The plots typically were warmer than the air temperature. However, on November 11th recording was performed during a rain event and the soil temperature read below the recorded temperature for the day (Figure 101).

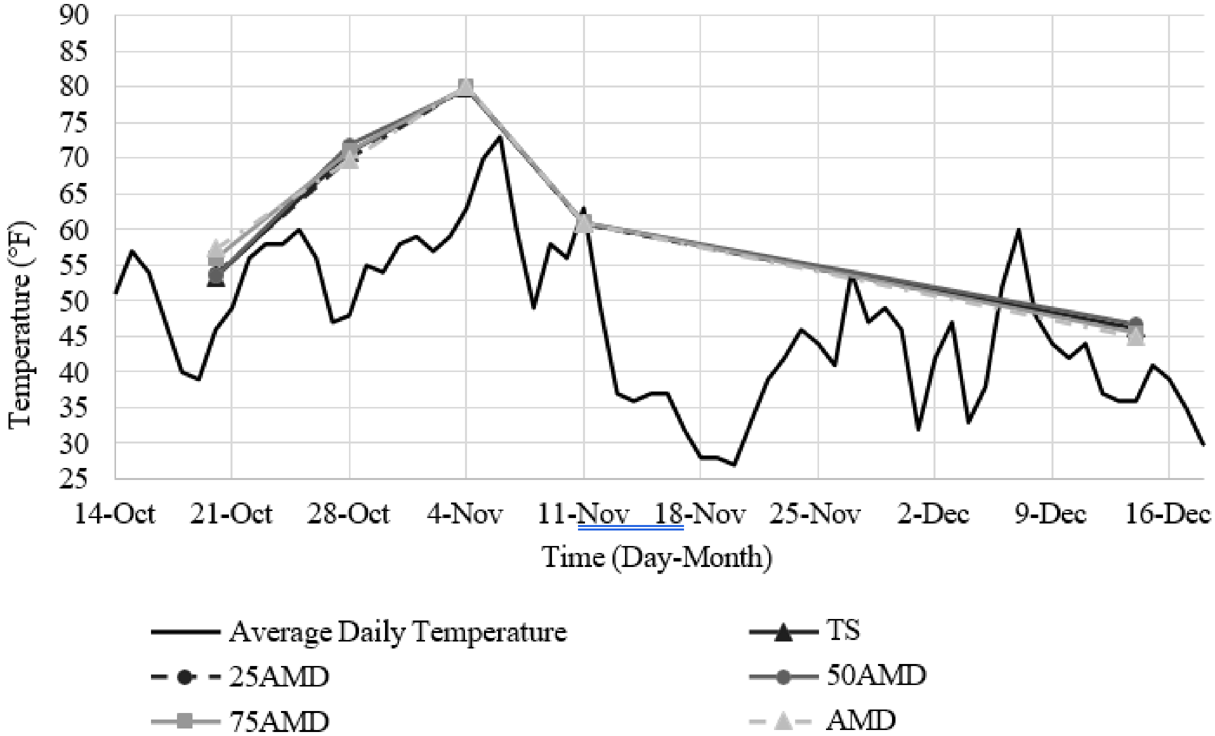

Figure 101. Average soil temperature by mixture compared to average daily temperature. Recorded by NWS Station Located in Morgantown, WV (NOAA 2022b).

Moisture readings for treatments with higher AMD concentrations generally yielded higher moisture contents. Percent moisture readings ranged from 9% to 46%. The lowest moister week after week was the total soils mixture, recorded at the low 9% and a high at 25% (Figure 102).

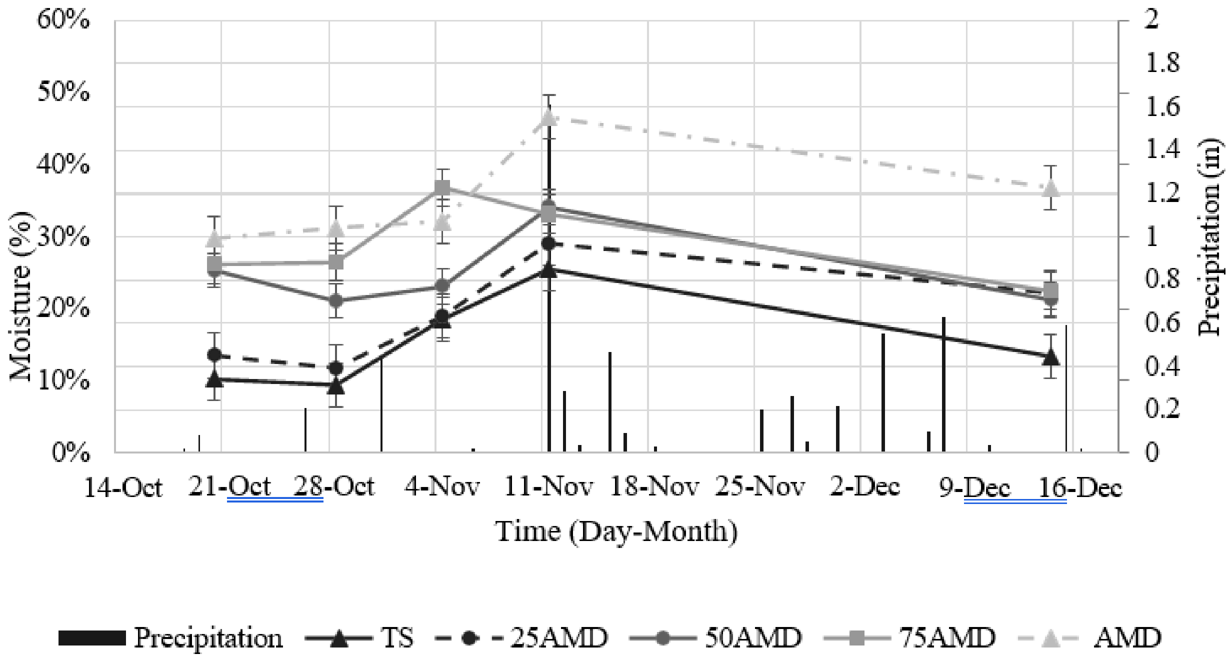

Figure 102. Average soil moisture percentage by mixture.

Average electrical conductivity generally followed the trend of treatments with higher concentrations of AMD showed higher readings. Values ranged from 0.0 to 0.38 mS/cm. Total soil mixture was the lowest values over the study, ranging from 0.0 to 0.06 mS/cm (Figure 103).

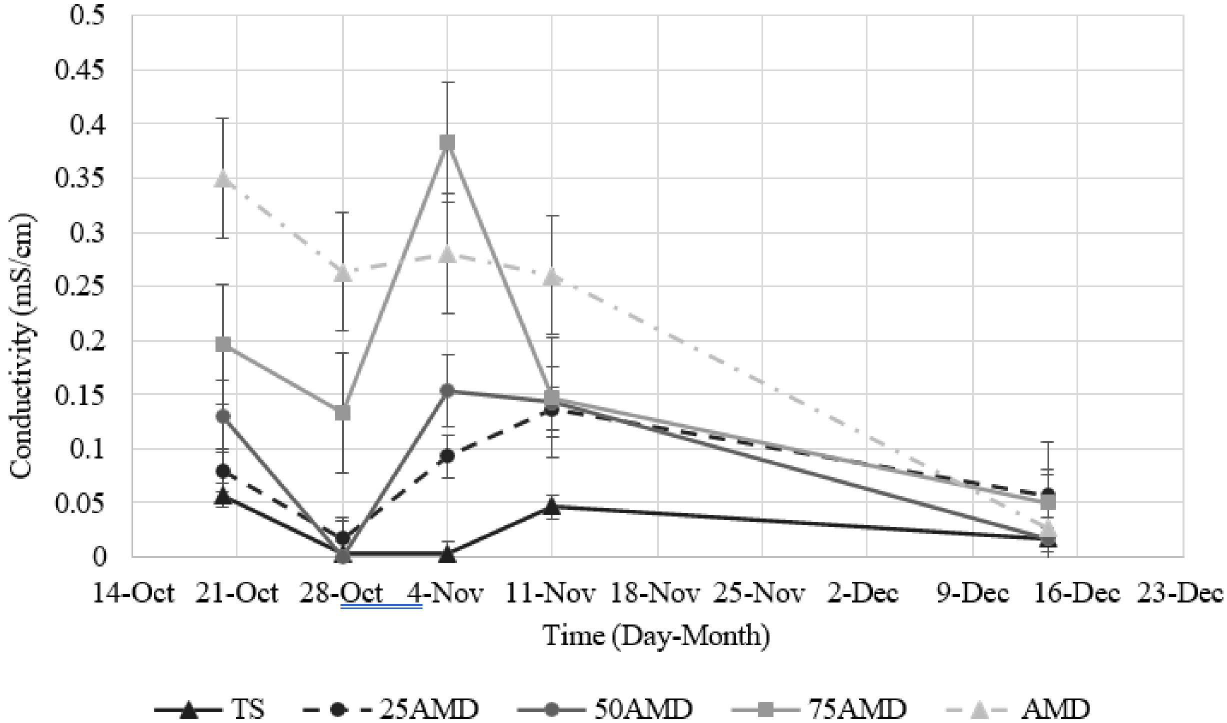

Figure 103. Average conductivity plotted by mixture.

Lab analysis

Results can be seen in the tables below (Table 56, Table 57, Table 58). EPA 6010D tests are reported as half the detection limit if the concentration was not over. Any value over 32.3 ppm was the actual tested value, the rest were reported as half the detection limit.

Table 56. Percent moisture from Pace Analytical SM2540G-2015 testing.

Sludge ID	Moisture (%)
Growth Study	94.8
1	91.9
2	94.2
3	98.4
4	93.3

Table 57. Mineral concentrations from Pace Analytical EPA 6010D testing. (Values reported as half the detection limit in italics).

Sludge ID	Arsenic (ppm)	Barium (ppm)	Chromium (ppm)	Lead (ppm)	Selenium (ppm)	Silver (ppm)
Growth Study	*10.6*	*11.0*	*11.2*	1310	*20.3*	*8.2*
1	*3.4*	*3.6*	*3.6*	*3.0*	*6.6*	*2.6*
2	*4.9*	*5.1*	*5.2*	*4.3*	*9.4*	*3.8*
3	*16.9*	462	*17.8*	*14.8*	*32.3*	*13.0*
4	*4.2*	*4.3*	*4.4*	*3.7*	*8.0*	*3.2*

Table 58. Mercury concentrations from Pace Analytical EPA 7471B testing (Values reported as half the detection limit in italics).

Sludge ID	Mercury (ppm)
Growth Study	*0.18*
1	*0.06*
2	*0.08*
3	*0.29*
4	*0.07*

Discussion

The primary takeaway from the study is that the data shows that AMD does not significantly inhibit grass growth, which allows further research and possible WVDEP implementation.

Within the grass coverage data it was observed that the 25% and 50% AMD mixtures performed better than the only topsoil mixture in the early stages of growth. When comparing growth and moisture data the trend shows that the more AMD within the mixture increases moisture content readings. Moisture retention seemed to lag with the addition of more AMD into the soil matrix (Figure 104). This indicates that AMD seems to act similar to covered soil or a soil with increased organics within the soil matrix. Each of which is a method for keeping more moisture within the sample for vegetation.

The soil pH was more alkaline than expected, which is primarily influenced by the pH of the topsoil coming from the factory at about 8.0 pH. A pH range of 7.5 to 8.1 is within healthy soil ranges and is a good factor for soil health.

Figure 104. Needle structured ice crystals within soil matrix, from December 14th site visit.

Moisture content readings from the sludge confirm the similar extremely high moisture content that is expected from AMD sludge. The electrical conductivity readings were to be expected with values higher in the higher % AMD mixtures. Soil moisture plays a direct role in the measurement of electrical conductivity, where an increase in moisture corelates to an increase in electrical conductivity readings. Electrical conductivity in soils can be valued as the availability of minerals for plant uptake. The values converge in December due to the soil and ground having frozen elements within the matrix. It appears that the water that was held within the AMD sludge froze and expanded, which would directly affect the available water within the soil. That correlation is shown within the moisture data. The freeze thaw degradation of plots did have a noticeable effect and was directly related to the amount of AMD within the soil. The resulting loss of volume would be a concern in larger applications. In the event of a high sludge mixture on an engineered slope, worries of localized or total topsoil failure would be valid. Larger grass coverage and root mass could combat this issue by holding the soil in place.

Soil Samples from each of the mixtures within the growth study were sent to AgSource for agronomic testing. It should be noted that percent organic matter (%OM) should be entirely from the topsoil mix. Nitrogen, phosphorus, and potassium (N, P, K) were all added through the initial 10/10/10 fertilizer application. It appears that only potassium is still readily available within the soil. There were notable concentrations of Mg, Ca, S, Fe & Na. The pH was more alkaline than expected, which is probably due to the topsoil mixture reading at a pH of 8.1 and the availability of calcium within the AMD sludge. The sludge soils had a more favorable pH for grass growth (Table 59). Other notable minerals detected include a high lead (Pb) content found from the total waste analysis within the sludge used for the growth study.

Table 59. Table of sludge characteristic data from AgSource testing.

Parameter	100AMD	75AMD25T	50AMD50T	25AMD75T	100T
OM (%)	14.3	30.2	36.4	41.2	39
N (ppm)	10.9	2.7	2	1.5	2.4
P (ppm)	-	8	17	30	95
K (ppm)	-	501	538	639	732
Mg (ppm)	-	295	278	293	341
Ca (ppm)	-	2777	3003	2895	3728
S (ppm)	-	490	275	135	109
Zn (ppm)	-	15.64	11.74	6.66	7.71
Mn (ppm)	-	4	4.5	9.1	10.4
Cu (ppm)	-	2.4	1.8	1.2	1.3
Fe (ppm)	-	107.8	88.6	80.6	120.3
B (ppm)	-	0.8	0.7	0.7	1.1
pH	7.5	7.5	7.7	7.7	8.1
Soluble Salts (mmhos/cm)	-	1.79	1.11	0.69	0.66
Na (ppm)	-	177	104	96	81
CEC	-	18.4	19.2	19	23.7

Nitrogen values were within reasonable values for soils. Phosphorus rates ranged from low to high with the increase of topsoil in the mixture. This would be due to the topsoil mix containing phosphorous for plant growth. Potassium values tested high across all mixtures. Future recommendations would include not adding fertilizer with K. Magnesium values tested medium. Sulphate (S) tested high and would be a leaching concern. Zinc, Copper, and Magnesium content was sufficient for plant growth (AgSource 2023). Soluble salts were marginal to suitable for plant growth, values >1.0 are considered marginally good for plants (Davis 2001) (Table 59).

The metals content results tested lower than other similar AMD studies (Chi et al. 2021; Ko et al. 2015; Sun et al. 2014; and Demers et al. 2016). This and the variance between the 5 samples tested (Table 57) shows the high variance and site specificness to AMD. Differences in treatment between studies would also lead to this variation. The lead content is an issue that would need to be retested to check for possible errors. High lead content would prevent EPA compliance for land applications at the tested concentrations (Davis 2001). Concerns of leaching for the higher metal and mineral contents became apparent with this study. Natural soil lead concentrations should be <50 ppm and in urban areas often tests around 200 ppm (CDC 2019).

When checking the seed mix for invasive species, Perennial Ryegrass and Kentucky Bluegrass (*Lolium perenne* and *Poa pratensis*) are reported on the invasive plant species list for West Virginia (WVDNR 2014). They are listed on a scale of 2 (moderate) out of a range 1-4 for invasiveness. This is an issue that a combined 16% of the seed mix is moderately invasive to West Virginia. Suggestions to change the grasses to something similar for growth but not invasive would be recommended for the longevity of the biodiversity of West Virginia vegetation.

When checking for the chosen seed mix and seeding date for the study with the WVDEP recommended seeding dates, the seed was planted close to the end of the seeding period. After October 1st the seeds and young seedlings are at a risk of freezing. Freezing of young seeds can damage and kill the grass, which is shown when looking at the decline in grass coverage in the December field visit (WVDEP 2012).

Complete a field study: Spring planting

Results include evaluating the statistical analysis, and the mean values among treatments over the course of the study duration for ground cover, volumetric water content, electrical conductivity, and temperature. Evaluation of biomass statistical analysis was included, along with the statistical analysis that was performed with the results from the saturated media extract report.

Ground cover

Mean ground cover among all treatments that contained topsoil increased from 30% to 60% at the beginning of the study to 60% to 80% at the conclusion of monitoring. The threshold of average 70% ground cover, value required for NPDES construction permit release, was reached by August 23, 2023 (WVDEP, 2016). Mean ground cover for the AMD treatments remained less than 40% throughout the duration of the study (Figure 105), was significantly less than all other treatments when considering only final ground cover (Figure 106), and was significantly less than all other treatments when considering ground cover over the full study duration (Figure 107). Less variability was observed among the other treatments (i.e., TS, 25AMD, 50AMD, and 75AMD). Gound cover for the 75AMD treatment was less than the 25AMD and 50AMD treatments throughout the study period (Figure 105), and this difference was not statistically significant (Figure 106, Figure 107). Similarly, the TS treatment had the greatest ground cover throughout the study (Figure 105), but there were no significant differences in ground cover among TS, 25AMD, and 50AMD (Figure 106, Figure 107).

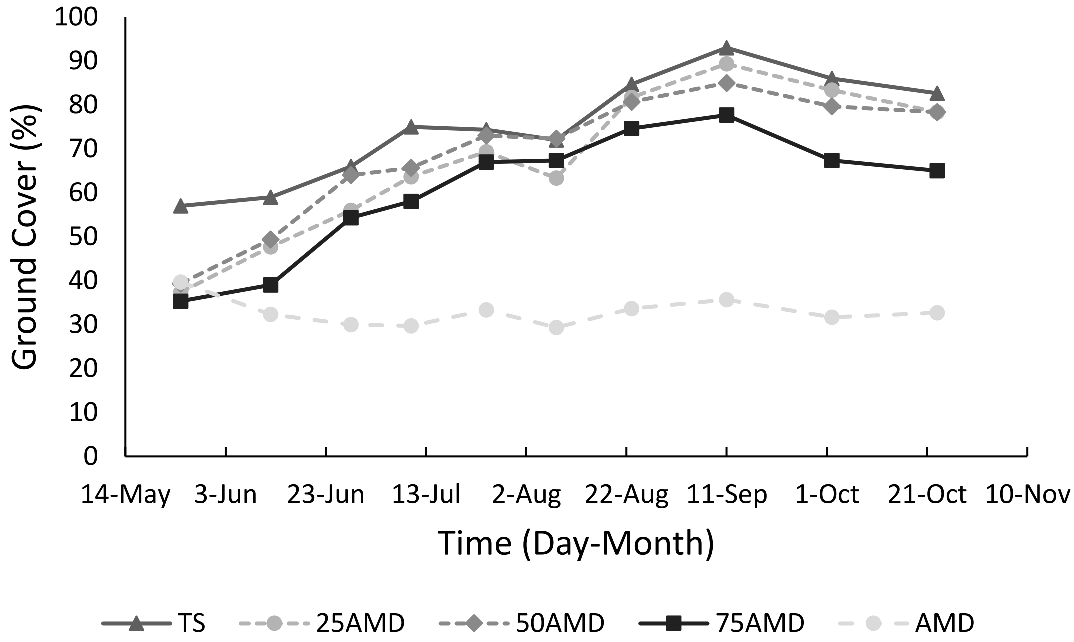

Figure 105. Comparison of mean ground cover among treatments.

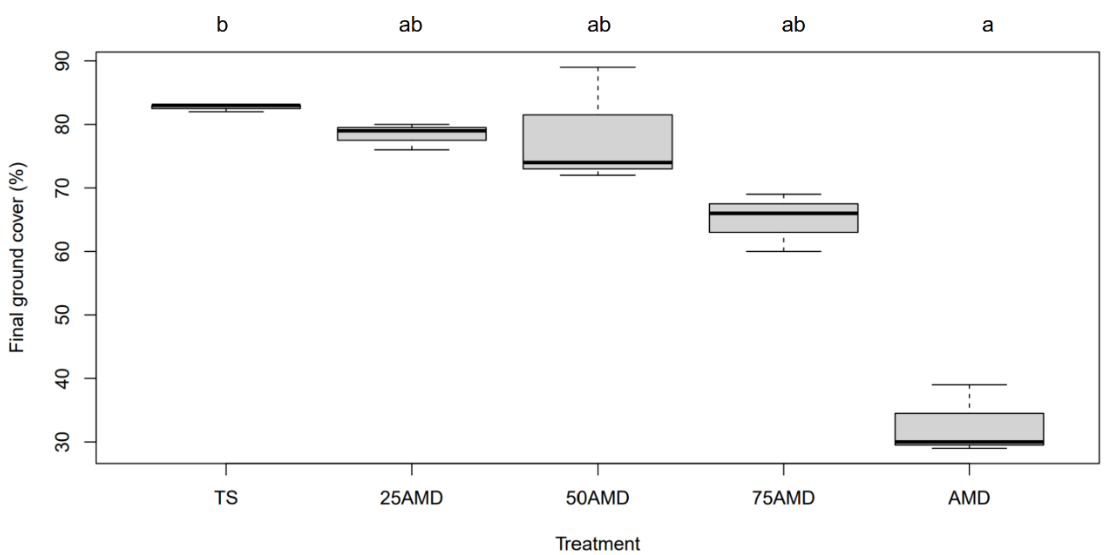

Figure 106. Comparison of final ground cover (n=3, α =0.05).

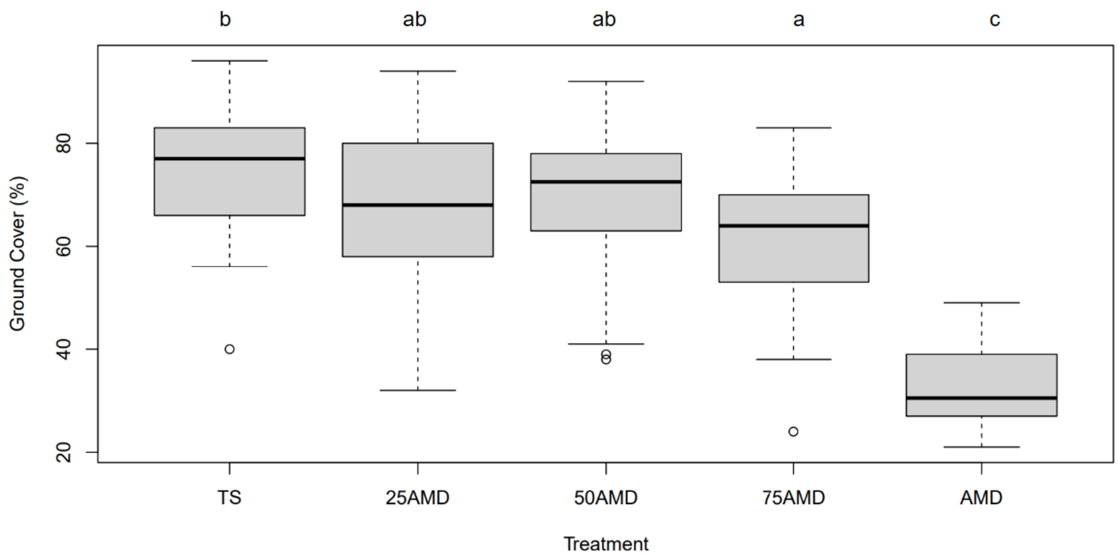

Figure 107. Comparison of all ground cover measurements (n=30, α =0.05).

Volumetric Water Content

Mean soil moisture among all treatments that contained topsoil increased from 6% to 18% at the beginning of the study to 8% to 18% at the conclusion of monitoring. Mean soil moisture for the AMD treatment remained higher than all treatments that contained topsoil throughout the duration of the study (Figure 108), was greater than all other treatments when considering only final ground cover (Figure 109), and was significantly greater than all other treatments when considering soil moisture over the full duration of the study (Figure 110). Final soil moisture for TS, 25AMD, 50AMD, and 75AMD treatments did not show any statistical significance (Figure 109). Likewise for comparing the treatments over the course of the study (Figure 110). AMD treatments had the highest soil moisture throughout the study, but there were no significant differences among TS, 25AMD, 50MAD and 75AMD (Figure 109, Figure 110).

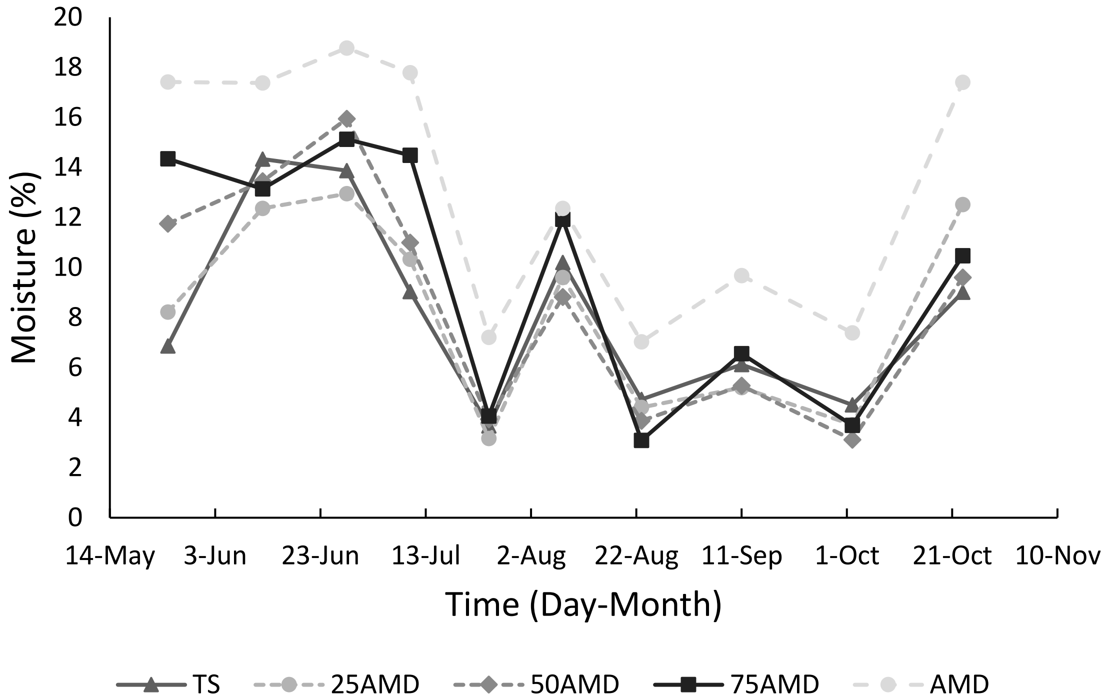

Figure 108. Comparison of mean soil moisture content among treatments.

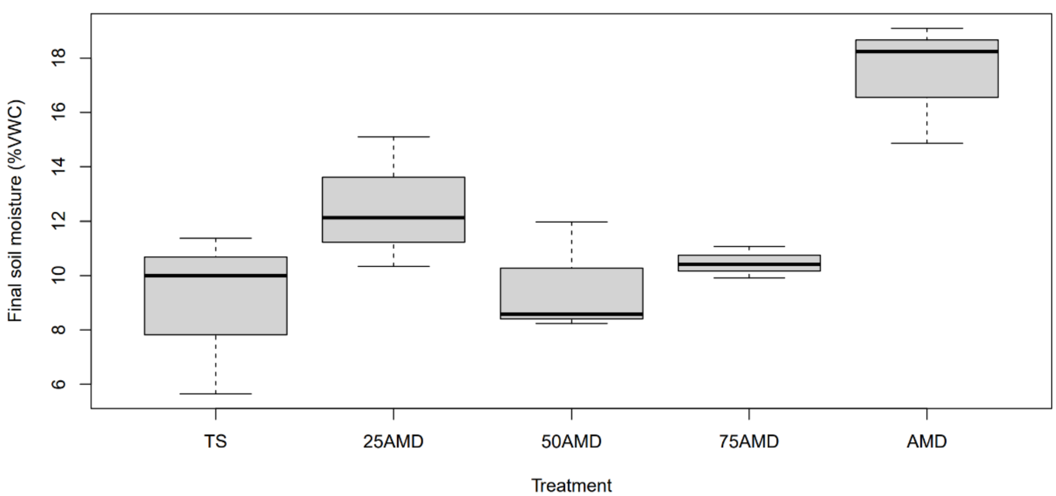

Figure 109. Comparison of final soil moisture (n=3, α =0.05).

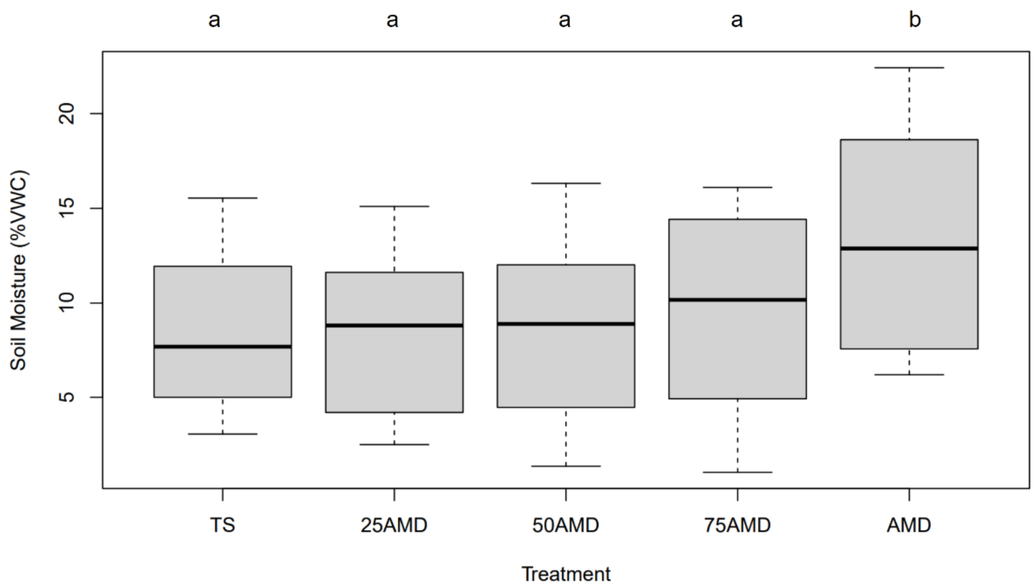

Figure 110. Comparison of soil moisture among treatments (n=30, α =0.05).

Electrical Conductivity

Mean electrical conductivity among all treatments ranged from 0.025-0.25 mS/in at the beginning of the study to 0.025-0.01 mS/in at the conclusion of monitoring. The variability for all the treatments decreased throughout the duration of the study (Figure 111), AMD treatment was the highest considering only final conductivity (Figure 112), and AMD treatment was the highest when considering the full study duration (Figure 113). AMD treatment had the highest electrical conductivity throughout the study period, but there were no significant differences between any of the treatments (Figure 112, Figure 113).

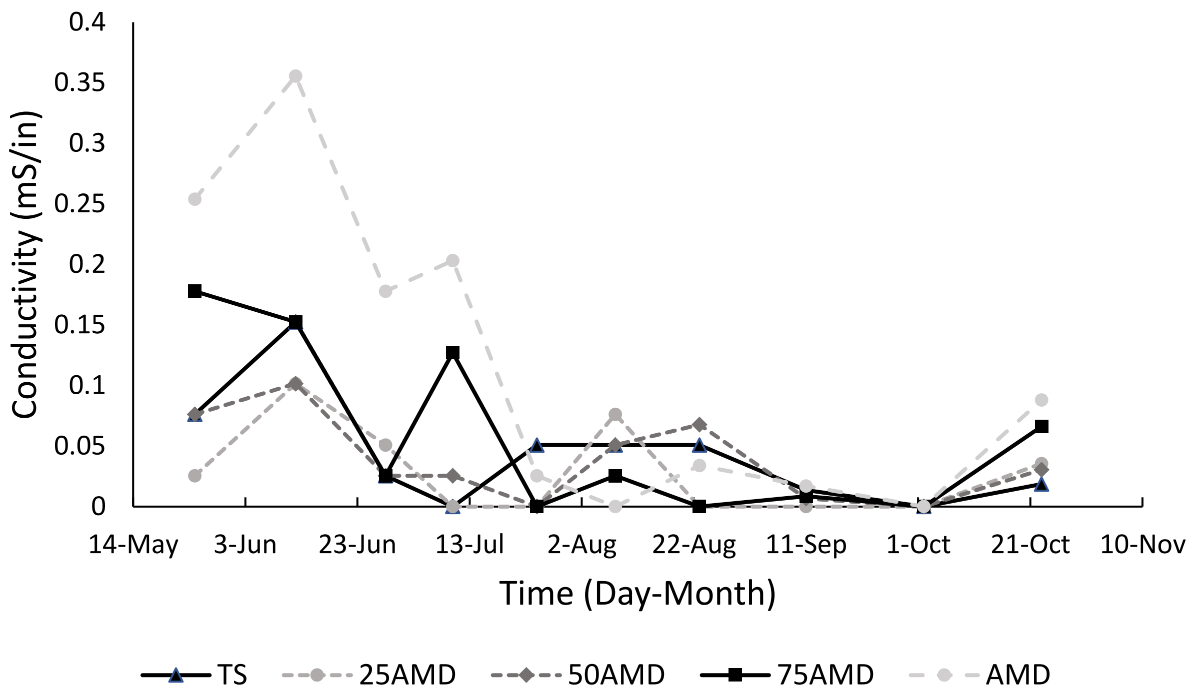

Figure 111. Comparison of mean conductivity among treatments.

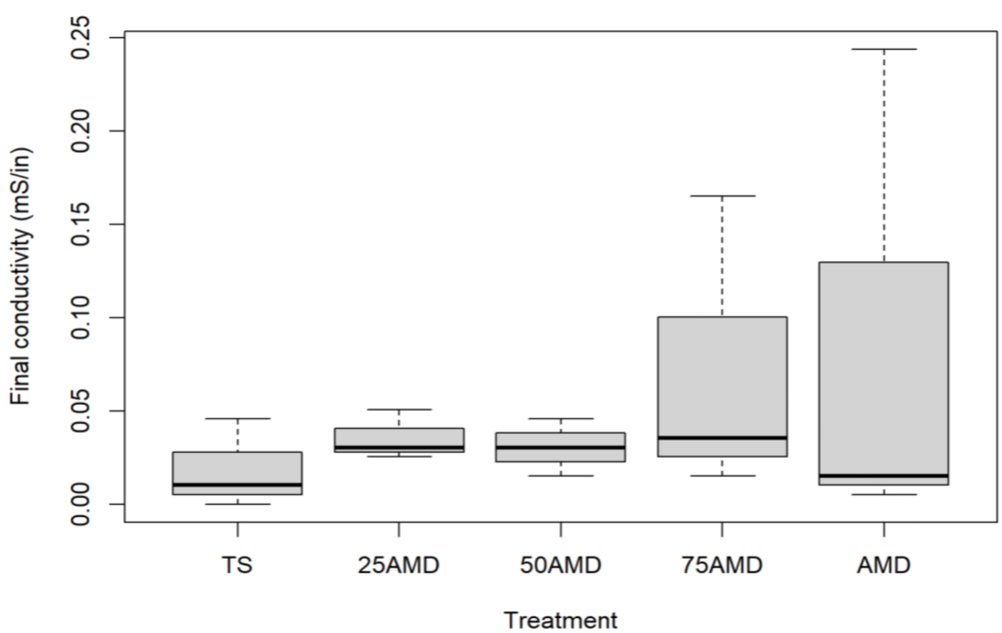

Figure 112. Comparison of final soil electrical conductivity (n=3, α=0.05).

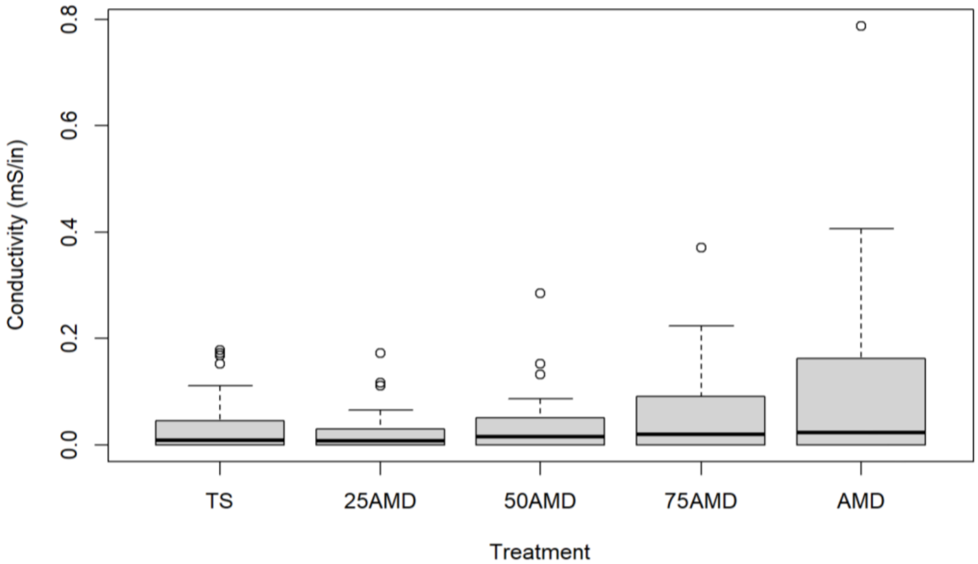

Figure 113. Comparison of conductivity for all measurements (n=30, α =0.05).

Temperature

Mean soil temperature among all treatments ranged from 62-80 ˚F throughout the duration of the study (Figure 114). The mean soil temperature for AMD treatment was lower than the other treatments while only considering the final temperature (Figure 115), and all treatments had a very similar mean when considering the soil temperature across the duration of the study (Figure 116). There were no significant differences experienced between the treatments for soil temperature (Figure 115, Figure 116).

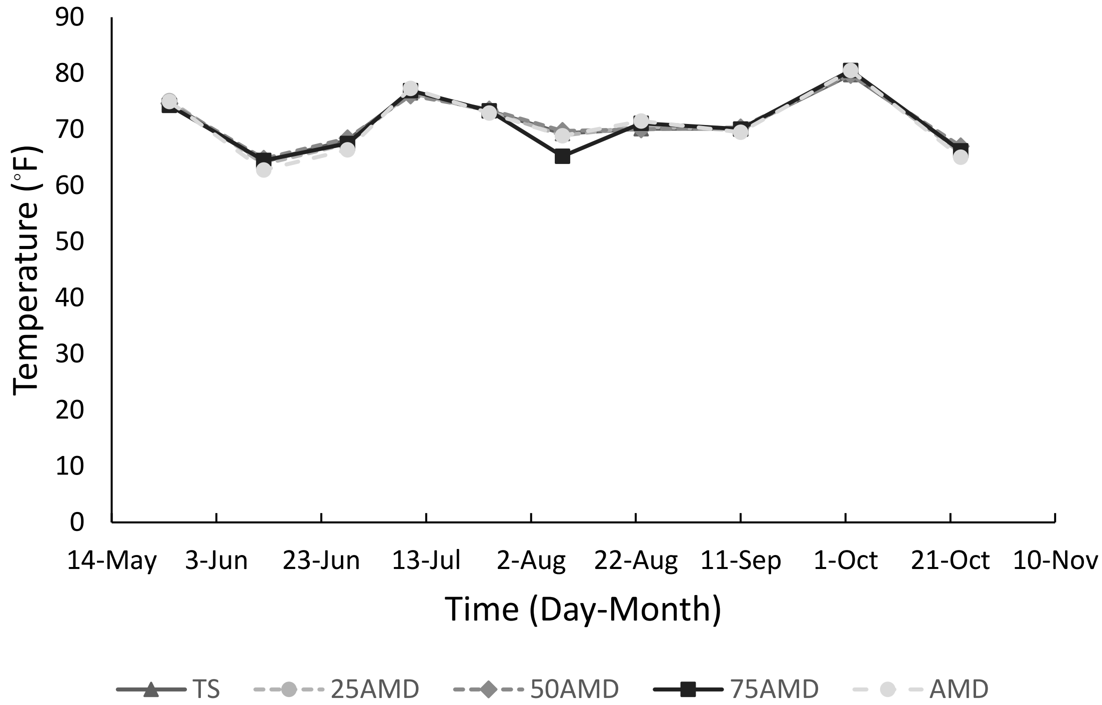

Figure 114. Comparison of mean soil temperature among treatments.

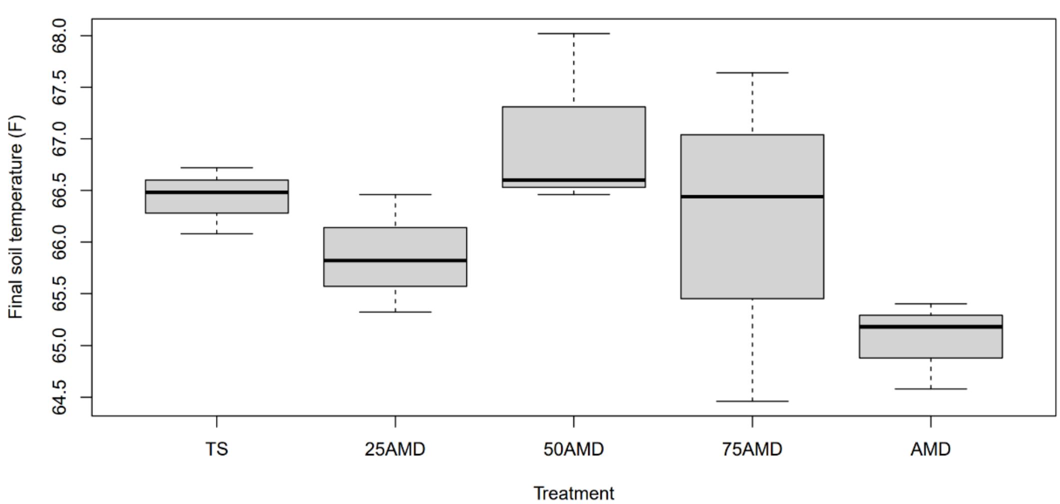

Figure 115. Comparison of final soil temperature (n=3, α =0.05).

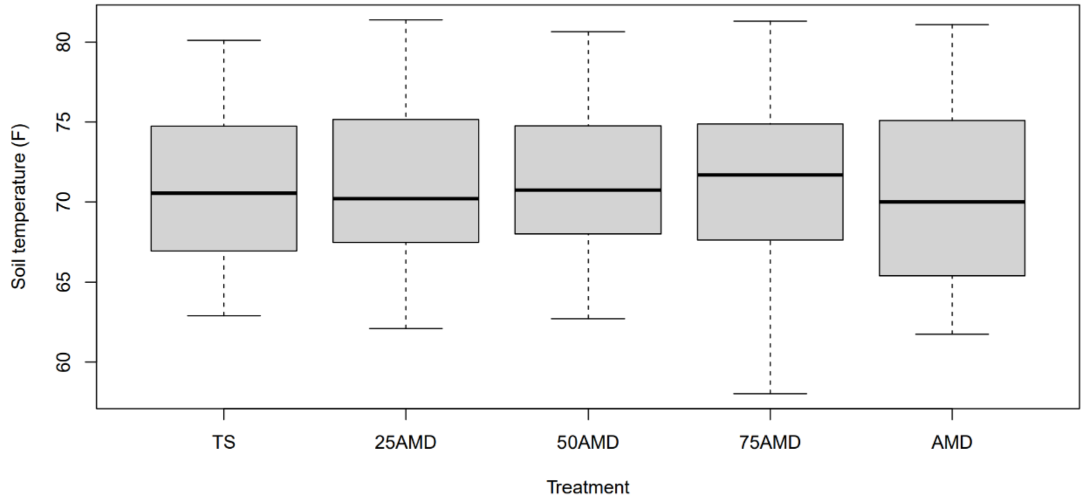

Figure 116. Comparison of soil temperature for all measurement (n=30, α =0.05).

Biomass

The mean biomass for all the treatments containing topsoil ranged from 0.13-0.20 lbs. and were above 0.10 lbs. (Figure 28). AMD treatment was less than 0.10 lbs., however, was not significantly different than the other treatments (*p*-value= 0.08) (Figure 117).

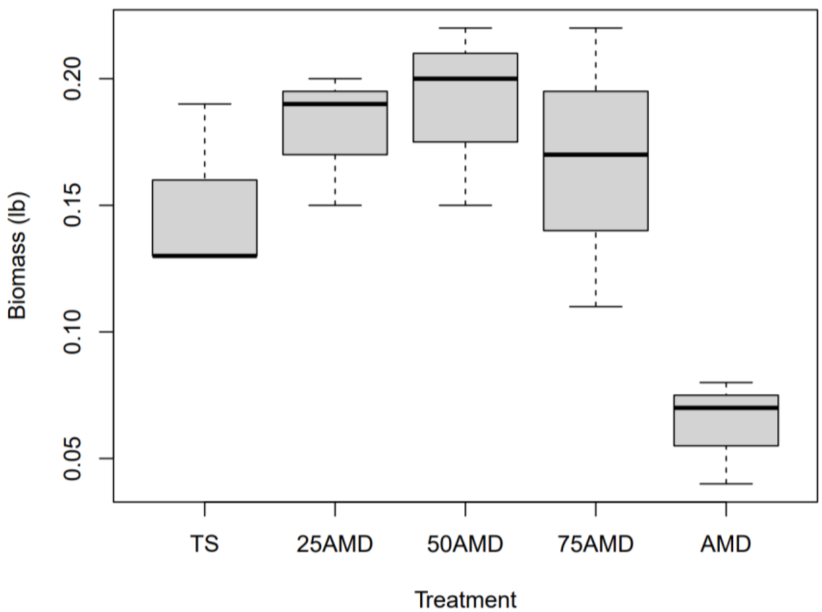

Figure 117. Comparison of biomass (n=3, α =0.05).

.

Soil data

Results from the saturated media extract report include the treatments that had topsoil and can be found in Appendix B. Statistical analysis was completed for the mean soil results for each treatment (Table 60). Phosphorus was significantly greater than the other treatments. Calcium was significantly greater in topsoil treatment than 75AMD, 75AMD was significantly less than topsoil, and 25AMD and 50AMD experienced no differences, likewise for magnesium. For sodium, topsoil was significantly less than 50AMD, 50AMD was significantly greater than topsoil, and 25AMD and 75AMD experienced no differences. While sulfur had a *p*-value less than 0.05, there were no significant differences experienced between the treatments, likewise for boron. For iron, topsoil was the highest, but was not significantly different, 75AMD was significantly less than 50AMD, and topsoil and 25AMD experienced no significant differences. For manganese, 75AMD was significantly less than topsoil, while 25AMD and 50AMD experienced no differences. For zinc, 25AMD was significantly greater than 75AMD, while topsoil and 50AMD experienced no differences. For copper, topsoil was significantly greater than 75AMD, while 25AMD and 50AMD had no differences.

Table 60. Statistical analysis of mean soil treatments.

Analysis	**Treatments**				***p*-value**
	TS	**25AMD**	**50AMD**	**75AMD**	
Nitrate (ppm)	1.00	1.00	1.00	1.00	0.3916
Phosphorus (ppm)	2.10_{b}	0.25_{a}	0.25_{a}	0.25_{a}	0.01325
Potassium (ppm)	116.00	109.33	88.67	73.00	0.3709
pH (S.U.)	7.13	7.1	7.03	7.07	0.5716
Calcium (ppm)	167.00_{b}	127.67_{ab}	82.00_{ab}	71.33_{a}	0.0216
Magnesium (ppm)	39.33_{b}	34.00_{ab}	30.33_{ab}	26.00_{a}	0.0207
Conductivity (mmho/in)	2.05	2.46	2.42	2.25	0.4784
Sodium (ppm)	9.67_{b}	22.00_{ab}	40.00_{a}	42.67_{ab}	0.0332
Sulfur (ppm)	9.67_{a}	62.33_{a}	82.67_{a}	81.00_{a}	0.0479
Boron (ppm)	0.27_{a}	0.23_{a}	0.13_{a}	0.07_{a}	0.0345
Iron (ppm)	129.27_{ab}	64.70_{ab}	46.27_{a}	24.20_{b}	0.0273
Manganese (ppm)	9.77_{b}	3.03_{ab}	1.17_{ab}	0.37_{a}	0.0266
Zinc (ppm)	3.70_{ab}	4.40_{a}	2.70_{ab}	1.77_{b}	0.0325
Copper (ppm)	0.70_{b}	0.47_{ab}	0.30_{ab}	0.20_{a}	0.0188

Discussion

Considering the results, there were some considerations that need to be addressed, as well as future recommendations.

The spring planting study conducted a study previous to this one and the results concluded that AMD could improve soil moisture, which in this study was the case. Results showed that mean soil moisture for the AMD treatment was significantly greater than all other treatments when considering the full duration of the study.

AMD treatments had less biomass than all the other treatments, however, the results were not statistically significant. One conclusion behind the decrease in biomass is due to the plots not being placed 6 inches into the ground. AMD sludge has a high-water content and the disturbance from wind, rain, and surface runoff decreased the size of the plots, which left less biomass to be collected at the end of the treatment.

AMD's properties include low pH, high specific conductivity, high concentrations of iron (Fe), aluminum (Al), and manganese (Mn), and low concentrations of toxic heavy metals (Akcil, 2006). The chemical composition is mostly composed of Mn, Fe, copper (Cu), zinc (Zn), arsenic (As), cadmium (Cd), and lead (Pb) (Fuchida et al. 2020). Soil results concluded that pH and conductivity experienced no significant differences among the treatments. Copper was highest in topsoil, zinc was the highest in topsoil and 25AMD, iron was highest in topsoil, likewise for manganese. Factors such as the volumetric mixture for each plot was hand mixed and the sludge was applied as a wet sludge. Meaning the soil samples collected at each plot may not have been a completely uniform mixture.

Future recommendations would include placing the plots 6 inches into the surface of the soil, place fencing around the plots so wildlife cannot disturb the plots, having a mixer on site to get a uniform mixture and collect surface runoff data from the site to be included within the statistical analysis. Future considerations would include applying the AMD sludge as a dry sludge and including different seeding mixtures, along with trees, brush, and bushes that are native to the area.

CONCLUSION

Objective #1 Develop methods to enhance AMD geotube dewatering with internal lateral drains.

Characterize geotechnical properties: Column filtration testing

This study tested five different geotextile fabrics and two different AMD sludges. The geotextile fabrics and AMD sludges were evaluated to determine the filtration efficiency and hydraulic conductivity changes in order to select the optimum fabric and optimum geotextile for lateral drainage applications. Preliminary findings tend to indicate that:

- With and without polymer the 1100N nonwoven fabric has the highest filtration efficiency.
- Without polymer the MD88 Typar fabric has the higher filtration efficiency (95.61% vs 94.7%) but has a lower hydraulic conductivity which means the fabric clogs faster than the MD7407 Typar fabric.
- The amount of polymer affects the hydraulic conductivity. The 20 ppm T&T material's hydraulic conductivity stabilized at $3x10^{-5}$ cm/s and the Raw (no polymer) Omega material stabilized at $3x10^{-4}$ cm/s.
- The systems (filter cake + geotextile) hydraulic conductivity was found to be independent of the geotextile used. This implies that the filter cake hydraulic conductivity controls drainage. The drainage process requires that the geotextile filter is developed, and a stable filter cake is developed.
- The Apparent Opening Size (AOS) of the fabric had an effect on the clogging of the fabric. Where fabrics with a smaller AOS (MD88) clogged faster than those with a larger AOS (GT500). This process impacts whether the fabric blinds-off drainage flow or whether a stable filter cake is formed. For the lateral drainage, the prefabricated vertical drain and typar fabric blinds-off and does not develop a lower hydraulic conductivity filter before the larger AOS geobag fabric does. The typar fabric blinding diminishes drainage (10X) compared to the nonwoven geotextiles (1100N and 140NC).

Design Recommendations

Considering the performance and analysis of the column tests running the two wick drain typar fabrics (MD88 and MD7407), it is recommended that the MD88 fabric be used when constructing the prototype geotextile bags intended to test field scale dewatering. The MD88 typar fabric has a higher filtration efficiency, which is due to its smaller AOS. A testing alternative is install the MD88 as the internal lateral drain and have the drain wrapped by 1100N fabric to limit the clogging, promote filter cake formation, and develop a stable drainage filter.

From the performance and analysis of the column tests running the non-woven fabrics (1100N and 140NC), it is recommended that the 1100N fabric be used in the filtration and dewatering in other geotextile bag designs. Between the two nonwoven fabrics (1100N and 140NC) the 1100N showed better filtration capabilities when running the lime dosed slurry. This is done by removing the outlier with the filtration efficiency is 82%. By removing this outlier, the rest of the data shows that the filtration efficiency is higher than the 140NC fabric.

When running the tests, the filtration efficiencies varied and were generally more efficient when the incoming slurry total solids was greater than 0.75% when compared to the tests that had the total solids in the slurry under 0.75%. Therefore, the optimum conditions to have the most efficient treatment is to have the total solids of the slurry to be greater than 0.75%. To catch the solid particles more effectively and there will be a larger filter cake.

Characterize geotechnical properties: Moisture distribution tests

This testing was conducted in order to determine the moisture and total solids distribution throughout geotextile tubes that are in the field. The bags that were selected were based on the pumping schedule that was being conducted at the AMD treatment site where the samples were collected. The goal was to collect samples from differently aged bags. The first tests that were conducted only had 1 sample per bag in order to figure out what was being tested for and what type of samples we wanted to collect. These tests provided how the distribution looks in the vertical direction only and where the moisture is expected to pool in the center of the bags. Which the older of the bags had more solids at the top and the newer bag had more solids at the bottom. The next set of tests were conducted to compare the distribution of moisture between different bags. These tests showed a cross sectional area of where the sample was collected. Based on these profiles, there is inconsistent flow trends. Where none of the three bags are similar in the layering of material and inconsistent in where majority of the solids pool together. The final test was conducted to compare the distribution within a single bag. These profiles in are similar in their layering because of where in the bag the sample is pumped.

The significant findings from this testing indicate:

- There is no clear trend in the moisture profiles that indicate preferential sludge dewatering
- There are no preferential drainage paths which indicate there are no clear placement of the lateral drains
- Moisture within the geotextile tubes have to do with the use of a polymer, the polymer dose, the injection time, and the tube's age.
- It is not possible to differentiate the zones of high polymer or low polymer within the geotextile tubes

The profiles that were created in this section will be used to be compared against in the next section, where numerical models will be created to create flow paths of how moisture is expected to flow in the material and out the geotextiles.

Numerical modeling

A finite element model was developed for analysis of moisture flow inside a geotextile tube using Plaxis 2D. The Plaxis 2D Groundwater results were able to predict the change in hydraulic conductivity (filter development) and the change in water content (drainage) in a cross-sectional profile of a geotextile tube calibrated using field and lab data. The models shown here are used to show what the expected flow in a geotextile tube is right now. The lateral drains were not included in modeling due to the inability to make it work in Plaxis 2D. In future work there will be models created in order to show how the introduction of a drainage core in the center would change the flow paths and all the other components.

The significant findings from the modeling are:

- The expected unsaturated flow has the flowlines traveling radially towards the external geotextile layer. With hydraulic mounding occurring, where the oldest material is displaced to the bottom of the cross section.
- By showing an increase in filter cake buildup it is expected there to be an increase in solids around the geotextile and there to be a decrease in dewatering out of the system.
- In comparison to the moisture distribution testing the results from the expected (modeled) moisture content does not equal the values that were collected from the field (no effective calibration).
- In comparison to the column filtration testing the hydraulic conductivity is expected to reduce and the filter cake thickness is expected to increase.
- The AMD Total Solids are not predictable in field geobags

Field-scale testing: Hanging Bag Tests (Test Set 1)

The experiment findings for Test Set 1 are listed below. The experiment findings were arrived at based on the content of the Field Operation, Laboratory Monitoring, Performance Testing Procedure, and Experimentation Results sections.

The marginalized intimate contact of AMD sludge filter cake with the internal drain and geotextile shell at time greater than 40 days after the timer was started was a major factor in AMD sludge dewatering behavior. This is illustrated in Figure 118 by the AMD precipitate having a high affinity for itself and forming clods.

Figure 118. HB-A (left), HB-B (middle), HB-C (right) (Source: Author).

Identified limitations of the field operation were as follows:

- There was an unknown and variable flow rate entering each bag from the manifold hose.

- The exposed location of the hanging bags with variable conditions for an extended period made data reproducibility and experimental results more questionable than it otherwise would be if bags were tested exclusively in a controlled environment.
- The AMD sludge was not enclosed within the bags (field scale geobags are entirely enclosed).
- The remote site location made filling and monitoring the bags on a consistent basis difficult. Limited filling of bags resulted in a smaller mass of AMD sludge being pumped into the hanging bags which limited the intimate contact window during which internal drainage systems could be properly assessed for dewatering performance.

Prior to the loss of CCF/sludge contact, the HB-B (2 ribbon “V”) displayed a higher dewatering rate than both HB-A and HB-C.

The data indicates that advancing to a larger (field) scale (more AMD sludge) is required to determine impact that internal drainage fibers have in aiding dewaterability. That is, having a larger internal drainage surface area combined with a larger mass of AMD sludge would more definitively conclude that internal lateral drainage enhancement increases dewatering performance of geobags by allowing longer sustained intimate contact and a larger surface on which intimate contact could occur.

Field-scale testing: Hanging Bag Tests (Test Set 2)

The experiment findings for Test Set 2 are listed below. The experiment findings were arrived at based on the content of the Field Operation, Laboratory Monitoring, Performance Testing Procedure, and Experimentation Results sections.

Initial fracturing of the filter cake was observed roughly 21 days after the timer start (Figure 119).

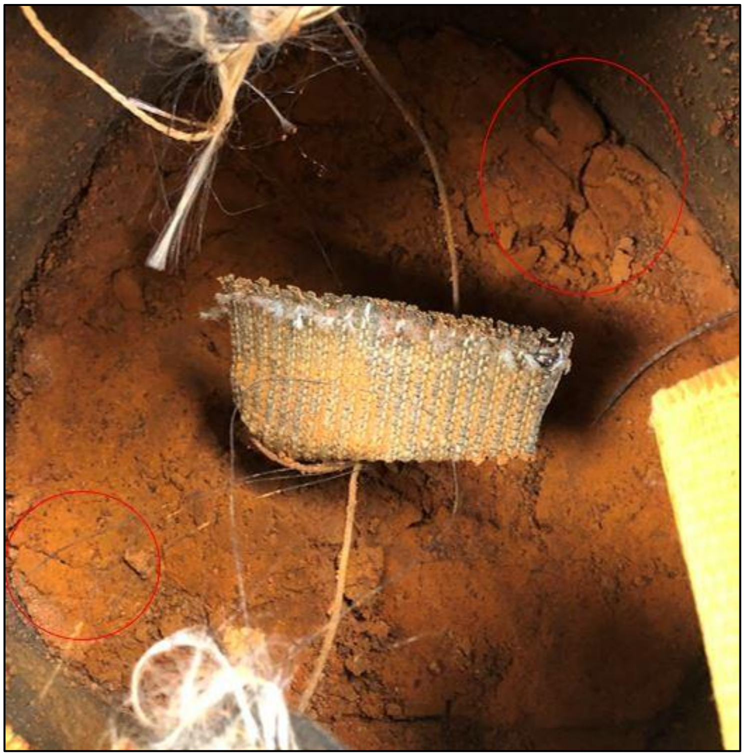

Figure 119. HB#4 at 21 days in the Lab (Source: Author).

Initial loss of intimate contact occurred roughly 31 days after the timer start. Significant loss of intimate contact of AMD sludge filter cake with internal drain and geotextile shell was confirmed 57 days after the timer start by fracturing of filter cake mass and self-cohesion of filter cake fragments. At this point the experiment was concluded.

CCF configured bags generally outperformed the standard bags in measures of dewaterability at less than 31 days after the timer start, but factors such as obtaining bag samples and progressive intimate contact loss could have impacted later time step bag sample data, making it more difficult to discern dewatering behavior among bags. This further confirmed the need to scale-up testing with larger sample sizes.

Field-scale testing: Geotube Dewatering Tests (Test Set 3)

The experiment findings for Test Set 3 are listed below. The experiment findings were arrived at based on the content of the Field Operation, Laboratory Monitoring, Performance Testing Procedure, and Experimentation Results sections.

1. CCF bag configurations and standard bags performed. The reason that the CCF and standard GDT bags displayed similar dewatering performance was likely a result of there not being enough AMD sludge mass within the GDT bags to maintain intimate contact with the CCF fabrics for a long enough period for the CCF configured bags to display positive separation in measures of dewaterability from the standard bags. The lateral positioning of the CCF fabrics intersecting mid-depth within the GDT bags also meant that as dewatering progressed the majority of the AMD sludge mass receded to the

internal bottom surface of the GDT bag geotextile and intimate contact with the mid-depth internal CCF fabrics was lost.

2. CCF bag configurations and standard bags both outperformed the PVD bag configurations with respect to Normalized Change in Bag Mass and normalized difference for Gravimetric Moisture Content. This was primarily due to the PVDs clogging in the field and losing drainage functionality and the fact that the AMD sludge surcharge acting on the PVDs decreased over the course of the experiment (see Prefabricated Vertical Drain (PVD) overview) while CCFs did not rely on a surcharge load to perform as intended (see Capillary Channel Fiber (CCF) overview) contributed to performance results.
3. Obtaining bag samples could have impacted later bag sample data via disturbance.
4. Identified limitations of the field operation were identical to those identified in the "Findings" section of the Test Set 1 section except for the following.
    a. The late field operation start date limited the number of bag fillings due to onset of freezing conditions.
    b. Unlike the HBTs in Test Set 1 and 2, the GDT bags were entirely enclosed. This made the structural design of the GDT bags more similar to those of field scale geobags.
5. Loss of intimate contact between the AMD sludge filter cake and the internal drainage fibers could have impacted data collection later in the test duration. However, this was more difficult to observe for Test Set 3 due to the enclosed nature of the GDT bags. Proper identification would have required cutting open the bags for observation as in Stephens (2007), which would have effectively ended the tests and prevented further data collection.

Objective #2: Evaluate the use of AMD as soil amendment

Evaluate soil development at a reclaimed site

The study site shows no evidence of AMD treatment within soil horizons. The soil appears to be stable chemically and no evidence of strong mineral leaching is present. The thin topsoil onsite overtops a seemingly compacted overburden fill material seems to be impeding natural succession and limiting the soils usage to grass and pastureland. This thin layer of topsoil would make it challenging for larger vegetation with deeper roots to thrive. Evidence is in the form of how the site was over 40 years reclaimed and is still only grassland. The site could be a great testing area for succession and reclamation testing to see if certain factors play a greater role in rehabilitation. The baseline can be the existing reclamation that is similar to many other sites across West Virginia. Soil chemical and biological testing could provide more insight into what is present and contributing to the current conditions at the site. Optimizing the topsoil for microbes, through amendments, could cause a significant increase in soil development when compared to current status.

Complete a small-scale growth study

This study evaluates land application as an alternative means of disposal for AMD sludge. Results suggest land application meets regulatory standards for one location and supports growth of one grass species. Even though ground cover only met permit limits for one sample, we could observe that the addition of AMD up to 50% did not reduce ground cover significantly as compared to a commercially available topsoil. The 50% sludge treatments performed close to the only-topsoil treatments. Additional studies are needed to understand the variation in AMD to meet regulations.

Complete a field study: Spring planting

When adding AMD sludge to a soil matrix, it appears that it acts similar to soils with higher organic contents or soils with coverage. The AMD amendment holds water that is accessible to vegetation, and raising the lag time between soil moisture decreases after rain events, effectively raising the moisture of the soil. In lower mixtures, around 25% AMD to topsoil, AMD appears to aid the growth of grasses. The increase in moisture affects the electrical conductivity of soils which can increase the amount of minerals available to vegetation within the soil matrix. Temperature variation does not seem to be a factor with the increased water content within AMD treatments. However, when freezing the larger AMD mixtures showed topsoil degradation due to freeze expansion. Once thawed the topsoil lost overall volume and can be a strength concern in larger scale testing.

The presence of high concentrations of lead within the AMD sludge was a concern. The sludge will need to be retested to check for testing errors. If the concentration is a similar high ppm, then concerns of toxicity and leaching would become apparent (CDC 2019 and Davis 2001). For vegetation Mg and Cu are adequate. Fe, S, K, and Zn are high (AgSource 2023). However, it does not appear to effect vegetation growth.

Complete a field study: Fall planting

The overall intent of this research was to evaluate the use of AMD sludge, a waste by-product, as a soil amendment to support vegetation establishment and persistence. The major results include the following:

- Mean ground cover for the AMD treatment was significantly less than all other treatments when considering only final ground cover, and was significantly less than all other treatments when considering the full study duration.
- Mean soil moisture for the AMD treatment was significantly greater than all other treatments when considering the full duration of the study.
- AMD treatment had the highest electrical conductivity throughout the study period, but there were no significant differences between any of the treatments.
- There were no significant differences experienced between the treatments for soil temperature.

- AMD treatment was the lowest for biomass, however, was not significantly different than the other treatments.
- Soil results experienced no significant differences in pH, or electrical conductivity, concluding the study.
- AMD sludge is composed of high concentrations of iron, copper, manganese, and zinc, however the highest concentrations from the soil results were found in the topsoil treatment.

The findings from this study will serve as a purpose for using AMD sludge, a waste by-product, in reclaiming AMLs to transform it back to its natural vegetative state. From the results of the study, AMD sludge can be used to grow native vegetation, but further research is advised to apply the future recommendations and considerations from this study.

REFERENCES

Ackman, T. E. 1982. Sludge disposal from acid mine drainage treatment. U.S. Department of the Interior, Bureau of Mines.

Adler, P. R., and P. L. Sibrell. 2003. *Sequestration of Phosphorus by Acid Mine Drainage Floc*. Journal of Environmental Quality, **32**(3): 112211–29. DOI: 10.2134/jeq2003.1122.

AgSource, 2022. Understanding a Soil Health Assessment. AgSource Laboratories. Retrieved from: https://agsourcevascom.wpenginepowered.com/wp-content/uploads/2022/05/Understanding-Soil-Health-Assessment_F-2486477865.pdf 9/12/2022

AgSource. “Agronomy Understanding a Soil Report.” *Agsource.com*, Accessed 25 April 2023. https://agsource.com/wp-content/uploads/2022/05/Understanding-a-Soil-Report-Tech-Bulletin_F-2570760112.pdf.

Akcil, Ata, and Soner Koldas. “Acid Mine Drainage (AMD): Causes, Treatment and Case Studies.” *Journal of Cleaner Production*, vol. 14, no. 12–13, Jan. 2006, pp. 1139–45. *DOI.org (Crossref)*, https://doi.org/10.1016/j.jclepro.2004.09.006.

Alder, P.R., and P.L. Sibrell. 2003. Sequestration of phosphorus by acid mine drainage floc. *Journal of Environmental Quality* 32, 1122-1129.

Amanda, N., and S.S. Moersidik. 2019. *Characterization of sludge generated from acid mine drainage treatment plants*. Journal of Physics: Conference Series, **1351**(1): 012113. DOI: 10.1088/1742-6596/1351/1/012113

Anwar, R., M. Ahmed, P. Seats, Q. Huag, and L-S Lian. 2021. *Prospect of Utilizing Coal Mine Drainage Sludge as an Iron Source for Value-Creating Applications*. Reviews in Environmental Science and Bio/Technology. **20**(3): 679–95. DOI: 10.1007/s11157-021-09584-y

ASTM D854-14 Standard test methods for specific gravity of soil solids by water pycnometer. ASTM International - Standards Worldwide. (2014). Retrieved from https://www.astm.org/standards/d854

ASTM Designation D7880/D7880M - 13. (2013). “Standard Test Methods for Determining Flow Rate of Water and Suspended Solids Retention from a Closed Geosynthetic Bag.” Annual Book of ASTM Standards, American Society of Testing Materials, West Conshohocken, PA.

ASTM International (American Society for Testing and Materials). (2019). ASTM D2216-19. Standard Test Methods for Laboratory Determination of Water (Moisture) Content of Soil and Rock by Mass. West Conshohocken, PA: ASTM International

ASTM International (American Society for Testing and Materials). (2018). ASTM D3385 − 18. Standard Test Method for Infiltration Rate of Soils in Field Using Double-Ring Infiltrometer. West Conshohocken, PA: ASTM International

ASTM International (American Society for Testing and Materials). (2004). ASTM D6913-04. Standard Test Methods for Particle-Size Distribution (Gradation) of Soils Using Sieve Analysis. West Conshohocken, PA: ASTM International

Azevedo, M., & Zornberg, J. (2013). Capillary barrier dissipation by new wicking geotextile. Advances in Unsaturated Soils, 559–565. https://doi.org/10.1201/b14393-88

Bouazza, A., Zornberg, J. G., McCartney, J. S., & Nahlawi, H. (2006). Significance of Unsaturated Behaviour of Geotextiles in Earthen Structures. *Australian Geomechanics Journal, Vol. 41, No. 3*, pp. 133–142.

CDC. “Lead (PB) Toxicity: What Are U.S. Standards for Lead Levels?” *Centers for Disease Control and Prevention*, Centers for Disease Control and Prevention, 2 July 2019, https://www.atsdr.cdc.gov/csem/leadtoxicity/safety_standards.html#:~:text=The%20EPA's%20standard%20for%20lead,cleanup%20projects%20using%20federal%20funds.

Chi, Y., Lin, Q., Zhuang, R., Xiong, M., and Ye, Z. “Evaluation Of Acid Mine Drainage Sludge as Soil Substitute For The Reclamation Of Mine Solid Wastes.” *Environmental Science and Pollution Research*. 2021, 29, 21184-21197 https://doi.org/10.1007/s11356-021-17290-z.

Ciolkosz, E. J., Cronce, R. C., Cunningham, R. L., & Petersen, G. W. (1985). Characteristics, genesis, and classification of pennsylvania minesoils: *Soil Science*, *139*(3), 232–238. https://doi.org/10.1097/00010694-198503000-00007

Dalen, S. 2021. Erosion and sediment controls on mine refuse impoundments. Graduate Theses, Dissertations, and Problem Reports. 8066. https://researchrepository.wvu.edu/etd/8066/

Davis, Sherry. “Regulated Metals: The Rule of 20.” *Studylib.net*, Pollution Prevention Institute, Dec. 2001, https://studylib.net/doc/18196608/regulated-metals--the-rule-of-20.

Demers, I., Mbonimpa, M., Benzaazoua, M., Bouda, M., Awoh, S., Sylvian, L., and Gagnon, M. “Use of Acid Mine Drainage Treatment Sludge by Combination with a Natural Soil as an Oxygen Barrier Cover for Mine Waste Reclamation: Laboratory Column Tests and Intermediate Scale Field Tests.” *Minerals Engineering*, vol. 107, 2017, pp. 43–52., https://doi.org/10.1016/j.mineng.2016.11.017.

Elzinga, C.L., Salzer, D.W., and Willoughby, J.W. “Measuring and Monitoring Plant Populations.” *Journal of Range Management*, vol. 52, no. 5, 1999, p. 544., https://doi.org/10.2307/4003786.

Fannin, J. (2007). “Multifunctional uses of geosynthetics in civil engineering.” Geosynthetics in Civil Engineering, pp. 97–126., doi:10.1533/9781845692490.2.127.

Faulkner, B.B., M. Reese, W. Snider, R. Phillips, A. McCartney, D. Gillum, and R. Green. (2000). Reduction in acid loads at the Alton Project. Paper presented at the West Virginia Surface Mine Drainage Task Force Symposium, 4/4/2000, Morgantown, WV.

Franks, C.D., and K.A. Goings. 1997. Above-Ground (Plant) Determinations. National Soil Survey Center, National Resources Conservation Service. USDA. Lincoln, Nebraska. https://www.nrcs.usda.gov/Internet/FSE_DOCUMENTS/nrcs142p2_051916.pdf.

Fuchida, Shigeshi, et al. “Understanding the Biogeochemical Mechanisms of Metal Removal from Acid Mine Drainage with a Subsurface Limestone Bed at the Motokura Mine, Japan.” *Scientific Reports*, vol. 10, no. 1, Dec. 2020, p. 20889. *DOI.org (Crossref)*, https://doi.org/10.1038/s41598-020-78069-9.

Gabr, M. A.,1997. “Prefabricated well injection depth extraction WIDE system for enhanced soil flushing.” Disclosure Document No.422400 under 37 CFR Sec 1.21 (c), U.S. Patent and TrademarkOffice.

Haering, K. C., Daniels, W. L., & Galbraith, J. M. (2004). Appalachian mine soil morphology and properties: Effects of weathering and mining method. *Soil Science Society of America Journal*, *68*(4), 1315–1325. https://doi.org/10.2136/sssaj2004.1315

Haering, K. C., Daniels, W. L., & Roberts, J. A. (1993). Changes in mine soil properties resulting from overburden weathering. *Journal of Environmental Quality*, *22*(1), 194–200. https://doi.org/10.2134/jeq1993.00472425002200010026x

Howard, J. (2017). Anthropogenic soils (Vol. 231). Cham, Switzerland: Springer International Publishing.

Khiari, L., L.E. Parent, A. Pellerin, A.R. Alimi, C. Tremblay, R.R. Simard, and J. Fortin. 2000. An agri-environmental phosphorus saturation index for acid coarse-textured soils. J. Environ. Qual. 29:1561–1567

Ko, M., Kim, J., Park, H., and Kim, K. 2015. “Field Assessment of Arsenic Immobilization in Soil Amended with Iron Rich Acid Mine Drainage Sludge,” *Journal of Cleaner Production*, 108, 1073-1080 https://doi.org/10.1016/j.jclepro.2015.06.076

Koerner, G., & Koerner, R. (2006). Geotextile tube assessment using a hanging bag test. Geotextiles and Geomembranes, 24, 129-137.

Lovett, R. and P. Ziemkiewicz. 1991. Calcium peroxide for treatment of acid mine drainage. p. 35-46. In: Proceedings, Second International Conference on the Abatement of Acidic Drainage, 16-18 Sept. 1991, MEND, Montreal, Canada.

Luckner, L., Van Genuchten, M. T., & Nielsen, D. R. (1989). A consistent set of parametric models for the two-phase flow of immiscible fluids in the subsurface. *Water Resources Research*, *25*(10), 2187–2193. https://doi.org/10.1029/wr025i010p02187

Minnesota Pollution Control Agency (Minnesota PCA). 2011. Characteristic Hazardous Wastes. Accessed December 5, 2022. https://www.pca.state.mn.us/sites/default/files/w-hw2-04.pdf.

National Centers for Environmental Information (NCEI). https://www.ncei.noaa.gov/. Accessed 16 Jan. 2024.

Northeast Region Certified crop adviser (NRCCA) study resources. Certified Crop Advisor study resources (Northeast region). (n.d.). Retrieved from https://nrcca.cals.cornell.edu/soil/CA2/CA0212.1-3.php#:~:text=The%20volumetric%20soil%20moisture%20content,to%2055%25%20for%20clay%20soils.

Ott, R. L. and M. Longnecker. 2001. An introduction to statistical methods and data analysis. Pacific Grove, CA: Duxbury.

Rawls, W. J., Gish, T. J., & Brakensiek, D. L. (1991). Estimating soil water retention from soil physical properties and characteristics. *Advances in Soil Science*, 213–234. https://doi.org/10.1007/978-1-4612-3144-8_5

Richart, FE. 1957. A review of the theories for sand drains. Journal of the Soil Mechanics and Foundations Division 83(3), 1-38.

Roberts, J. A., Daniels, W. L., Burger, J. A., & Bell, J. C. (1988). Early stages of mine soil genesis in a southwest virginia spoil lithosequence. *Soil Science Society of America Journal*, *52*(3), 716–723. https://doi.org/10.2136/sssaj1988.03615995005200030023x

Santos, I. L. (2022). *Methodology for enhanced filtration and dewatering of fine-grain AMD precipitate using geocomposites for Rare Earth Elements recovery* (dissertation). West Virginia University.

Scagline-Mellor, S., Griggs, T., Skousen, J., Wolfrum, E., & Holásková, I. (2018). Switchgrass and giant miscanthus biomass and theoretical ethanol production from reclaimed mine lands. *BioEnergy Research*, *11*(3), 562–573. https://doi.org/10.1007/s12155-018-9915-2

Schoeneberger, P.J., Wysocki, D.A., Benham, E.C., and Soil Survey Staff. “Field Book for Describing and Sampling Soils.” *National Soil Survey Center, Natural Resources Conservation Service, U.S. Department of Agriculture*, 2012.

Sencindiver, J.C. and Ammons, J.T. (2000). Minesoil Genesis and Classification. In Reclamation of Drastically Disturbed Lands (eds R.I. Barnhisel, R.G. Darmody and W. Lee Daniels). https://doi.org/10.2134/agronmonogr41.c23

Sibrell, P.L., G. A. Montgomery, K. L. Ritenour, K.L., and T. W. Tucker. 2009 *Removal of Phosphorus from Agricultural Wastewaters Using Adsorption Media Prepared from Acid Mine Drainage Sludge*. Water Research, **43**(8): 2240–2250. DOI: 10.1016/j.watres.2009.02.010

Skousen, J, A Sexstone, P Ziemkiewicz. 2000. Acid mine drainage control and treatment. Reclamation of Drastically Disturbed Lands, 2nd ed. American Society of Agronomy, Madison, WI, 131-168.

Skousen, J. G., P. F. Ziemkiewicz, and L. M. McDonald. 2019. *Acid mine drainage formation, control and treatment: Approaches and strategies*. The Extractive Industries and Society, **6**(1): 241–249. DOI: 10.1016/j.exis.2018.09.008

Skousen, J., C. E. Zipper, A. Rose, P. F. Ziemkiewicz, R. Nairn, L. M. McDonald, and R. L. Kleinmann. 2017. *Review of passive systems for acid mine drainage treatment*. Mine

Water and the Environment, **36**(1): 133–153. DOI: 10.1007/s10230-016-0417-1

Skousen, J.G., A. Rose, G. Geidel, J. Foreman, R. Evans, and W. Hellier. 1998. Handbook of Technologies for Avoidance and Rernediation of Acid Mine Drainage, ADTI of the USOSM, Published by the National Mine Land Reclamation Center, WVU, Morgantown, WV.

Skousen, J.G., P.F. Ziemkiewicz, L.M. McDonald. 2019. Acid mine drainage formation, control and treatment: Approaches and strategies. *The Extractive Industries and Society* 6, 241-249.

Stephens, T. (2007). "Three New Tests Allow Accurate Assessment of Geotube Dewatering Technology," News Bulletin G2007-05, TenCate Geosynthetics North America, http://www.tencate.com/amer/Images/nb_geotube_3tests_tcm29- 12838.pdf

Stormont, J. C., & Morris, C. E. (2000). Characterization of unsaturated nonwoven geotextiles. *Advances in Unsaturated Geotechnics*. https://doi.org/10.1061/40510(287)10

Sun, M., Xiao, T., Ning, Z., Xiao, E., and Sun, W. "Microbial community analysis in rice paddy soils irrigated by acid mine drainage contaminated water." *Applied Microbiology & Biotechnology*, 2014, 99(6), 2911–2922 https://doi.org/10.1007/s00253-014-6194-5.

Thomas, K.A., J.C. Sencindiver, JG Skousen, and JM Gorman. (2000). Soil horizon development on a mountaintop surface mine in southern West Virginia. Green Lands 30: 41-52.

Tolonen, E-T., A. Sarpola, T. Hu, J. Rämö, and U. Lassi. 2014. *Acid mine drainage treatment using by-products from quicklime manufacturing as neutralization chemicals*. Chemosphere, **117**: 419-424. DOI: 10.1016/j.chemosphere.2014.07.090

Tyson, J. (2023). *Laboratory experimentation and numerical modeling to enhance drainage in geotextile tubes* (thesis). West Virginia University.

United States Environmental Protection Agency (USEPA). Guide for industrial waste management. Retrieved December 9, 2022, from: https://www.epa.gov/sites/default/files/2016-03/documents/industrial-waste-guide.pdf

US Environmental Protection Agency (USEPA). 2007. Developing your stormwater pollution prevention plan: A guide for construction sites. Retrieved from: https://www.epa.gov/sites/production/files/2015-10/documents/sw_swppp_guide.pdf

van Genuchten, M. T., Leij, F. J., & Yates, S. R. (1991, December). *The RETC code for quantifying the hydraulic functions of unsaturated soils*. EPA. Retrieved February 8, 2023, from https://cfpub.epa.gov/si/si_public_record_Report.cfm?dirEntryId=130162

Vanapalli, S. K., Sillers, W. S., & Fredlund, M. D. (1998). *The meaning and relevance of residual state to unsaturated soils*. Retrieved from http://by.genie.uottawa.ca/~vanapall/papers/conference/1998/cgs98_residual.pdf

Warren, K. A., Gabr, M. A., & Quaranta, J. D. (2006). Field study to investigate wide technology for TCE extraction. Journal of Geotechnical and Geoenvironmental Engineering, 132(9), 1111–1120.

Web soil survey—Home. (n.d.). Retrieved March 13, 2024, from https://websoilsurvey.nrcs.usda.gov/app/

Weggel, J. R., & Dortch, J. (2012). A model for filter cake formation on geotextiles: Experiments. *Geotextiles and Geomembranes*, *31*, 62–68. https://doi.org/10.1016/j.geotexmem.2011.10.003

Wei, X., R. C. Viadero, and S. Bhojappa, S. 2008. *Phosphorus removal by acid mine drainage sludge from secondary effluents of municipal wastewater treatment plants*. Water Research, **42**(13): 3275–3284. DOI: 10.1016/j.watres.2008.04.005

Woods, Alan J., Omernik, James M., and Brown, Douglas Brown D., (1999). "Level III and IV Ecoregions of Delaware, Maryland, Pennsylvania, Virginia, and West Virginia." *U.S. Environmental Protection Agency.* 1999

WVDEP. "Erosion and Sediment Control Best Management Practice Manual." West Virginia Department of Environmental Protection: Division of Water and Waste Management. Aug. 2016.

WVDEP. "West Virginia Erosion and Sediment Control Field Manual." *West Virginia Department of Environmental Protection: Office of Oil and Gas*. May 2012.

Zhang, X., Presler, W., Li, L., Jones, D., & Odgers, B. (2014). Use of wicking fabric to help prevent frost boils in Alaskan pavements. Journal of Materials in Civil Engineering, 26(4), 728–740. https://doi.org/10.1061/(asce)mt.1943-5533.0000828

Zinck, J. 2006. Disposal, reprocessing and reuse options for acidic drainage treatment sludge. Poster paper presented at the 7th International Conference on Acid Rock Drainage (ICARD), March 26-30, 2006, St. Louis MO. R.I. Barnhisel (ed.) Published by the American Society of Mining and Reclamation (ASMR)

APPENDIX A: OBJECTIVE 1

Characterize geotechnical properties: Column filtration testing

Test Instructions

Preparation:

1.) Attach a clear tube with a ruler taped to the front and back to the stand using the white pipe strap. Only adjust the screws of the left side of the tube. Ensure the tube is level
2.) Cut about a 3-inch diameter piece of geotextile and tighten to the bottom of the tube using a hose clamp. Record dry mass of geotextile on the Tube Test data sheet
    a. Ensure the geotextile is pulled tight at the bottom of the tube so that it is flush. The geotextile should extend past the hose clamp in all directions.
    b. Be sure geotextile is facing the correct direction (heated side down)
3.) Place a 1000 mL graduated cylinder with a funnel underneath the bottom of the tube to collect the outflow
4.) Place a funnel on the top of the tub to pour the slurry in to the tube
5.) Obtain set volume of slurry (typically 500-1000 mL)
6.) Ensure that slurry is mixed thoroughly so that it is homogenous throughout while being careful to not break the floc structure
7.) Acquire three moisture content samples directly after slurry is mixed

Begin Test

1.) Once slurry is thoroughly mixed, start a stopwatch and immediately start to pour slurry into the tube
    a. The funnel should be tilted while pouring the slurry to allow the slurry to run down the side of the tube to avoid the slurry splashing into the bottom of the tube as.

Figure 1. Tilted Funnel (Source: Nasiadka 2021)

2.) Once pouring is finished, record head, filter cake thickness and volume passed every 5 minutes where:

a. Head is the height of the water column in the tube
b. Volume passed is the volume that is collected in the bottom flask/graduate cylinder.
c. Filter cake thickness is the height of the filter cake (This may not be able to be read for the first couple minutes of the test)

Figure 2. Difference in head and thickness of filter cake

3.) Once head is equal to filter cake thickness, pour DI or recirculate outflow (depending on the type of test). Record this in the data sheet
   a. Pour at the same rate of approximately 1 Liter per minute
   b. Use a small funnel and tilt to the side when pouring in an attempt to not damage the filter cake. The funnel should be rotated around the inside diameter of the tube to evenly distribute the pour around the circumference of the tube filter cake. This avoids an angled or uneven surface on top of the filter-cake
4.) Repeat step 4 for however many passes are necessary to develop a satisfactory system
5.) The test is complete when either:
   a. The filter cake thickness stops changing or
   b. Cracks start becoming visible within the filter cake
6.) Once complete, loose the hose clamp, carefully twist the and pull down to release the filter cake. Hold a bowl underneath the tube to catch the filter cake as it is pulled out of the tube. Liquid sample may come off.
7.) Record the moisture content of the filter cake from the top, bottom, and middle immediately after removing the filter cake.

8.) Scrape off all leftover filter cake from the geotextile and dry the geotextile in the oven. Weigh the dried geotextile to find the percent loss of solids.

Once the above parameters are dried and recorded the % Retained, % Lost, % Passing, Filtration Efficiency, and the hydraulic conductivity are calculated as shown by the equations below

$$\% \, Retained \; = \frac{solids \; retained \; (g)}{total \; solids \; (g)} x \; 100 \tag{1}$$

$$\% \, Lost \; = \frac{solids \; stuck \; in \; fabric \; (g)}{total \; solids \; (g)} x \; 100 \tag{2}$$

$$\% \, Passing \; = \frac{solids \; passing \; through \; fabric \; (g)}{total \; solids \; (g)} x \; 100 \tag{3}$$

$$Filtration \; Efficiency \, \% \; = \frac{total \; solids \; (g) - passing \; solids \; (g)}{total \; solids \; (g)} x \; 100 \tag{4}$$

$$Moisture \; Content \; (w\%) = \frac{water \; in \; filter \; cake \; (g)}{water \; in \; filter \; cake \; (g) + solids \; in \; filter \; cake \; (g)} x \; 100 \tag{5}$$

$$Hydraulic \; Conductivity: k \; = \frac{aL}{A\Delta t} ln(\frac{h1}{h2}) \tag{6}$$

Where:

a = cross-sectional area of the reservoir containing the influent liquid (cm^2)

L = length of the specimen (cm)

A = cross-sectional area of the specimen (cm^2)

Δt = elapsed time between determination of h1 and h2

h1 = head loss across the specimen, at time t1, m or cm

h2 = head loss across the specimen at time t2, m or cm

Hydraulic conductivity was calculated for each time step during testing. k values were averaged for each test once the steady state was reached per ASTM D5088-16a (ASTM 2016).

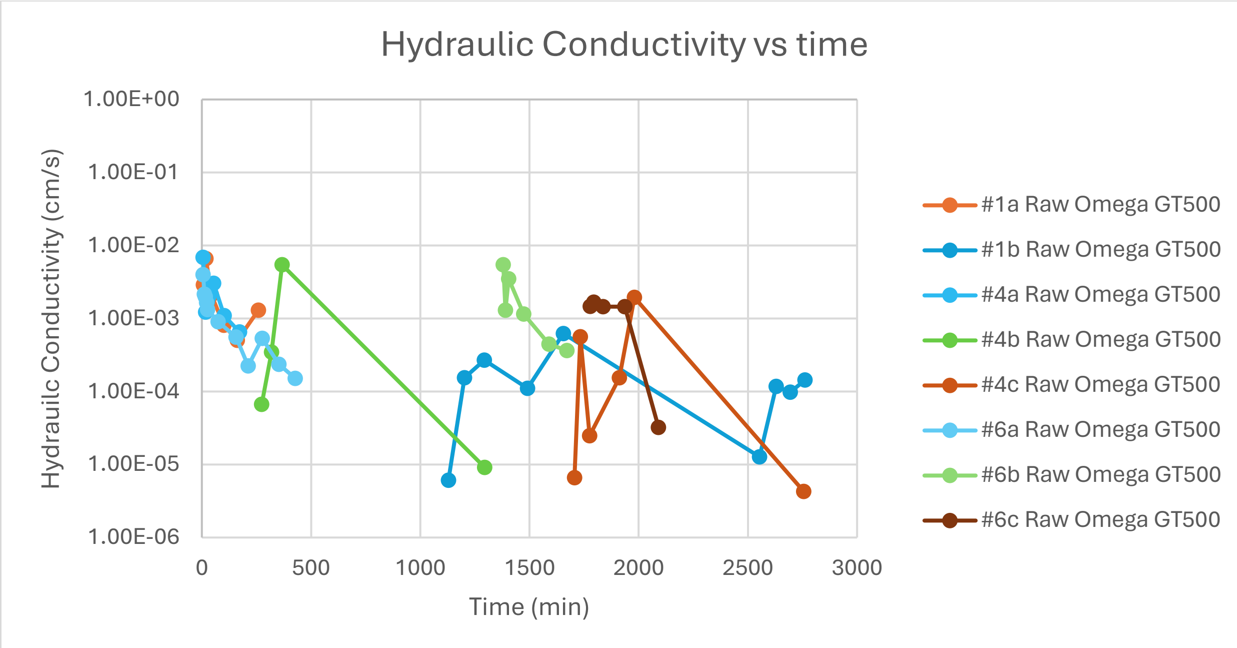

Figure 3. No Polymer Omega Test Set 1 Using GT500 - Hydraulic Conductivity vs Time

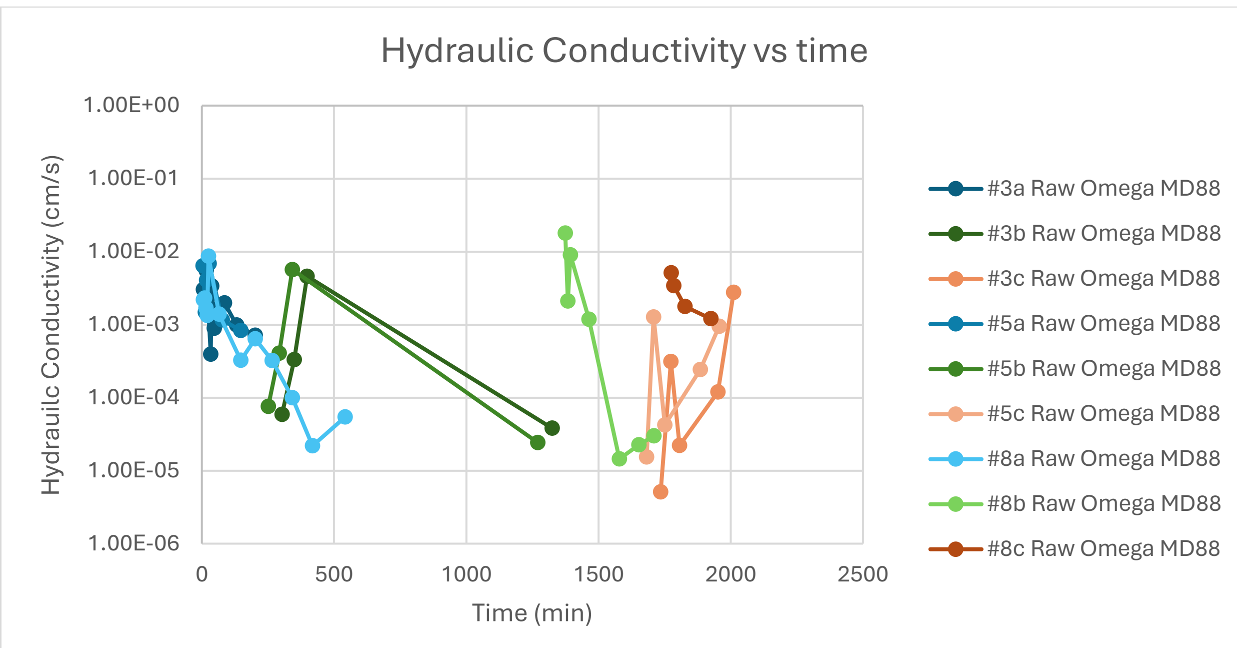

Figure 4. No Polymer Omega Test Set 1 Using MD88 Typar - Hydraulic Conductivity vs Time

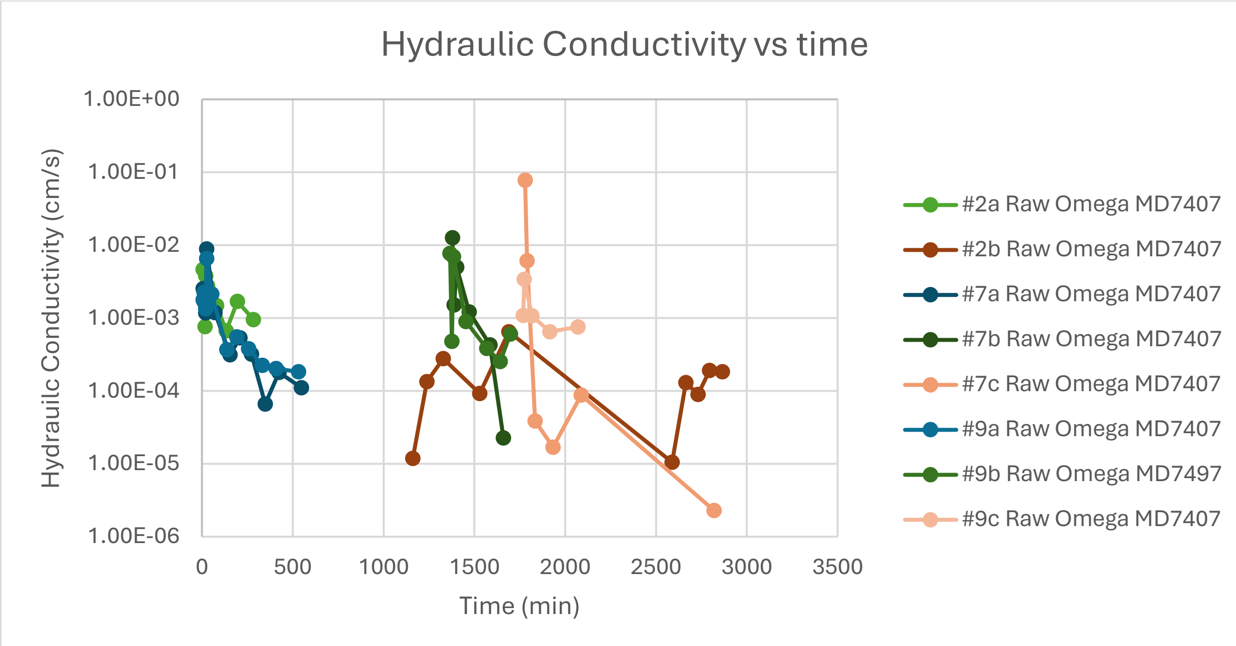

Figure 5. No Polymer Omega Test Set 1 Using MD7407 Typar – Hydraulic Conductivity vs Time

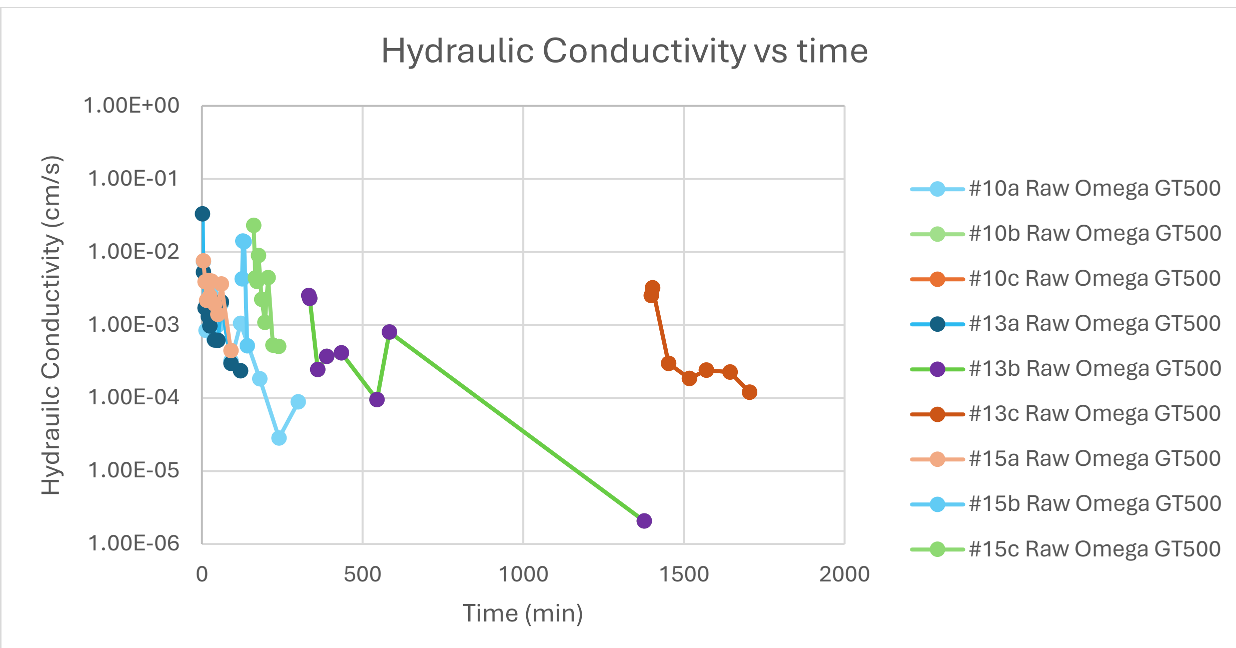

Figure 6. No Polymer Omega Test Set 2 Using GT500 – Hydraulic Conductivity vs Time

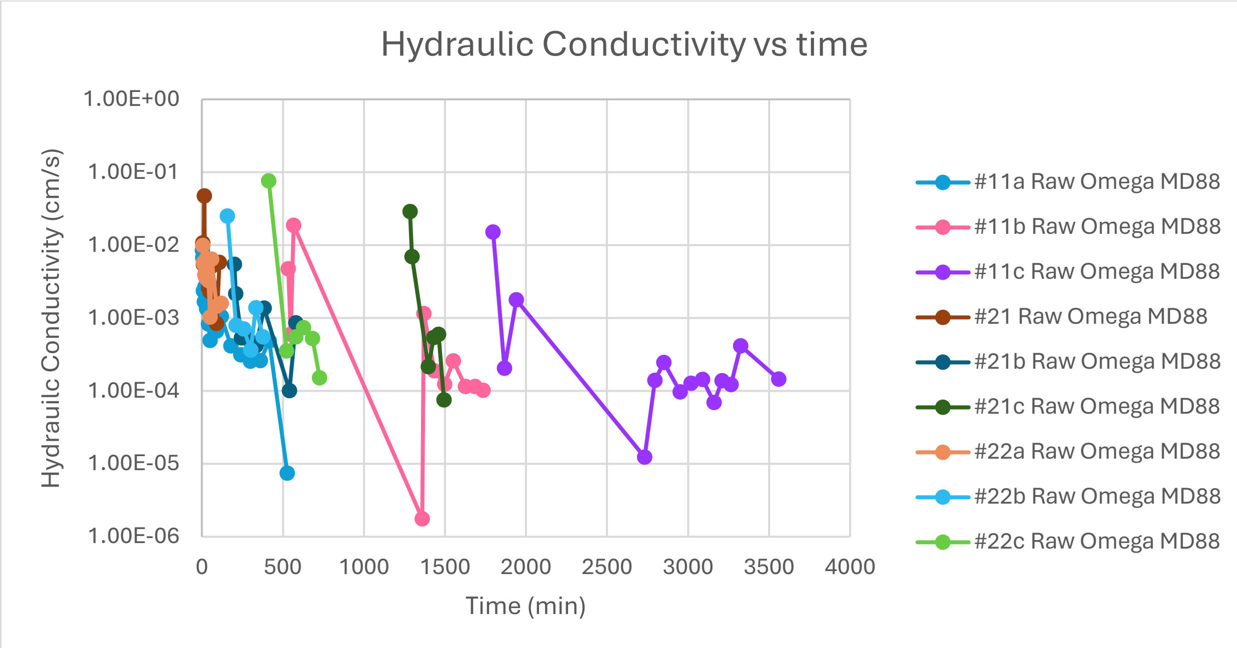

Figure 7. No Polymer Omega Test Set 2 Using MD88 Typar – Hydraulic Conductivity vs Time

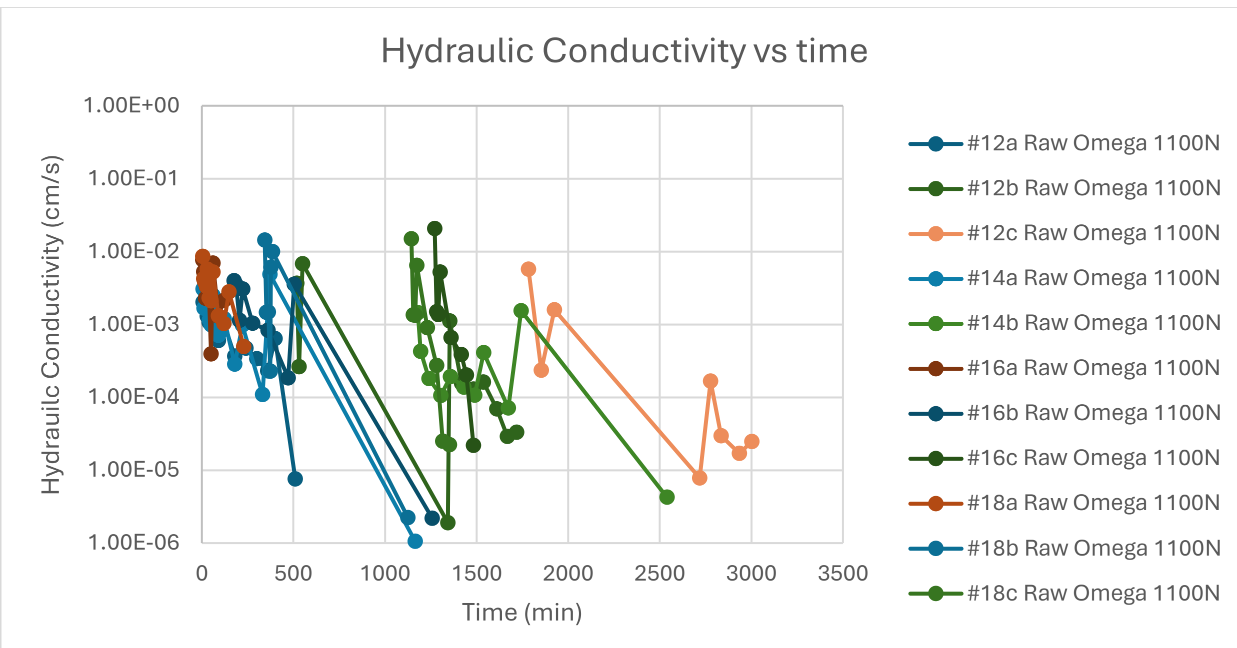

Figure 8. No Polymer Omega Test Set 2 Using 1100N – Hydraulic Conductivity vs Time

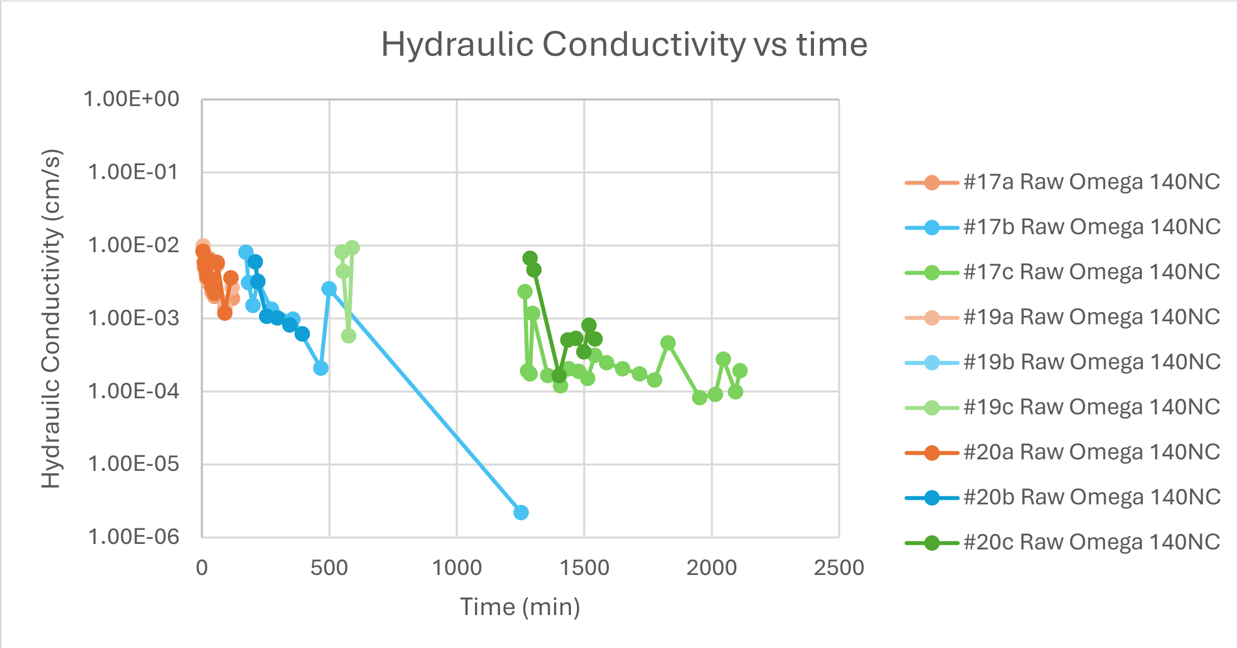

Figure 9. No Polymer Omega Test Set 2 Using 140NC – Hydraulic Conductivity vs Time

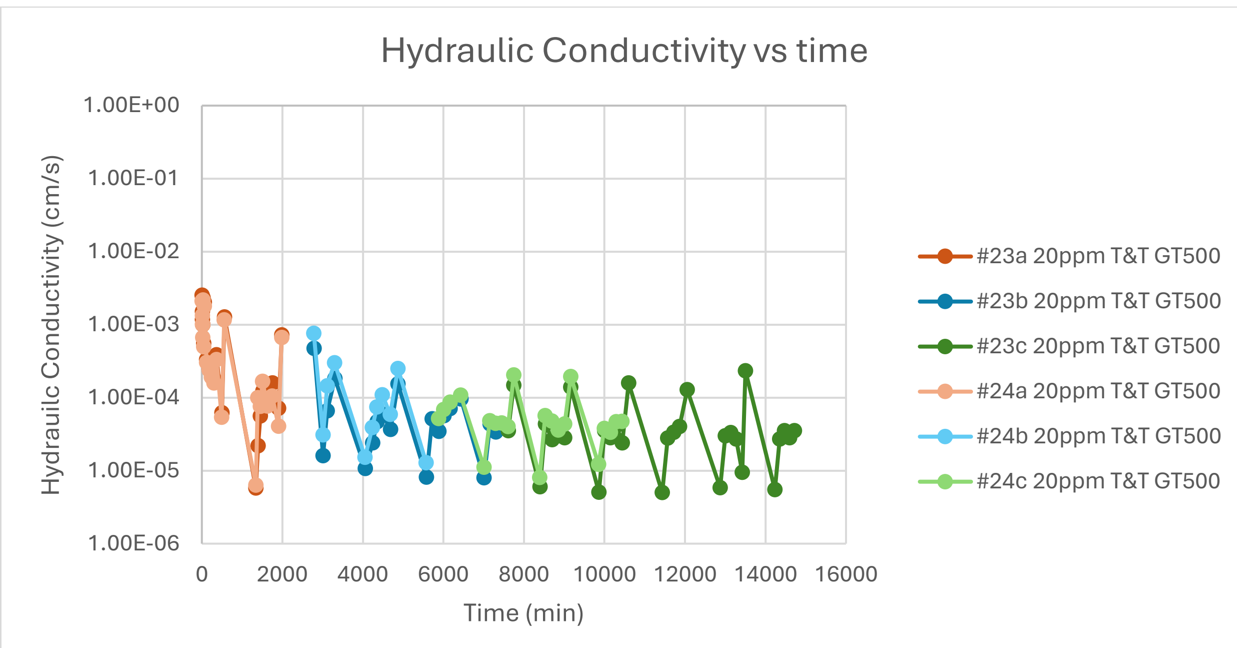

Figure 10. 20 ppm Dosed T&T Using GT500 – Hydraulic Conductivity vs Time

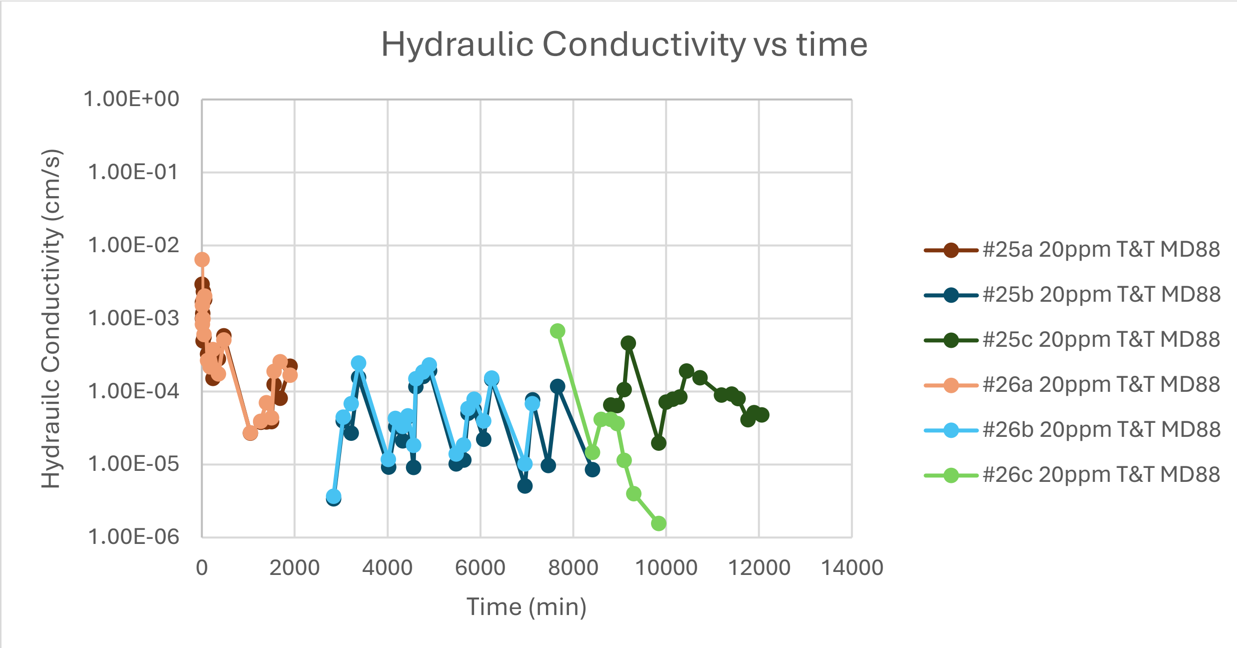

Figure 11. 20 ppm Dosed T&T Using MD88 Typar – Hydraulic Conductivity vs Time

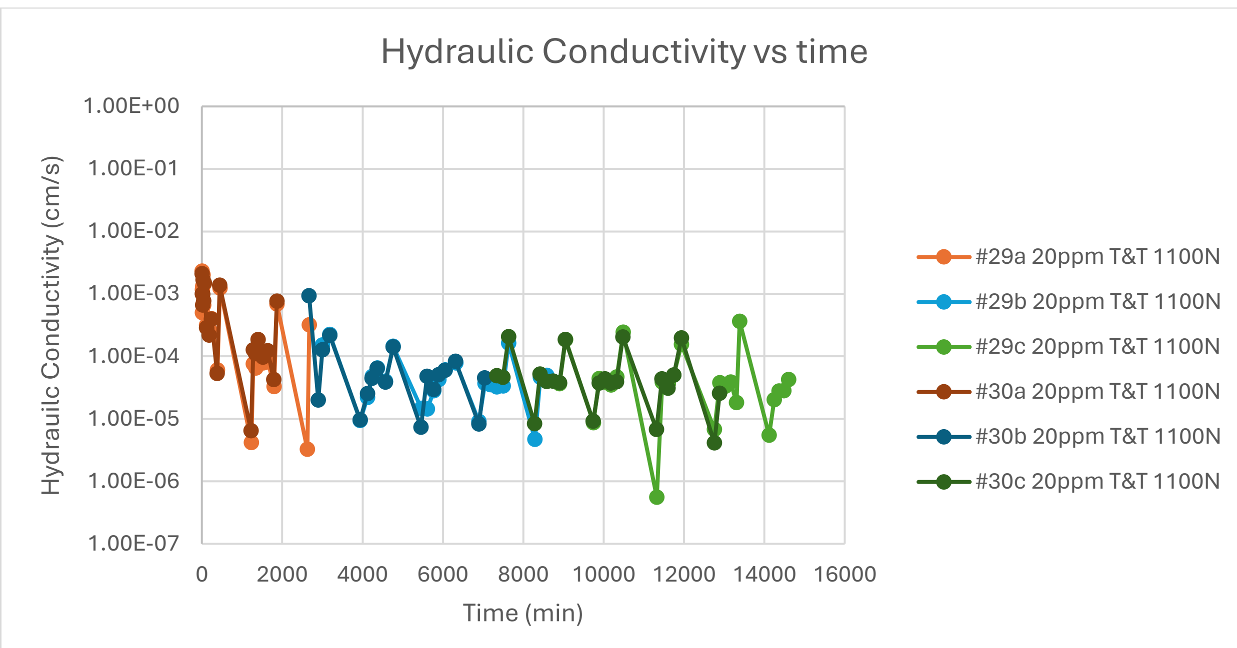

Figure 12. 20 ppm Dosed T&T Using 1100N – Hydraulic Conductivity vs Time

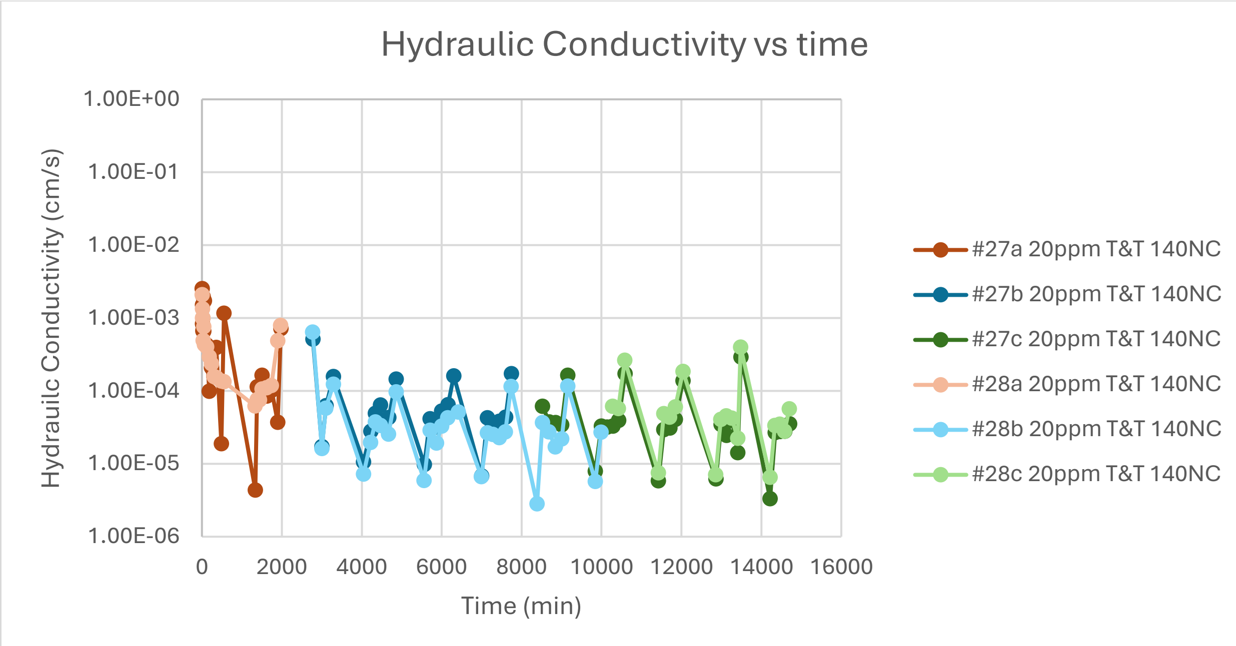

Figure 13. 20 ppm Dosed T&T Using 140NC – Hydraulic Conductivity vs Time

Characterize geotechnical properties: Moisture distribution tests

Testing

Materials Needed:

- Obtain 6 tubes (for each dig being conducted) with a sealable lid to transport samples from field back to the lab
- Obtain a spoon or flat edge spatula
- Large metal spoon
- Constructed Sampler
- 5-gallon buckets (1 for each cross section)
- Duct Tape
- Sharpie
- Wooden 2x4
- Rubber Mallet/Hammer
- Scissors
- Cutting Knife
- Metric Tape Measure
- Slip Wrench

Collection:

1) Determine the field geotextile tube that will be collected from and count the number of bags from the far wall down to the one chosen. With the selected bag choose which center port or cross section will be collected from.
2) With the chosen bag and cross section selected measure from the edge of the bag closest to the open edge. Also measure the distance from the center port to the sides of the bags.
3) Starting from the center port push down the sampler until it cannot be pushed down anymore. From here take the 2x4 and the rubber mallet and drill down as far as possible or until all the holes are submerged. Shown in Figure 12 is how the board should be used.

Figure 12: Moisture Distribution Sampler with 2x4 board (Source: Tyson 2022)

4) With the submerged sampler in the sludge start twisting in the direction of the sampler's openings, as to scoop the sludge in with the aluminum slices. Rotate the sampler until there is hardly any friction resisting motion.

Figure 13: Removal of Sludge Sampler (Source: Tyson 2022)

5) Remove the sampler from the hole, carefully not to lose any samples. Figure 13 illustrates the sampler should be removed. Then with the spoon/spatula scoop the sludge from the blades and in the hole and deposit into labeled tubes depicting the dig, the hole number, and the geotextile tube being tested on.

Figure 14: Removed Sampler read for Sample to be Collected (Source: Tyson 2022)

6) Before moving on to the next sample location, the sampler should be cleaned of any excess material as to not cross contaminate into other holes or bags.
7) Continue to the next hole in the cross section by measuring an even distance from the center port (even distance meaning where you could do 3 or 4 holes across the cross section). Using the knife to cut into the geobag, cut a wide enough hole (create a cross in the bag and fold the flaps upwards) to allow for the sampler to fit inside. Follow the same steps as 3-6 for this hole. After the sampler has been removed using the duct tape on the slits in the geobag to close the hole.
8) Repeat Step 7 for each of the holes in the cross section.
9) Before leaving the geobag, collect enough material to fill about a third of a 5-gallon bucket to determine the specific gravity

Moisture Content:

1) When back in the lab take out 3 moisture content tins for each of the sample tubes that were filled.
2) Taking note of the label on each of the moisture content tins, write down the name and the empty weight of each.
3) Fill each moisture content tin with about a third of the sample that was collected from the site. Weigh the filled moisture content tin and place into the oven at 110 degrees Celsius for at least 16 hours.
4) With the dried samples take them out of the oven and weigh the dried weight before calculating the moisture content for each of the tins.

Specific Gravity:

1) Take some of the material from the bucket and place into a large bowl to place into the oven. This is done due to the high moisture content of the material.
2) Once the material is dried take it out of the oven and measure about 50grams of dried material and place to the side to be used in the specific gravity testing
3) Grab an empty pycnometer and grab the empty weight. Fill the pycnometer with deionized water and start deairing it at the vacuum pumps.
4) With a full pycnometer of deaired water, grab the full weight before emptying into a 600-1,000 mL beaker.
5) With the full beaker place a thermometer to determine the temperature of the deaired water.
6) While collecting the temperature start pouring the oven dried material into the pycnometer using a funnel and a squirt bottle to make sure all material goes into the pycnometer.
7) Pour some deaired water into the pycnometer, be sure not to fill all the way to the top. Swirl the pycnometer before hooking it up to the vacuum pump. This step should be done until the water reaches the line in the spoke of the pycnometer.
8) Weigh the filled pycnometer and then pour into a dry bowl before being placed into the oven. This is done to determine the mass of the soil.

9) After weighing the dried bowl, place all the data into the calculations to determine the specific gravity for the material in the specific cross section.

Table 1. Omega Geobag 5 Center Port

5/23/2022	WVU	Jonah Tyson
Bag 5	Cross Section A	Center Port
Depth (cm)	Moisture Content	Total Solids %
0	93.37%	6.63%
10		
20	93.93%	6.07%
30		
40	93.72%	6.28%
50		
60	93.81%	6.19%
70		
80	94.40%	5.60%
90		
100	94.45%	5.55%
110		

Table 2. Omega Geobag 7 Center Port

6/3/2022	WVU	Jonah Tyson
Bag 7	Cross Section A	Center Port
Depth (cm)	Moisture Content	Total Solids %
0	93.67%	6.33%
9		
20	93.62%	6.38%
29		
40	94.75%	5.25%
49		
60	90.78%	9.22%
69		
80	92.64%	7.36%
89		

Table 3. Omega Geobag 7 1.12m Right of Center

6/8/2022	WVU	Jonah Tyson
Bag 7	**Cross Section A**	**1.12m From Center**
Depth (cm)	**Moisture Content**	**Total Solids %**
0	93.75%	6.25%
9		
20	93.88%	6.12%
29		
40	92.60%	7.40%
49		
60	94.68%	5.32%
69		
80	90.22%	9.78%
89		
100	90.64%	9.36%
109		

Table 4. Omega Geobag 7 2.24m Right of Center

6/8/2022	WVU	Jonah Tyson
Bag 7	**Cross Section A**	**2.24m From Center**
Depth (cm)	**Moisture Content**	**Total Solids %**
0	93.78%	6.22%
9		
20	88.65%	11.35%
29		
40	94.49%	5.51%
49		
60	93.26%	6.74%
69		
80	92.74%	7.26%
89		
100	93.65%	6.35%
109		

Table 5. Omega Geobag 7 3.05m Right of Center

<table>
<tr><th>6/8/2022</th><th>WVU</th><th>Jonah Tyson</th></tr>
<tr><th>Bag 7</th><th>Cross Section A</th><th>3.05m From Center</th></tr>
<tr><th>Depth (cm)</th><th>Moisture Content</th><th>Total Solids %</th></tr>
<tr><td>0</td><td rowspan="2">93.40%</td><td rowspan="2">6.60%</td></tr>
<tr><td>9</td></tr>
<tr><td>20</td><td rowspan="2">93.18%</td><td rowspan="2">6.82%</td></tr>
<tr><td>29</td></tr>
<tr><td>40</td><td rowspan="2">92.48%</td><td rowspan="2">7.52%</td></tr>
<tr><td>49</td></tr>
<tr><td>60</td><td rowspan="2">94.07%</td><td rowspan="2">5.93%</td></tr>
<tr><td>69</td></tr>
<tr><td>80</td><td rowspan="2">94.33%</td><td rowspan="2">5.67%</td></tr>
<tr><td>89</td></tr>
</table>

Table 6. Omega Geobag 9 Center Port

<table>
<tr><th>9/9/2022</th><th>WVU</th><th>Jonah Tyson</th></tr>
<tr><th>Bag 9</th><th>Cross Section A</th><th>Center Port</th></tr>
<tr><th>Depth (cm)</th><th>Moisture Content</th><th>Total Solids %</th></tr>
<tr><td>0</td><td rowspan="2">92.55%</td><td rowspan="2">7.45%</td></tr>
<tr><td>9</td></tr>
<tr><td>20</td><td rowspan="2">91.29%</td><td rowspan="2">8.71%</td></tr>
<tr><td>29</td></tr>
<tr><td>40</td><td rowspan="2">91.54%</td><td rowspan="2">8.46%</td></tr>
<tr><td>49</td></tr>
<tr><td>60</td><td rowspan="2">90.69%</td><td rowspan="2">9.31%</td></tr>
<tr><td>69</td></tr>
<tr><td>80</td><td rowspan="2">90.19%</td><td rowspan="2">9.81%</td></tr>
<tr><td>89</td></tr>
<tr><td>100</td><td rowspan="2">91.52%</td><td rowspan="2">8.48%</td></tr>
<tr><td>109</td></tr>
</table>

Table 7. Omega Geobag 1.2m Right of Center

9/9/2022	WVU	Jonah Tyson
Bag 9	Cross Section A	1.2m From Center
Depth (cm)	Moisture Content	Total Solids %
0	92.33%	7.67%
9		
20	92.90%	7.10%
29		
40	91.61%	8.39%
49		
60	90.94%	9.06%
69		
80	91.81%	8.19%
89		
100	93.54%	6.46%
109		

Table 8. Omega Geobag 9 2.2m Right of Center

9/9/2022	WVU	Jonah Tyson
Bag 9	Cross Section A	2.2m From Center
Depth (cm)	Moisture Content	Total Solids %
0	92.22%	7.78%
9		
20	93.38%	6.62%
29		
40	92.06%	7.94%
49		
60	91.57%	8.43%
69		
80	92.70%	7.30%
89		
100	94.38%	5.62%
109		
120	94.48%	5.52%
129		

Table 9. Omega Geobag 9 3.1m Right of Center

9/9/2022	WVU	Jonah Tyson
Bag 9	Cross Section A	3.1m From Center
Depth (cm)	Moisture Content	Total Solids %
0	89.69%	10.31%
9		
20	90.62%	9.38%
29		
40	90.71%	9.29%
49		
60	92.29%	7.71%
69		
80	94.42%	5.58%
89		
100	93.39%	6.61%
109		

Table 10. Omega Geobag 11 CS A Center Port

11/2/2022	WVU	Jonah Tyson
Bag 11	Cross Section A	Center Port
Depth (cm)	Moisture Content	Total Solids %
0	95.47%	4.53%
9		
20	95.10%	4.90%
29		
40	94.93%	5.07%
49		
60	94.93%	5.07%
69		
80	94.65%	5.35%
89		
100	93.25%	6.75%
109		

Table 11. Omega Geobag 11 CS A 1m Right of Center

11/2/2022	WVU	Jonah Tyson
Bag 11	Cross Section A	1m From Center
Depth (cm)	Moisture Content	Total Solids %
0	95.09%	4.91%
9		
20	94.62%	5.38%
29		
40	94.98%	5.02%
49		
60	94.78%	5.22%
69		
80	94.76%	5.24%
89		
100	93.36%	6.64%
109		

Table 12. Omega Geobag 11 CS A 2m Right of Center

11/2/2022	WVU	Jonah Tyson
Bag 11	Cross Section A	2m From Center
Depth (cm)	Moisture Content	Total Solids %
0	93.57%	6.43%
9		
20	94.00%	6.00%
29		
40	94.65%	5.35%
49		
60	94.53%	5.47%
69		
80	94.83%	5.17%
89		
100	93.02%	6.98%
109		

Table 13. Omega Geobag 11 CS A 2.9m Right of Center

11/2/2022	WVU	Jonah Tyson
Bag 11	Cross Section A	2.9m From Center
Depth (cm)	Moisture Content	Total Solids %
0 9	93.64%	6.36%
20 29	94.75%	5.25%
40 49	94.11%	5.89%
60 69	94.14%	5.86%
80 89	92.79%	7.21%

Table 14. Omega Geobag 11 CS B Center Port

11/2/2022	WVU	Jonah Tyson
Bag 11	Cross Section B	Center Port
Depth (cm)	Moisture Content	Total Solids %
0 9	95.74%	4.26%
20 29	95.28%	4.72%
40 49	94.54%	5.46%
60 69	95.04%	4.96%
80 89	94.77%	5.23%
100 109	94.16%	5.84%

Table 15. Omega Geobag CS B 0.8m Right of Center

11/2/2022	WVU	Jonah Tyson
Bag 11	Cross Section B	0.8m From Center
Depth (cm)	Moisture Content	Total Solids %
0	95.05%	4.95%
9		
20	95.00%	5.00%
29		
40	95.13%	4.87%
49		
60	95.09%	4.91%
69		
80	94.58%	5.42%
89		
100	94.44%	5.56%
109		

Table 16. Omega Geobag CS B 1.6m Right of Center

11/2/2022	WVU	Jonah Tyson
Bag 11	Cross Section B	1.6m From Center
Depth (cm)	Moisture Content	Total Solids %
0	94.90%	5.10%
9		
20	94.87%	5.13%
29		
40	94.60%	5.40%
49		
60	94.85%	5.15%
69		
80	94.10%	5.90%
89		
100	93.78%	6.22%
109		

Table 17. Omega Geobag 11 CS B 2.3m Right of Center

11/2/2022	WVU	Jonah Tyson
Bag 11	Cross Section B	2.3m From Center
Depth (cm)	Moisture Content	Total Solids %
0	93.86%	6.14%
9		
20	94.59%	5.41%
29		
40	94.37%	5.63%
49		
60	94.60%	5.40%
69		
80	93.69%	6.31%
89		

Table 18. Omega Geobag 6 Center Port

1/17/2023	WVU	Jonah Tyson
Bag 6	Cross Section A	Center Port
Depth (cm)	Moisture Content	Total Solids %
0	92.65%	7.35%
9		
20	94.61%	5.39%
29		
40	93.40%	6.60%
49		
60	93.64%	6.36%
69		
80	92.99%	7.01%
89		
100	93.05%	6.95%
109		

Table 19. Omega Geobag 6 0.75m Right of Center

1/17/2023	WVU	Jonah Tyson
Bag 6	Cross Section A	0.75m From Center
Depth (cm)	Moisture Content	Total Solids %
0	93.03%	6.97%
9		
20	94.62%	5.38%
29		
40	93.01%	6.99%
49		
60	93.26%	6.74%
69		
80	93.15%	6.85%
89		
100	93.66%	6.34%
109		

Table 20. Omega Geobag 6 1.5m Right of Center

1/17/2023	WVU	Jonah Tyson
Bag 6	Cross Section A	1.5m From Center
Depth (cm)	Moisture Content	Total Solids %
0	93.11%	6.89%
9		
20	95.10%	4.90%
29		
40	93.49%	6.51%
49		
60	92.77%	7.23%
69		
80	93.78%	6.22%
89		
100	93.54%	6.46%
109		

Table 21. Omega Geobag 6 2m Right of Center

1/17/2023	WVU	Jonah Tyson
Bag 6	Cross Section A	2m From Center
Depth (cm)	Moisture Content	Total Solids %
0	92.75%	7.25%
9		
20	94.75%	5.25%
29		
40	92.80%	7.20%
49		
60	93.02%	6.98%
69		
80	93.59%	6.41%
89		
100	93.58%	6.42%
109		

Field-scale testing: Hanging Bag Tests (Test Set 1)

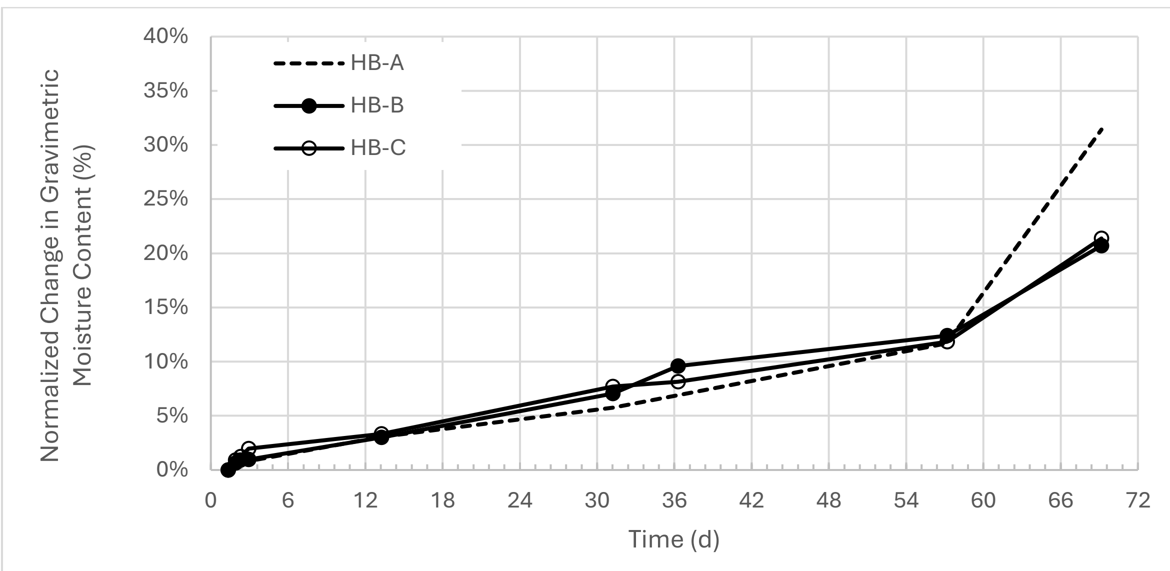

Figure 14. Normalized Change in Gravimetric Moisture Content (%) vs Time (d) for HB-A, HB-B, and HB-C.

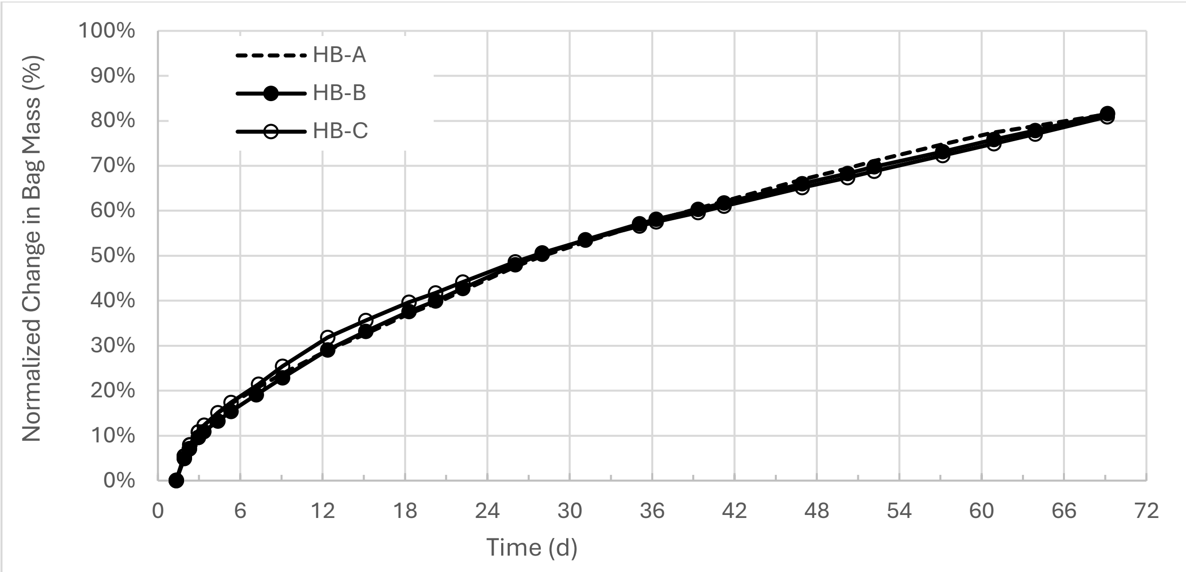

Figure 15. Normalized Change in Bag Mass (%) vs Time (d) for HB-A, HB-B, and HB-C.

Field-scale testing: Hanging Bag Tests (Test Set 2)

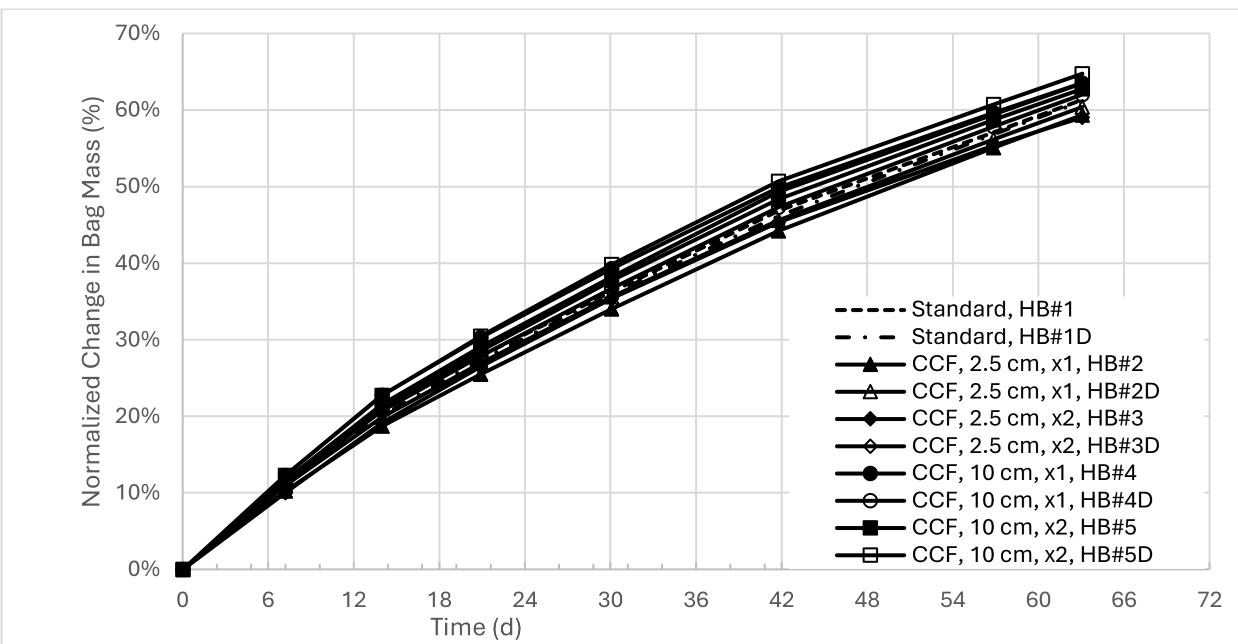

Figure 16. Normalized Change in Bag Mass (%) vs Time (d) for all 10 Test Set 2 Hanging Bags.

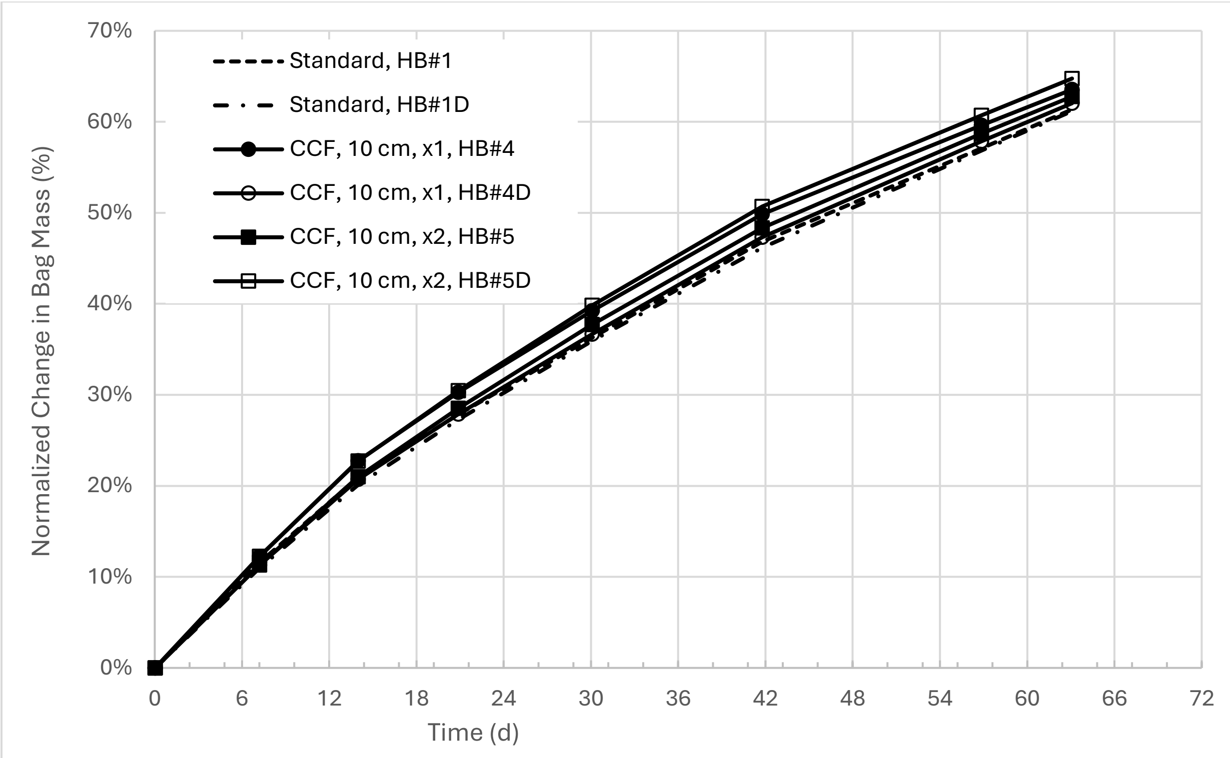

Figure 17. Normalized Change in Bag Mass (%) vs Time (d) for HB#1, HB#1D, HB#4, HB#4D, HB#5 and HB#5D.

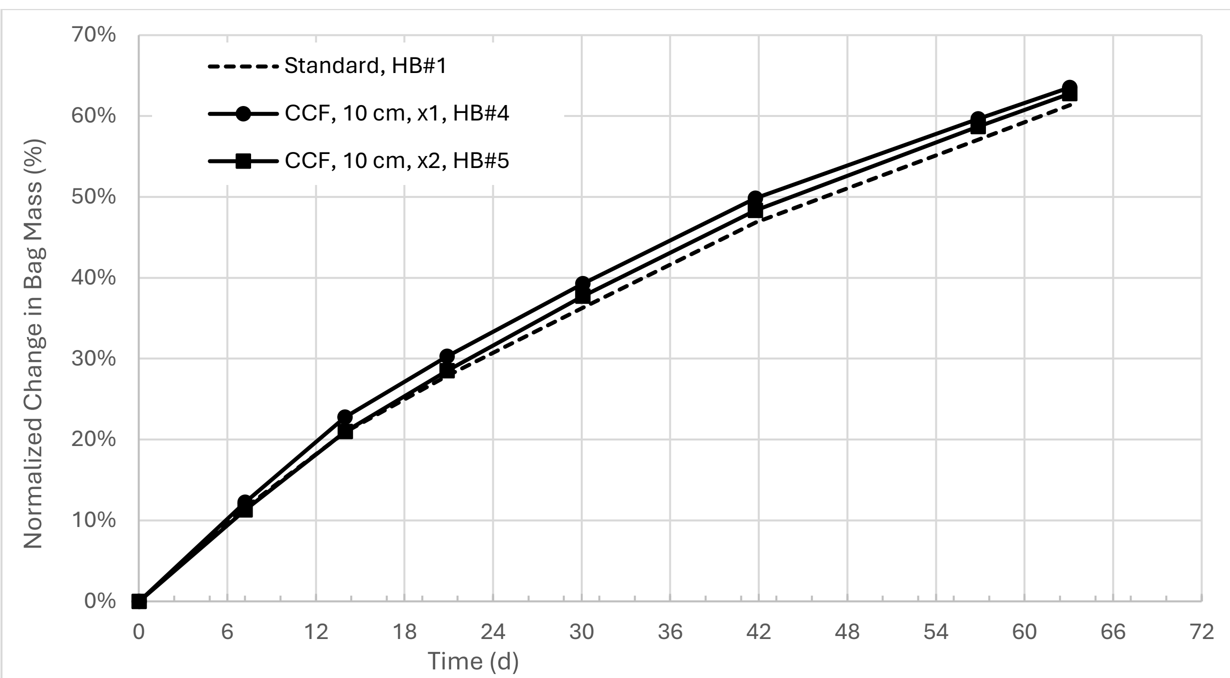

Figure 18. Normalized Change in Bag Mass (%) vs Time (d) for HB#1, HB#4, and HB#5.

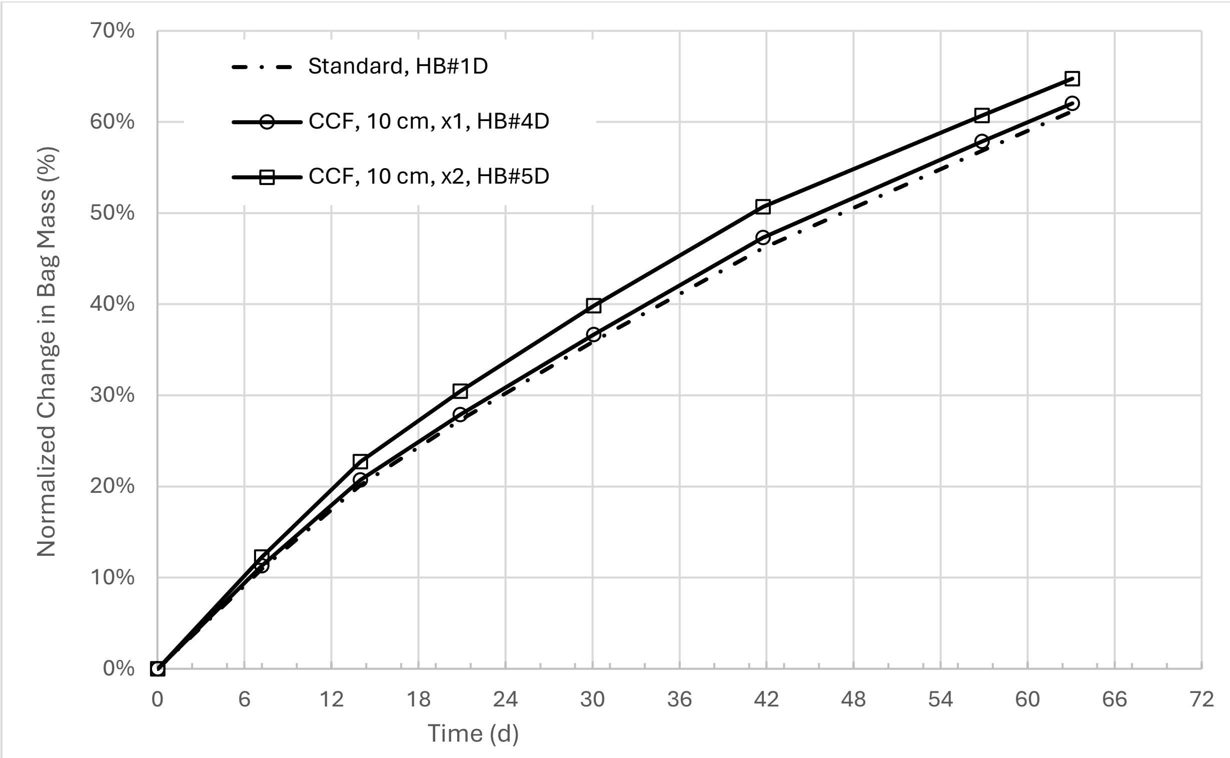

Figure 19. Normalized Change in Bag Mass (%) vs Time (d) for HB#1D, HB#4D, and HB#5D.

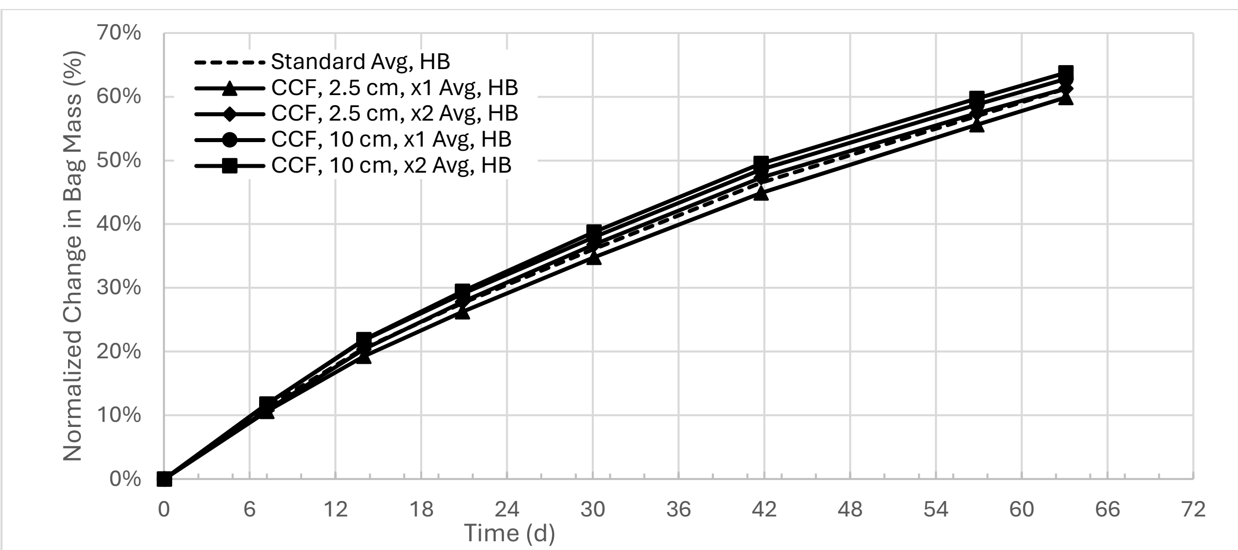

Figure 20. Normalized Change in Bag Mass (%) vs Time (d) for all Test Set 2 Hanging Bag Configuration Averages.

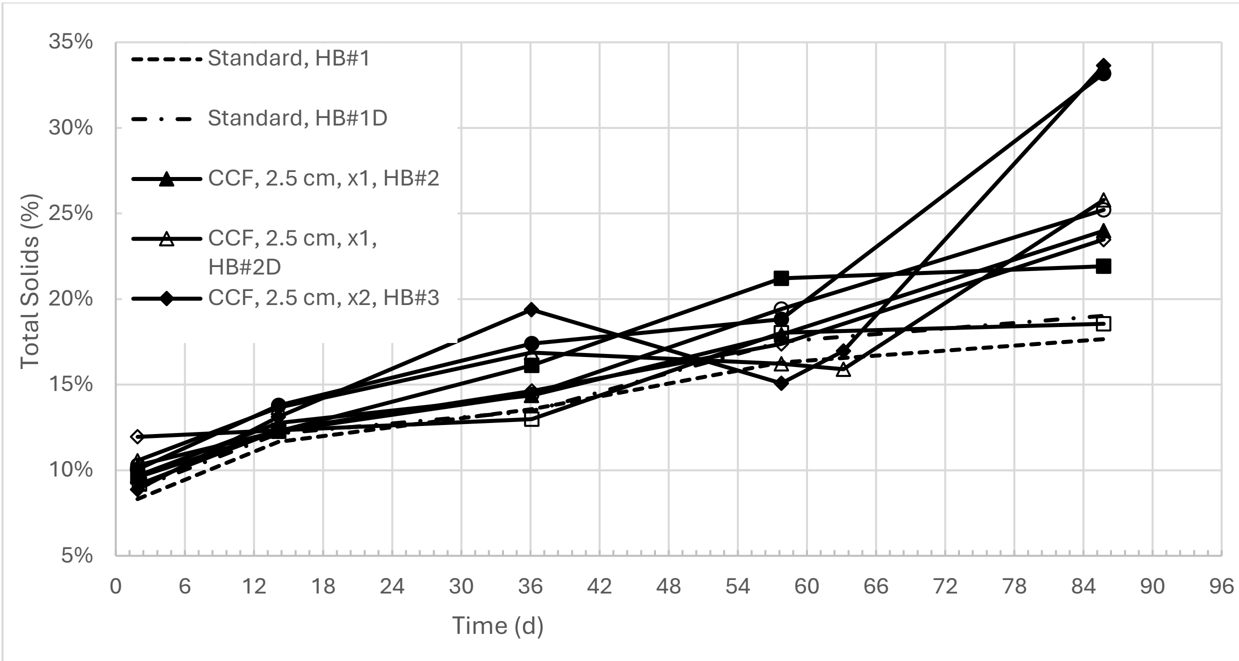

Figure 21. Total Solids (%) vs Time (d) for all 10 Test Set 2 Hanging Bags.

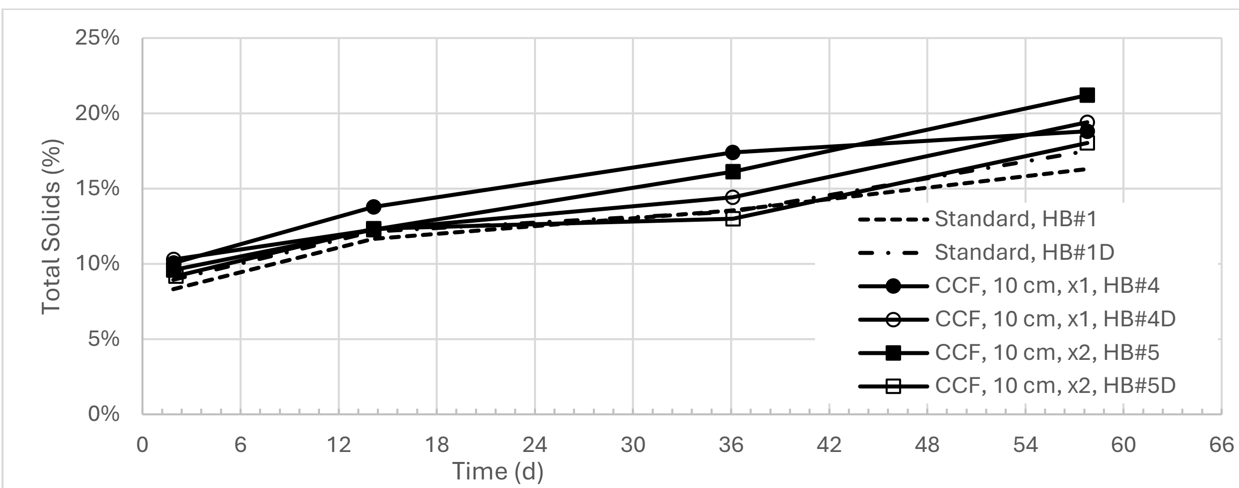

Figure 22. Total Solids Content (%) vs Time (d) for HB#1, HB#1D, HB#4, HB#4D, HB#5 and HB#5D.

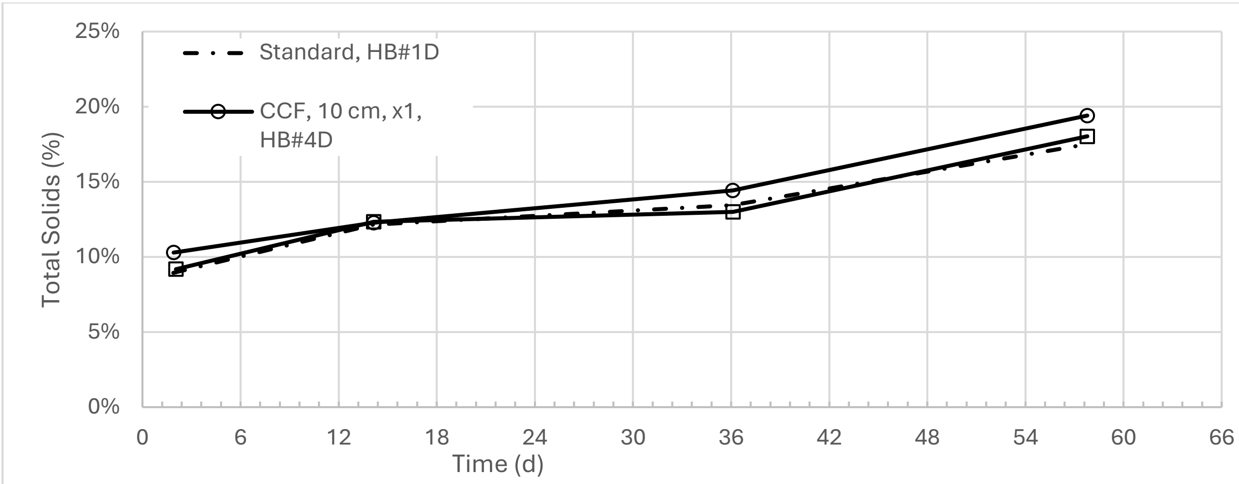

Figure 23. Total Solids Content (%) vs Time (d) for HB#1D, HB#4D, and HB#5D.

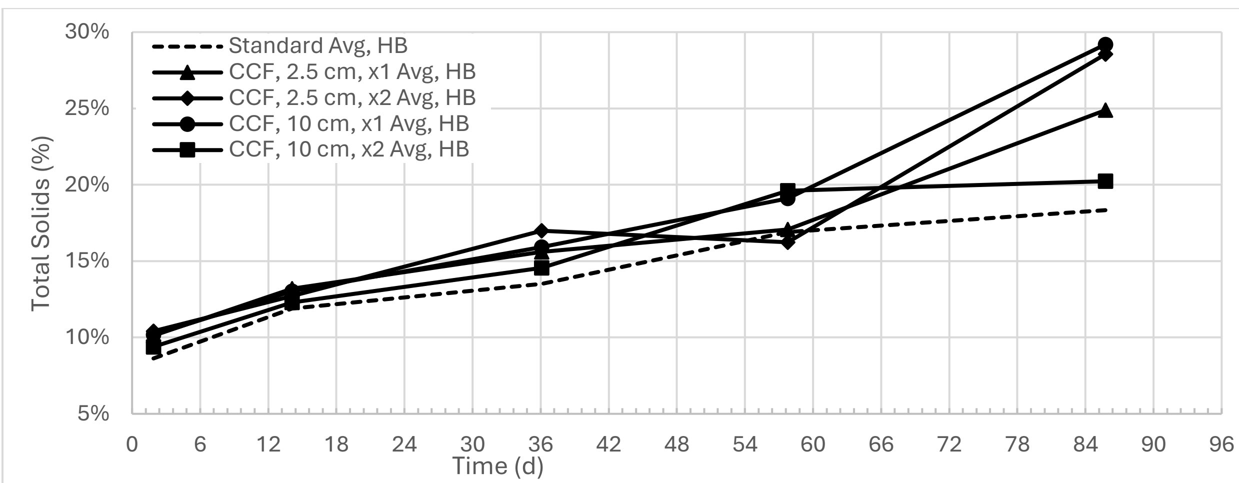

Figure 24. Total Solids (%) vs Time (d) for all Test Set 2 Hanging Bag Configuration Averages.

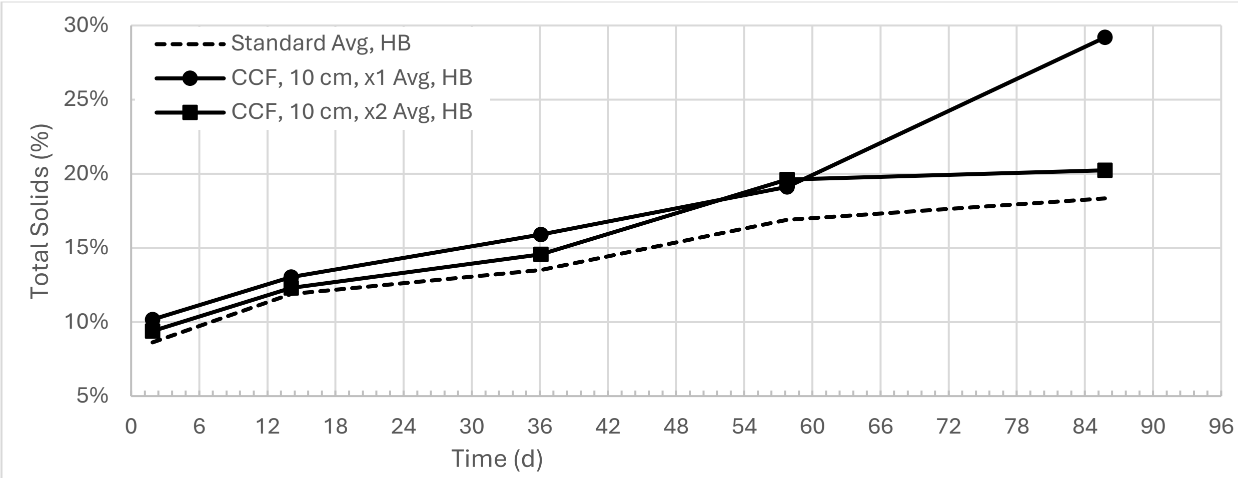

Figure 25. Total Solids Content (%) vs Time (d) for Standard, [CCF, 10 cm, x1], and [CCF, 10 cm, x2] Configuration Average.

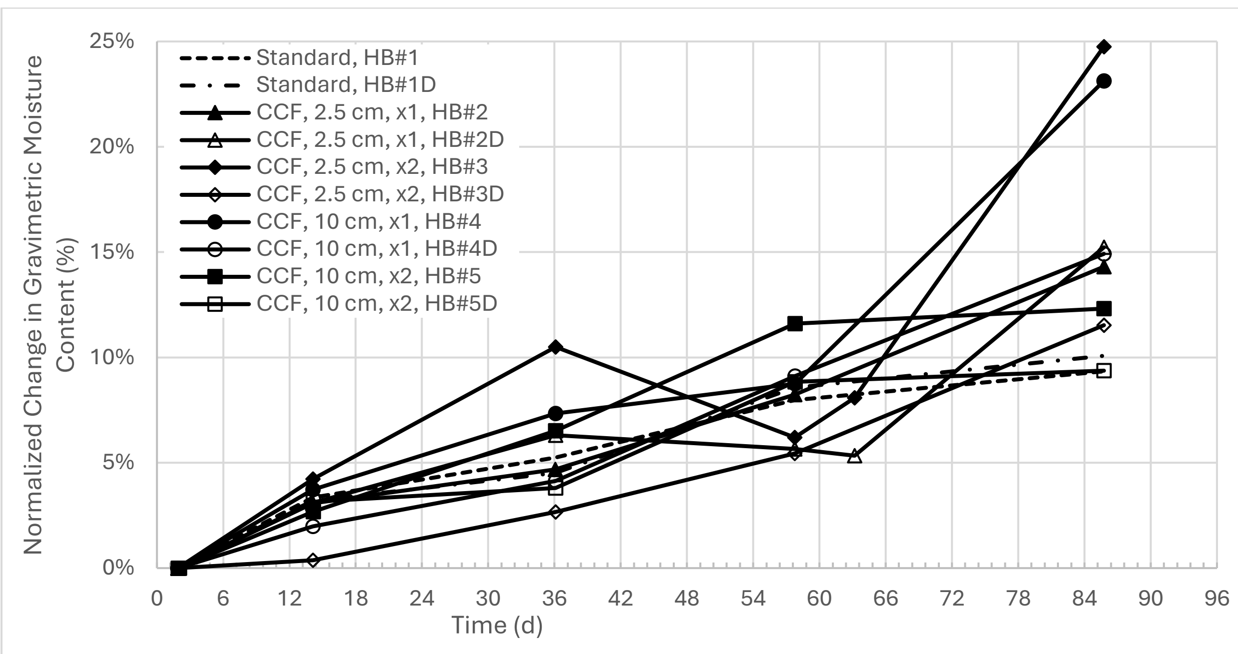

Figure 26. Normalized Change in Gravimetric Moisture Content (%) vs Time (d) for all 10 Test Set 2 Hanging Bags.

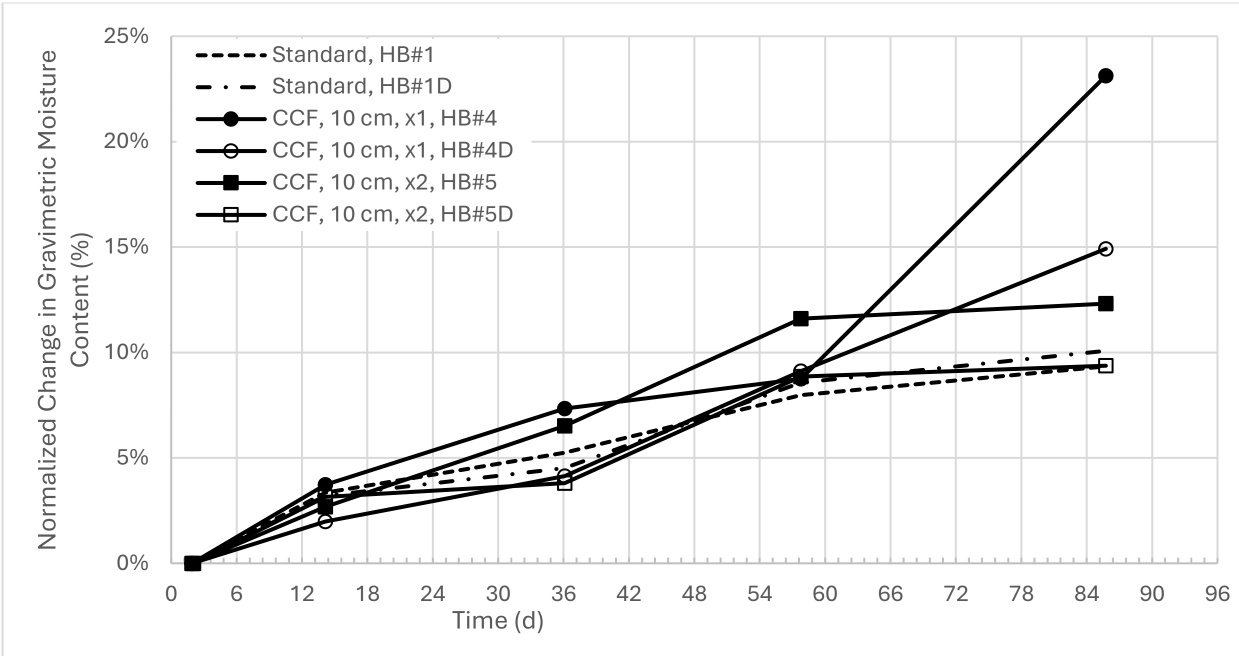

Figure 27. Normalized Change in Gravimetric Moisture Content (%) vs Time (d) for HB#1, HB#1D, HB#4, HB#4D, HB#5, and HB#5D.

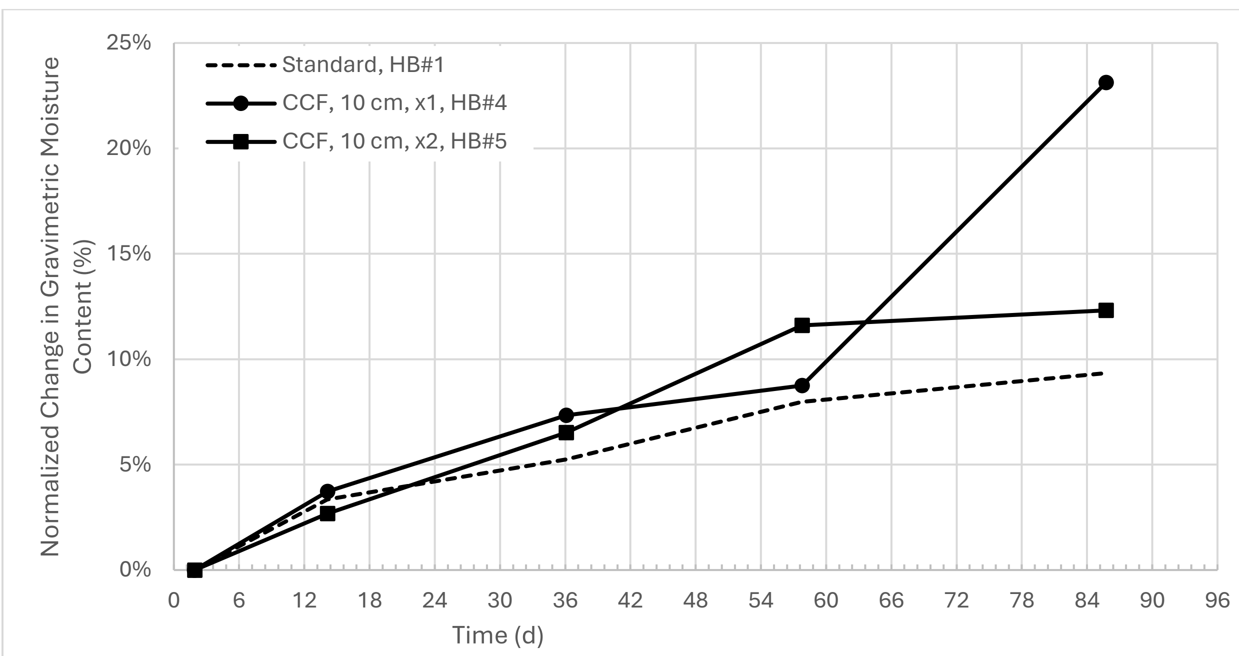

Figure 28. Normalized Change in Gravimetric Moisture Content (%) vs Time (d) for HB#1, HB#4, and HB#5.

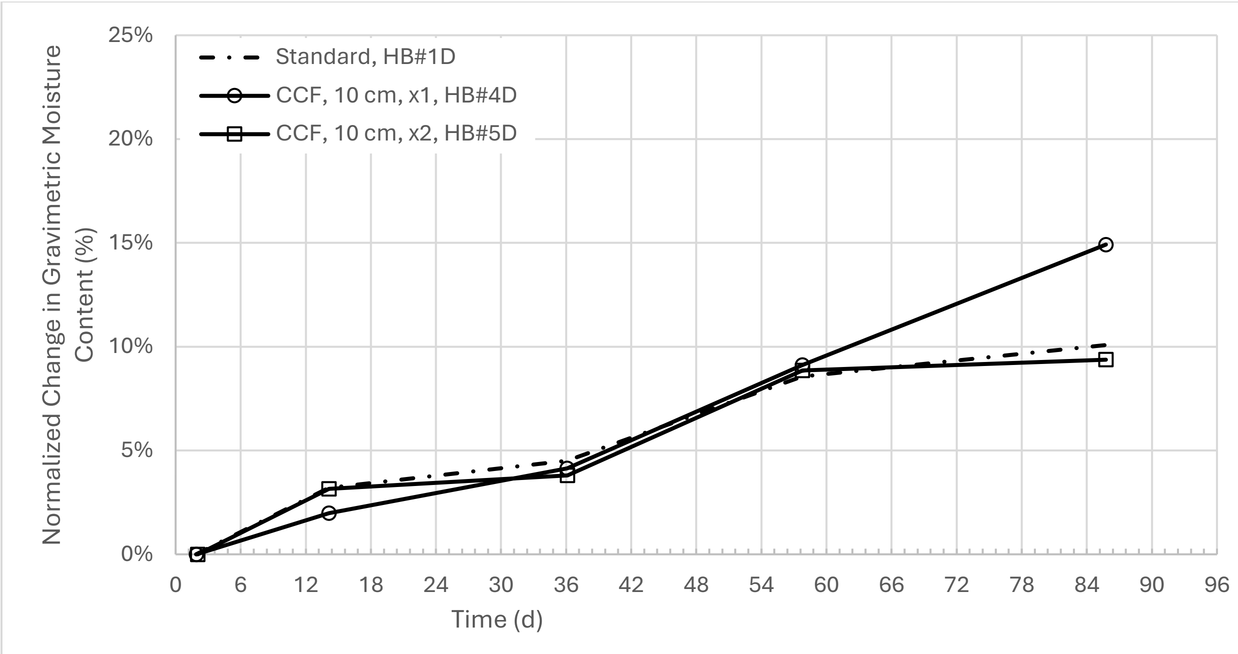

Figure 29. Normalized Change in Gravimetric Moisture Content (%) vs Time (d) for HB#1D, HB#4D, and HB#5D.

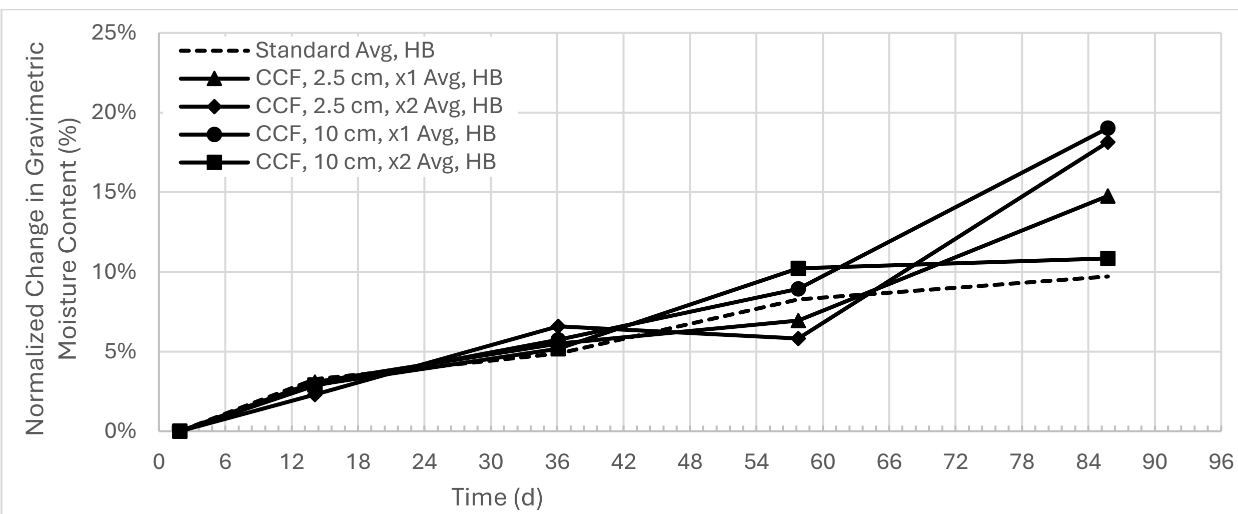

Figure 30. Normalized Change in Gravimetric Moisture Content (%) vs Time (d) for all Test Set 2 Hanging Bag Configuration Averages.

Field-scale testing: Geotube Dewatering Tests (Test Set 3)

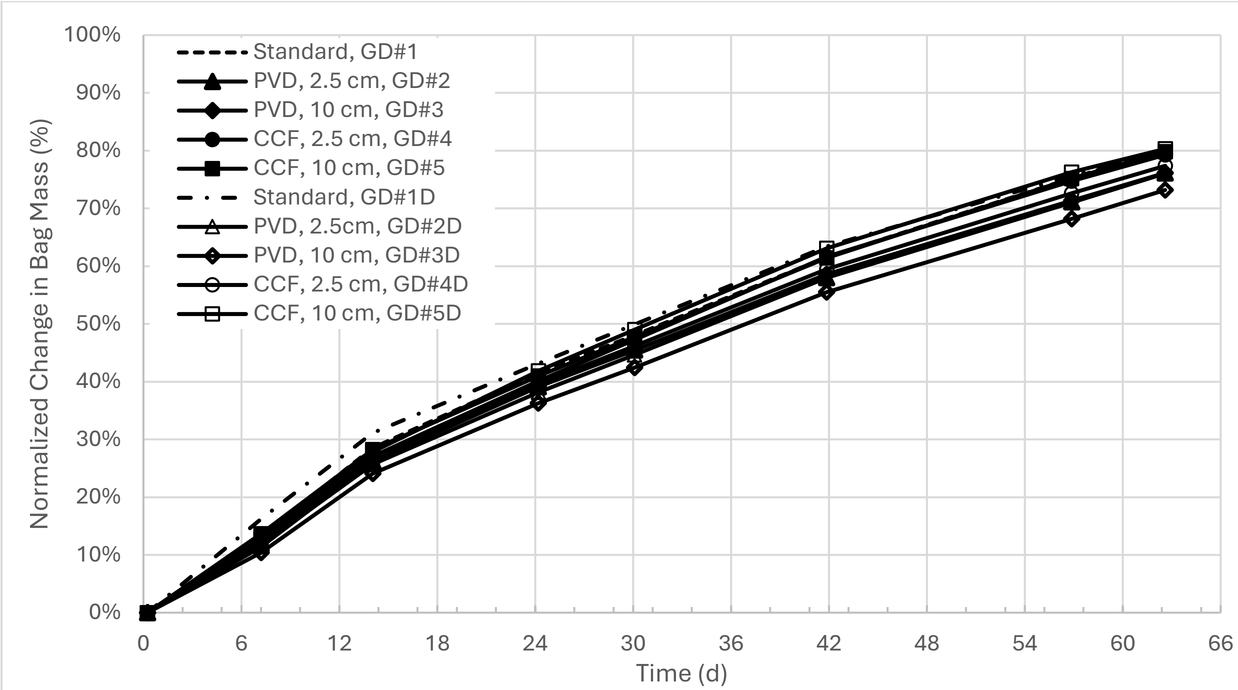

Figure 31. Normalized Change in Bag Mass (%) vs Time (d) for all 10 Test Set 3 GDT Bags.

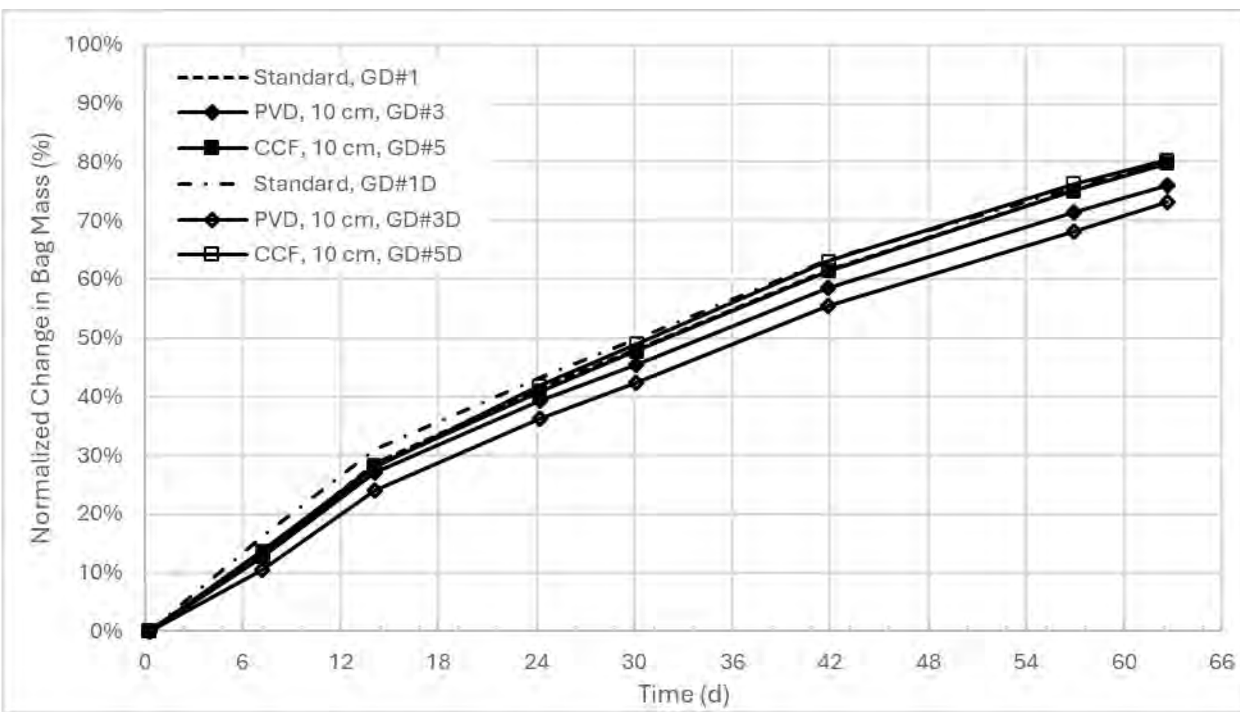

Figure 32. Normalized Change in Bag Mass (%) vs Time (d) GD#1, GD#1D, GD#3, GD#3D, GD#5, and GD#5D.

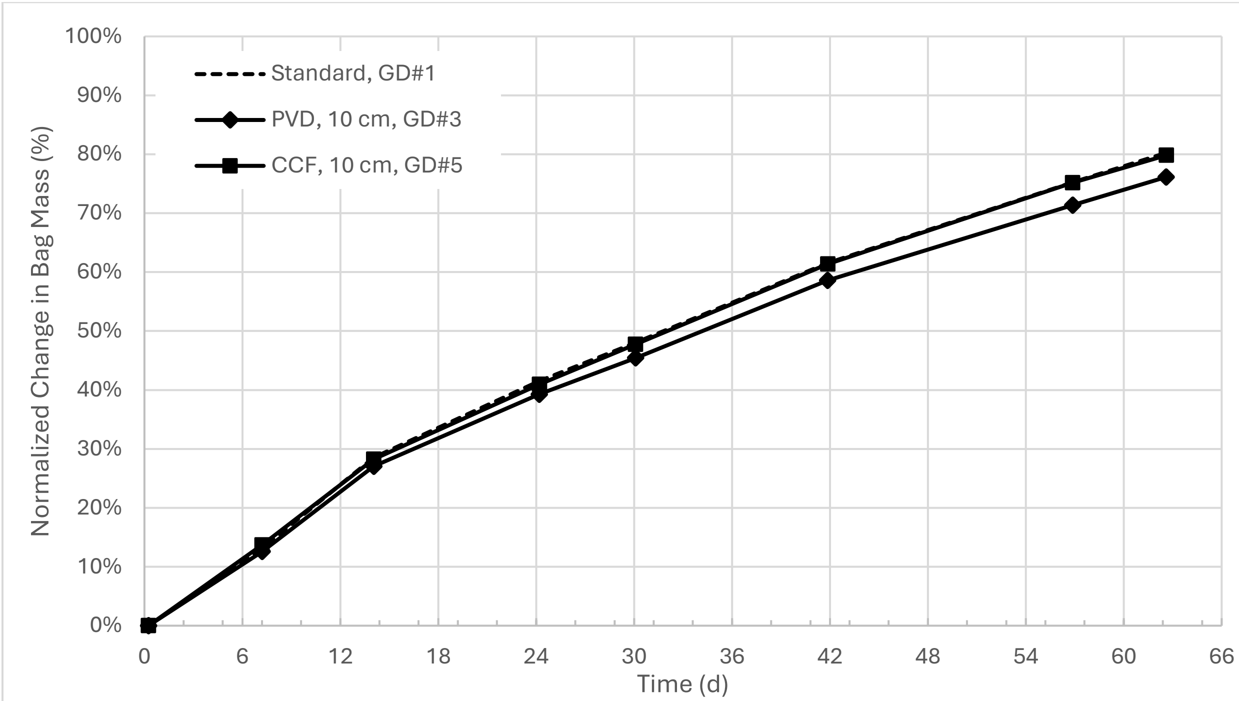

Figure 33. Normalized Change in Bag Mass (%) vs Time (d) GD#1, GD#3, and GD#5.

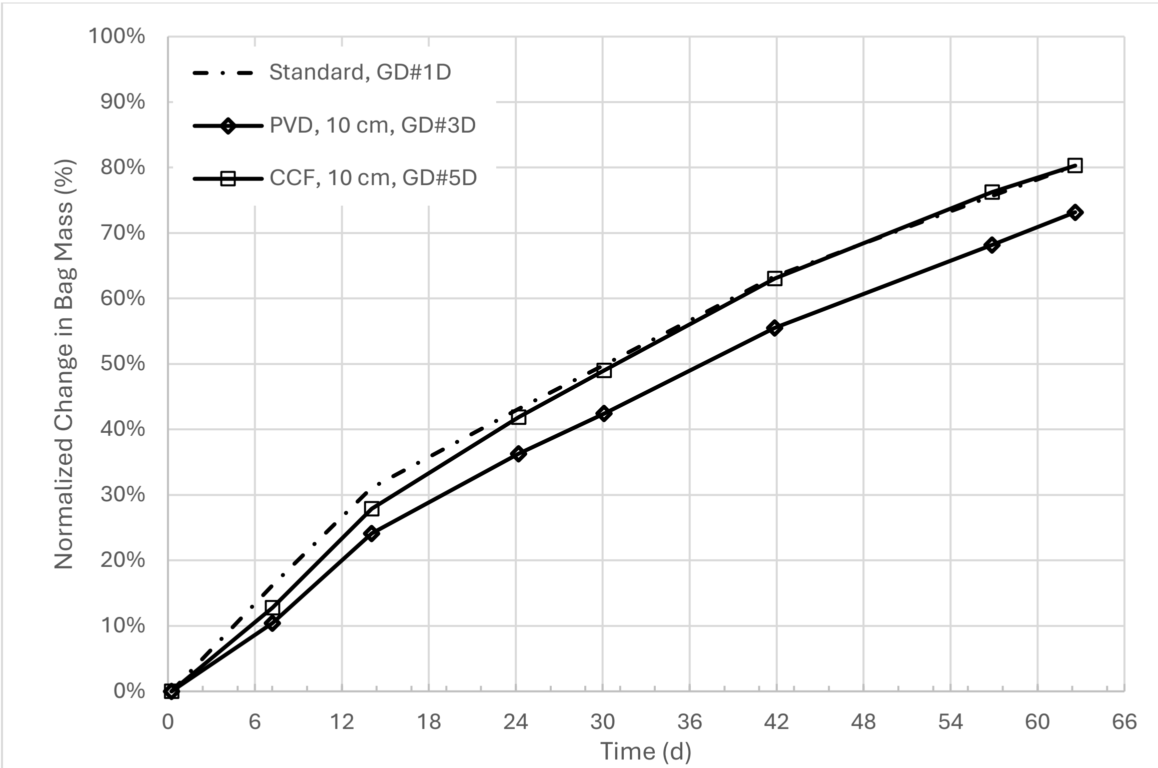

Figure 34. Normalized Change in Bag Mass (%) vs Time (d) for GD#1D, GD#3D, and GD#5D.

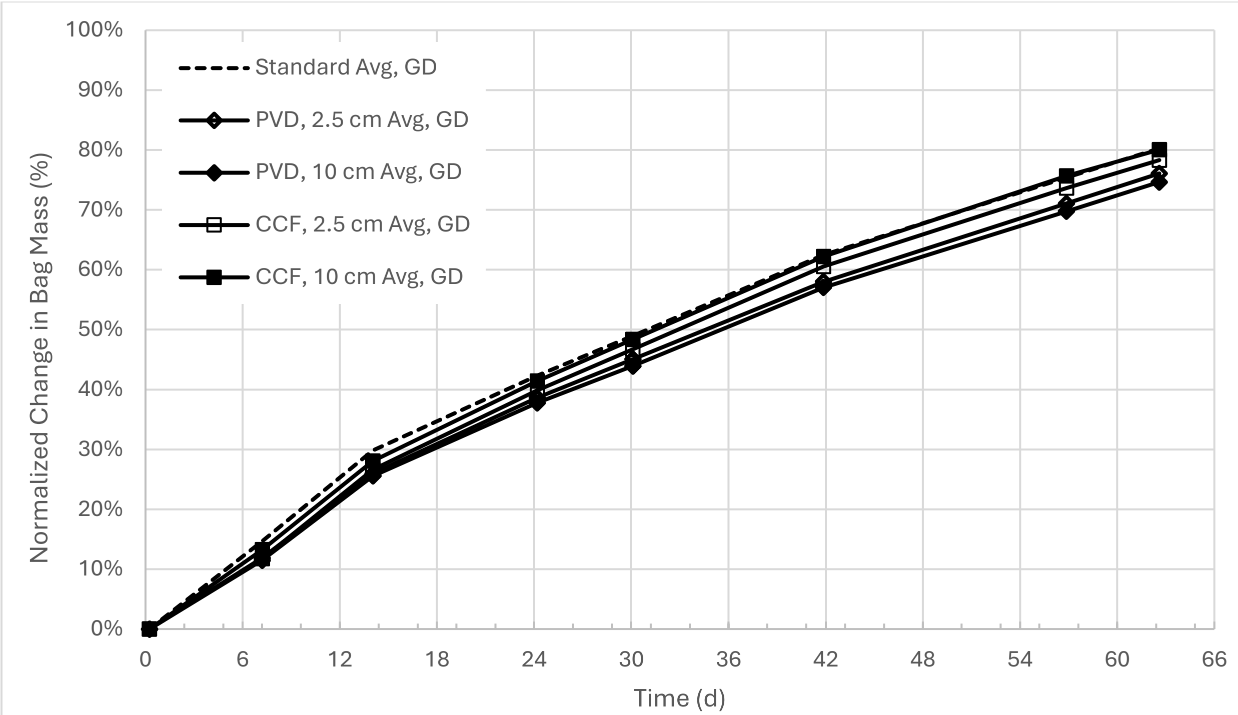

Figure 35. Normalized Change in Bag Mass (%) vs Time (d) for all Test Set 3 GDT Bag Configuration Averages.

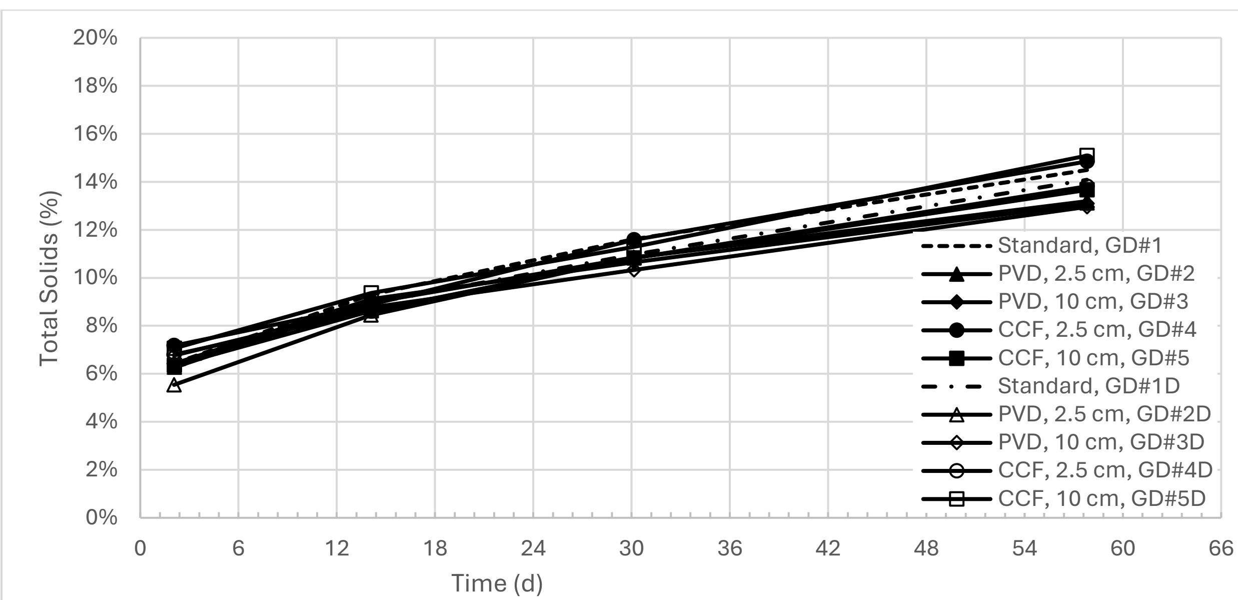

Figure 36. Total Solids (%) vs Time (d) for all 10 Test Set 3 GDT Bags.

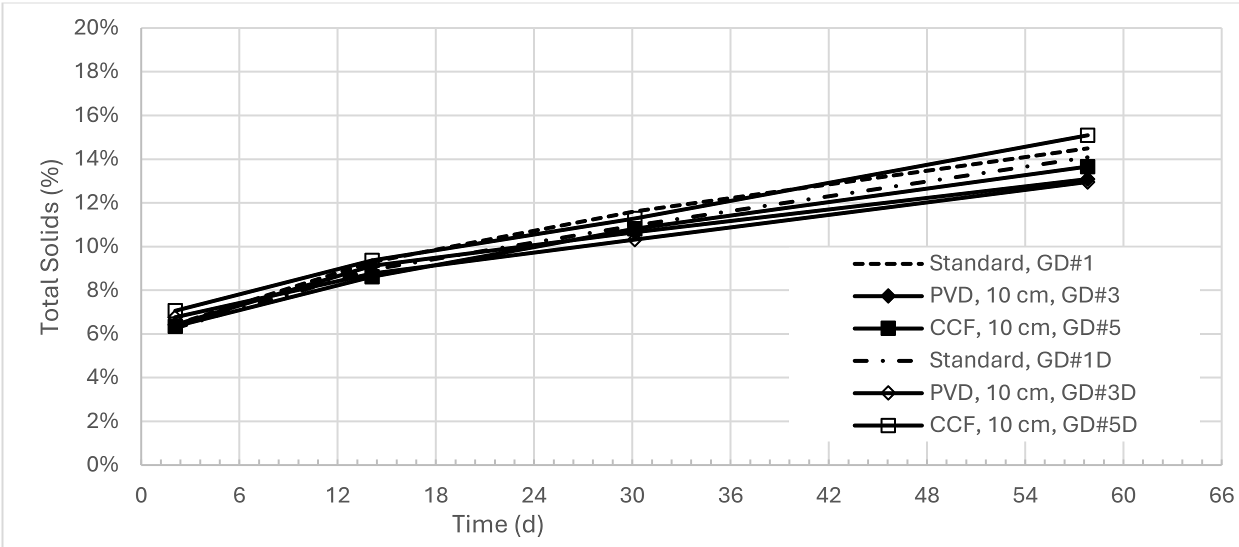

Figure 37. Total Solids Content (%) vs Time (d) GD#1, GD#1D, GD#3, GD#3D, GD#5, and GD#5D.

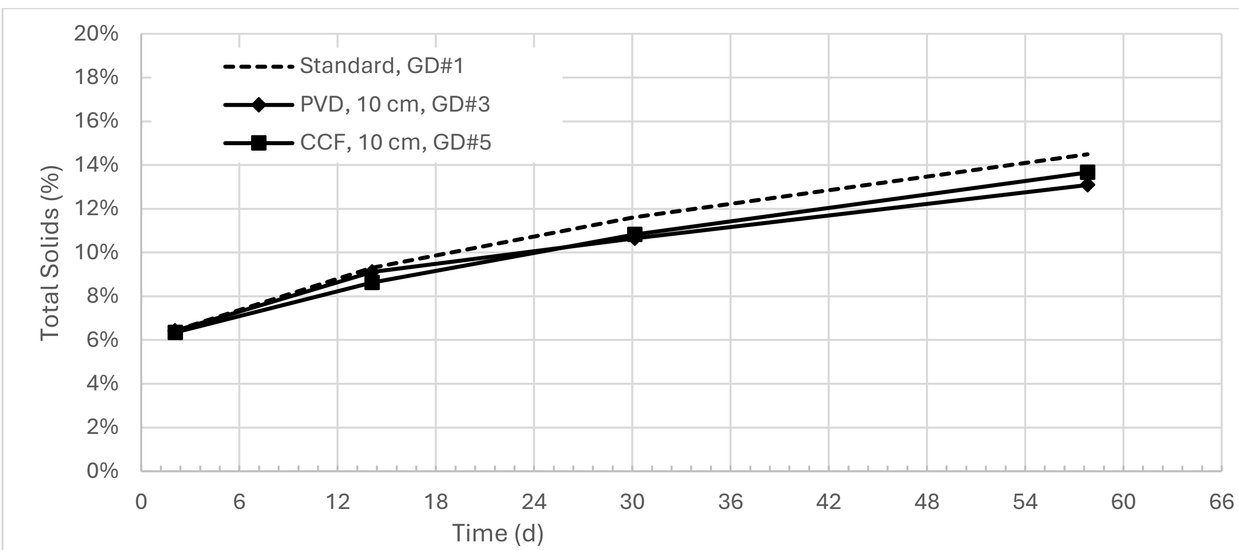

Figure 38. Total Solids Content (%) vs Time (d) for GD#1, GD#3, and GD#5.

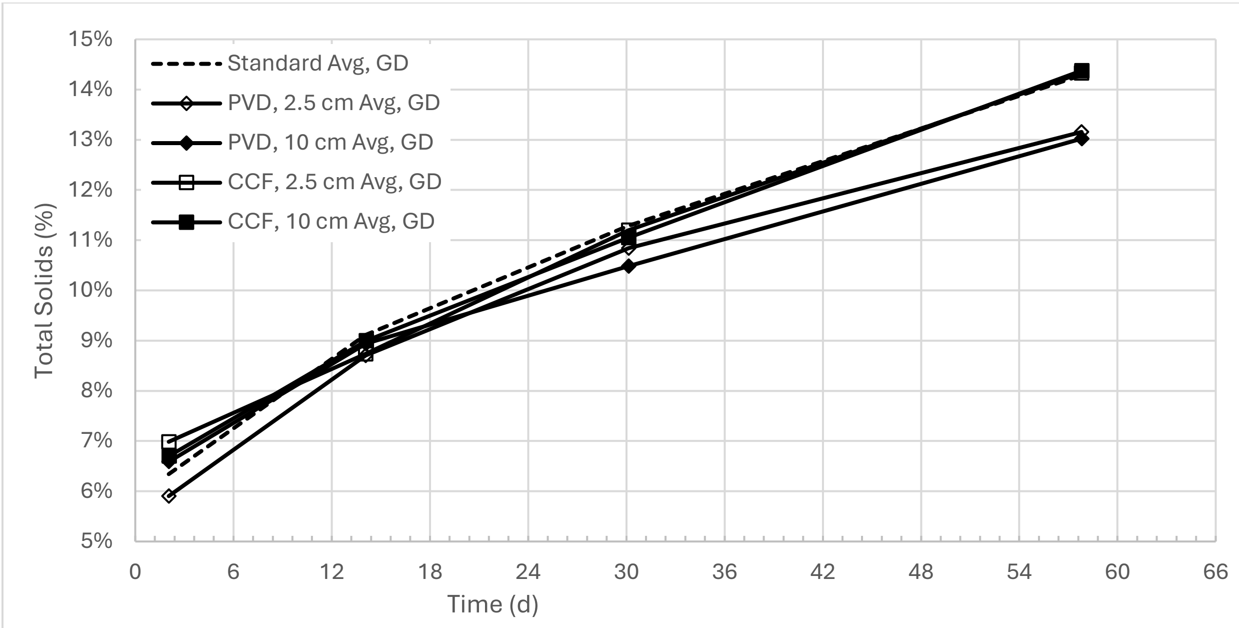

Figure 39. Total Solids (%) vs Time (d) for all Test Set 3 GDT Bag Configuration Averages.

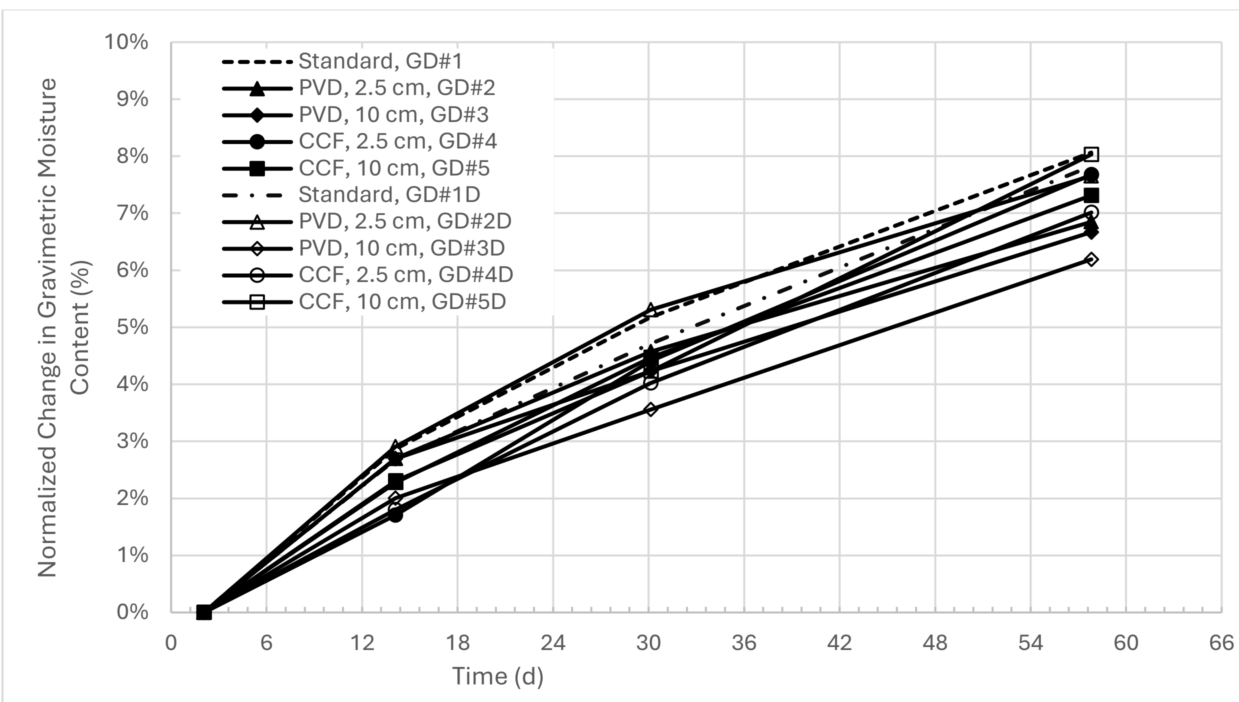

Figure 40. Normalized Change in Gravimetric Moisture Content (%) vs Time (d) for all 10 Test Set 3 GDT Bags.

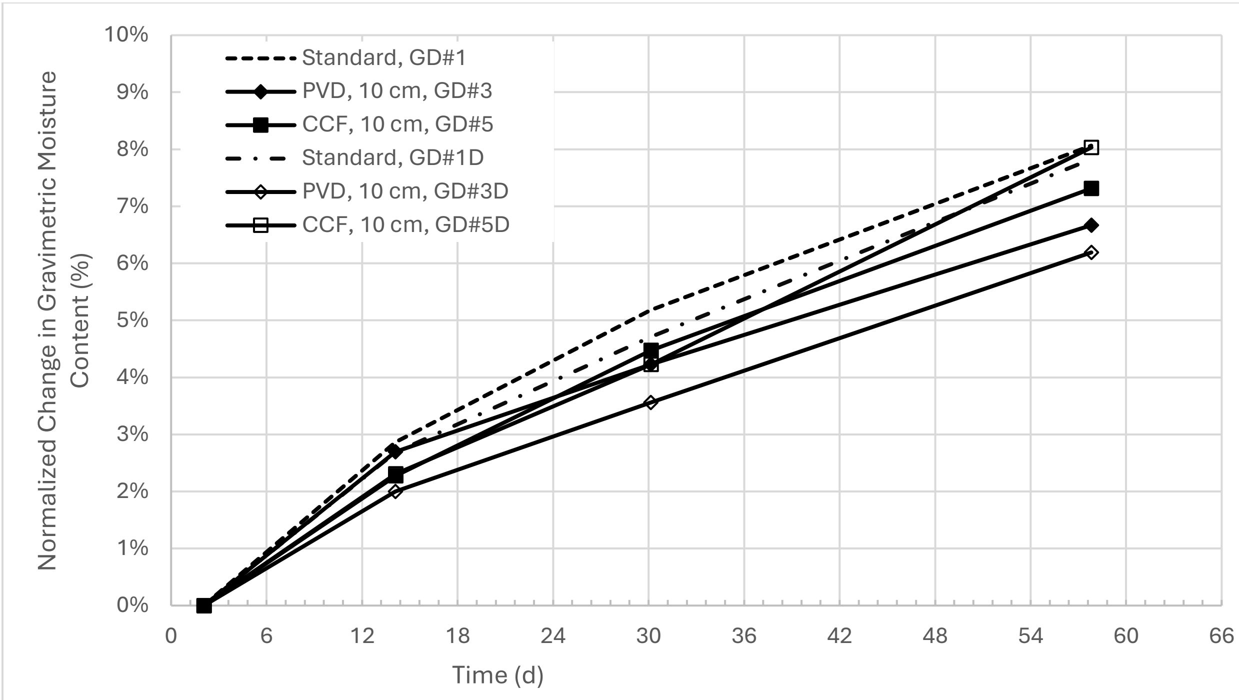

Figure 41. Normalized Change in Gravimetric Moisture Content (%) vs Time (d) for GD#1, GD#1D, GD#3, GD#3D, GD#5, and GD#5D.

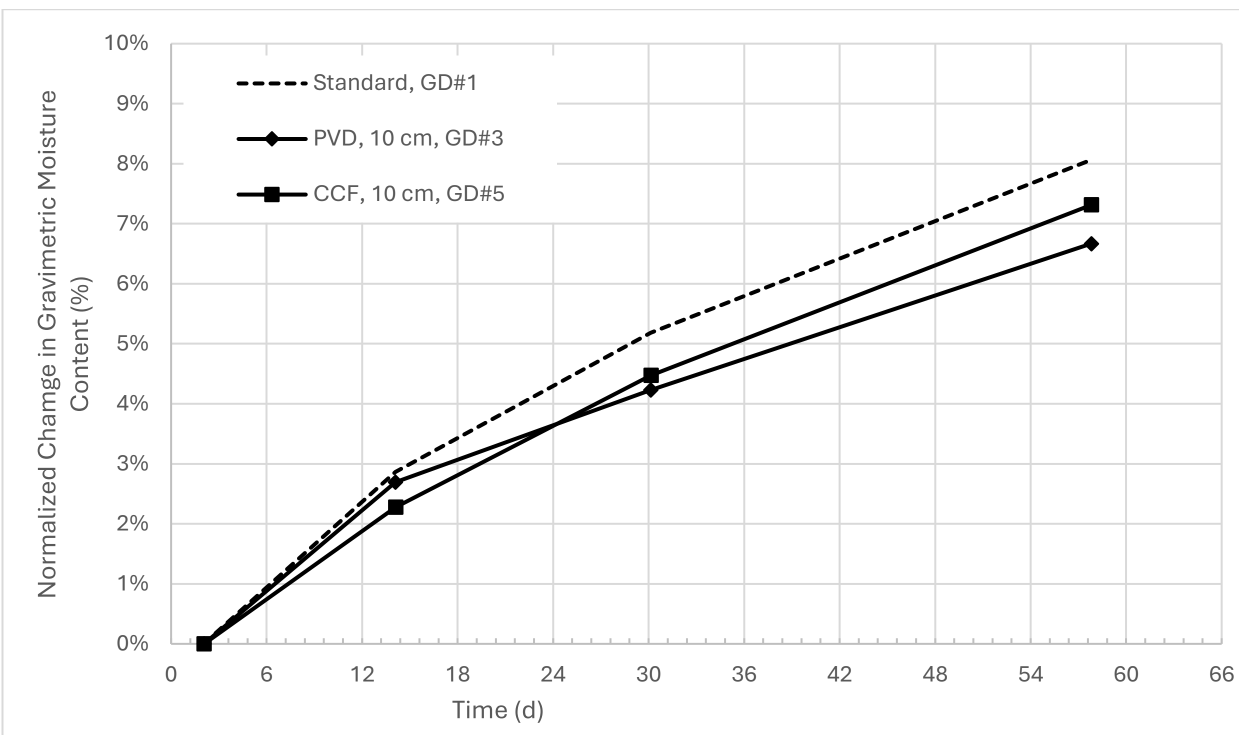

Figure 42. Normalized Change in Gravimetric Moisture Content (%) vs Time (d) for GD#1, GD#3, and GD#5.

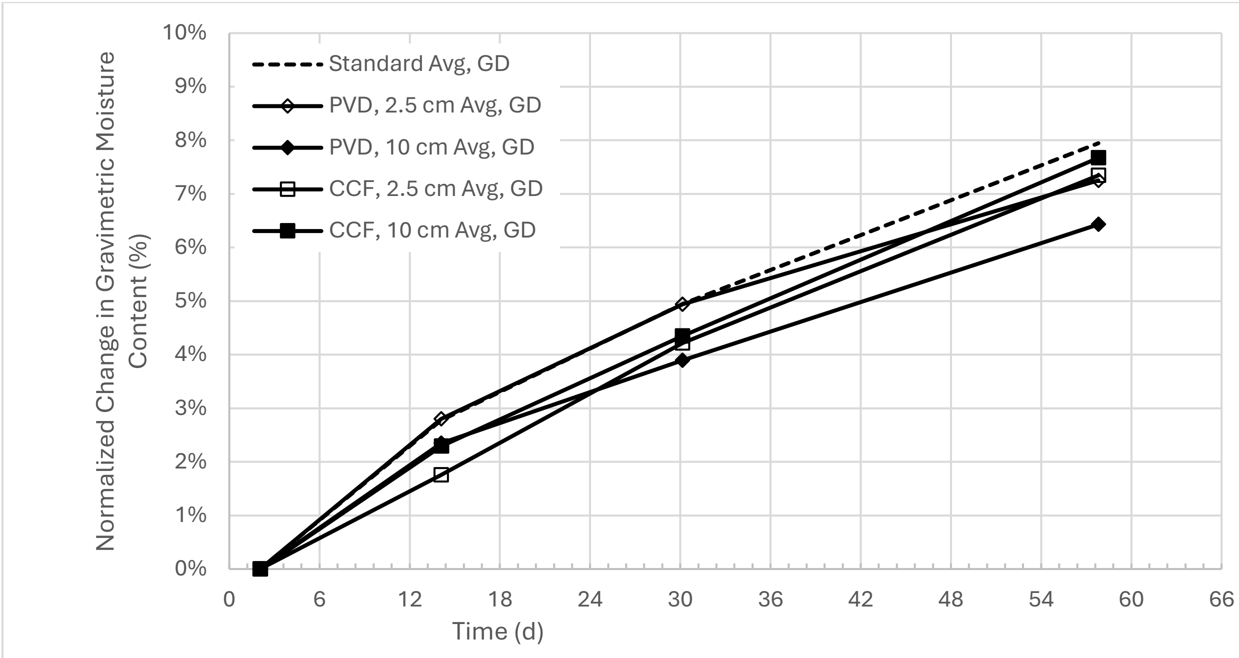

Figure 43. Normalized Change in Gravimetric Moisture Content (%) vs Time (d) for all Test Set 3 GDT Bag Configuration Averages.

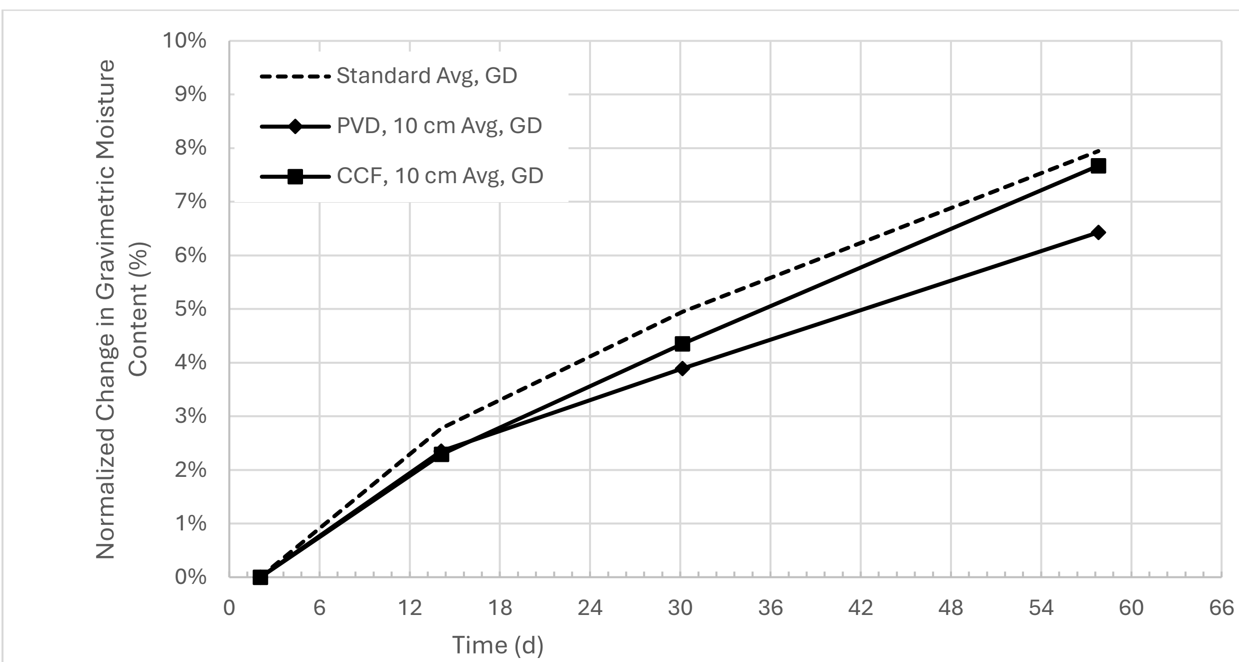

Figure 44. Normalized Change in Gravimetric Moisture Content (%) vs Time (d) for Standard, [PVD, 10 cm], and [CCF, 10 cm] Configuration Average.

APPENDIX B: OBJECTIVE 2

Evaluate soil development at a reclaimed site

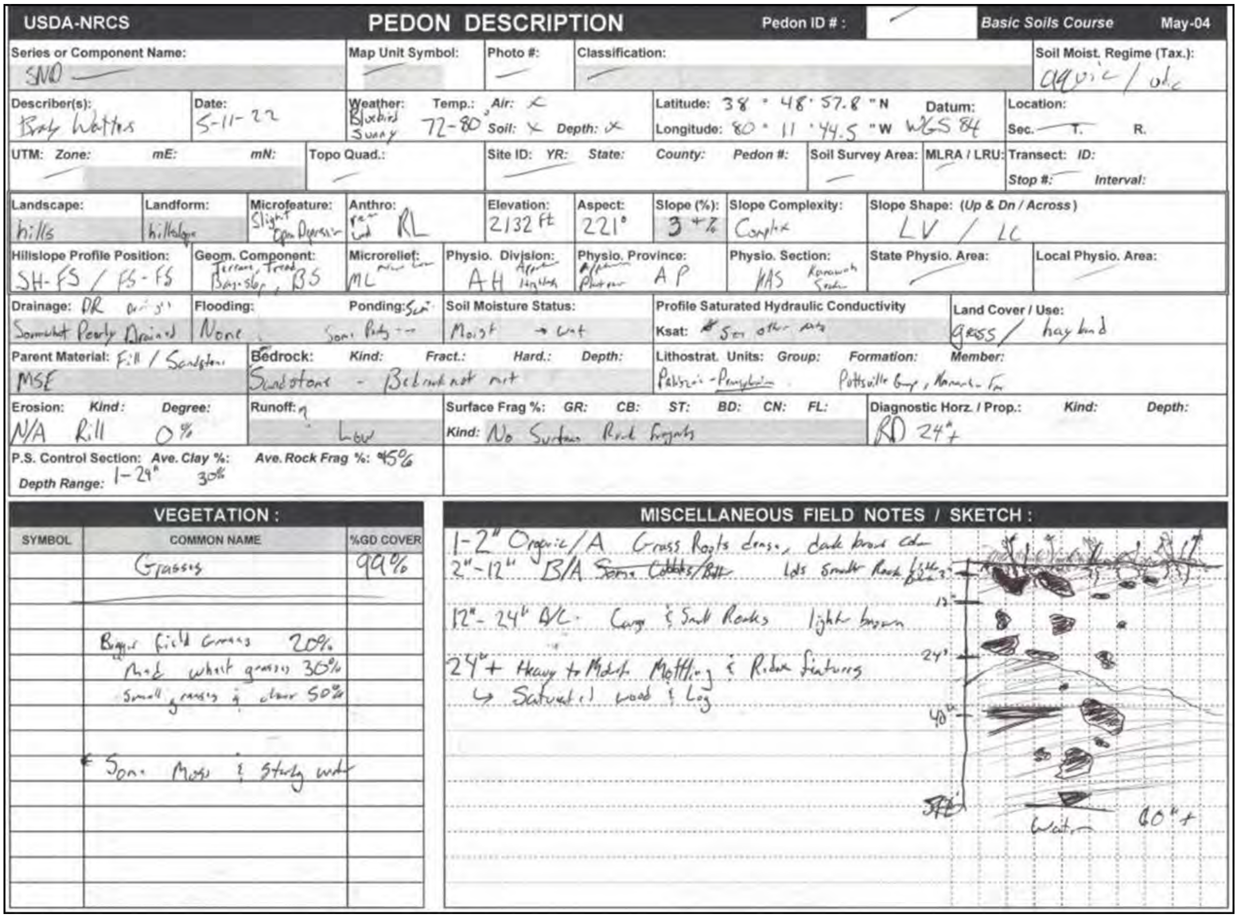

USDA-NRCS **PEDON DESCRIPTION** Pedon ID #: — Basic Soils Course May-04

Series or Component Name: SND — | Map Unit Symbol: — | Photo #: — | Classification: — | Soil Moist. Regime (Tax.): aquic / udic

Describer(s): Brady Watters | Date: 5-11-22 | Weather: Bluebird Sunny | Temp.: 72-80° Air: × Soil: × Depth: × | Latitude: 38 ° 48 ' 57.8 " N | Longitude: 80 ° 11 ' 44.5 " W | Datum: WGS 84 | Location: Sec. — T. R.

UTM: Zone: mE: mN: | Topo Quad.: | Site ID: YR: State: County: Pedon #: | Soil Survey Area: | MLRA / LRU: | Transect: ID: Stop #: Interval:

Landscape: hills | Landform: hillslope | Microfeature: Slight Open Depression | Anthro: RL | Elevation: 2132 Ft | Aspect: 221° | Slope (%): 3+% | Slope Complexity: Complex | Slope Shape: (Up & Dn / Across) LV / LC

Hillslope Profile Position: SH-FS / FS-FS | Geom. Component: BS | Microrelief: ML | Physio. Division: AH | Physio. Province: AP | Physio. Section: KAS | State Physio. Area: | Local Physio. Area:

Drainage: DR Somewhat Poorly Drained | Flooding: None | Ponding: Some Pockets | Soil Moisture Status: Moist → wet | Profile Saturated Hydraulic Conductivity Ksat: | Land Cover / Use: Grass / hay land

Parent Material: Fill / Sandstone MSE | Bedrock: Kind: Fract.: Hard.: Depth: Sandstone - Bedrock not met | Lithostrat. Units: Group: Formation: Member: Pottsville Grp

Erosion: Kind: Degree: N/A Rill 0% | Runoff: Low | Surface Frag %: GR: CB: ST: BD: CN: FL: Kind: No Surface Rock Fragments | Diagnostic Horz. / Prop.: Kind: Depth: RD 24"+

P.S. Control Section: Depth Range: 1-24" Ave. Clay %: 30% Ave. Rock Frag %: 45%

VEGETATION :

SYMBOL	COMMON NAME	%GD COVER
	Grasses	99%
	Bigger field Grass 20%	
	Med wheat grass 30%	
	Small grasses & clover 50%	
	Some Moss & Sticky weed	

MISCELLANEOUS FIELD NOTES / SKETCH :

1-2" Organic / A Grass Roots dense, dark brown color

2"-12" B/A ~~Some Cobbles/Bolt~~ Lots Small Rock frags

12"- 24" B/C Large & Small Rocks light brown

24"+ Heavy to Mod. Mottling & Redox features

↳ Saturated wood & Log

12" 24" 40" Water 60"+

Figure 45. Soil pit Pedon Sheet (front)

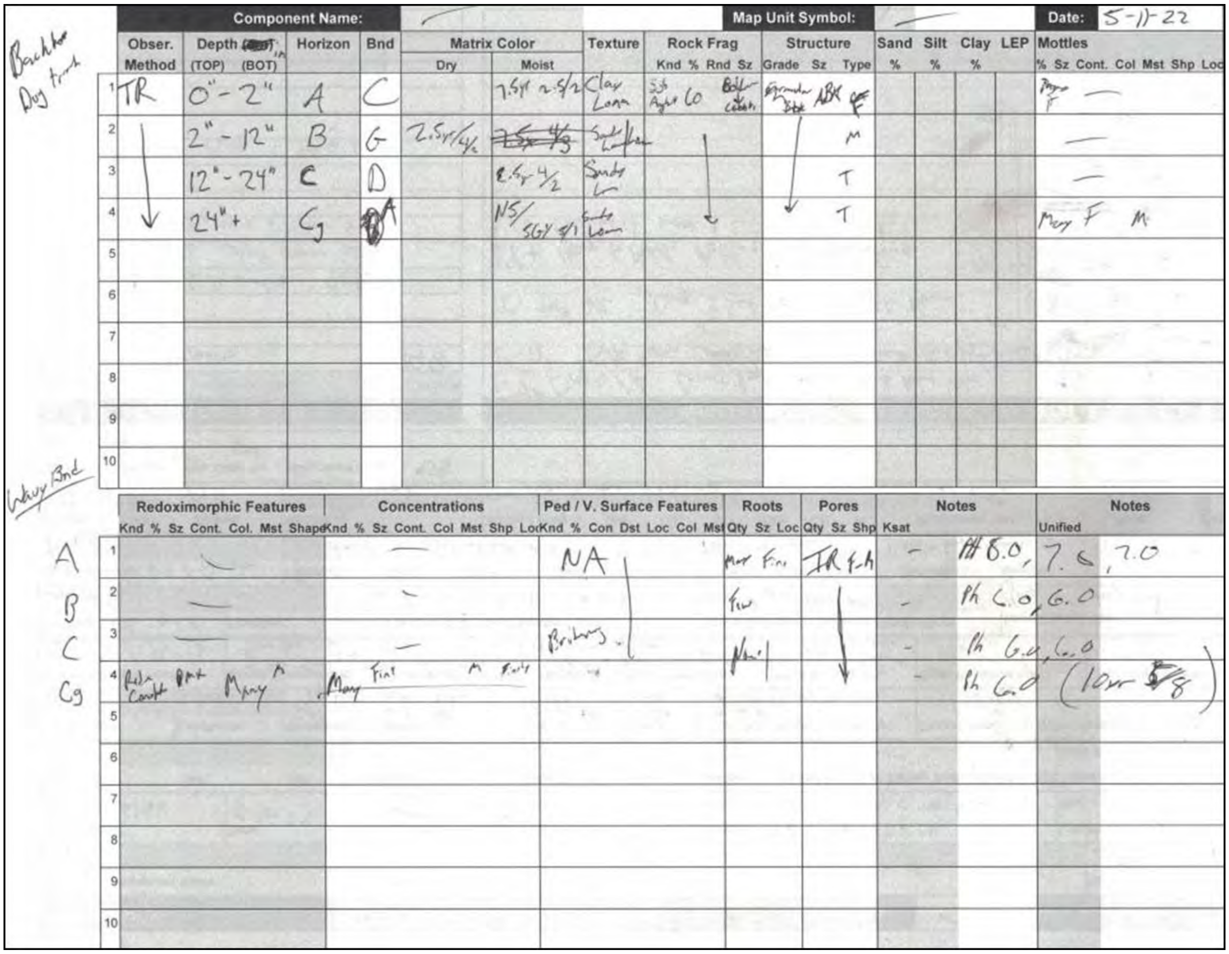

Backhoe Dug trench

Component Name:	Map Unit Symbol:	Date: 5-11-22
—	—	

	Obser. Method	Depth (TOP) (BOT) in	Horizon	Bnd	Matrix Color Dry	Matrix Color Moist	Texture	Rock Frag Knd % Rnd Sz	Structure Grade Sz Type	Sand %	Silt %	Clay %	LEP	Mottles % Sz Cont. Col Mst Shp Loc
1	TR	0"-2"	A	C		7.5YR 2.5/2	Clay Loam	Sub Angular Co Boulder cobbles	Granular Str ABK F					Many F —
2		2"-12"	B	G	2.5YR 4/4	~~7.5YR 4/3~~	Sandy Loam		M					—
3		12"-24"	C	D		2.5Y 4/2	Sandy L		T					—
4		24"+	Cg	A		N5/ 5GY 5/1	Sandy Loam		T					Many F M
5														
6														
7														
8														
9														
10														

Wavy Bnd

		Redoximorphic Features Knd % Sz Cont. Col. Mst Shape	Concentrations Knd % Sz Cont. Col Mst Shp Loc	Ped / V. Surface Features Knd % Con Dst Loc Col Mst	Roots Qty Sz Loc	Pores Qty Sz Shp	Notes Ksat	Notes Unified
A	1	—	—	NA	Many Fine	IR F-M	—	pH 8.0, 7.6, 7.0
B	2	—	—		Few		—	Ph 6.0, 6.0
C	3	—	—	Bridging	Many		—	Ph 6.0, 6.0
Cg	4	Redox Conc [illegible] Many	Many Fine M Faint				—	Ph 6.0 (10YR 5/8)
	5							
	6							
	7							
	8							
	9							
	10							

Figure 46. Soil pit Pedon Sheet (back)

Table 22. Infiltrometer Test 1: Tabulated Data

Test 1				
Time (hr:min)	Time Elapsed		Reading (cm)	Ksat (cm/hr)
	min	sec		
10:20	10	580	0.5	0.000862
10:26	16	930	0.9	0.000968
10:28	18	1065	1.0	0.000939
10:33	23	1353	1.3	0.000961
10:36	25	1518	1.5	0.000988
10:40	30	1793	1.7	0.000948
10:44	33	2003	2.0	0.000999
10:51	41	2455	2.4	0.000978
10:55	44	2665	2.6	0.000957
11:00	50	2972	2.9	0.000976
11:04	53	3205	3.2	0.000998
11:11	60	3590	3.5	0.000975
11:15	64	3867	3.7	0.000957
11:22	71	4279	4.1	0.000958
11:28	77	4637	4.5	0.000970
11:35	84	5035	4.9	0.000973
11:41	90	5395	5.0	0.000927

Table 23. Infiltrometer Test 2: Tabulated Data

Test 2				
Time (hr:min)	Time Elapsed		Reading (cm)	Ksat (cm/hr)
	min	sec		
12:05	15	900	3.2	0.00356
12:20	30	1828	5.9	0.00323
12:35	45	2712	7.6	0.00280
12:41	52	3122	8.5	0.00272
12:48	58	3489	9.0	0.00258

Table 24. Infiltrometer Test 3: Tabulated Data

Test 3				
Time (hr:min)	Time Elapsed		Reading (cm)	Ksat (cm/hr)
	min	sec		
12:57	4	235	0.5	0.002128
1:07	14	816	0.8	0.000980
1:16	22	1346	1.0	0.000743
1:28	34	2025	1.2	0.000593
1:46	52	3104	1.4	0.000451
1:59	65	3929	1.7	0.000433
2:07	73	4380	1.8	0.000411

Table 25. Infiltrometer Test 4: Tabulated Data

Test 4				
Time (hr:min)	Time Elapsed		Reading (cm)	Ksat (cm/hr)
	min	sec		
2:29	11	665	3.5	0.00526
2:38	20	1174	4.4	0.00375
2:46	28	1671	4.5	0.00269
2:58	40	2405	4.9	0.00204
3:12	53	3209	5.2	0.00162
3:17	59	3535	5.8	0.00164
3:19	61	3664	6.1	0.00166

Table 26. Grain size distribution Test 1: Tabulated data

TEST 1 - Topsoil - 0-2"						
Sieve ID	Particle Diameter (mm)	Percent Passing	Percent Retained	Sieve Weight (g)	Sieve Retained (g)	Retained Weight (g)
1in	25.000	99.99	0.01	584.41	584.44	0.03
3/4in	19.000	92.00	8.00	581.32	606.76	25.44
3/8in	9.500	89.23	10.77	555.89	564.71	8.82
#4	4.750	83.48	16.52	524.99	543.29	18.30
#10	2.000	65.48	34.52	469.20	526.50	57.30
#20	0.850	47.57	52.43	373.94	430.94	57.00
#40	0.450	28.96	71.04	377.03	436.27	59.24
#60	0.250	15.28	84.72	320.98	364.52	43.54
#100	0.150	8.05	91.95	345.83	368.87	23.04
#140	0.106	5.15	94.85	356.47	365.68	9.21
#200	0.075	2.94	97.06	337.95	344.99	7.04
Pan		0.00	100.00	372.21	381.57	9.36
					Measured Tot.	Total
					318.15	318.32

Table 27. Grain size distribution Test 2: Tabulated data

TEST 2 - Soil A - 2-12"						
ieve ID	Particle Diameter (mm)	Percent Passing	Percent Retained	Sieve Weight (g)	Sieve Retained (g)	ed Weight (g)
1in	25.000	89.51	10.49	584.41	727.78	143.37
3/4in	19.000	80.86	19.14	581.35	699.41	118.06
3/8in	9.500	63.70	36.30	555.91	790.34	234.43
#4	4.750	50.13	49.87	525.00	710.49	185.49
#10	2.000	37.06	62.94	469.23	647.67	178.44
#20	0.850	27.69	72.31	373.96	501.98	128.02
#40	0.450	17.67	82.33	377.05	514.00	136.95
#60	0.250	10.10	89.90	320.98	424.46	103.48
#100	0.150	6.25	93.75	345.84	398.36	52.52
#140	0.106	4.52	95.48	356.47	380.08	23.61
#200	0.075	3.42	96.58	337.95	353.05	15.10
Pan		0.00	100.00	372.23	418.92	46.69
					Measured Tot.	Total
					1363.9	1366.17

Table 28. Grain size distribution Test 3: Tabulated data

TEST 3 - Soil B - 12-24"						
Sieve ID	Particle Diameter (mm)	Percent Passing	Percent Retained	Sieve Weight (g)	Sieve Retained (g)	Retained Weight (g)
1in	25.000	95.68	4.32	584.39	640.70	56.31
3/4in	19.000	91.69	8.31	581.34	633.27	51.93
3/8in	9.500	79.15	20.85	555.88	719.30	163.42
#4	4.750	63.43	36.57	524.98	729.82	204.84
#10	2.000	47.06	52.94	469.20	682.57	213.37
#20	0.850	35.39	64.61	373.94	526.01	152.07
#40	0.450	23.35	76.65	377.03	533.92	156.89
#60	0.250	13.62	86.38	320.97	447.75	126.78
#100	0.150	8.57	91.43	345.83	411.55	65.72
#140	0.106	6.14	93.86	356.47	388.16	31.69
#200	0.075	4.49	95.51	337.95	359.51	21.56
Pan		0.00	100.00	372.22	430.66	58.44
					Measured Tot.	Total
					1305.72	1303.04

Table 29. Grain size distribution Test 4: Tabulated data

TEST 4 - Soil C - 24"+						
Sieve ID	Particle Diameter (mm)	Percent Passing	Percent Retained	Sieve Weight (g)	Sieve Retained (g)	Retained Weight (g)
1in	25.000	95.33	4.67	584.40	657.87	73.47
3/4in	19.000	89.98	10.02	581.36	665.53	84.17
3/8in	9.500	74.57	25.43	555.85	798.42	242.57
#4	4.750	58.93	41.07	524.71	770.79	246.08
#10	2.000	44.62	55.38	469.19	694.25	225.06
#20	0.850	34.87	65.13	373.94	527.50	153.56
#40	0.450	24.06	75.94	377.09	547.16	170.07
#60	0.250	15.11	84.89	320.82	461.65	140.83
#100	0.150	10.41	89.59	345.92	419.88	73.96
#140	0.106	8.10	91.90	356.51	392.83	36.32
#200	0.075	6.65	93.35	337.92	360.73	22.81
Pan		0.00	100.00	363.62	468.26	104.64
					Measured Tot.	Total
					1574.9	1573.54

Complete a small-scale growth study

Table 30. Watering schedule

Small scale Growth Analysis - Watering schedule			
Y	N	DATE	OBSERVATIONS
		9/29/2021	Planting day
		9/30/2021	250 ml
		10/1/2021	250 ml
		10/2/2021	skipped
		10/3/2021	it rained
		10/4/2021	It was soaking wet due to the rain
		10/5/2021	It's still too wet.
		10/6/2021	250 ml
		10/7/2021	skipped
		10/8/2021	it rained
		10/9/2021	it rained
		10/10/2021	250 ml
		10/11/2021	skipped
		10/12/2021	250 ml
		10/13/2021	skipped
		10/14/2021	250 ml
		10/15/2021	skipped
		10/16/2021	it rained
		10/17/2021	skipped
		10/18/2021	skipped
		10/19/2021	250ml
		10/20/2021	skipped
		10/21/2021	250 ml
		10/22/2021	it rained
		10/23/2021	it rained
		10/24/2021	skipped
		10/25/2021	it rained
		10/26/2021	it rained
		10/27/2021	it rained
		10/28/2021	skipped
		10/29/2021	it rained
		10/30/2021	it rained
		10/31/2021	it rained

		11/1/2021	steam size analysis (skipped)
		11/2/2021	it rained
		11/3/2021	
		11/4/2021	
		11/5/2021	
		11/6/2021	
		11/7/2021	skipped - night frostings kept the samples wet during the next day.
		11/8/2021	
		11/9/2021	
		11/10/2021	
		11/11/2021	250ml
		11/12/2021	it rained
		11/13/2021	it rained
		11/14/2021	it rained
		11/15/2021	it rained
		11/16/2021	skipped
		11/17/2021	skipped
		11/18/2021	it rained
		11/19/2021	skipped
		11/20/2021	skipped
		11/21/2021	skipped
		11/22/2021	it rained
		11/23/2021	skipped
		11/24/2021	skipped
		11/25/2021	skipped
		11/26/2021	it rained
		11/27/2021	skipped
		11/28/2021	skipped
		11/29/2021	skipped
		11/30/2021	it rained
		12/1/2021	it rained
		12/2/2021	Last pictures

Table 31. Ground cover data table

	Ground Cover (%)								
	Week1	**Week 2**	**Week 3**	**Week 4**	**Week 5**	**Week 6**	**Week 7**	**Week 8**	**Week 9**
A100T	0.36	29.43	50.96	51.96	47.00	47.26	59.59	45.49	56.97
B100T	0.40	33.83	58.65	56.82	52.58	53.95	57.21	52.95	60.77
C100T	0.50	24.57	55.27	57.26	56.10	55.75	58.16	54.22	66.43
D100T	0.51	26.29	46.22	50.11	45.55	52.48	55.59	50.73	58.25
A10S90T	0.28	30.28	48.23	54.26	47.87	46.37	52.60	47.27	56.41
B10S90T	0.48	25.77	46.68	49.22	39.76	43.18	46.05	45.30	53.09
C10S90T	0.34	21.18	50.26	49.36	51.91	46.37	48.31	43.97	55.48
D10S90T	0.22	31.08	56.12	52.55	53.06	54.17	56.16	47.98	57.32
A20S80T	0.20	33.37	50.43	52.94	46.62	48.82	53.62	48.85	57.79
B20S80T	0.45	24.71	54.24	53.97	45.21	47.28	52.13	48.67	59.47
C20S80T	0.26	26.04	49.80	52.40	49.32	46.49	51.58	43.81	53.50
D20S80T	0.40	30.23	49.88	52.42	53.71	49.82	51.83	47.02	54.85
A30S70T	0.12	32.75	48.19	48.74	44.70	45.73	46.76	43.27	58.83
B30S70T	0.18	28.20	52.99	52.22	46.07	48.12	53.47	45.22	56.85
C30S70T	0.32	29.99	44.03	53.41	53.16	50.44	53.11	48.98	63.68
D30S70T	0.28	26.90	52.41	52.08	51.84	50.04	53.60	42.93	55.38
A40S60T	0.34	35.19	54.42	56.29	53.40	55.05	57.69	51.86	60.33
B40S60T	0.49	26.30	42.48	49.17	44.56	44.40	46.35	41.72	48.15
C40S60T	0.23	31.02	45.21	56.67	50.77	53.97	57.88	54.40	64.82
D40S60T	0.53	23.79	43.02	48.05	47.41	46.51	49.93	44.58	53.51
A50S50T	0.30	35.19	56.69	62.16	58.18	58.93	63.36	59.71	70.07
B50S50T	0.29	21.41	42.01	51.39	48.04	48.11	52.80	49.58	60.17
C50S50T	0.22	27.96	41.55	59.32	56.34	56.00	60.45	58.37	61.94
D50S50T	0.05	1.33	7.86	10.89	13.10	9.81	9.10	10.64	14.26

Table 32. Biomass data table

	Biomass weight (grams)			
	Container A	Container B	Container C	Container D
100T	4.92	5.62	5.40	4.86
10S90T	4.68	4.51	3.87	4.58
20S80T	4.56	4.40	4.65	3.91
30S70T	4.77	3.80	4.53	4.24
40S60T	4.88	4.10	5.31	3.93
50S50T	6.12	5.45	6.22	1.41

Table 33. Stem height data table

	100T	10S90T	20S80T	30S70T	40S60T	50S50T
Container A	3.4	4.6	4.7	4.5	4.5	5.3
	5.1	3.8	5.4	3.9	4.2	5.7
	4.1	3.6	4.6	4.7	4.0	5.1
	3.3	3.6	4.6	4.3	3.9	5.6
	3.4	3.2	4.5	3.6	4.1	5.5
	3.8	4.2	4.2	4.9	3.7	5.3
	4.4	3.5	3.5	5.0	3.8	4.4
	4.1	3.6	4.1	4.5	4.1	5.3
	5.1	3.4	3.0	4.1	3.4	5.8
	4.7	2.8	2.9	4.5	3.1	4.6
Container B	5.0	3.3	4.3	5.1	3.2	5.2
	4.2	3.4	4.3	4.9	5.5	4.6
	3.2	3.7	4.6	4.7	4.2	4.5
	4.7	3.3	4.2	4.4	4.4	4.8
	3.5	4.3	4.1	5.1	5.2	5.5
	3.2	3.0	3.5	3.6	4.1	3.8
	3.6	3.7	3.6	3.6	3.5	4.2
	4.4	3.8	4.7	5.1	3.4	4.3
	3.2	3.8	3.9	3.8	3.5	5.0
	3.8	3.0	3.7	3.2	3.7	3.5
Container C	4.1	4.0	4.6	4.2	6.0	3.8
	3.7	5.8	4.9	4.1	6.0	3.4
	4.1	5.8	3.4	3.8	6.0	3.3
	5.0	4.5	3.5	4.8	5.5	4.3
	3.4	4.2	3.9	3.8	4.1	4.6
	3.0	3.8	3.2	4.3	3.7	3.9
	3.9	4.2	3.7	4.6	3.3	4.7
	4.9	3.8	3.5	4.3	3.3	4.2
	5.2	4.0	4.1	4.5	2.3	4.1
	3.5	3.8	5.0	4.2	6.0	5.0
Container D	4.3	4.6	4.2	4.7	4.3	3.1
	3.5	3.7	4.0	4.2	3.8	4.3
	3.9	4.1	5.8	4.2	4.2	2.2
	4.5	3.4	5.7	4.4	5.0	4.5
	3.6	4.2	4.0	4.5	4.7	4.8
	5.2	4.5	3.8	3.8	3.3	3.2
	4.3	4.6	5.3	4.0	4.0	3.7
	4.0	4.4	5.1	4.0	4.5	3.8
	4.2	4.1	3.7	3.2	3.5	3.2
	4.5	4.8	4.1	3.2	3.7	3.1

10.06.21	10.13.21	10.20.21
		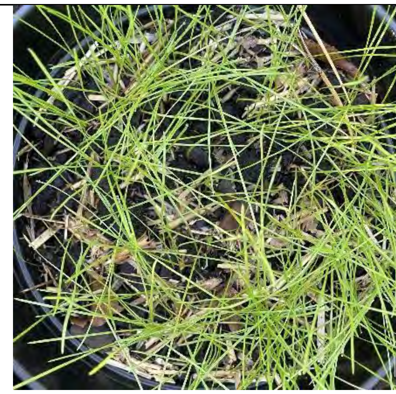
10.27.21	11.01.21	11.10.21
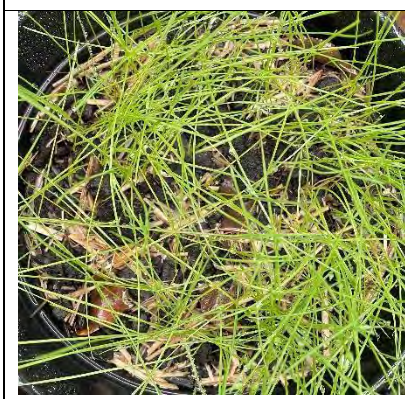		
11.17.21	11.27.21	02.12.21
		

Figure 47. Pictures used for ground cover calculations: A 100T treatment.

10.06.21	10.13.21	10.20.21
	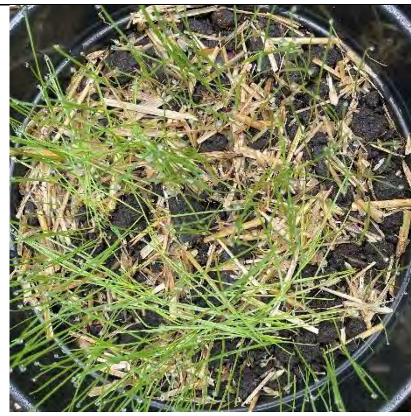	
10.27.21	11.01.21	11.10.21
		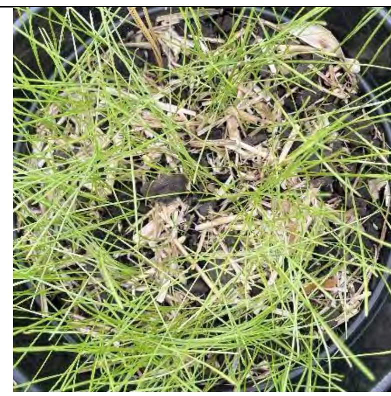
11.17.21	11.27.21	02.12.21
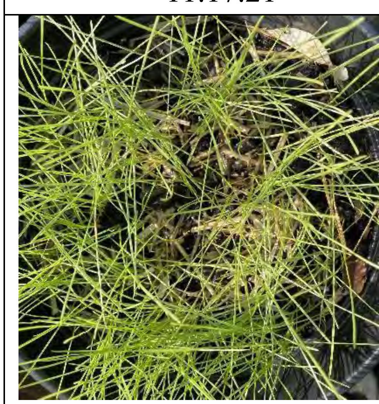		

Figure 48. Pictures used for ground cover calculations: A 10S90T treatment.

10.06.21	10.13.21	10.20.21
		
10.27.21	11.01.21	11.10.21
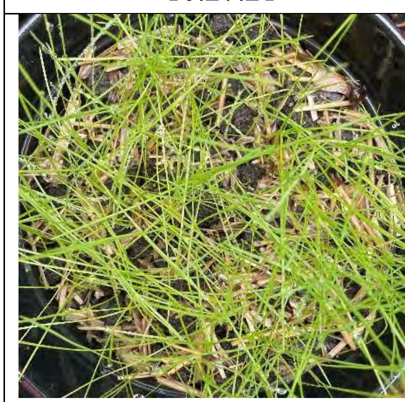		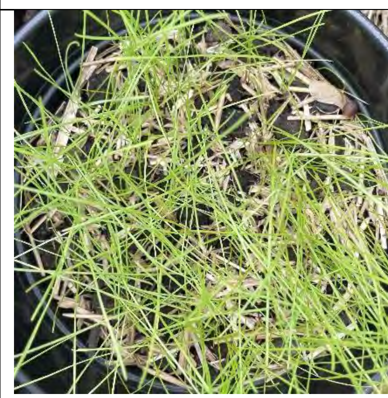
11.17.21	11.27.21	02.12.21
		

Figure 49. Pictures used for ground cover calculations: A 20S80T treatment

10.06.21.	10.13.21	10.20.21
		
10.27.21	11.01.21	11.10.21
		
11.17.21	11.27.21	02.12.21
		

Figure 50. Pictures used for ground cover calculations: A 30S70T treatment.

10.06.21	10.13.21	10.20.21
		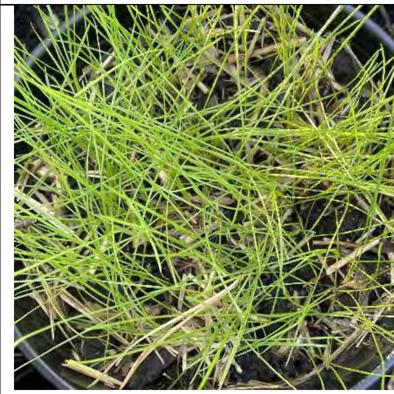
10.27.21	11.01.21	11.10.21
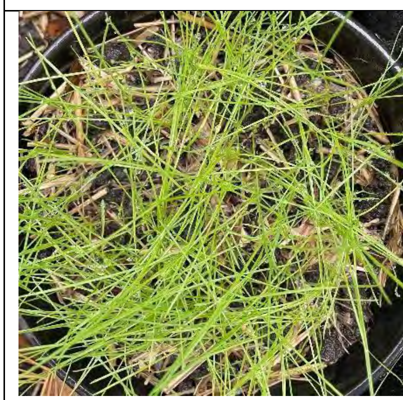		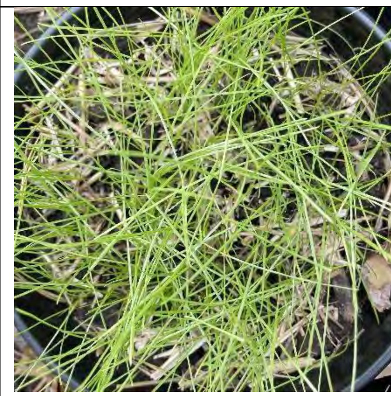
11.17.21	11.27.21	02.12.21
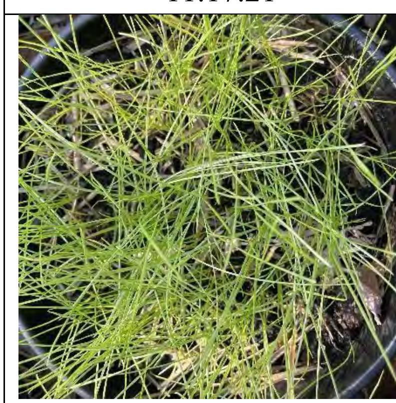		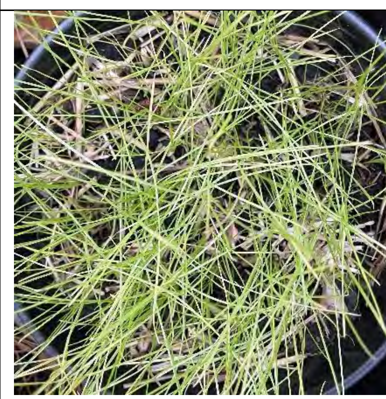

Figure 51. Pictures used for ground cover calculations: A 40S60T treatment.

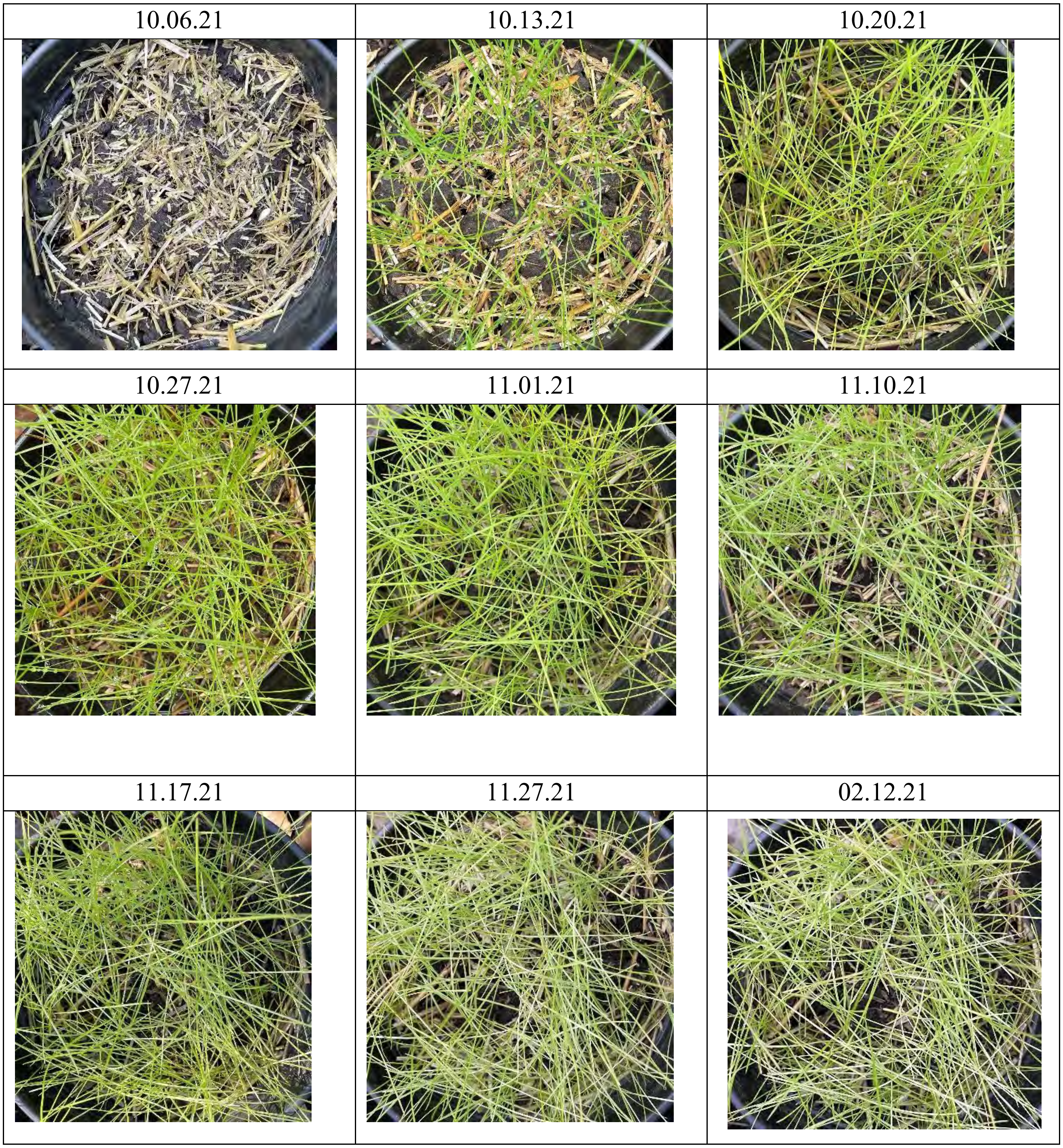

Figure 52. Pictures used for ground cover calculations: A 50S50T treatment.

10.06.21	10.13.21	10.20.21
	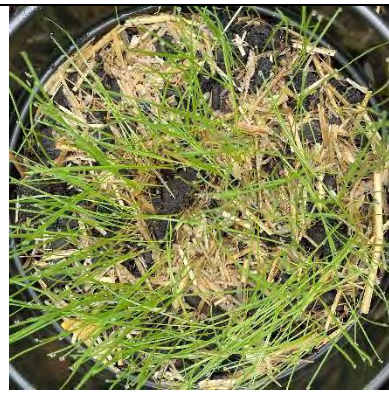	
10.27.21.	11.01.21	11.10.21
		
11.17.21	11.27.21	02.12.21
		

Figure 53. Pictures used for ground cover calculations: B 100T treatment.

10.06.21	10.13.21	10.20.21
		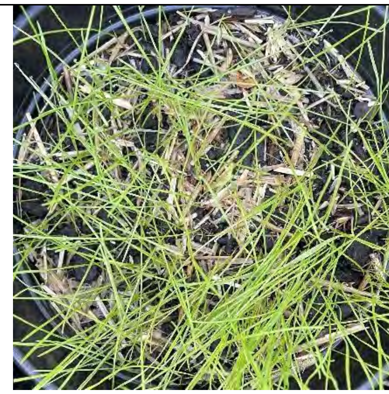
10.27.21	11.01.21	11.10.21
		
11.17.21	11.27.21	02.12.21
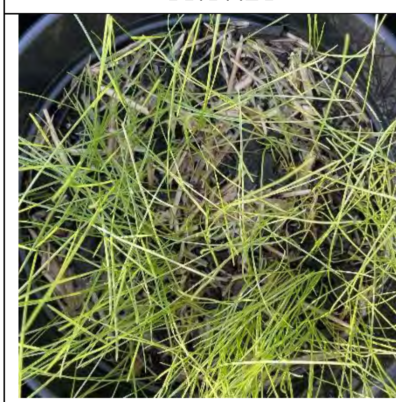		

Figure 54. Pictures used for ground cover calculations: B 10S90T treatment.

10.06.21	10.13.21	10.20.21
		
10.27.21	11.01.21.	11.10.21
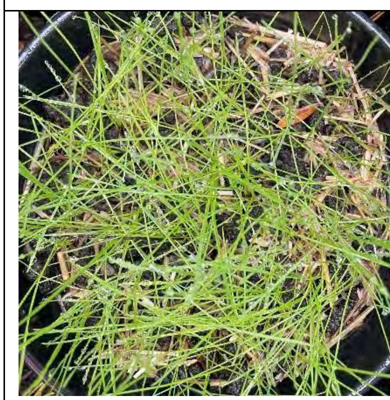	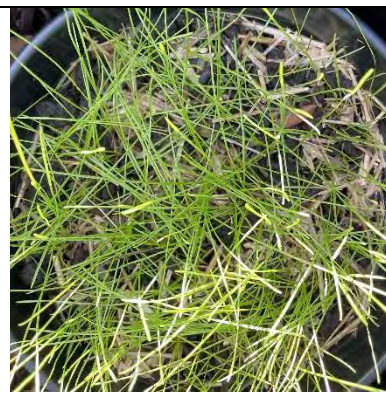	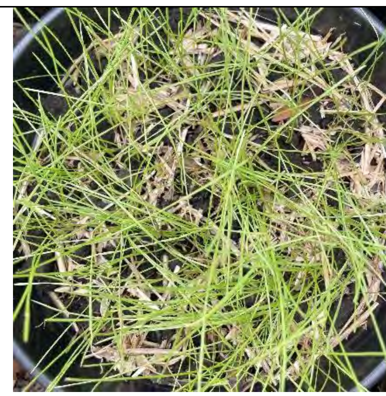
11.17.21	11.27.21	02.12.21
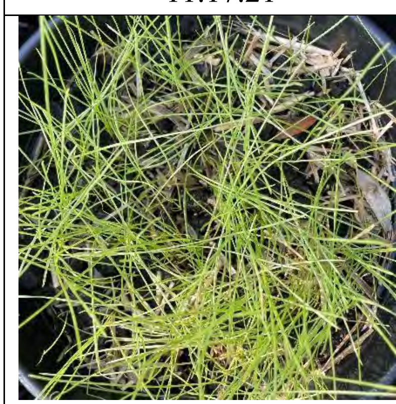		

Figure 55. Pictures used for ground cover calculations: B 20S80T treatment.

10.06.21	10.13.21	10.20.21
		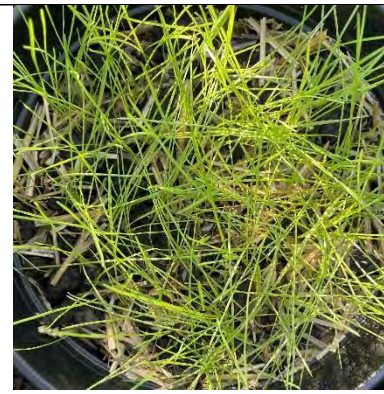
10.27.21	11.01.21	11.10.21.
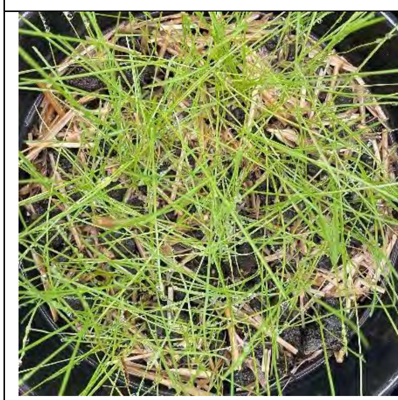		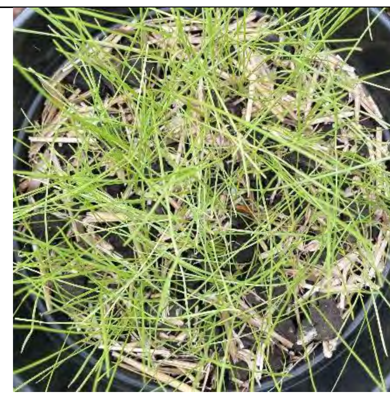
11.17.21	11.27.21	02.12.21
		

Figure 56. Pictures used for ground cover calculations: B 30S70T treatment.

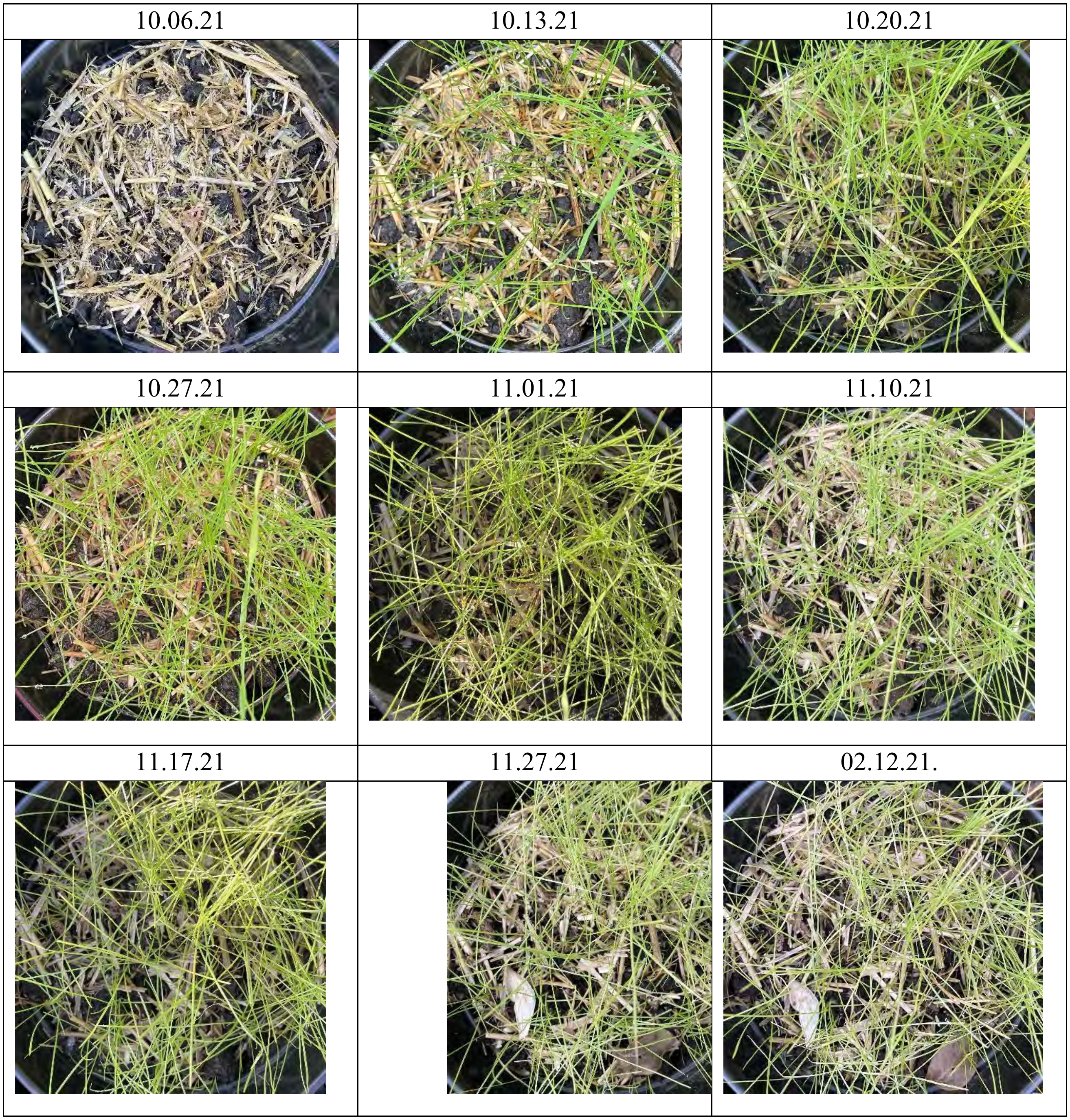

Figure 57. Pictures used for ground cover calculations: B 40S60T treatment.

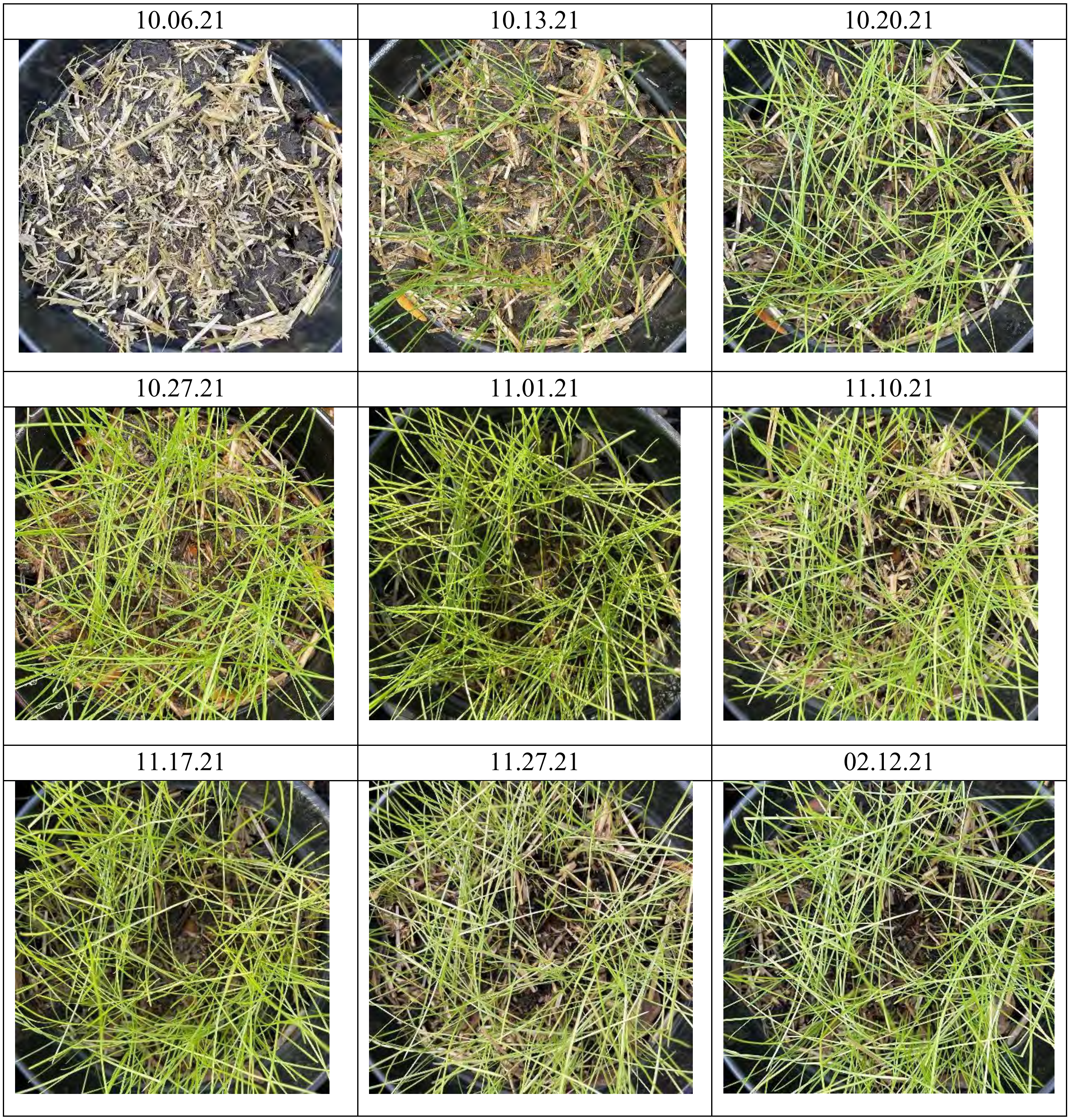

Figure 58. Pictures used for ground cover calculations: B 50S50T treatment.

10.06.21	10.13.21	10.20.21
		
10.27.21	11.01.21	11.10.21
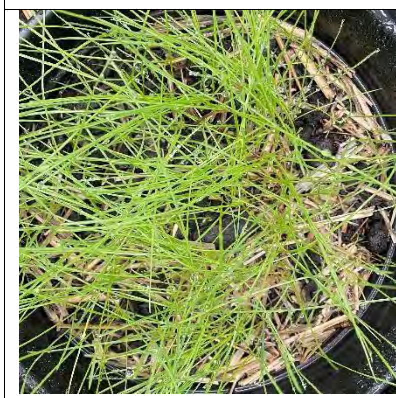		
11.17.21	11.27.21.	02.12.21
		

Figure 59. Pictures used for ground cover calculations: C 100T treatment.

10.06.21	10.13.21	10.20.21
		
10.27.21.	11.01.21	11.10.21
	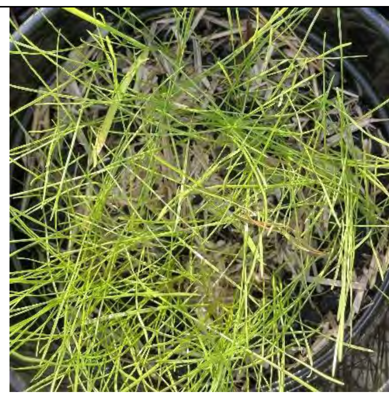	
11.17.21.	11.27.21	02.12.21.
		

Figure 60. Pictures used for ground cover calculations: C 10S90T treatment.

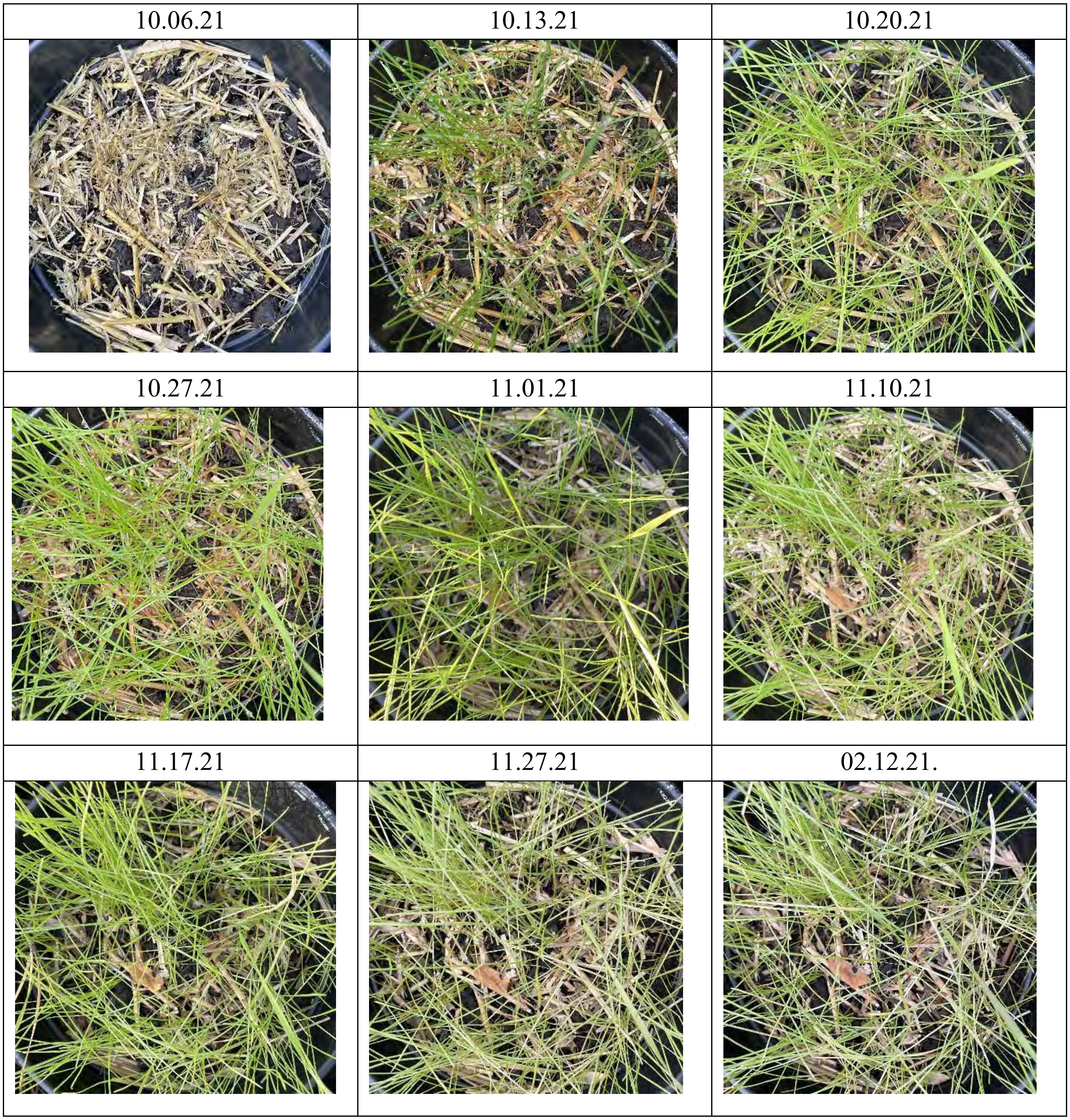

Figure 61. Pictures used for ground cover calculations: C 20S80T treatment.

10.06.21	10.13.21	10.20.21
		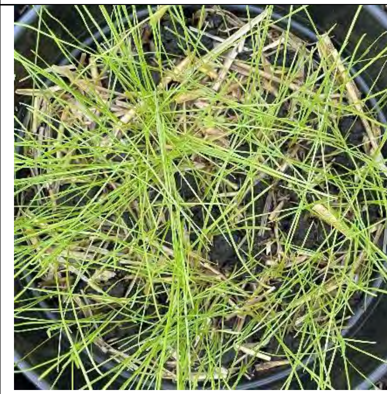
10.27.21	11.01.21	11.10.21
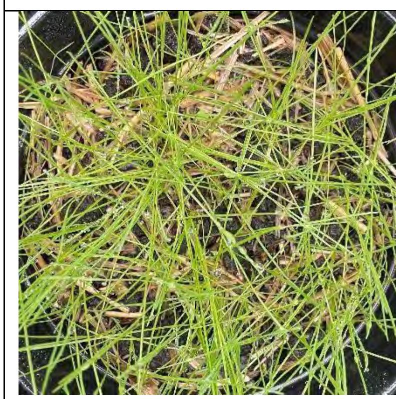		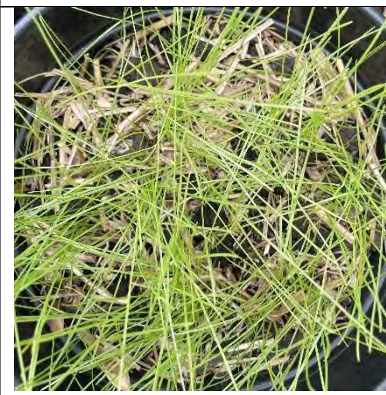
11.17.21	11.27.21	02.12.21
		

Figure 62. Pictures used for ground cover calculations: C 30S70T treatment.

10.06.21	10.13.21	10.20.21
	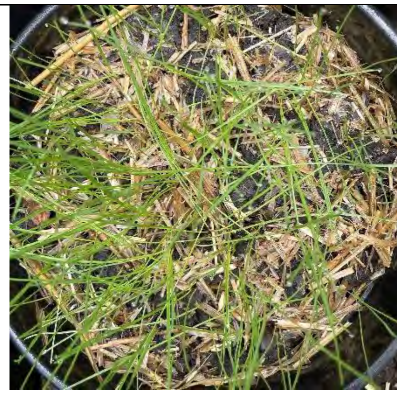	
10.27.21	11.01.21	11.10.21
	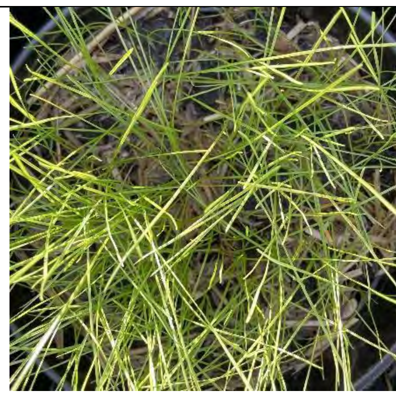	
11.17.21	11.27.21	02.12.21
		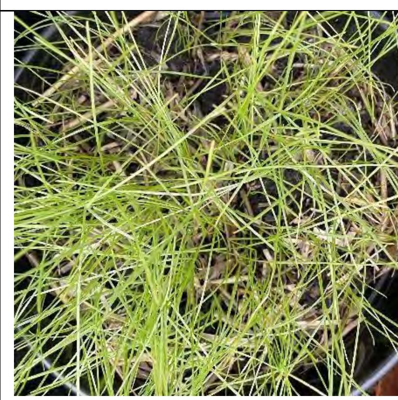

Figure 63. Pictures used for ground cover calculations: C 40S60T treatment.

10.06.21	10.13.21	10.20.21
		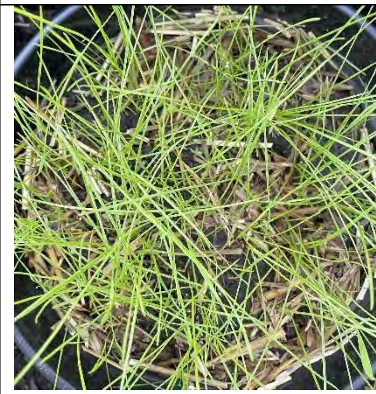
10.27.21	11.01.21	11.10.21
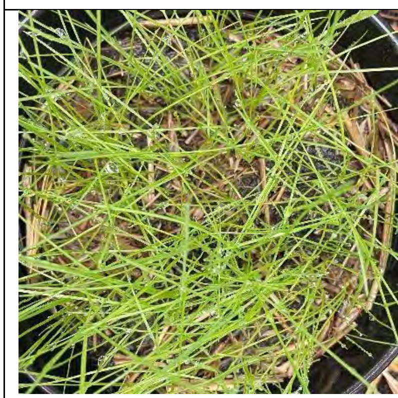	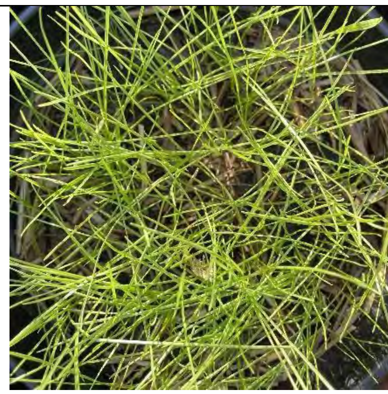	
11.17.21	11.27.21	02.12.21
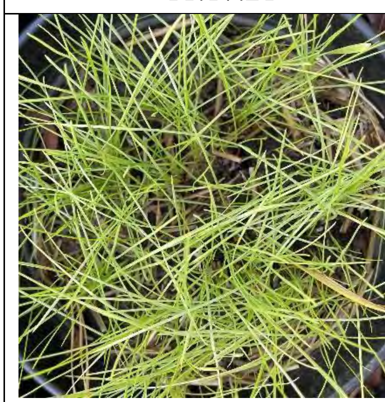	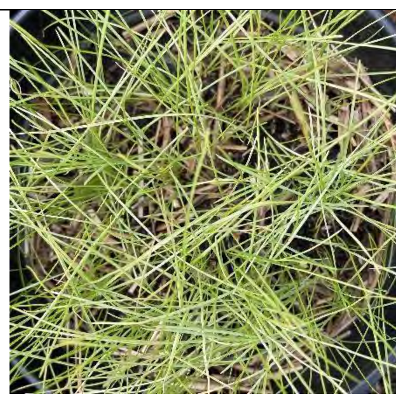	

Figure 64. Pictures used for ground cover calculations: C 50S50T treatment.

10.06.21	10.13.21	10.20.21
		
10.27.21	11.01.21.	11.10.21
		
11.17.21	11.27.21	02.12.21.
		

Figure 65. Pictures used for ground cover calculations: D 100T treatment.

10.06.21	10.13.21	10.20.21
		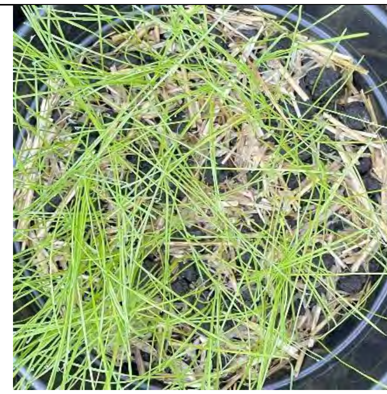
10.27.21.	11.01.21	11.10.21
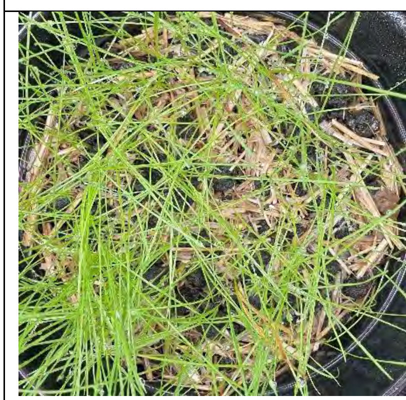		
11.17.21	11.27.21	02.12.21
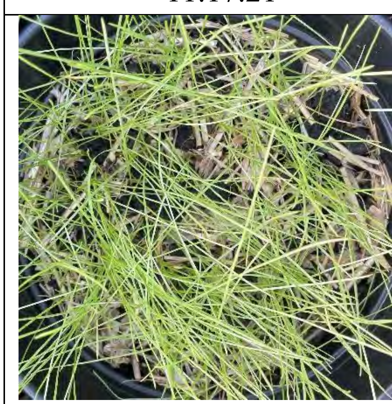		

Figure 66. Pictures used for ground cover calculations: D 10S90T treatment.

10.06.21	10.13.21	10.20.21
		
10.27.21.	11.01.21	11.10.21
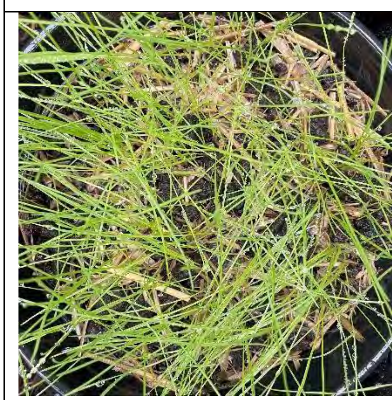	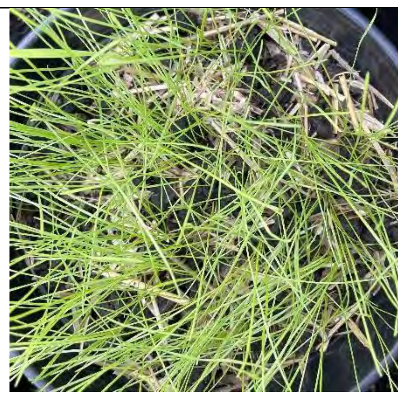	
11.17.21	11.27.21	02.12.21
		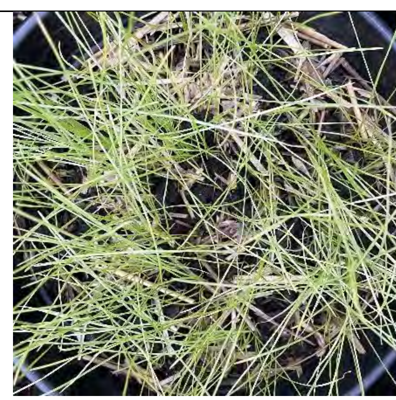

Figure 67. Pictures used for ground cover calculations: D 20S80T treatment.

10.06.21	10.13.21	10.20.21
		
10.27.21	11.01.21	11.10.21
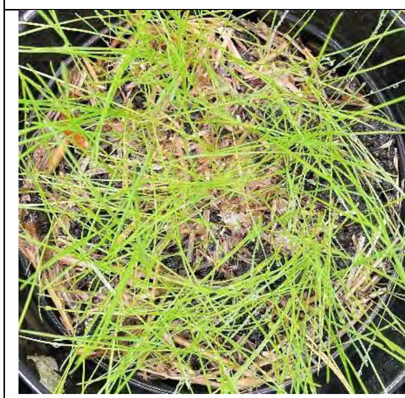	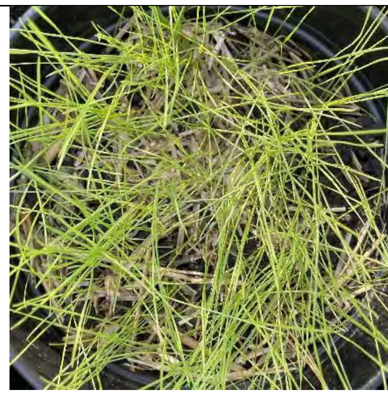	
11.17.21	11.27.21	02.12.21
		

Figure 68. Pictures used for ground cover calculations: D 30S70T treatment.

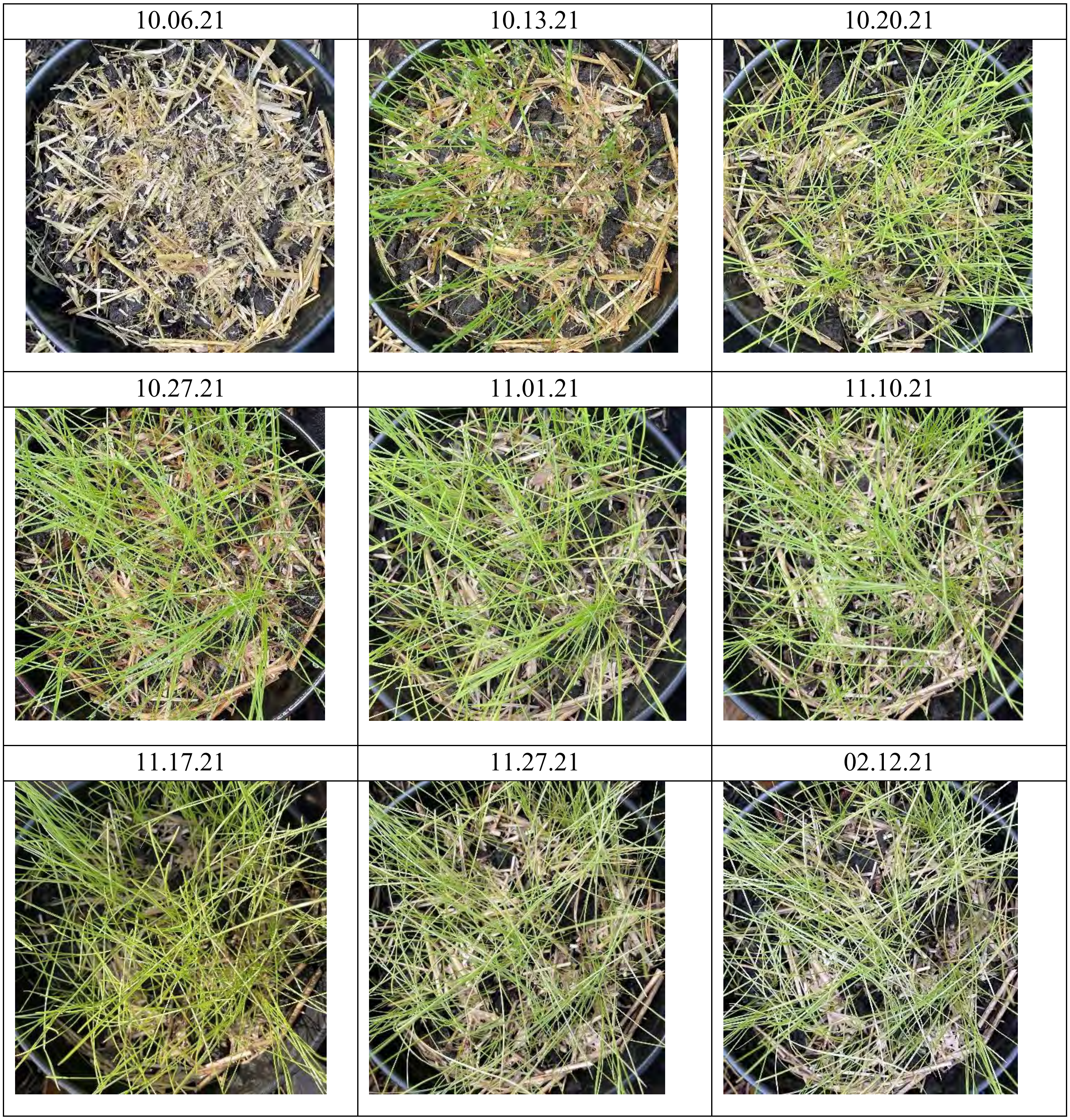

Figure 69. Pictures used for ground cover calculations: D 40S60T treatment.

10.06.21	10.13.21	10.20.21
		
10.27.21	11.01.21	11.10.21
		
11.17.21	11.27.21	02.12.21
		

Figure 70. Pictures used for ground cover calculations: D 50S50T treatment.

Figure 71. Topsoil used for media mixing.

Figure 72. Sludge as received from the site.

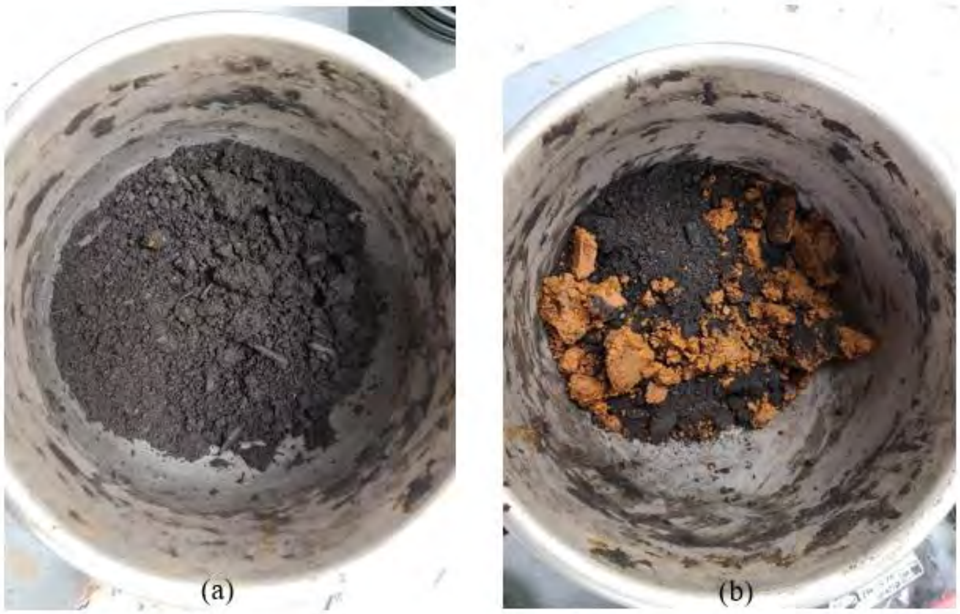

Figure 73. Topsoil (a) and Topsoil + Sludge (b) on mixer pan, before mixing (09/24/21).

Figure 74. Pots with labels.

Figure 75. Fenced study area.

(a) (b)

Figure 76. Seeding process: (a) Seeds weighing and (b) Containers with 2g of Kentucky 31 tall fescue grass seed (*Festuca arundinacea*) (Pennington seed inc., Greenfield, MO).

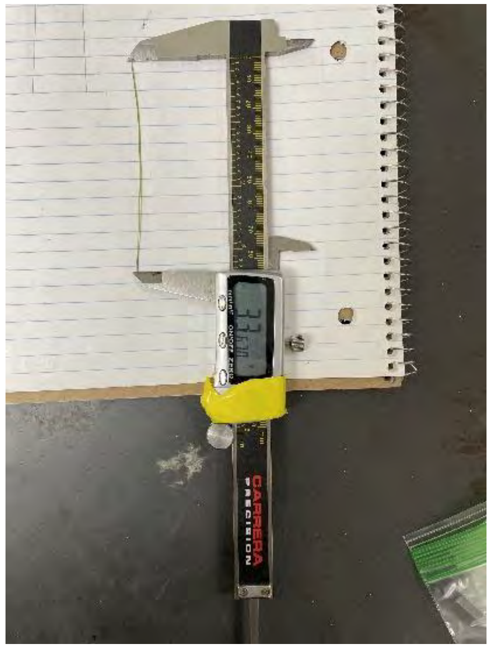

Figure 77. Stem Size measurement procedure (11/01/21).

Figure 78. Pots on breaking down day, just before biomass collection and weighing (12/09/21).

Complete a field study: Fall planting

Table 52. Summary Table: Average Soil Moisture for December 14th, 2022

12/14/2022	* Frozen Ground	
Avg. Moisture		23.2%
TS	Avg. Moisture (%)	13.4%
25AMD	Avg. Moisture (%)	22.2%
50AMD	Avg. Moisture (%)	21.3%
75AMD	Avg. Moisture (%)	22.5%
AMD	Avg. Moisture (%)	36.8%

Table 53. Summary Table: Average Electrical Conductivity for December 14th, 2022

14-Dec	* Frozen Ground	
Avg. Conductivity (mS/cm)		0.03
TS	Avg. Conductivity (mS/cm)	0.02
25AMD	Avg. Conductivity (mS/cm)	0.06
50AMD	Avg. Conductivity (mS/cm)	0.02
75AMD	Avg. Conductivity (mS/cm)	0.05
AMD	Avg. Conductivity (mS/cm)	0.03

Figure 79. October 28 AMD plot

Figure 80. November 4 AMD plot

Figure 81. November 11 AMD plot

Figure 82. October 28 75AMD plot

Figure 83. November 4 75AMD plot

Figure 84. November 11 75AMD plot

Figure 85. October 28 50AMD plot

Figure 86. November 4 50AMD plot

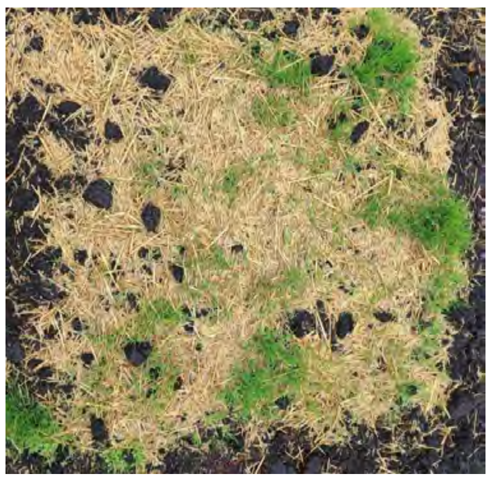

Figure 87. November 11 50AMD plot

Figure 88. October 28 25AMD plot


Figure 89. November 4 25AMD plot


Figure 90. November 11 25AMD plot


Figure 91. October 28 TS plot


Figure 92. November 4 TS plot


Figure 93. November 11 TS plot

Complete a field study: Spring planting

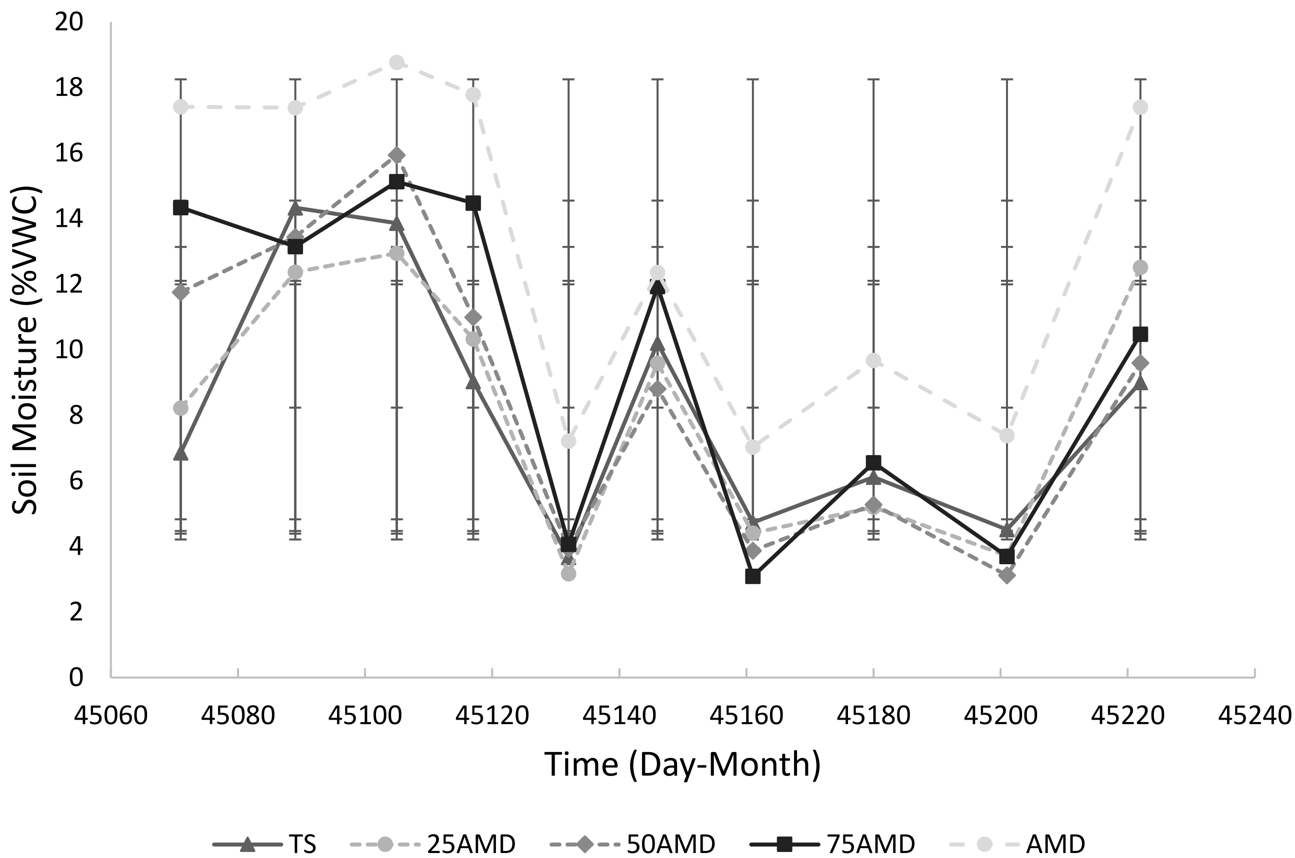

Figure 94: Comparison of mean soil moisture content among treatments with standard error bars

Table 54: Results from saturated media extract report

Treatment	NO_3- (ppm)	P (ppm)	K (ppm)	pH (S.U.)	Ca (ppm)	Mg (ppm)	EC (mS/in)	Na (ppm)	S (ppm)	B (ppm)	Fe (ppm)	Mn (ppm)	Zn (ppm)	Cu (ppm)
TS-A	1	0.9	117	7.4	165	34	1.9	10	5	0.3	119	10.9	4.3	0.7
TS-B	1	3.6	117	7.2	175	40	2.0	11	8	0.3	107.2	13.4	4.1	0.6
TS-C	1	1.8	114	6.8	161	44	2.3	8	16	0.2	161.6	5	2.7	0.8
25AMD-A	1	<0.5	137	7.1	121	37	2.9	30	78	0.3	65.5	2.3	4.8	0.5
25AMD-B	1	<0.5	108	7.1	130	32	2.2	18	51	0.2	70.3	4.6	4.2	0.5
25AMD-C	1	<0.5	83	7.1	132	33	2.2	18	58	0.2	58.3	2.2	4.2	0.4
50AMD-A	1	<0.5	138	7	91	32	2.9	39	87	0.2	44.7	2.3	3.2	0.3
50AMD-B	1	<0.5	67	7.1	78	30	2.3	49	93	0.1	26.3	0.2	2.1	0.2
50AMD-C	1	<0.5	61	7	77	29	2.0	32	68	0.1	67.8	1	2.8	0.4
75AMD-A	1	<0.5	62	7	68	27	1.9	21	66	<0.1	21.2	<0.1	1.6	0.2
75AMD-B	1	<0.5	43	7.1	65	23	2.2	66	99	<0.1	24.8	<0.1	1.7	0.2
75AMD-C	1	<0.5	114	7.1	81	28	2.7	41	78	0.1	26.6	1	2	0.2

Site visit on June 12, 2023

Figure 95: Overview of plots (side view)

Figure 96: Overview of plots (front view)

Figure 97: 75AMD-A

Figure 98: AMD-C

Figure 99: AMD-A

Figure 100: 25AMD-B

Figure 101: 75AMD-C

Figure 102: 25AMD-A


Figure 103: TS-A


Figure 104: TS-C

Figure 105: 25AMD-C

Figure 106: TS-B

Figure 107: 50AMD-A

Figure 108: 50AMD-C

Figure 109: 50AMD-B

Figure 110: AMD-B

Figure 111: 75AMD-B

Site visit on June 28, 2023

Figure 112: Overview of plots (side view)

Figure 113: Overview of plots (front view)

Figure 114: 75AMD-A

Figure 115: AMD-C

Figure 116: AMD-A

Figure 117: 25AMD-C

Figure 118: 75AMD-C

Figure 119: 50AMD-A

Figure 120: TS-A

Figure 121: TS-C

Figure 122: 25AMD-A

Figure 123: 50AMD-B

Figure 124: AMD-B

Figure 125: 25AMD-B

Figure 126: TS-B

Figure 127: 50AMD-C

Figure 128: 75AMD-B

Site visit on July 10, 2023

Figure 129: Overview of plots (side view)


Figure 130: Overview of plots (front view)

Figure 131: 75AMD-B

picture of outdoor field plot

Figure 132: 50AMD-C

Figure 133: TS-B

Figure 134: 25AMD-B

Figure 135: AMD-B

Figure 136: 50AMD-B

Figure 137: 25AMD-A

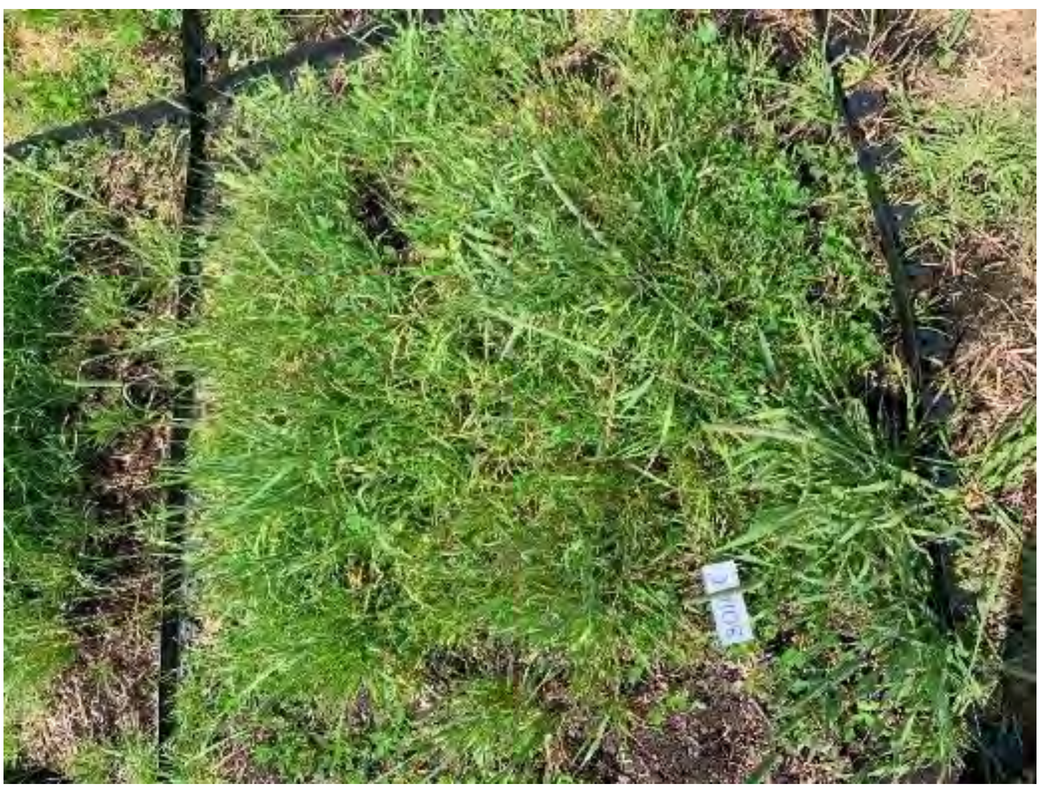

Figure 138: TS-C

Figure 139: TS-A

Figure 140: 50AMD-A

Figure 141: 75AMD-C


Figure 142: 25AMD-C

Figure 143: AMD-A

Figure 144: AMD-C

Figure 145: 75AMD-A

Site visit on July 25, 2023

Figure 146: Overview of plots (side view)

Figure 147: Overview of plots (front view)

Figure 148: 75AMD-A

Figure 149: AMD-C

Figure 150: AMD-A

Figure 151: 25AMD-C

Figure 152: 75AMD-C

Figure 153: 50AMD-A

Figure 154: TS-A

Figure 155: TS-C

Figure 156: 25AMD-A

Figure 157: 50AMD-B

Figure 158: AMD-B

Figure 159: 25AMD-B

Figure 160: TS-B

Figure 161: 50AMD-C

Figure 162: 75AMD-B

Site visit on August 8. 2023

Figure 163: Overview of plots (side view)

Figure 164: Overview of plots (front view)

Figure 165:75AMD-A

Figure 166: AMD-C

Figure 167: AMD-A

Figure 168: 25AMD-C

Figure 169: 75AMD-C


Figure 170: 50AMD-A

Figure 171: TS-A

Figure 172: TS-C

Figure 173: 25AMD-A

Figure 174: 50AMD-B

Figure 175: AMD-B

Figure 176: 25AMD-B

Figure 177: TS-B

Figure 178: 50AMD-C

Figure 179: 75AMD-B

Site visit on August 8 23, 2023

Figure 180: Overview of plots (side view)

Figure 181: Overview of plots (front view)

Figure 182: 75AMD-A

Figure 183: AMD-C

Figure 184: AMD-A

Figure 185: 25AMD-C

Figure 186: 75AMD-C

Figure 187: 50AMD-A

Figure 188: TS-A

Figure 189: TS-C

Figure 190: 25AMD-A

Figure 191: 50AMD-B

Figure 192: AMD-B

Figure 193: 25AMD-B

Figure 194: TS-B

Figure 195: 50AMD-C

Figure 196: 75AMD-B

<u>Site visit on September 11, 2023</u>

Figure 197: Overview of plots (side view)

Figure 198: Overview of plots (front view)


Figure 199: 75AMD-A


Figure 200: AMD-C

Figure 201: AMD-A

Figure 202: 25AMD-C

Figure 203: 75AMD-C

Figure 204: 50AMD-A

Figure 205: TS-A

Figure 206: TS-C

Figure 207: 25AMD-A

Figure 208: 50AMD-B

Figure 209: AMD-B

Figure 210: 25AMD-B

Figure 211: TS-B

Figure 212: 50AMD-C

Figure 213: 75AMD-B

Site visit on October 2, 2023

Figure 214: Overview of plots (side view)

Figure 215: Overview of plots (front view)

Figure 216: 75AMD-A

Figure 217: AMD-C

Figure 218: AMD-A

Figure 219: 25AMD-C

Figure 220: 75AMD-C

Figure 221: 50AMD-A

Figure 222: TS-A

Figure 223: TS-C

Figure 224: 25AMD-A

Figure 225: 50AMD-B

Figure 226: AMD-B

Figure 227: 25AMD-B

Figure 228: TS-B

Figure 229: 50AMD-C

Figure 230: 75AMD-B

Site visit on October 23, 2023

Figure 231: Overview of plots (side view)

Figure 232: Overview of plots (front view)

Figure 233: 75AMD-A

Figure 234: AMD-C

Figure 235: AMD-A

Figure 236: 25AMD-C

Figure 237: 75AMD-C

Figure 238: 50AMD-A

Figure 239: TS-A

Figure 240: TS-C

Figure 241: 25AMD-A

Figure 242: 50AMD-B

Figure 243: AMD-B

Figure 244: 25AMD-B

Figure 245: TS-B

Figure 246: 50AMD-C

Figure 247: 75AMD-B

Use of Acid Mine Drainage (AMD) Waste as a Soil Amendment

Technical Transfer Products

Refereed Journal Articles

- Rodrigues Silva*, A., B. Watters*, L. Hopkinson, J. Quaranta. 2022. Evaluation of the use of AMD sludge as soil amendment. *Proceedings of the West Virginia Academy of Science*. 94(3): 17-23. DOI: 10.55632/pwvas.v94i3

Invited talks (Presenter in bold)

- **Hopkinson, L., J. Quaranta, A. Rodrigues*, J. Tyson, B. Watters***. 2022. Use of Acid Mine Drainage (AMD) Waste as a Soil Amendment. Appalachia Region Technology Transfer TEAMS Call. June 6. Virtual.

Poster Presentations (Presenter in bold)

- **Kerr, G**. L. Hopkinson. 2024. Utilizing acid mine drainage (AMD) sludge in reclamation. 2024 IECA Conference & Expo. Feb. 25-28. Spokane, WA.
    - First Place, Student Poster Competition
- **Rodrigues*, A.**, B. Watters*., J. Quaranta, L. Hopkinson. 2022. Evaluation of the use of AMD sludge as soil amendment. Annual West Virginia Academy of Science Meeting, April 23, Fairmont University.
    - First Place, Student Poster Competition

M.S. Theses

- Watters, Brady, "Exploring the Usage of Acid Mine Drainage Sludge as a Soil Amendment for Reclaimed Mine Lands" (2023). *Graduate Theses, Dissertations, and Problem Reports*. 11713. https://researchrepository.wvu.edu/etd/11713
- Tyson, Jonah G., "Laboratory Experimentation and Numerical Modeling to Enhance Drainage in Geotextile Tubes" (2023). *Graduate Theses, Dissertations, and Problem Reports*. 11864. https://researchrepository.wvu.edu/etd/11864
- Daugherty, Luke William, "Study of Capillary Channel Fiber Augmented Geobags for Accelerated Dewatering of High Moisture Content Fine-Grained Acid Mine Drainage Precipitate" (2023). *Graduate Theses, Dissertations, and Problem Reports*. 12080. https://researchrepository.wvu.edu/etd/12080
- Rodrigues Silva, Amanda, "Evaluating potential soil amendments and geomorphic methods for mine land reclamation" (2022). Chapter 2. *Graduate Theses, Dissertations, and Problem Reports*. 11524. https://researchrepository.wvu.edu/etd/11524
- Kerr, G.K. Evaluation of Probable Maximum Precipitation (PMP) for West Virginia to Predict Current and Future PMP & Utilizing Acid Mine Drainage (AMD) Sludge in Reclamation *Graduate Theses, Dissertations, and Problem Reports*. Chapter 3. (Expected May 2024.)

Use of Acid Mine Drainage (AMD) Waste as a Soil Amendment

Authors: Leslie Hopkinson and John Quaranta
Affiliation: West Virginia University, Morgantown, WV

Project Description and Objectives:

Costs associated with acid mine drainage (AMD) sludge management and handling are high, often several times greater than the cost of chemical treatment. This work developed methods to enhance AMD geotube dewatering and evaluated the use AMD sludge as a soil amendment to support vegetation establishment and persistence.

Hanging bag test evaluating dewatering of geobags with internal modifications

Applicability to Mining and Reclamation:

The ability to dewater AMD sludge (up to 2,500% moisture content) reduces the area needed for sludge disposal and simplifies methods for reuse. There is potential for the of AMD sludge through land application as part of the reclamation process.

Methodology:

To evaluate the process of geotube dewatering, the following series of tasks were completed:

1. Characterized geotechnical properties through column filtration testing and moisture distribution tests,
2. Designed a prototype dewatering system,
3. Evaluated dewatering through numerical modeling, and
4. Completed field testing of dewatering system through hanging bag tests and geotube dewatering tests.

Geobag dewatering tests

Final version of sludge sampler developed in this study

The use of AMD sludge as a soil amendment was completed by evaluating soil development at a reclaimed site, characterizing the sludge, and completing a series of growth studies (small-scale study with planters, plot study with a fall planting date, and plot study with a spring planting date).

Continued on Back >

Results and Findings:

Capillary channel fibers (CCFs) are geosynthetic yarns formed with microgrooves and set into bundled arrangements capable of wicking water, via capillary action, from fine grained soils. This research studied CCF augmented fabrics and prefabricated vertical drain (PVD) geocomposites positioned mid-depth in geobags filled with AMD precipitate to accelerate drainage via a shortened drainage path. A potential decrease in dewatering times using the combination of CCF geotextiles with internal lateral drainage was observed.

Field tests suggested that the addition of AMD sludge may result in increased soil moisture content. This result could be tested with different application techniques because the AMD sludge was mixed while wet in this study.

Geobag cut open to expose AMD sludge used in plot study

Final set-up of small-scale growth study

Development of plots for spring planting field test

Evaluating soil development at a reclaimed location

Fact Sheet Contact Information

PRINCIPAL INVESTIGATOR (PI):
Leslie Hopkinson, Leslie.Hopkinson@mail.wvu.edu, 304-293-9932, West Virginia University

PROJECT TECHNICAL REPRESENTATIVE (PTR):
Miles, Ronald R – rmiles@osmre.gov
Office of Surface Mining Reclamation and Enforcement

Utilizing acid mine drainage (AMD) sludge in reclamation

Grace Kerr, Leslie Hopkinson

West Virginia University
BENJAMIN M. STATLER COLLEGE OF ENGINEERING AND MINERAL RESOURCES

Wadsworth Department of Civil and Environmental Engineering, West Virginia University, Morgantown, WV 26506

Introduction

Acid mine drainage (AMD) occurs when sulfide-bearing material is exposed to oxygen and water that forms an acidic, sulfate rich drainage. AMD's properties include low pH, high specific conductivity, high concentrations of iron (Fe), aluminum (Al), and manganese (Mn), and low concentrations of toxic heavy metals (Akcil and Koldas, 2006). The chemical composition is mostly composed of Mn, Fe, copper (Cu), zinc (Zn), arsenic (As), cadmium (Cd), and lead (Pb) (Fuchida et al. 2020). AMD can occur naturally from iron sulfide aggregated rocks, but mostly mining activities contribute to the production of AMD. AMD can affect vegetation, humans, wildlife, aquatic species, and contaminate ground waters if not treated (Simate and Ndlovu, 2014).

Treatment of AMD results in a hydroxide sludge that must be managed. There are three most common types of sludge disposal methods: 1) disposal into a deep mine, 2) retention ponds, and 3) burial onsite (Ackman, 1982). The cost associated with AMD sludge disposal is high, and there needs to be a reclamation plan to reduce the cost (Masindi et al. 2022).

Objectives

This research evaluated the use of AMD sludge, a waste by-product, as a soil amendment to support vegetation establishment and persistence.

Methods

The study site was located in Monongalia County, West Virginia (Fig. 1).The site consists of fifteen study plots (three repetitions of five treatments) (Fig. 2). The treatments included topsoil mixed with AMD sludge in volumetric ratios: 1) 25% AMD sludge/75% topsoil (25AMD), 2) 50% AMD sludge/50% topsoil (50AMD), 3) 75% AMD sludge/25% topsoil (75AMD), 4) 100% AMD sludge (100AMD), and 5) 100% topsoil (Topsoil, control).

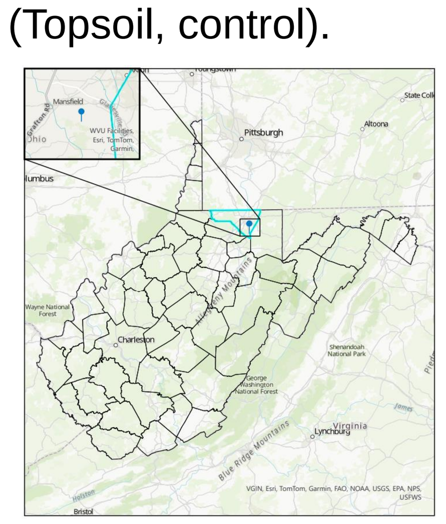

Figure 1. Study location

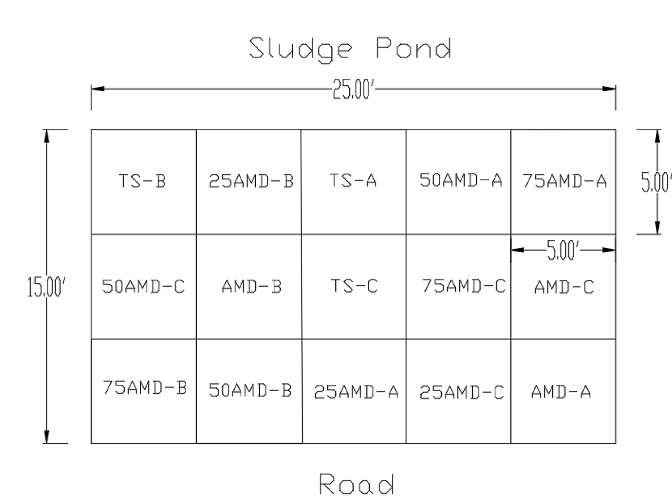

Figure 2. Plot layout

The plots were developed on September 26, 2022 (Fig. 3). Each plot was created by a specific volume of AMD/soil ratio that was hand mixed. After the plots were formed, fertilizer and seed mixture was applied using the WVDEP seeding procedure guidelines. Plots were monitored for ground cover, electrical conductivity, temperature, and soil moisture from May 25, 2023 to October 23, 2023 using the Field Scout TDR 150 and 3.28 ft^2 device (Fig. 4). At the end of the data collection phase, soil and above-ground biomass samples were collected from each plot. The biomass samples were collected by taking a 1 ft^2 square area (Fig. 5) and randomly placing it on top of each of the plots. From there, the area that was enclosed by the PVC square was trimmed, placed into bags, and weighed.

Figure 3. Plots in September 2022

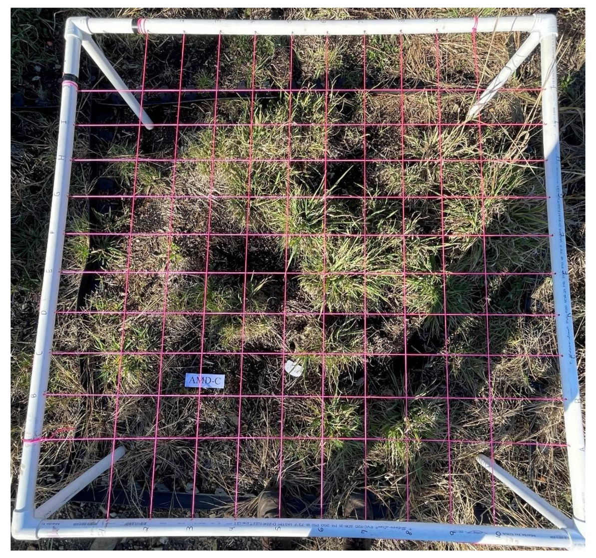

Figure 4. Ground cover measurement

Figure 5. Biomass

Results

Statistical analysis was completed in R Studio for ground cover, electrical conductivity, temperature, and biomass samples. The One-way Kruskal Wallis test was completed, with α = 0.05. From there, if the *p*-value was less than 0.05, then the analysis was continued with the Dunns test for pairwise comparisons. Results include comparison of ground cover (Fig. 6-8), soil moisture (Fig. 9-11), electrical conductivity (Fig. 12-14), temperature (Fig.15-17) for final measurements and all measurements, and biomass (Fig. 18). Final measurements were collected on October 23, 2023 (Fig. 19).

Ground Cover

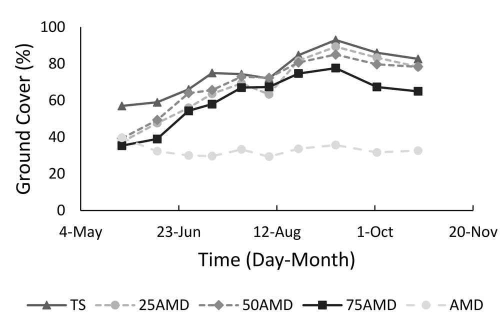

Figure 6. Mean ground cover over time

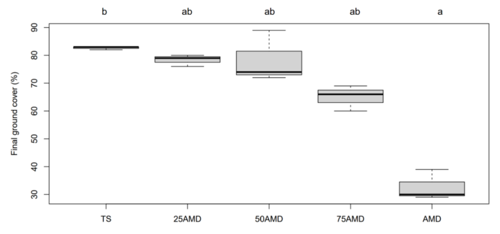

Figure 7: Comparison of ground cover for final measurements

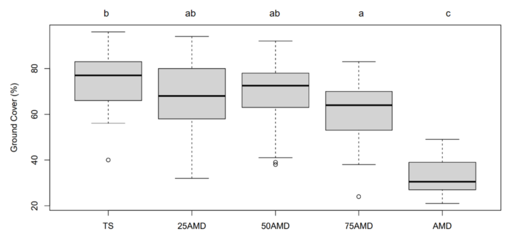

Figure 8: Comparison of ground cover for all measurements

Volumetric Water Content

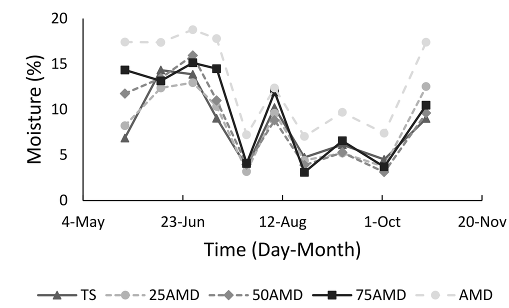

Figure 9. Mean volumetric water content over time

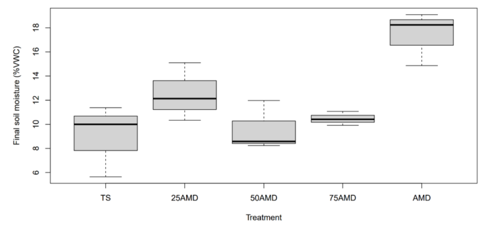

Figure 10: Comparison of ground cover for final measurements

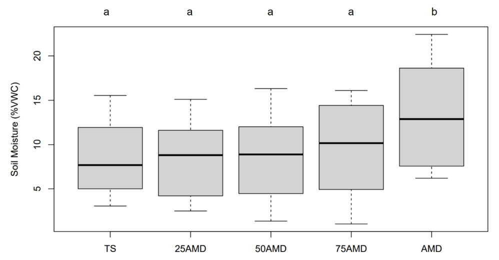

Figure 11: Comparison of ground cover for all measurements

Electrical Conductivity

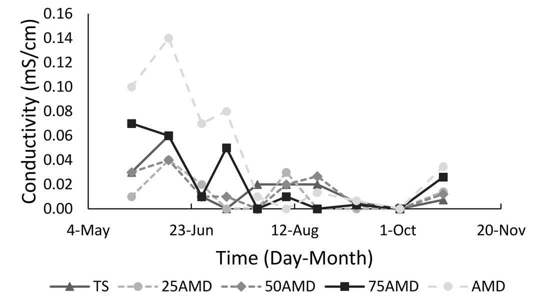

Figure 12. Mean EC over time

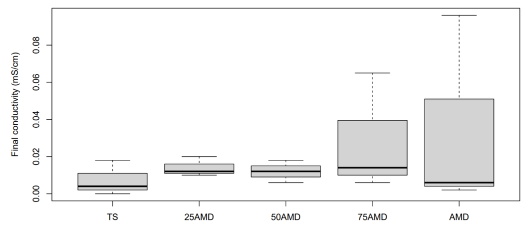

Figure 13: Comparison of EC for final measurements

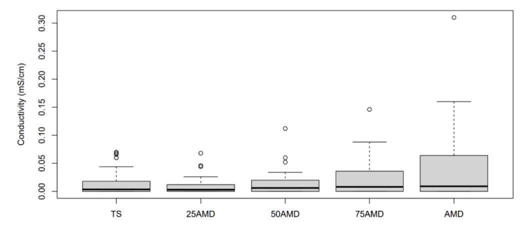

Figure 14: Comparison of EC for all measurements

Temperature

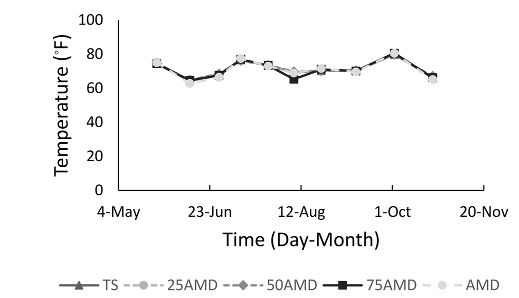

Figure 15. Mean soil temperature over time

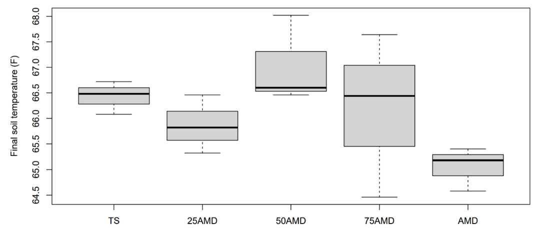

Figure 16: Comparison of soil temperature for final measurements

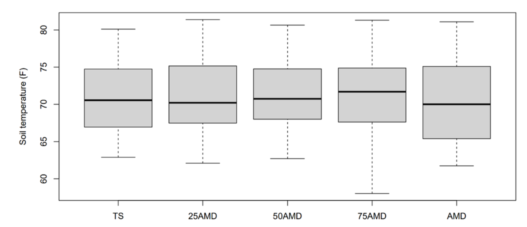

Figure 17: Comparison of soil temperature for all measurements

Biomass

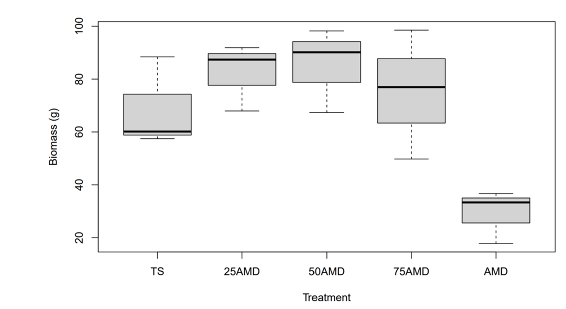

Figure 18. Comparison of biomass

Figure 19. Plots at end of study period

Conclusions

The major takeaways from this research include:

- Ground cover showed AMD mixture was significantly less than other treatment's when considering the full duration of the study (Fig. 8)
- Soil moisture showed AMD mixture was significantly greater than all other treatments when considering soil moisture over the full duration of the study (Fig. 11)

Future considerations include digging 6-in into the surface to place plots, use fence to keep wildlife from disturbing plots, and consider runoff from the site.

Acknowledgements

This research is supported by Grant/Cooperative Agreement Number S21AC10054 from the Office of Surface Mining, Reclamation, and Enforcement. Its contents are solely the responsibility of the authors and do not necessarily represent the official views of the OSM. This work is also in collaboration with the West Virginia Department of Environmental Protection, Office of Special Reclamation.

References

Ackman, T. E. Sludge Disposal from Acid Mine Drainage Treatment. Report of Investigations/1982. PB-82-257148, Bureau of Mines, Pittsburgh, PA (USA). Pittsburgh Research Center, 1 June 1982. www.osti.gov, https://www.osti.gov/biblio/6611776.

Akcil, Ata, and Soner Koldas. "Acid Mine Drainage (AMD): Causes, Treatment and Case Studies." Journal of Cleaner Production, vol. 14, no. 12–13, Jan. 2006, pp. 1139–45. DOI.org (Crossref), https://doi.org/10.1016/j.jclepro.2004.09.006.

Fuchida, Shigeshi, et al. "Understanding the Biogeochemical Mechanisms of Metal Removal from Acid Mine Drainage with a Subsurface Limestone Bed at the Motokura Mine, Japan." Scientific Reports, vol. 10, no. 1, Dec. 2020, p. 20889. DOI.org (Crossref), https://doi.org/10.1038/s41598-020-78069-9.

Masindi, V., et al. "Challenges and Avenues for Acid Mine Drainage Treatment, Beneficiation, and Valorisation in Circular Economy: A Review." Ecological Engineering, vol. 183, Oct. 2022, p. 106740. DOI.org (Crossref),https://doi.org/10.1016/j.ecoleng.2022.106740.

Simate, Geoffrey S., and Sehliselo Ndlovu. "Acid Mine Drainage: Challenges and Opportunities." *Journal of Environmental Chemical Engineering*, vol. 2, no. 3, Sept. 2014, pp. 1785–803. *DOI.org (Crossref)*, https://doi.org/10.1016/j.jece.2014.07.021.